

Studies of Hip Impingement Diagnosis

A thesis submitted for the degree of Doctor of Philosophy

By

Mahshid Yazdi Far

College of Engineering, Design and Physical Sciences

Brunel University

August 2014

Copyright

Copyright © 2014 Mahshid Yazdi Far. All rights reserved.

The copyright of this thesis rests with the Author. Copies (by any means) either in full, or of extracts, may not be made without prior written consent from the Author.

**This thesis is dedicated to my parents Mahnaz and Majid for
their endless love, support and encouragement**

Abstract

Hip impingement is a hip associated abnormality which develops among young and middle-aged individuals. It reduces the activity of those affected and if it is not detected at early stage, it can result in osteoarthritis. In this thesis a reliable framework for studying impingement detection is developed.

Current clinical methods in detecting hip impingement involve measuring three angles, first the patient's leg being flexed until maximum angle, second patient's leg being flexed until 90° then adducted until maximum angle, and third patient's leg being flexed until 90° afterwards internally rotated until the maximum angle also known as FADIR (Flexion, adduction in 90° flexion and internal rotation in 90° flexion) test. This is a manual method and relies heavily on surgeons experience and even pain tolerance of the patient and the method is prone to error. The use of computational programmes are known to be more accurate and reliable as the kinematic of contact can easily be studied using the digitised bones of the hip joint assuming that the impingement is determined by bone to bone contact kinematics. Current impingement studies assume that the kinematics of hip joint can be studied by assuming the centre of rotation is fixed for hip joint. For highly conforming joints this assumption is acceptable but for cases where conformity is poor the presence of soft tissue and soft tissue loading becomes very important. The important need in orthopaedics field is to develop a model without too much simplification.

In this thesis for the first time the complete computational model of hip with soft tissue has been used to detect the impingement in a specific patient. The effect of centre of rotation and soft tissue are considered on impingement detection.

In this study the femur, acetabulum, cartilage and ligaments of specific patients were modelled in MIMICs (Materialise' Interactive Medical Image Control System) using both MRI and CT scan. 3D hip models with and without soft tissues of normal hip, hip with impingement and hip with impingement after reshaping were modelled. The hip models were meshed in 3-Matic. The hip models were imported to Abaqus and boundary conditions were applied. Impingement zone and impingement angle was detected in Abaqus. Different centre of rotation was applied to consider the effect of centre of rotation to detect impingement.

Experimental studies were set up to validate the hip models. Mocap, Wiimote, MotionNode and goniometer were used together at the same time to measure the flexion, adduction and internal rotation in 90⁰ of flexion in twenty two healthy volunteers. Validity and reliability of all of the methods were calculated. It is the first time that reliability and validity of Wiimote and MotionNode are considered to be used in medical application.

Our results show that the model with soft tissue is closer to the experimental results. It shows that the soft tissue in hip model affects hip impingement angle and hip biomechanics. This finding also shows that, if the boundary condition is closer to the real hip, then the results of computer-aided program will be more reliable.

List of Publications and Award Achieved From This Thesis

- **Mahshid Yazdifar**, Mohammad Reza Yazdifar, Jamaluddin Mahmud, Ibrahim Esat, Mahmoud Chizari, “*Evaluating the hip range of motion using goniometer and video tracking methods*” Paper presented at Malaysian International Tribology Conference 2013 (MITC2013)
- **Mahshid Yazdifar**, Mohammadreza Yazdifar, Pooyan Rahmanivahid, Saba Eshraghi, Ibrahim Esat, Mahmoud Chizari, “*Evaluation of hip impingement kinematics on range of motion*” paper presented at 15th International Conference on Human-Computer Interaction (HCII), Mirage Hotel, Las Vegas, Nevada, USA.
- **Mahshid Yazdifar**, Nikolaos Bardakos, Richard Field, Mohamadreza Yazdifar, Ibrahim Esat, Mahmoud Chizari, “*The femoroacetabular impingement may be affected by changing the centre of rotation*” Paper presented at 19th Iranian Conferences of Biomedical Engineering (ICBME91), Tehran, Iran, 2012
- **Mahshid Yazdifar**, Nikolaos Bardakos, Richard Field, Mohamadreza Yazdifar, Ibrahim Esat, Mahmoud Chizari, “*The effect of centre of rotation on hip joint with impingement*” Paper presented at 25th annual SIMULIA UK regional user meeting, Cheshire, UK, 2012.
- **Mahshid Yazdifar**, Radhakrishna Suppanee, Nikolaos Bardakos, Richard Field, Saba Eshraghi, Mohamadreza Yazdifar, Ibrahim Esat, Mahmoud Chizari, “*The femoroacetabular impingement may be effected by changing the kinematic of the hip joint*” Paper presented at 17th annual conference of society of design and processing (SDPS) in Berlin, Germany, 2012.
- **Mahshid Yazdifar**, Radhakrishna Suppanee, Ibrahim Esat, Mahmoud Chizari, Nikolaos Bardakos, Karthig Rajakulendran , “*Motion Analysis of the hip joint at a femoroacetabular impingement*” Paper presented at 24th annual SIMULIA UK regional user meeting in Gloucestershire, 2011.
- **Mahshid Yazdi Far**, Ibrahim Esat, “*The Effect of Soft Tissue on 3D modelling of Hip*” paper presented in 5th annual research student conference (Rescon13), 2013, Brunel University, London, UK.
- **Mahshid Yazdi Far**, Ibrahim Esat, “*Does changing the kinematic of motion affect on femoroacetabular impingement?*” paper presented in 5th annual research student conference (Rescon12), 2012, Brunel University, London, UK.
- **Mahshid Yazdi Far**, Ibrahim Esat, “*The effect of range of motion on the femoroacetabular impingement.*” Poster presented in graduate school poster conference 2012, Brunel University, London, UK.
- Radhakrishna Suppanee, **Mahshid Yazdifar** , Mahmoud Chizari, Ibrahim Esat, Nikolaos V. Bardakos , Richard E. “*Field Simulation osteoarthritis: the effect of*

the changing thickness of articular cartilage on the kinematics and pathological bone-to-bone contact in a hip joint with femoroacetabular impingement”, journal of European orthopaedics and traumatology Volume4 number2 June 2013,DOI: 10.1007/s12570-013-0196-0.

- **Mahshid Yazdifar**, Mohammadreza Yazdifar, Pooyan Rahmanivahid, Saba Eshraghi, Ibrahim Esat, Mahmoud Chizari ,”*Evaluation of hip impingement kinematics on range of motion*” Springer, Human-Computer Interaction.Part V, volume 8008, pp. 262–269, 2013.
- Winner of Brunel University Vice-Chancellor's travel prize for postgraduate research students academic year 2011/2012
- Winner of Brunel University Vice-Chancellor's travel prize for postgraduate research students academic year 2012/2013

Acknowledgment

I would like to express the sincere gratitude to my supervisor Professor Ibrahim Esat, who continually and persuasively conveyed a spirit of adventure in regard to research. Without his supervision and constant help this thesis would not have been possible.

A great thank to Gopal Jeyasandra and Ioannis Paraskevopoulos for providing Motion Capture and Wiimote lab. In addition, thank to Doctor Mahmoud Chizari. I also would like to thank Epsom Hospital, Brunel University and School of engineering and design for cooperation, great information and providing facilities in the thesis.

I would like to show appreciation to Amir Ghajar, Mohammad Reza Yazdifar, Saba Eshraghi and Tony Morris who gave me courage and support through my PhD. I would never be able to finish my thesis without my parent's supports.

List of Contents

Chapter 1 Introduction	1
Introduction.....	1
1.1 Motivation.....	1
1.2 Research Goals	3
1.3 Outline of Chapters	4
Chapter 2 Basic Background	6
Basic Background	6
2.1 Introduction.....	6
2.2 Hip Structure.....	6
2.2.1 Pelvis.....	7
2.2.2 Femur	7
2.2.3 Hip Joint Cartilage	9
2.2.4 Hip Joint Ligaments.....	10
2.2.5 Hip Joint Muscles	12
2.3 Biomechanics of Hip Joint.....	14
2.4 Femoroacetabular Impingement (FAI)	16
2.4.1 Type of Impingement.....	16
2.4.1.1 Cam Impingement.....	16
2.4.1.2 Pincer Impingement	18
2.4.1.3 Combined Cam and Pincer Impingement	19
2.4.2 Role of FAI to Induce OA	20
2.4.3 Effects of FAI	22
2.4.4 Who Has Impingement?	22
2.4.5 Treatment of FAI	22
2.4.5.1 Resectional Osteoplasty	24
2.4.5.2 Arthroscopy of hips	24
2.5 Conclusion	24
Chapter 3 Literature Review	25
Literature Review	25
3.1 Introduction.....	25
3.2 Hip Modelling.....	25
3.2.1 Experimental Hip Modelling	26
3.2.2 Analytical Modelling	27
3.2.3 Computational Modelling	28
3.2.3.1 Constitutive Models for Bone and Cartilage	28

3.2.3.2 Finite Element Modelling	29
3.2.3.3 Discrete Element Analysis	30
3.3 Hip Impingement Analysis via Computer Modelling.....	31
3.3.1 Detection of Impingement	32
3.3.1.1 Physical or Clinical Examinations	32
3.3.1.1.1 FABER TEST.....	35
3.3.1.1.2 FADIR TEST	36
3.3.1.2 Radiographic Parameters Examinations	37
3.3.2 Previous researche on FAI.....	41
3.3.2.1 Experimental Research	42
3.3.2.2 Computational Research	44
3.4 Conclusions.....	47
Chapter 4 Research Method	48
Research Methods.....	48
4.1 Introduction.....	48
4.1.1 Impingement Angle (FADIR Test).....	49
4.1.2 Impingement Zone (Clock Method)	51
4.2 Finite Element Analysis (FEA).....	51
4.3 Experiments	54
4.4 Validation of FEA with Experimental Analysis	55
Chapter 5 Hip Modelling	57
Hip Modelling.....	57
5.1 Introduction.....	57
5.2 MIMICs	57
5.2.1 Importing Medical Images	58
5.2.2 Thresholding of Medical Images	60
5.2.3 Region Growing.....	62
5.2.4 Segmentation Density Mask	62
5.2.5 Generating 3D Model	63
5.2.6 Smoothing and Reduce Triangle Reduction	64
5.3 3-Matic.....	65
5.3.1 Element Type.....	65
5.3.2 Remesh.....	66
5.3.3 Quality of Mesh	67
5.4 Abaqus	70
5.4.1 Volumetric Mesh	71

5.4.2 Assemble.....	72
5.4.3 Material Properties.....	73
5.4.4 Location of Hip Joint Centre	74
5.4.5 Contact Algorithm	76
5.4.6 Boundary Condition.....	76
5.4.7 Impingement Angle and Impingement Zone	79
5.4.8 Collision Detection of Impingement.....	80
5.5 Conclusion	84
Chapter 6 Hip Modelling Results	85
Hip Modelling Results	85
6.1 Introduction.....	85
6.2 Case Studies	86
6.3 Methododology	86
6.3.1 Fixed centre of Rotation	86
6.3.2 Changing the Centre of Rotation	87
6.3.3 Free Centre of Rotation.....	89
6.3.4 Hip Models with Soft Tissues.....	90
6.4 Results.....	90
6.4.1 Fixed Centre of Rotation.....	96
6.4.2 Changing the Centre of Rotation	99
6.4.3 Free centre of rotation.....	103
6.4.4 Hip Models with Soft Tissues.....	104
6.5 Discussion.....	106
6.6 Conclusion	107
Chapter 7 Experiments on FADIR Test	109
Experiments on FADIR Test	109
7.1 Introduction.....	109
7.2 Methodology	110
7.2.1 Subjects.....	110
7.2.2 Motion Capture	111
7.2.2.1 Calibration	113
7.2.2.2 Accuracy of Motion Capture	115
7.2.2.3 Data Recording	117
7.2.3 Wii-Remote.....	122
7.2.3.1 Calibration	124
7.2.3.2 Data Recording	125
7.2.4 MotionNode	128

7.4.2.1 Calibration	129
7.2.4.2 Data Recording	130
7.2.5 Adjustable goniometer	133
7.2.6 Statistical Analysis.....	135
7.3 Results and Discussion	136
7.3.1 Validity	141
7.3.2 Reliability.....	145
7.4 Conclusion	148
Chapter 8 Summary and Conclusion.....	149
Summary and Conclusion	149
8.1 Summary	149
8.2 Conclusions.....	154
8.3 Future Work.....	155
Bibliography	157
Appendixes	169

List of Figures

Figure 1: a) Torsion angle of hip b) normal and abnormal angle of inclinations (coxa vara and coxa valga) in the femur bone (Gauresh, 2009).....	8
Figure 2: Hip joint cartilage and ligament attachment point (Jones, 2013).....	10
Figure 3: Anterior and posterior view of hip joint ligaments (Jones, 2013).....	12
Figure 4: Flexor muscles of hip joint (anterior view) (Anderson, 2013).....	13
Figure 5: Adductor muscle of hip joint (anterior view) (Anderson, 2013).....	13
Figure 6: Rotator muscle of hip joint (anterior view) (Anderson, 2013).....	14
Figure 7: Movements of the hip joint; a) flexion and extension b) abduction and adduction c) external and internal rotation (Drake, et al., 2010)	15
Figure 8: Radiography picture of cam impingement. White arrow shows the place of bump in impingement (Filigenzi & Bredella, 2008).....	17
Figure 9: Radiographic picture of pincer impingement. White arrow shows the place of bump in impingement (Filigenzi & Bredella, 2008).....	18
Figure 10: Schematic pictures of all of the impingement types (Marti & Tashman, 2010)	19
Figure 11: Schematic view of hip arthroscopy to treat hip impingement (Horisberger , et al., 2010)	23
Figure 12: Impingement test to locate hip pain area which is C sign pain around hip (Kuhlman & Domb, 2009).....	33
Figure 13: Angles measurement in FABER and FADIR test as two experimental tests to detect impingement a) maximum flexion, b) maximum abduction in 90°flexion, c) maximum adduction in 90°flexion, d) maximum external rotation in 90°flexion, e) maximum internal rotation (Nussbaumer, et al., 2010)	36
Figure 14: Measurement of Centre Edge Angle (Lever & O’Hara, 2008) b)AP radiograph of a 23-year-old female patient (anterior view of hip weight bearing) (Marti & Tashman, 2010)	38
Figure 15: Measurement of adult Acetabular Index of supine position (anterior view of hip) (Lever & O’Hara, 2008).....	38
Figure 16: Measurement of alpha angle in supine position (Taunton , 2011)	39
Figure 17: X-ray of typical pistol grip deformity (anterior view of hip weight bearing) (Lever & O’Hara, 2008)	39
Figure 18: Alpha angle and normal head-neck offset in the lateral view a) normal hip b) Cam impingement (anterior view of hip weight bearing) (Hossain & Andrew, 2008) ..	40
Figure 19: Impingement angle a) flexion, b) adduction in 90° flexion, c) internal rotation in 90° flexion.....	50
Figure 20: The clock method to measure the impingement zone (Kubiak-Langer, et al., 2007)	51
Figure 21: Outline of FEA method and results in Chapters 5 and 6.....	53
Figure 22: Outline of experimental method and results in Chapter 7.....	55
Figure 23: Outline of validating FEA with experimental results in Chapter 8.....	56
Figure 24: Different views in MIMICs program a) axial b) sagittal c) coronal d) 3D views of the pathological left hip joint	59
Figure 25: Segmentation of the cortical bones from the soft tissues and soft tissues from bone. a) Threshold value and segmentation of bone from soft tissues b) Threshold value and segmentation of compact bone c) Threshold value and segmentation of soft tissues	61

Figure 26: Filling pelvic mask manually a) a slide of pelvic mask was chosen b) pelvic mask was filled manually (yellow area) c) all of the pelvic was filled in the mask	63
Figure 27: 3D model of the pathological hip joint of the volunteer after filling cavity in MIMICs a) with soft tissues b) without soft tissues	64
Figure 28: Smoothing a) acetabulum before smoothing b) acetabulum after smoothing	64
Figure 29: Quality mesh histogram that shows the amount of triangle that have certain quality according to the threshold value. Tool bar under the histogram shows the number of elements a) with minimum quality b) between minimum and maximum quality c) with maximum quality	68
Figure 30: Changing the quality of mesh by changing the parameters such as shape measure, inspection measure, geometric errors, and maximum triangle edge length	69
Figure 31: Volumetric mesh of a) femur b) acetabulum c, d, e) hip Ligaments f, g) hip cartilage in Abaqus	72
Figure 32: Assemble of hip model a) Without soft tissues b) with soft tissues.....	73
Figure 33: Fixed sphere top of the femur head to select centre of rotation. The centre of sphere is the centre of rotation	75
Figure 34: Coupling femur to centre of rotation	77
Figure 35: Ligaments and articular cartilage were tied to the femur and acetabulum....	78
Figure 36: Pinned area in hip model	78
Figure 37: Schematic of acetabulum before and after impingement happens (sagittal view of left hip).....	83
Figure 38: Stress-Impingement angle diagram of impinged area.....	84
Figure 39: Schematic centre of rotation displacement a) toward (-) and b) outward (+) the acetabulum	87
Figure 40: Calculation of the coordinate of the centre of rotation.....	89
Figure 41: The hip model with the free centre of rotation (Bedi, et al., 2011), (Bedi, et al., 2012)	90
Figure 42: Flexion angles of normal volunteer for a) hip model with fixed centre of rotation, b) hip model with free centre of rotation, c) hip model with soft tissues.....	91
Figure 43: Adduction in 90° flexion a) hip model with fixed centre of rotation, b) hip model with free centre of rotation, c) hip model with soft tissues.....	93
Figure 44: Internal rotation in 90° flexion a) hip model with fixed centre of rotation, b) hip model with free centre of rotation, c) hip model with soft tissues	95
Figure 45: Collision detection for flexion angle of the hip model with fixed centre of rotation	96
Figure 46: Collision detection for adduction angle of the hip model with fixed centre of rotation	97
Figure 47: Collision detection for internal rotation angle of the hip model with fixed centre of rotation	97
Figure 48: Flexion, adduction, internal rotation for normal, reshaped and impinged model with fixed centre of rotation.....	98
Figure 49: Comparison of our results with previous articles (Kubiak-Langer, et al., 2007) when centre of rotation is fixed to the centre of the femur	98
Figure 50: Flexion angle in terms of centre of rotation for the normal, impingement and reshaped hip	99
Figure 51: Adduction angle in terms of centre of rotation for the normal, impingement and reshaped hip	100
Figure 52: Internal rotation angle in terms of centre of rotation for the normal, impingement and reshaped hip	101

Figure 53: Impingement zone for normal, impingement and reshaped hip with different centre of rotations a) -4mm b)-3mm c) -2mm d)-1mm e) 0mm f) 1mm g) 2mm h) 3mm i) 4mm away from centre of the femur (lateral view of left hip).....	103
Figure 54: Comparison of impingement zone for normal, impingement and reshaped hip with free and fixed centre of rotation a) free centre of rotation b) fixed centre of rotation (lateral view of left hip)	104
Figure 55: Impingement zone for hip model with soft tissues (lateral view of left hip)	105
Figure 56: General view of the Motion Capture lab with seven cameras and large screen to show human motion.....	111
Figure 57: Vicon Blade software window start-up.....	112
Figure 58: Camera hardware reset	113
Figure 59: 3D space calibration window	114
Figure 60: Floor calibration marker view	115
Figure 61: Measuring the accuracy of the Motion Capture and movement of the hand was measured by ruler	116
Figure 62: Marker places on leg to measure flexion, adduction and internal rotation of hip	118
Figure 63: Measurement of flexion angle in the Motion Capture lab	119
Figure 64: Measurement of adduction in 90° flexion angle in the Motion Capture lab	120
Figure 65: Measurement of internal rotation in 90° flexion angle in the Motion Capture lab.....	121
Figure 66: Schematic procedure of Wii-remote control to get motion data of human.	123
Figure 67: Place of Wiimote on the body a) measuring flexion and adduction, b) measuring internal rotation	124
Figure 68: The calibration window of Wiimote	124
Figure 69: The take window of Wiimote.....	125
Figure 70: Sample of data recording for Wiimote in terms of time	126
Figure 71: Measurement of flexion, adduction in 90°of flexion and internal rotation 90°of flexion by Wiimote and Motion Capture at the same time.....	128
Figure 72: a) MotionNode device which is as small as a pound coin, b) X, Y, Z axis in MotionNode software	129
Figure 73: Calibration window in MotionNode software.....	129
Figure 74: MotionNode device view in MotionNode software, right hand side of the software shows the rotation changes around X, Y, Z axis during each take.....	130
Figure 75: Sample of data recording for MotionNode interms of time	132
Figure 76: Measurement of flexion, adduction in 90°of flexion and internal rotation 90°of flexion by MotionNode.....	133
Figure 77: Adjustable goniometer used in the experiments	134
Figure 78: Measurement of a) flexion, b) adduction in 90°of flexion, c) internal rotation 90°of flexion by goniometer	135
Figure 79: Angle of flexion in terms of time for three volunteers as a sample	138
Figure 80: Angle of adduction in 90° flexion in terms of time for three volunteers as a sample	139
Figure 81: Angle of internal rotation in 90° flexion in terms of time for three volunteers as a sample	140
Figure 82: Graph of reference method (Motion Capture) against the test methods (Goniometer, MotionNode, Wiimote) (correlation plot).....	144

Figure 83: Bland-Altman plot for goniometer, Motion Capture, MotioNode and
Wiimote 147

List of Tables

Table 1: Different parts of lower limb (Tortora, 2003)	6
Table 2: Physical examination of hip impingement (Kuhlman & Domb, 2009).....	34
Table 3: Radiographic parameters which are used to indicate the impingement (Hossain & Andrew, 2008)	41
Table 4: Range of motion for normal hip, hip with impingement and hip with impingement after reshaping (Kubiak-Langer, et al., 2007).....	45
Table 5: Number of elements for femur in 3-Matic by changing the mesh parameters such as inspection measure and Max triangle edge length, the red line is the changes while the black one remain constant.....	70
Table 6: Material property of the finite element model (Hewitt, et al., 2001), (Suppatee, et al., 2013), (Rho, et al., 1993)	74
Table 7: Nine different location of centre of rotation were introduced between femur and acetabulum to examine the effect of kinematic on the FAI	88
Table 8: Range of motion in free centre of rotation models	103
Table 9: Range of motion in free centre of rotation models according to the previous articles (Bedi, et al., 2011) (Bedi, et al., 2012)	103
Table 10: Flexion, adduction and internal rotation for hip model with soft tissues	105
Table 11: General information of all volunteers.....	111
Table 12: Comparison of Motion Capture and ruler measurement (n=10)	116
Table 13: Mean± SD volunteers ROM for each measurement device (n=44)	137
Table 14: Validity of the Wiimot, goniometer and MotionNode (MotionCapture was used as a reference device) for hip ROM (n=22).....	142
Table 15: Comparison of our finding (n=22) with the previous articles (Nussbaumer, et al., 2010)	142
Table 16: Reliability of Goniometer, Wiimote, Motion Capture and MotionNode for hip ROM	145
Table 17: Comparison of our finding with previous articles (Nussbaumer, et al., 2010)	146
Table 18: Results of different centre of rotations, 0 is the fixed centre of rotation (previous article (Kubiak-Langer, et al., 2007) used this centre) and -1 means that centre of rotation was moved 1 mm inward the acetabulum and +1 means that centre of rotation was moved 1 mm outward the acetabulum.....	151
Table 19: Results of different boundary conditions.....	152
Table 20: Reliability of the different measurement techniques	152
Table 21: Validity of Wimote, goniometer and MotionNode compared to the Motion Capture.....	153
Table 22: The comparison of the normal hip ROM for computer-aided programme and experimental results	154

Abbreviations

CT	Computed Tomography
CV	Coefficient of Variance
DEA	Discrete Element Analysis
ETS	Electromagnetic Tracking System
FAI	Femoroacetabulum Impingement
FEA	Finite Element Analysis
ICC	Intraclass Correlation Coefficient
LOA	Limit of Agreement
MIMCs	Materialise' Interactive Medical Image Control System
MRI	Magnetic Resonance Imaging
OA	Osteoarthritis
ROM	Range of Motion
SEM	Significant Error of Measurement
THR	Total Hip Replacement
1D	One dimensional
2D	Two Dimensional
3D	Three Dimensional

Notations

U_1	Displacement in X direction
U_2	Displacement in Y direction
U_3	Displacement in Z direction
UR_1	Rotation around X axis
UR_2	Rotation around Y axis
UR_3	Rotation around Z axis
X	Horizontal axis
Y	Vertical axis
Z	Third axis

Chapter 1

Introduction

1.1 Motivation

The hip joint is considered as an important joint because two thirds of the total body weight is carried by it and during daily activities, forces equal to five and a half times body weight are shifted between the femur and pelvis (Hodge, et al., 1986), (Bergmann, et al., 2001) (Bergmann, et al., 1997 Feb). Moreover, hip joint is a connector between the upper and lower body providing a wide range of motion. However, abnormal loading of the articular cartilage often leads to it becoming damaged and this degeneration is termed osteoarthritis (OA). One significant hip joint disease is hip impingement which can lead to OA (Mankin, 1974; Mow, et al., 1980).

With improved healthcare provisions people are living longer and some medical conditions are becoming more common due to old age. One such condition is osteoarthritis. In Wales and England during 2012 more than 160000 hip replacement were performed (Anon., 2012). The onset of OA is debatable but it is well accepted that Femoroacetabular Impingement (FAI) plays a substantial role.

FAI is a condition arising from abnormal contact (Ganz, et al., 2003) between the head of the femur and the acetabulum. “FAI is not a disease, but rather it is a pathomechanical process by which the human hip can miscarry” (Ganz, et al., 2003). A variety of abnormalities of the bony acetabulum and/or femur, combined with rigorous hip motion, can lead to repetitive collisions that damage the soft tissue structures

(labrum or cartilage) of the acetabular rim (Leunig, et al., 2005). These deformities in the structure of hip bones reduce the range of motion that a hip joint can make and thus patients who are suffering with FAI feel pain when contact occurs between the head of the femur and the acetabulum (Ganz, et al., 2003).

FAI develops increasingly among young generation, as they become more active and sporty. So there is a need to develop an accurate and reliable method to detect the FAI. 10%-15% of the adult population are clinically diagnosed with FAI (Leunig & Ganz, 2005). Most of the patients diagnosed with FAI are young, active and sporty adults. Also the population of the male diagnosed with FAI are higher than female diagnosed with FAI.

The development of OA leads to Total Hip Replacement (THR) surgery. However, for younger patients, this may not be the best solution for their hip pain, because it can lead to numerous difficult revisions later in life. As hip impingement usually happens to young active adults (Leunig, et al., 2005), early detection and treatment can avoid OA and subsequent THR.

Impingement surgery is one of the most common operations taking place in sports medicine. The cost of such intervention is hard to evaluate because medical centres claimed that the details regarding their charges and costs are proprietary information. However, reports from one academic medical centre indicated the cost of hip impingement surgery is less than the cost of THR surgery (Kolata, November 2011) which may suggest that the early detection of FAI could reduce the cost burden of surgery for the NHS.

As the life style choices of people change and more, particularly younger ones, are keen to take up sports, more of the population may encounter hip impingement and thus, over the past few decades, this matter has become the focus of extensive academic writing. Impingement has been studied by many authors (Eijer , et al., 2001), (Ganz, et al., 2003), (Jäger , et al., 2004), (Murphy , et al., 2004), (Siebenrock , et al., 2003), (Strehl & Ganz , 2005), (Leunig, et al., 2009) with some of the literature addressing its assessment and treatment.

The mean time for the symptom from start to the final diagnosis is 3 years (Clohisy, et al., 2009). Early diagnosis is very challenging since many of FAI patients have insidious onset of symptoms that is the same as other muscle dysfunction diseases. Many of the FAI patients experience delay in diagnosis, incorrect diagnosis and

ineffective treatment recommendation (Clohisy, et al., 2009). Late diagnosis of FAI causes OA and damage to soft tissue. As FAI occurs in young and active adults who need the full range of motion, there is a requirement to detect FAI in early stage. There is a major need to investigate reliable, valid and easy impingement detection framework. 74% of the FAI patients have reported to have significant reduction in flexion and internal rotation in flexion (Clohisy, et al., 2009).

Murray (Murray, 1965) was the first person to report FAI theory in 1965 and then 10 years later Stulberg and his colleague (Stulberg & Harris, 1974) expanded the FAI theory of Murray by studying morphology of hip in 1974. Harris reported that 80% of patients diagnosed with OA had FAI (Harris, 1986). After this point, the number of articles about FAI started to increase. Publications on impingement have increased between 1997 and 2007 because of improved diagnostic of impingement (Leunig, et al., 2009).

1.2 Research Goals

The overall aim of this project is to propose a reliable framework for studying impingement. In order to achieve the main aim, several goals were defined. One of the goals of this thesis is to develop a complete and clinically realistic hip model. In order to achieve this goal, a finite element analysis method (FEA) with the incorporation of soft tissue is established. This is the first time that a complete model with soft tissue is being modelled by using CT and MRI of the specific patient. Many numerical and theoretical models have been designed in the past to model hip joint; however none of them presents a real model of ligaments and cartilage from the MRI. Hence, this model aids improved understanding of the biomechanics of hip.

This research is focused on addressing the following three main goals: firstly, in this study the limitations of computer based impingement detections are clarified. Although computer aided programmes are used to assist patients and doctors, there are various limitations and factors that affect the accuracy of the modelling that they generate.

Secondly, the effects of soft tissue have been studied in respect to the accurate detection of impingement. All previous work on detecting impingement has ignored the factor of soft tissue. In this study a hip model with soft tissue is used with three

ligaments and articular cartilage being modelled by using patients' MRI. Thus, the complete hip model with soft tissue, specific to each patient, is employed to study the biomechanics of hip diseases.

Thirdly, the study focused on comparing the results of our computer aided program with experimental results in order to validate the computational models. Four different experimental methods were set up to measure volunteer's flexion as well as their adduction and internal rotation in 90⁰ flexion. Reliability and validity of all methods were calculated, and then replace a reliable, valid, easy to use and convenient method instead of the present clinical method to detect impingement, have been achieved.

The following objectives are summarized and achieved in this thesis:

- Develop reliable and valid framework to detect FAI. Most of the FAI patients are either misdiagnosed with others hip diseases or diagnosed late. In this study a valid and reliable framework was developed to diagnose the FAI in the early stages.
- Develop a complete and real hip model with soft tissues. The hip model is based on CT and MRI of the specific person. It is the first model of its kind with soft tissues and real hip joint geometry.
- Design a collision detection of FAI based on stress to detect the impingement angle. The collision detection was designed to detect FAI based on stress-impingement angle diagram. It is the first collision detection based on stress.
- The effect of centre of rotation and boundary condition on hip modelling has been considered.
- Compared the validity and reliability of current clinical methods with Motion Capture laboratory, experimental results.

1.3 Outline of Chapters

The structure of this dissertation is organized to address the essential questions that arise when surgeons aim to detect, cure and treat hip impingement. The thesis also studies on limitations of computer aided programming in the detection of hip joints with impingement. The focus of Chapter 2 is to provide a knowledge base that serves as a reference for the topics encompassed in the subsequent Chapters. In Chapter 2 the

following are discussed: bone, ligaments, cartilage and muscle structure of hip joint. In addition, the principle of hip impingement is introduced and issues such as types, causes and treatment of impingement are explained.

In Chapter 3, previous research work on hip modelling and impingement is reviewed. This contains related work that has involved experimental, numerical and finite element analysis of hip modelling. Moreover, recent articles discussing the clinical detection of hip impingement and computer aided modelling for detection of hip impingement are covered.

Chapter 4 briefly introduces the research plan and research methods. Also this Chapter outlines the main investigation plot and their relationship to the aim of the thesis.

In Chapter 5 the methods that are used in Chapter 6 are explained and justified. Computational modelling of the hip and finite element tools is explained. Furthermore, method of the 3D modelling are covered for the femur, acetabulum, articular cartilage and ligaments of the hip made in MIMICs by using CT and MRI data. In this Chapter there is also an explanation of how 3-Matic is used to mesh the parts and to check the quality of the mesh and how Abaqus is used to assemble the parts with boundary conditions and surface interaction defined in Abaqus, together with the detection of impingement angle and impingement zone in Abaqus.

The outcomes of finite element modelling of the hip with impingement are discussed and compared with each other and previous work in Chapter 6. In addition, the results of the simulation in Abaqus for different hip models are shown. The hip models discussed are the hip model with; a fixed centre of rotation, a free centre of rotation, different centre of rotation and the hip model with and without soft tissues.

Chapter 7 demonstrates the experimental methodology and results. The method and the results of four devices, Wiimote, Motion Capture, MotionNode and goniometer are explained. The volunteers are asked to take part and flexion, adduction in 90° of flexion and internal rotation in 90° of flexion are measured by applying different measurement methods. The reliability and validity all the measurement methods are compared.

Chapter 8 summarizes and draws some conclusions on all Chapters, in particular comparing the results of Chapters 6 and 7. Also, in Chapter 8 future research and improvements arising from the thesis are proposed.

Chapter 2

Basic Background

2.1 Introduction

This Chapter consists of three background studies: the hip structure, the hip biomechanics and the FAI. In hip structure, general information about different parts of hip joint is delivered. Basic hip kinematics is described in biomechanics section. In FAI part, information about different types of impingement, causes and treatment of impingement according to previous research works is discussed.

2.2 Hip Structure

Lower- limb supports the body weight as well as allowing motion and maintains the balance. The lower limb is made of four parts as shown in Table 1.

Table 1: Different parts of lower limb (Tortora, 2003)

Lower limb Segmen	Bone	Connection formed
Hip	Hip bone and hip joint	Skeleton of the limb to the vertebral column
Thigh	Femur and patella	Connection between hip and knee
Leg	Tibia and fibula	Between knee and ankle
Foot	Tarsus , metatarsus and phalange	Between ankle and foot

The hip joint, also known as congruent joints, forms connection between lower limb and the pelvic girdle (Levangie & Norkin, 2001). The hip joint is mainly responsible for supporting the body weight as well as controlling most of the daily activities such as walking, seating, running and so on (Levangie & Norkin, 2001). The hip joint is structured by articulation of femoral head and pelvis's acetabulum (Drake, et al., 2010), (Levangie & Norkin, 2001). The two parts outlines a socket and ball configuration which forms three degree of freedom. The 1-2 mm gap between these two segments is filled with synovial fluid.

2.2.1 Pelvis

The pelvic girdle is made of hip bone, coccyx and sacrum. It provides supports for organs within the pelvic region as well as a dynamic connection between vertebral column and the lower limb (Levangie & Norkin, 2001). The hip bone is made of three segments; ilium (superior), ischium (interior and posterior) and pubis (inferior and anterior). These bones remain separated by a tri-radiated cartilage until the age of 15-17 and then fuse together and form a single bone (Levangie & Norkin, 2001).

Ilium: This is the largest part of hip bone. It comprises two sections, body and ala and forms the superior section of the acetabulum (Levangie & Norkin, 2001).

Ischium: This bone forms the inferior and posterior part of hip bone. It consists of a body and ramus (Levangie & Norkin, 2001).

Pubis: This bone is the anteromedial part of hip bone. The pubis consists of superior and inferior rami. The anterior and lateral parts of pubis are named pubic crest and pubic tubercle respectively (Levangie & Norkin, 2001).

2.2.2 Femur

Femur is the heaviest and longest bone in the human body (Tortora, 2003). Femur consists of head, neck and shaft. The round shape proximal and distal parts of femur articulate with acetabulum and tibia, respectively (Tortora, 2003). Fovea capitis is the small dent on top of the femoral head which is connected to the acetabulum by ligament (Levangie & Norkin, 2001). The femoral neck is considered to be the tensed

region and connects the head of the femur to the shaft. Shaft ends at the knee joint and connects to the femoral neck by two large projection of bone known as greater and lesser trochanter (Tortora, 2003). In normal healthy individual the femoral head forms a 120° - 135° angle to femoral neck.

The torsion angle is the angle between longitudinal axis of the head, neck, greater trochanter of the femur and transverse axis of the femoral condyles distally as shown in Figure 1a. The torsion angle reduces with age. In case of newly born child, this angle is 40° which decrease in the first 2 years. The torsion angles is about 15° in adults but also varies up to 30° (Levangie & Norkin, 2001).

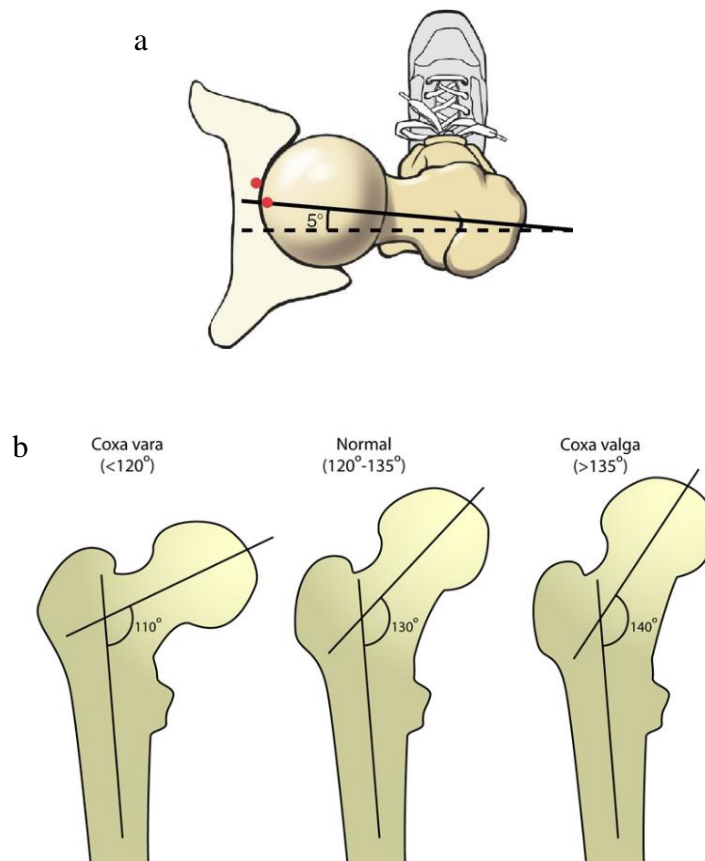


Figure 1: a) Torsion angle of hip b) normal and abnormal angle of inclinations (coxa vara and coxa valga) in the femur bone (Gauresh, 2009)

The inclination angle is present within the frontal region by the neck and head of femur and the longitudinal axis of the shaft of femur as shown in Figure 1b (Levangie & Norkin, 2001). The abnormal and normal inclination angles are shown in Figure 1b.

Inclination angles abnormality change the stability of hip joint (Levangie & Norkin, 2001).

The inclination angle is about 150° in child, 125° in adults and 120° in elderly people (Levangie & Norkin, 2001). The coxa valga and coxa vara are termed as the pathologic increment and pathologic decrement within angulations between shafts of head and neck respectively. These are shown in Figure 1b. Abnormal angles increase stress on the hip joint and affect gait (Gauresh, 2009).

Pelvis and femur are made of bone. Bone is the main constituent of the skeletal system and differs from the connective tissues in rigidity and hardness. These characteristic of bones result from inorganic salts impregnating the matrix, which consists of collagen fibres, a large variety of non-collageneous proteins and minerals (Cowin, 2001). A typical adult bone consists of a central cylindrical shaft, or diaphysis, and two wider and rounded ends, the epiphyses. Conical regions called the metaphysis connect the diaphysis with each epiphysis (Cowin, 2001).

In fact, the epiphyseal and metaphyseal bone supports the articular cartilage, which makes the epiphysis and metaphysic wider than the diaphysis. Indeed, the diaphysis is composed of mainly the cortical bone whereas the epiphysis and metaphysis contain mostly cancellous bone with a thin shell of cortical bone (Cowin, 2001). Besides, cortical bone is a dense, solid mass with only microscopic channels. About 80% of the skeletal mass in the adult human skeleton is cortical bone, which forms the outer wall of all bones and is largely responsible for the supportive and protective function of the skeleton (Cowin, 2001). On the other hand, the remaining 20 % of the bone mass is cancellous bone, a lattice of large plates and rods known as trabecula, found in the inner parts of the bones (Cowin, 2001).

2.2.3 Hip Joint Cartilage

Cartilage covers articulating surfaces of bones and acts like a shock absorber in the hip joint (Daenen, et al., 1998). It decreases the amount of bone friction and prevents bone from rubbing. Articular cartilage consists of a porous extracellular matrix (ECM) of type II collagen, proteoglycans, and other non-collagenous proteins interspersed with interstitial water and electrolytes (El-Khoury , et al., 2004) (Eckstein, et al., 2000). Articular cartilage does not contain nerves, blood vessels, or lymphatics,

and therefore, it is nourished and drained only by diffusion or convection from the surrounding synovial fluid. Articular cartilage contains cells, called chondrocytes, which are embedded in the ECM, but are sparse, making up less than 5–10% of the total volume (Ross & Craig , 2007).

Acetabulum encloses a layer of articular cartilage with its thickness ranges between 1.2 to 2.3 mm in case of adults (Sittek, et al., 1996). The whole femoral head encompasses a soft and thin layer of articular cartilage. The thickness of femoral cartilage ranges from 1 to 2.5 mm in normal adults (Sittek, et al., 1996). The articular cartilage covers inferior and central parts of acetabulum but not the fossa (Sittek, et al., 1996) as shown in Figure 2.

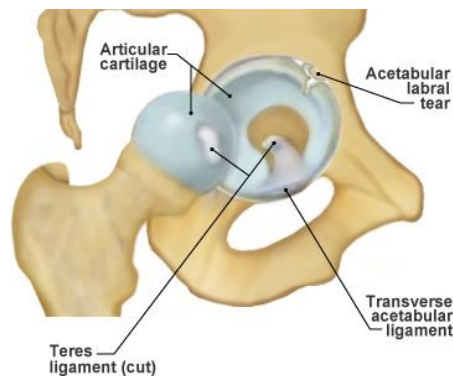


Figure 2: Hip joint cartilage and ligament attachment point (Jones, 2013)

2.2.4 Hip Joint Ligaments

Hip joint ligaments mainly perform two functions;

1) **Restricts motion range.** Ligaments are found in each and every joint in the body. They regulate and stabilise the degree of hip bones and hip joint connection and the extent at which hip joint can be expanded. As a result, they protect joints from excessive tension and dislocation and also maintain the balance (Fagerson, 1998).

2) **Joint and body protection.** The articular surface area of hip joints and the neck of femur are rounded by the powerful ligaments (Fagerson, 1998). These ligaments give protection to the surface area of hip joint and thus protecting the neck of femur (Fagerson, 1998). When injury occurs ligaments move stealthily and act like the shock absorber of any type of shock.

Ligaments are primarily composed of elastin fibres, proteoglycans and collagen (mostly type I and some type III). Elastin acts like a rubber band to return the ligament

to its original length after a stress is removed. Proteoglycans aid in the regulation of water movement within the tissue (Ross & Craig , 2007).

The collagen in the middle section of the ligament is arranged in fibres that aggregate to form fascicles. The fibres are generally oriented along the long axis of the ligament in order to resist tensile forces, although some fibres align off-axis. Close to the points where the ligament inserts into bone, the composition and structure of the ligament changes so that it is stiffer, which may help to reduce the risk of tearing at the bone–ligament interface.

The fibrous capsules are armoured through three powerful longitudinal fibrous named as iliofemoral, ischiofemoral and pubofemoral as shown in Figure 3 and an extra capsular ligament (Levangie & Norkin, 2001). These ligaments are initiated on pelvis and ended on the femur.

The iliofemoral ligament, also known as Bigelow's Y ligament and shown in Figure 3, prevents hyperextension of the hip joint during standing (Levangie & Norkin, 2001). The ligament's apex is associated with the anterior inferior iliac spine and the two arms are attached with the femur's intertranchantric line (Levangie & Norkin, 2001).

Pubofemoral ligament arises from anterior part of pubic ramus which passes to tranchantric fossa interiorly (Levangie & Norkin, 2001). The pubofemoral ligaments initiate a Z shaped structure over the capsule anteriorly. It tightens during extension and abduction and prevents hip joint from over-abducting (Levangie & Norkin, 2001).

An ischiofemoral ligament is located at the posterior side and is linked with the acetabulum rim and labrum posteriorly. Some fibres of this ligament are curved around the neck of femur and blended with zona orbicularis (Levangie & Norkin, 2001). Its other fibres are placed in a horizontal way and linked to the tranchanter interiorly. Similar to iliofemoral segment it also prevents the hip joint from hyperextension (Levangie & Norkin, 2001).

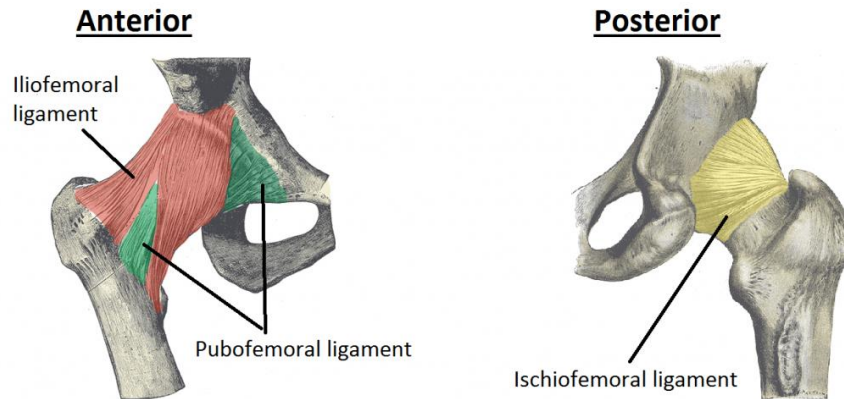


Figure 3: Anterior and posterior view of hip joint ligaments (Jones, 2013)

2.2.5 Hip Joint Muscles

The muscles work over the hip joints to ensure the joint stability (Fagerson, 1998) as well as produce movement and support body weight (Levangie & Norkin, 2001). An individual skeletal muscle may be made of muscle fibres bundled together and bound in a connective tissue covering. These muscles made of 70% water, 20% protein, 5% carbohydrates (as glycogen), 5% fats and salts (Levangie & Norkin, 2001). Muscles are categorized according to their movement: hip extensors, hip flexors, hip adductors, hip abductors, hip medial rotators, and hip lateral rotators.

The extensors of hip joint include group of hamstrings muscles and gluteus maximus muscle (Levangie & Norkin, 2001) and this muscle is the major hip extensors (Griffin, 2007). It also gives assistance to the hip's lateral rotation (Fagerson, 1998). The gluteus maximus has been found as the biggest muscle of lower edge muscle and this muscle constitutes about 13% of total lower extremity muscles (Levangie & Norkin, 2001).

The hip joint's flexors act like functional muscles when the limbs do not bear weight for the purpose of bringing lower level of extremity throughout the ambulation (Levangie & Norkin, 2001). The flexors can resist powerful extension forces of hip which takes place. Nine muscles are present along with the anterior view of hip joint (Levangie & Norkin, 2001). Iliacus, tensor fascia lata and iliopsoas are the main muscles of hip flexion as shown in Figure 4. The iliopsoas muscles are known as crucial muscles of the main muscles of hip flexors (Gauresh, 2009). This muscle consists of two muscles named as psoas muscle and iliacus muscle and these are attached with femur through muscle tendons as shown in Figure 4 (Drake, et al., 2010).

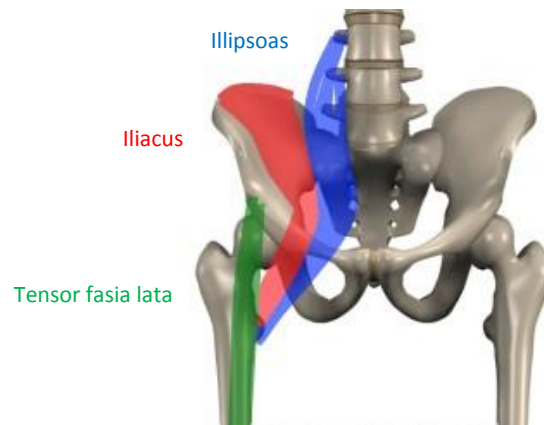


Figure 4: Flexor muscles of hip joint (anterior view) (Anderson, 2013)

The adductor muscles of hip covers adductor gracilis, adductor magnus, adductor pectineus, adductor brevis and adductor longus (Levangie & Norkin, 2001). Three adductor muscles named as adductor brevis, adductor longus and adductor pectineus helps in the rotation and the flexions of thigh and it depends on hip's position As shown in Figure 5 (Fagerson, 1998). The adductor gracilis muscle has been considered as the 2- joint adductor muscle shown in Figure 5.

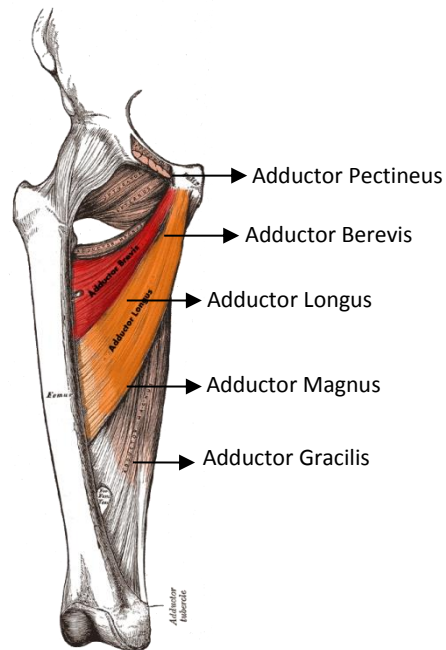


Figure 5: Adductor muscle of hip joint (anterior view) (Anderson, 2013)

The gluteus minimus and gluteus medius contributes towards an active hip abduction (Levangie & Norkin, 2001). Additionally, muscle tensor fascia lata is considered to be an effective abductor at the time of flexion of hip, thus it is recognised for its powerful contribution (Lavigne , et al., 2004).

Medial rotations are controlled by 3 main hip muscles called tensor fascia latae, gluteus medius and gluteus minimus. These three muscles have the simplest functions compare to the other hip muscles (Levangie & Norkin, 2001).

There are six muscles which controls lateral rotations (Levangie & Norkin, 2001). The names of these muscles are: piriformis muscles, gemellus inferior and superior, quadrates femoris, obturator internus & externus (Levangie & Norkin, 2001). Figure 6 shows these six muscles. In an alternative way, there is unavailability of muscles which may perform the function of medial rotations (Levangie & Norkin, 2001). But some muscles like gluteus minimus, gluteus medius and tensor fascia lata are present which perform their secondary actions of medial rotation (Lavigne , et al., 2004).

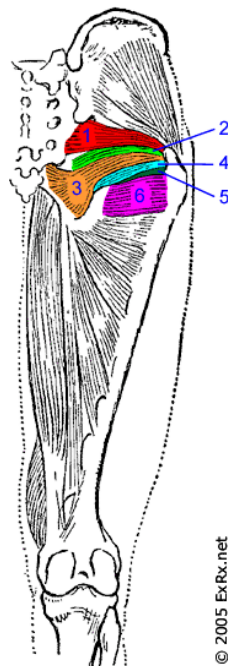


Figure 6: Rotator muscle of hip joint (anterior view) (Anderson, 2013)

2.3 Biomechanics of Hip Joint

Biomechanics defines the mechanics of body parts in human (Levangie & Norkin, 2001). It includes kinetics and kinematics. The kinematics includes the

motions with no regards to joint forces (Levangie & Norkin, 2001). Kinetics is concerned with the forces that establishes balancing or develops movements (Levangie & Norkin, 2001). With the help of strong kinetics, an individual is able to have control over the movement of the body (Levangie & Norkin, 2001).

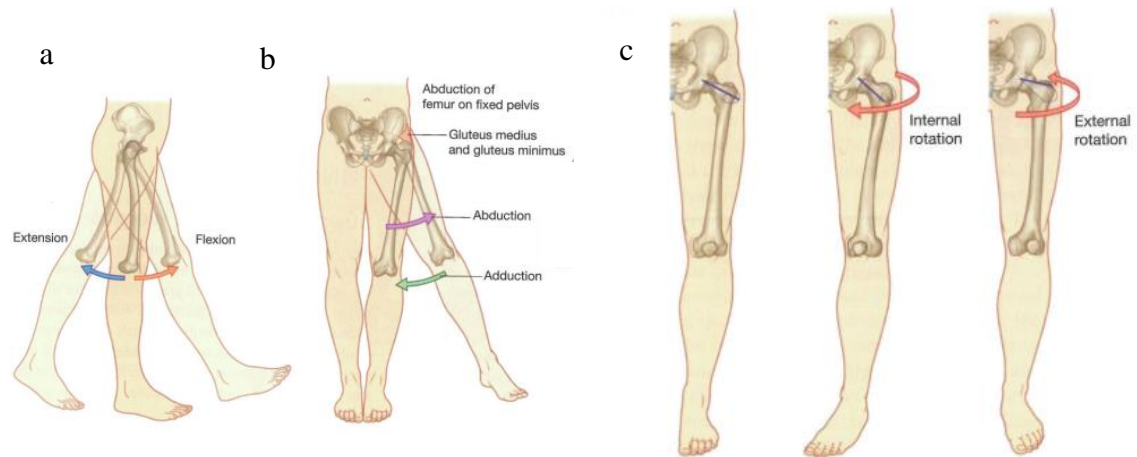


Figure 7: Movements of the hip joint; a) flexion and extension b) abduction and adduction c) external and internal rotation (Drake, et al., 2010)

The hip joint covers the motion of convex head of femur in the acetabulum's concavity (Levangie & Norkin, 2001). Figure 7 shows the hip movement. Figure 7a indicates the flexion and extension of the hip. Figure 7b shows the adduction and abduction of the hip. Figure 7c shows the internal and external rotation of the hip.

The femur's movements explain the availability of motions at the joints of hip (Levangie & Norkin, 2001). The hip flexion is about 90° and 120° by extension and flexion of knee respectively (Levangie & Norkin, 2001). The adduction of femur can be 30° and abduction can be 50° maximum (Levangie & Norkin, 2001). The hip's lateral and medial rotation can be measures with flexion of about 90° in hip joints. The normal way of walking necessitates abduction and adduction and medial and lateral rotation of 5° , flexion of 90° and hyper- extension of 10° (Levangie & Norkin, 2001). However, for an abnormal way of walking, these figures may vary slightly. But, overall, the correct way of walking in practice should be somewhere around these figures only (Levangie & Norkin, 2001).

2.4 Femoroacetabular Impingement (FAI)

A Femoroacetabular impingement condition is defined as an abnormal contact between acetabulum and head of femur (Ganz, et al., 2003). It is not found as a disease but it is a pathomechanical way through which hip can stop working (Leunig, et al., 2009). The abnormalities of acetabulum or femur with accurate or inaccurate motions can give rise to some repetitive impacts which may harm cartilage or labrum of rim of acetabulum (Leunig, et al., 2009), (Kubiak-Langer, et al., 2007)

Ganz et.al, (Ganz, et al., 2008) studied the morphology of hip which is one of the important factors to develop FAI. FAI is found as an activation of OA of hip (Ganz, et al., 2008). If this problem is not treated properly, then young people who are FAI affected, can have OA problem in hip later in life stages. High hip activities and high ROM adults can speed up the starting of hip FAI and OA. Thus, the treatment of FAI can decrease the amount of populations affected by the problem of hip OA (Ganz, et al., 2008).

2.4.1 Type of Impingement

Mainly two types of impingement is defined and each of this is featured with shape of deformity in the structure of the hip. These types are differentiated on the basis of impingement mechanism and origin, are termed as cam and pincer (Tannast, et al., 2007). The head of femur causes cam impingement which is blocked within the acetabulum (Iko, et al., 2001). The acetabulum abnormalities cause pincer impingement (Tannast, et al., 2007).

2.4.1.1 Cam Impingement

FAI divides into two types of impingement: cam and pincer. Each impingement is defined by the damaging of joints of hip or abnormalities in structure of the hip joint. Cam impingement is generated by the abnormality in structure of head of femur. So, the head of femur is blocked into acetabulum cavity and damages labrum. Figure 8 shows the radiography picture of cam impingement.

Cam impingement is more critical than the pincer impingement (Ganz, et al., 2008). In case of cam impingement, the damaging of cartilage of acetabulum cavity

takes place at faster rate and it spreads wider than pincer impingement. The symptoms of cam impingement are not properly defined. Moreover, the damaging patterns of rim of acetabulum in cam impingement are different from pincer impingement (Ganz, et al., 2008).



Figure 8: Radiography picture of cam impingement. White arrow shows the place of bump in impingement (Filigenzi & Bredella, 2008)

In Figure 8, white arrows are representing the bumps in head of the femur (Ganz, et al., 2008). As a result, cam impingement deteriorates the joints of hip (Ganz, et al., 2003). It is started by damaging of cartilage of acetabulum, detachment and degeneration of labrum and chondral avulsion (Tanzer & Noiseux , 2004) which cause pain in the patients. As a result, the labrum is detached and degenerated from the cartilage of acetabulum. The labrum degeneration terms as the secondary options to the detachment from acetabulum's cartilage (Ganz, et al., 2003). This type of FAI is most common amongst young males (20 - 30 years) with high sport activities in a routine way (Kubiak-Langer, et al., 2007).

Because of the jamming of head of femur into cavity of acetabulum at the time of motion, the cartilage of acetabulum is separated from the acetabulum as well as subchondral bone. This is caused by the shear force generated as the femoral head jams into the acetabulum (Ganz, et al., 2003). The labrum is not involved at the time of cam impingement for a long period (Ganz, et al., 2008). The fact is that cartilage avulsion from labrum and then subchondral bone takes place (Ganz, et al., 2008). In reality, cartilage cleavage can become as deep as 2mm and is destroyed with time. The head of femur goes into the defective part while larger area can be seen as combined narrowing of space within MRI (Ganz, et al., 2008). After that only spherical part of the

acetabulum's cartilage of femoral head is involved. The non- spherical cartilage of femoral head represent the damaging of surface in the impingement process (Ganz, et al., 2008).

2.4.1.2 Pincer Impingement

Pincer impingement is generated by abnormality in structure of acetabulum. The femoral head's morphology can be normal. As shown in Figure 9, the cavity of acetabulum may over cover the head of femur. Thus rim of acetabulum impacts directly and linearly on neck and head junctions within the over covering of acetabulum (Ganz, et al., 2008). The effects of pincer FAI is equal to the effects generated by cam FAI. The differences in effects of both of these impingements lie in the failure methods and the damaging patterns (Ganz, et al., 2008).



Figure 9: Radiographic picture of pincer impingement. White arrow shows the place of bump in impingement (Filigenzi & Bredella, 2008)

In Figure 9, white arrow represents bump's on pelvis within pincer impingement (Ganz, et al., 2008). The spherical femoral head's cartilage is kept normal for long period (Ganz, et al., 2003). The effects caused by pincer impingement are slower than cam impingement.

The cartilage of acetabulum is harmed in case of pincer impingement. Such damage is limited to a narrow piece just near to the labrum (Ganz, et al., 2008). Afterwards, the chronic leverage damages the posterior- inferior cartilage. The labral damaging is not linked with chondral damages in case of pincer impingement (Ganz, et al., 2003). Failure takes place towards the central and posterior- inferior osteoarthritis

(Ganz, et al., 2008). This type of impingement affects people with normal hip by imposing physiological demand on hip (Ganz, et al., 2008). This affects middle aged athletic women directly who perform activities with higher demands over their movements (Ganz, et al., 2008), (Griffin, 2007).

Labrum is damaged initially in case of pincer impingement (Ganz, et al., 2008). Then apposition of bone takes place at the rim of osseous just after the labrum and it pushes the labrum in forward direction. In fact, the cartilage of acetabulum is degenerated which is nearby the labrum (Ganz, et al., 2008). In the later stages of this impingement, the abrasion of cartilage may take place in the posterior inferior joints of head and neck of the acetabulum, are commonly termed as contrecoup lesion.

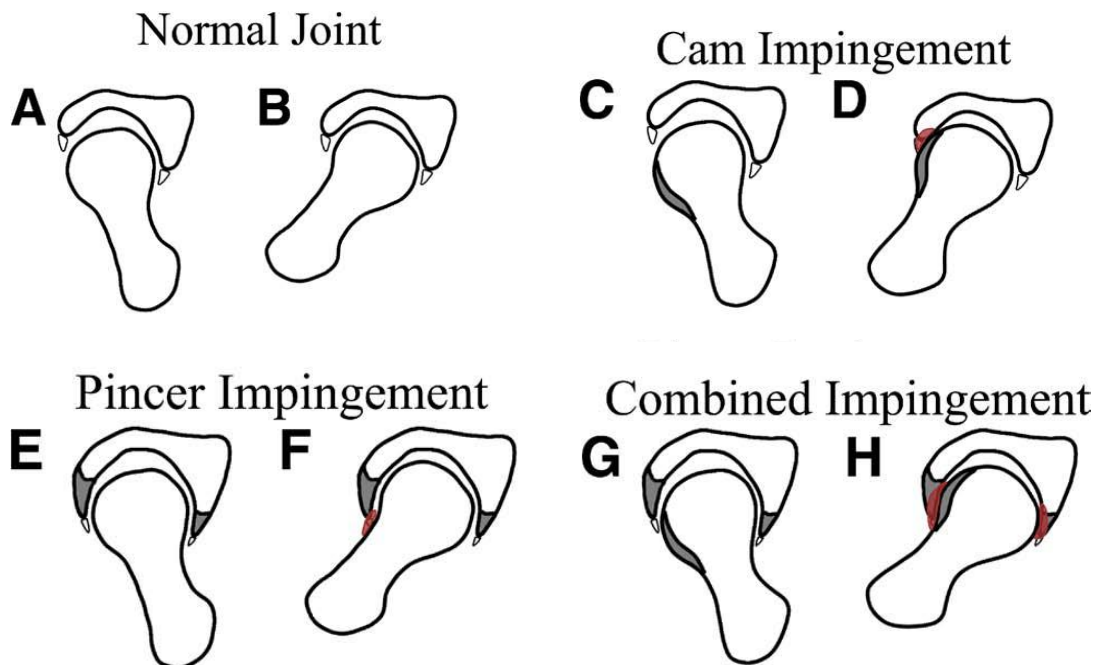


Figure 10: Schematic pictures of all of the impingement types (Marti & Tashman, 2010)

2.4.1.3 Combined Cam and Pincer Impingement

The combined pincer and cam impingement is diagnosed in so many patients (Ganz, et al., 2008) and Figure 10 shows different type of impingement in summary. The effects caused by both types of impingements are critical for labrum. The damages generated by pincer and cam impingement are found in the joints of hip. Chondral damages give rise to labral tears (Ganz, et al., 2008). At initial stages of process of cam and pincer impingement, the chondral damages are found without the

presence of labral tears (Ganz, et al., 2008). These damages are produced mainly on the hip joint's acetabulum (Ganz, et al., 2003), (Ganz, et al., 2008). These findings are studied through medical imaging techniques and arthroscopy within patients. The observed information provide proper assessment and interpretations of predictions which locates the position of impingements in joints of hip (Ganz, et al., 2008).

2.4.2 Role of FAI to Induce OA

Most researchers claimed that damages of joint in FAIs starts at impingement regions (Siebenrock , et al., 2003), (Beck , et al., 2005) . Two theories explain on deformities starting and osteoarthritis from FAI (Ganz, et al., 2008).

First theory is known as non-dysplasia theory. During the motions of hip, the defects on hip create a contact between acetabulum rim and proximal femur (Ganz, et al., 2003). Thus the lesions can occur in the cartilage of acetabulum or labrum of acetabulum. It has been shown in both active adults and young people both (Ganz, et al., 2003). The avoidance of the causes of both impingements can become more crucial. The lesions on chondral and labral side can continue for along period in adults and thus leads to joint's degeneration (Ganz, et al., 2003).

The dysplastic mechanism explained as the second method and this is an accepted theory (Ganz, et al., 2003). Such mechanism states the mechanical views of deformities of hip (Ganz, et al., 2003). The degeneration of cartilages is initiated by eccentric or concentric overloads (Ganz, et al., 2003), (Leunig, et al., 2005). The early stages of osteoarthritis of hips are generated by the mal-oriented articular surfaces (Ganz, et al., 2003). Such type of deformities decreases the contact region amongst acetabulum's rim and proximal femur. Therefore, anterior and superior parts of hips are overloaded in eccentric way, and osteoarthritis appears (Ganz, et al., 2003).

Some researchers like Ganz (Ganz, et al., 2003) and Leunig (Leunig, et al., 2005), addressed the weakness of this theory. The commonly accepted theory suggests that OA on hip is generated because of a reduced contact area within the dysplastic hip and then it generates overload on anterior superior areas eccentrically (Leunig, et al., 2005). The theory does not include the point that how the pressures develop the OA in young patient groups with normal hip (Ganz, et al., 2003). This theory does not cover the causes of hip osteoarthritis (Leunig, et al., 2005). Therefore, the osteoarthritis within

young people is recommended to be investigated with an alternative method (Leunig, et al., 2005).

Murray suggested the subtle types of deformity in femur that lead to the successive growth of osteoarthritis (Murray, 1965). After few decades, this recommendation was completed with the help of other researchers and then controversial mechanism was given on the study of OA (Ganz, et al., 2008), (Solomon , et al., 1982) .

Before this, the idiopathic and primary reasons were mainly responsible for the development of OA. The primary reasons consist the inflammation and the abnormalities within the cartilage (Ganz, et al., 2008). This point was strongly supported by Leunig who suggested that abnormal morphology of hip give rise to OA (Leunig, et al., 2005). Idiopathic reasons refer to the reason which takes place from ambiguous reasons suddenly. The alternative mechanisms include the minor deformities as the causes of hip OA (Ganz, et al., 2008). Such types of deformities become the reasons of triggering FAI and arthritis (Ganz, et al., 2008).

Leunig with other researchers argued on FAI that it is a mechanism which develops early OA within dysplastic hip (Leunig, et al., 2005). This point does not match with the arguments given by Ganz et.al, who suggested that impingements lead to osteoarthritis in normally deformed hip. As for the views of Leunig (Leunig, et al., 2004), the osteoarthritis takes place by the non- dysplastic hips. It clearly argues that hips without deformities can also be more susceptible to develop osteoarthritis. It also recommends that OA does not occur by hips' deformities (Ganz, et al., 2008).

Conversely, Tanzer & Noiseux (Tanzer & Noiseux , 2004) recommended that presence of impingements in people without any hip disease can also be caused by some variations within anatomy of proximal femur (Tanzer & Noiseux , 2004). The subtle variations are the results of variations within normal hip anatomy, subclinical problems and growing abnormalities (Tanzer & Noiseux , 2004). But more data is required for giving support to the made hypotheses.

2.4.3 Effects of FAI

FAI generates damages in the joints of the hip. As a result, patient feels discomfort and pain. FAI speeds up damages in the labrum (Tanzer & Noiseux , 2004) and delamination of cartilage of acetabulum (Griffin, 2007). Also it degenerates cartilage of acetabulum at anterior and superior rim of acetabulum. Moreover, the degeneration is spread all over hip and head of femur (Griffin, 2007). The effects caused by FAI in patients are groin pain, hip pain and then it spreads to the thighs. The pain may take place slowly or unexpectedly (Griffin, 2007).

2.4.4 Who Has Impingement?

Almost 35% of Olympic athletes and professional sport players have gone through hip surgery between September 2000 and April 2005, and have necessitated decompression of FAI (Philippon & Schenker, 2006). FAI generally takes place in young people with slower beginning of growing pain which is generally initiated just after traumatic attack. At initial stages, the groin pain is not regular and it may be intensified through excessive hip activities like athletics, long intensive walking, etc. (Ganz, et al., 2003).

Griffin has outlined the FAI as a condition which mainly has an impact on young adults (Griffin, 2007). The observance of FAI in young adults has also been supported by (Ganz, et al., 2003), (Ganz, et al., 2008) . The adduction in young adults with higher activities include squatting activities like surfing, kayaking, riding of car, power- lifting, cycling, dancing, aerobatics, tennis, soccer, yoga, ice hockey, bike riding, martial arts, golf, rugby, lacrosse, field hockey, horseback riding, mixed form of martial arts, etc. (Griffin, 2007).

2.4.5 Treatment of FAI

The major treatment of FAI is to go through the surgical methods (see Figure 11). The identification of proper timing for surgical methods to treat problems of FAI is still in the progress, even though the anti- inflammatory therapies or physiotherapy remains at first for treating muscular and skeletal damages and its advantages within the case of impingements are still problematic (Leunig, et al., 2009). The delays within

surgical procedure in symptomatic patients with abnormalities in bone can lead to the progressions of diseases in joints where the preservations of joints are not indicated for long period (Leunig, et al., 2009). With proper study of morphologies of FAIs, some approaches like arthroscopy have taken place (Leunig, et al., 2009), (Philippon , et al., 2007).

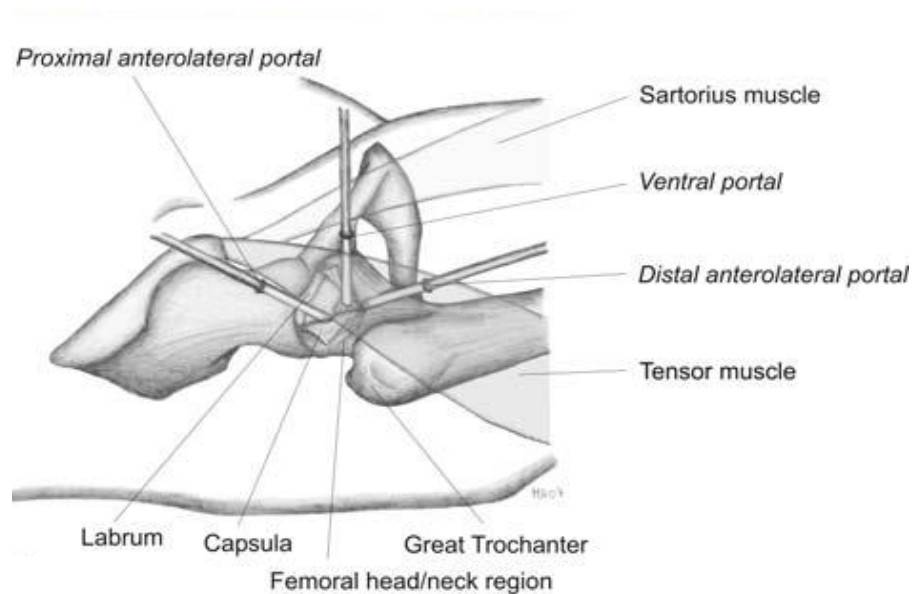


Figure 11: Schematic view of hip arthroscopy to treat hip impingement (Horisberger , et al., 2010)

In today's scenario, the complex types of abnormalities with pincer impingement, major hip deformities and some articular impingements can be treated by using some open methods (Leunig, et al., 2009). Number of options are available for curing impingements such as: removal of bump by using surgical instruments, non-surgical treatment, preservation of hip through using surgical instruments rather than replacing hips with artificial hips (Siebenrock , et al., 2003), (Lavigne , et al., 2004), (Rodrigo , et al., 2005). The surgical resections of anterior and lateral views of femoral head and femoral neck junction enhance the ratio of both head and neck; also it improves the motion before the appearance of impingement (Rodrigo , et al., 2005), (Beck, et al., 2004). However, the fracture of neck of femur is the biggest risk for this procedure where the surgical resection is subjected before settlement of integrity (Rodrigo , et al., 2005).

Two main surgical treatment of FAI are; resectional osteoplasty and arthroscopy.

2.4.5.1 Resectional Osteoplasty

This method excludes extra part of acetabulum's anterior rim as well as extra bony structure of junctions of femoral head and neck (Leunig, et al., 2005). For the head of femur, the goal of using this method is the recreation of normal curve lines of neck of femur (Leunig, et al., 2005). It is completed with the help of excluding the major part of non- spherical area of the head of femur.

2.4.5.2 Arthroscopy of hips

This method is also termed as key-hole surgical method which facilitates the debridement or reattachment of labral tears (Leunig, et al., 2005). This type of surgery is done with using incisions of size about 1cm (Tanzer & Noiseux , 2004). This method is less invasive than other methods. In the hip arthroscopy, dislocation of hip joint (dislocation of hips is an open surgery which is done to detect the impingement zone and damaged area of hip joint) is not needed which is traumatic for the patients and along with it also enhances the infections just after going through surgery (Leunig, et al., 2004).

(Further information is provided in Appendix A for the surgical procedure of FAI.)

2.5 Conclusion

This Chapter covered the current state of FAI which is a mechanical mismatch of hip joint and causes abnormal contact, pain and reduction in ROM in patients. Unrecognized and untreated FAI leads to OA and damages the soft tissue such as cartilage and labrum. Therefore, there is a need to develop a precise diagnostic tool to detect FAI at early stage in life. This also can be seen as a promising method to improve ROM in young and active people.

Chapter 3

Literature Review

3.1 Introduction

Hip modelling can be used to study the biomechanics of the hip in diagnosis and treatment of all hip diseases and disorder. In this chapter, previous studies on hip modelling and hip impingement are discussed. Experimental, numerical, finite element analysis and discrete element analysis hip modelling are clarified according to the previous meanings given in various articles. The importance of diagnosis, treatment and detection of hip impingement are discussed.

3.2 Hip Modelling

Hip modelling is used to study the biomechanics of the hip in order to predict the development of hip diseases. The hip joint is one of the most important joint and consequently many researchers have tried to understand its mechanics. In this section studies of hip joints are divided into three kinds according to the modelling employed: experimental, analytical and computational.

3.2.1 Experimental Hip Modelling

In the experimental modelling of the hip, the hip joints of cadavers are used in order to study the biomechanics of hip in a lab environment. Also data obtained from a gait lab are used to measure the load during daily activity.

In-Vitro study

Previous *in vitro* investigation on cadaver samples measured stress and strain on hip cartilage (Oh & Harris, 1978), (Dalstra, et al., 1995), (Ries, et al., 1989), (Finlay, et al., 1986).

Adams and his colleague (Adams & Swanson, 1985) developed a piezoelectric pressure transducer to measure the stress profile on the femur of several cadavers. Later on Ries et al. (Ries, et al., 1989) studied the effect of femur size on the acetabular strain. Their results showed that the normal size of the femur has the same strain distribution on the acetabular as the previous articles showed (Brown & Shaw, 1983). Their results also showed that changing the size of the femur changes the strain distribution in the acetabular. They observed that a 1mm oversized femur increased the strain on the acetabular (Brown & Shaw, 1983). Adams et al. (Adams, et al., 1999) tested stress distribution on the cadaver's articular hip cartilage by applying creep loading. Their results led to the claim that peak stress occurred at 12 o'clock and 3 o'clock of the acetabulum (Adams, et al., 1999). Kim et al. (Kim, et al., 2001) studied femoral cadavers. They measured the strain at the top of hip implants. They found that fitting the implant to the anatomical size of the hip reduced stress shielding and reduced the bending stiffness of the implant (Kim, et al., 2001)

Various researchers studied the peak value of stress on the femur with the use of piezoelectric sensors or films which are pressure sensitive (Rushfeldt, et al., 1979), (Rushfeldt, et al., 1981), (Macirowski, et al., 1994).

In-Vivo studies

The measurement methods of strain and stress on femur bone and pelvic bone are not available. Various attempts have been made to measure reaction and contact pressures on hip joints with the help of proper hip replacement instruments. The contact pressure can be measured with the help of instrumented prostheses by replacing

them in the patients (Bergmann, et al., 1997 Feb), (Bergmann, et al., 2001). *In vivo* studies usually measure the load acting on the hip joint using gait data.

Bergmann et al. (Bergmann, et al., 1997 Feb) studied the Motion Capture of several volunteers while they were walking and carrying load. The result showed that carrying a load on one side put heavy load on the other side of the hip. They also found that carrying load on both side reduces the load applied on both sides (Bergmann, et al., 1997 Feb). Their result showed that if a bag carried upward by adducting the arm reduces the load on the hip (Bergmann, et al., 1997 Feb).

In another study Bergmann et al. (Bergmann, et al., 2001) studied considered the load when climbing the stairs and walking. Their results showed that going upstairs put a greater load on the hip than normal walking (Bergmann, et al., 2001). Moreover, joint contact force was lower when going upstairs than when coming downstairs (Bergmann, et al., 2001).

In another study, a gait lab was used to measure the pressure during walking on cartilage of different thickness (Mann, 2002). The thickness of the cartilage was measured by using ultrasound (Mann, 2002). The results showed that pressure decreased when the thickness of the cartilage decreased (Mann, 2002).

3.2.2 Analytical Modelling

The analytical modelling for predicting the biomechanics of hip joints involves the use of static mechanisms or equations to find the reaction forces on the hip joints. Several points have been given for using analytical studies to explain these with the help of simple static equations; thus clearly demonstrating that it is not essential to discrete geometry or there is no requirement to use material properties. Michaeli et al. (Michaeli, et al., 1997) were among the first researchers to develop an analytical model of the hip to predict OA places at an early stage. Their analytical method was developed to predict maximum pressure and location of pressure in OA patients (Michaeli, et al., 1997). Later on they developed mathematical model of the hip to assess the peak stress on the hip (Mavcic, et al., 2002). The result showed that the size of the femur, its shape and width of the pelvis are the main parameters which can cause higher weight bearing, damaging the hip and increasing risk of OA (Mavcic, et al., 2002).

3.2.3 Computational Modelling

Computational modelling is a subsection of numerical modelling which necessitates the discretization of an object's geometry into easy numerical problems. Now that computational modelling has been developed, constitutive equations should be presented in a specific format. This is considered a helpful method for those studying biomechanics of the hip joints. Computational modelling is capable of predicting stresses and strains on bones as well as cartilage over all objects (Anderson, et al., 2010). After finding suitable imaging methods, the models of patients can be improved by isolating data which describe mechanical and geometrical properties involved. Thus, there is no need to simplify the geometry of the hip joint such as the articulation of the cartilage or the spherical geometry, etc. Computational models can be enhanced without involving any puncturing (except radiation exposure during CT) by using live subjects, allowing every patient to be evaluated (Anderson, et al., 2010).

Anderson et al. studied the effect of hip morphology on cartilage stress which causes OA (Anderson, et al., 2010). A complete sphere femur showed 50% lower peak pressure than a non-sphere did (Anderson, et al., 2010). They also studied the effect of different materials (deformable and rigid) on the hip. The model with rigid material was found to have been under higher pressure than the model with deformable material. They concluded that material properties and hip geometry play an important role in hip modelling.

3.2.3.1 Constitutive Models for Bone and Cartilage

Constitutive modelling is essential for providing insight into the involvement of various tissues in the behaviour of all tissues and showing the tissue properties in computational modelling. Bones can be taken as elastic objects (Van Rietbergen, et al., 1996). The cartilage can be used as various material forms, such as pro-elastic material (Afoke, et al., 1987), poro-viscoelastic material (Suh & Bai, 1998), isotropic-biphasic material (Mow, et al., 1980), (Mak & Mow, 1987), transverse isotropic-biphasic material and isotropic biphasic material (Hayes, et al., 1972).

The reactions are similar to non-compressible material at the times when the cartilage is forced upon (Mow, et al., 1980), (Mak & Mow, 1987), (Soltz & Ateshian, 2000). Linear-elastic models can sometimes be applied in some cases. In some

examples, using a linear elastic constitutive model could be applicable. The energy potential of strain leads to hyper-elasticity and then gives rise to a non-linear relationship between strains and stresses. The involvement of fluid and solid states in the behaviour of the cartilage is briefly described, using pro-elastic constitutive model. Those were enhanced for the purpose of defining soil mechanics (Truesdell & Toupin, 1960), (Terzaghi, 1943) and persistent for the cartilage by using biphasic concepts (Mow, et al., 1980).

3.2.3.2 Finite Element Modelling

Finite element modelling methods help researchers to find solutions for the dispersal of strains and stresses throughout the continuum subjected to loading and in such cases material properties are given. Arrangements of finite element modelling are made into three steps: pre-processing; provisions of loading and boundary conditions and post-processing. The first step in pre-processing is to discretize the geometry of object into some finite elements (Lee, et al., 2006), (Wang, et al., 2007). The provision of loading relates to stress, pressure, displacement, torque and also the way of loading (whether cyclic or constant load). Afterwards, boundary limitations are exercised for regulating the dislocation of separated parts. The discrete motion equations are functions of the energy which is determined for identifying the displacement field. Strains and stresses are obtainable from the displacement fields. The estimations for models are then post-processed in order to make data analysis and observation easier.

A 3D model of finite element analysis was developed by several researchers (Dalstra, et al., 1995), (Goel, et al., 1978), (Oonishi, et al., 1983) to predict hip bone stress.

Goel et al. (Goel, et al., 1978) developed a very basic computational model to measure the stress on hip bones by applying the muscle force on the acetabulum and femur (Goel, et al., 1978). This was one of the first attempts to study hip joint bones in FEA (Goel, et al., 1978). The authors' main finding was the peak stress of 0.57 Mpa on the pelvis (ilium region) (Goel, et al., 1978).

Oonishi et al. used a simple basic FEA program called 'ASKA' (Oonishi, et al., 1983). They used muscle force as a simple flange element (a flange element is one

dimensional stiffness in 3D space) (Oonishi, et al., 1983). The outcomes simply showed the von Mises stress on a pelvic surface (Oonishi, et al., 1983).

Dalstra et al. (Dalstra, et al., 1995) reported that Oonishi et al. had some unit errors in calculating muscle force using Newton but actually value was in Kg (Oonishi, et al., 1983). Dalstra et al. (Dalstra, et al., 1995) claimed that their model was more reliable than the previous one (Oonishi, et al., 1983). They also reported that the simplification of modelling affected FEA results (Dalstra, et al., 1995). They examined the stress- strain test on several pelvic cadavers and compared the results with their FEA model (Dalstra, et al., 1995). They claimed that the previous FEA model had overestimated the stress distribution in light of the experimental results (Dalstra, et al., 1995). They showed the simplification of the hip model did indeed significantly affect the FEA results (Dalstra, et al., 1995).

Ferguson et al. considered the effect of labrum and cartilage on contact pressure on the hip cartilage (Ferguson, et al., 2000). The results were presented in order to show contact pressure in terms of the position on the acetabulum. They used pro-elastic properties to define the cartilage and labrum. The model without labrum had significantly increased pressure and friction (92%) (Ferguson, et al., 2000). Moreover, in the model without labrum, the centre of contact was shifted towards the acetabulum rim (Ferguson, et al., 2000). The model without labrum had higher stress and strain on the cartilage which caused the fatigue of the cartilage layers. They also asserted that “labrum affected the lateral motion so that the joint with labrum preserved joint congruity” (Ferguson, et al., 2000).

Russell et al. used FEA to compare a dysplastic hip with a normal hip; their results indicated that the abnormal hip had greater stress on the hip bones than the normal hip (Russell, et al., 2006). They claimed that any abnormalities in the hip morphology caused higher stress on the articular cartilage (Russell, et al., 2006).

3.2.3.3 Discrete Element Analysis

Discrete element analysis (DEA) is a variant of the finite element method and has been used for evaluating the contact mechanism of hip joints (Genda, et al., 1995), (Genda, et al., 2001), (Yoshida, et al., 2006).

Genda et al. (Genda, et al., 1995) studied 112 normal hips and 66 hips diagnosed as dysplastic. They used the spring element as articular cartilage for the femur and acetabular to measure the maximum contact pressure (Genda, et al., 1995). They assumed 2mm of cartilage distributed around the femur and acetabulum. Their results showed that normal model with cartilage had higher contact pressure than the model without cartilage (Genda, et al., 1995). The results also showed that patients diagnosed with dysplastic hip had higher contact pressure.

Later on Genda et al. (Genda, et al., 2001) generated three-dimensional contact hip discrete element models of the hip by means of two dimensional radiographs, assuming that the head of the femur and acetabulum were spherical in shape (Genda, et al., 2001). They studied the effect of gender (men and women) and also the sphericity of the femur on the distribution of pressure on the femur and acetabulum (Genda, et al., 2001). They found that peak contact pressure greatly depended on gender and hip morphology (Genda, et al., 2001). The findings also showed that peak-contact pressure in DEA was less than the experimental data-revealed (Genda, et al., 2001). They claimed that the DEA model can be more effective for some limited cases, but practical proof has not yet been offered regarding the DEA models (Genda, et al., 2001).

Researchers such as Yoshida et al. (Yoshida, et al., 2006) enhanced the discrete element model for the purpose of studying the distribution of contact pressures in hip joints, using *in vivo* study data. They used compressed spring elements as cartilage in a DEA model to measure peak pressure during daily activity (Yoshida, et al., 2006). Their results indicated that peak pressure is higher when going up the stairs than when coming down (Yoshida, et al., 2006). They also showed that peak pressure in seating down is 2.8 times greater than in walking (Yoshida, et al., 2006). The acetabulum experiences peak pressure in one place when sitting down and in a different place when bending the knee and flexing the hip (Yoshida, et al., 2006). They also claimed that their results were different from the *in vivo* findings of previous researches (Bergmann, et al., 2001) , (Yoshida, et al., 2006).

3.3 Hip Impingement Analysis via Computer Modelling

The basic information about impingement type and treatment was explained in Chapter 2. In this section previous researches on impingement detection are described.

The main parameters used to detect FAI are also described according to the previous articles.

3.3.1 Detection of Impingement

Detecting of impingement in the early stages avoids OA as discussed in Chapter 2. However, detecting FAI is not an easy procedure and surgeons have misdiagnosed it with the other hip muscular diseases and it takes a long time to detect FAI. Clinical examination and radiography examinations are introduced by various articles in order to detect FAI correctly and accurately (Nussbaumer, et al., 2010), (Kuhlman & Domb, 2009).

3.3.1.1 Physical or Clinical Examinations

Dislocation technique of surgical hips was used for identifying FAI mechanism (Ganz, et al., 2008). In most of these cases, the patients complained on anterior groin pain which is then worsened by flexion on hip (Philippon & Schenker, 2006). Patients also complained for groin pain with long term sitting, problems in going inside and outside of the car. FAI has been considered as the main reason of hip pain, reduced ROM in athlete and reduced performance (Philippon & Schenker, 2006). The mean time from symptom of beginning of FAI to final diagnosis is 3 years (Clohisy, et al., 2009). Delayed diagnosis and inaccurate diagnosis are two main highlighted problems in FAI diagnosis (Clohisy, et al., 2009). Early and accurate diagnosis avoids OA and damaging soft tissue (Clohisy, et al., 2009).



Figure 12: Impingement test to locate hip pain area which is C sign pain around hip (Kuhlman & Domb, 2009)

Patients with FAI, usually have antero-lateral pain on hips. More often, the patients complain about pains in their antero-lateral hips as shown in Figure 12, by using fingers and thumb to have “c” shape pain area (Byrd, 2007). They have sharp pain while taking turn towards problematic side. It can get worse with long time sitting, leaning or going into and outside the car. Such pain appears slowly and progressively. The clinical examination of hip starts with proper assessment of the problem, palpation and motion range assessment. Such steps for hips are clearly specified in Table 2 which shows the detection stage of FAI and also different methods to detect FAI. The FADIR testing (flexion, adduction in 90° flexion and internal rotation in 90° flexion) has been taken as the most commonly used amongst different types of physical examination for FAI (Byrd, 2007), (Byrd & Jones , 2004). FADIR test also has been also used to examine FAI in clinical and computer aided programme (Kuhlman & Domb, 2009).

Several problems have been found with using physical testing, such as beginning of examination, rotation centre, limb’s longer axis, horizontal as well as vertical positions can be measured (Kuhlman & Domb, 2009). Furthermore, the traditional goniometers can be used with both hands without leaving hands free to stabilize the proximal part of femoral joints (Lea & Gerhardt, 1995). Some problems have also found to monitor the joints which are enclosed with soft tissues like hip (Lea

& Gerhardt, 1995). More additionally, goniometers are used for assessing flexibility of joints in 2 dimensions.

Table 2: Physical examination of hip impingement (Kuhlman & Domb, 2009)

<i>Inspection component</i>	<i>Findings and clarification</i>
Examination of hips	Asymmetry recommends SI joint dysfunction or leg-length discrepancy, either of which can cause SI joint pain, pubic symphysis pain, or muscle strain
Palpation of bone landmarks and muscles	Tenderness indicates that tissue is involved. Tenderness over the greater trochanter advises trochanteric bursitis, which can coincide with intra-articular hip disorder; mass advises tumor
Range of motion (flexion, extension, abduction, adduction, internal and external rotation) Passive (examiner moves the hip) Active (patient moves)	Consider for pain; localize pain Pain in a stretched muscle indicates strain; pain in groin suggests intra-articular hip disorder; pain with slight motion is concerning for septic arthritis Limitation of motion reflects severity of condition; pain helps to localize source of pain
Resisted (examiner resists motion to test muscle strength)	Weakness or pain in muscle suggests strain
Patrick (FABER) test	Groin pain indicates an iliopsoas strain or an intra-articular hip disorder; SI pain indicates SI joint disorder; posterior hip pain suggests posterior hip impingement
FADIR test	Reproducing the patient's anterolateral hip pain is dependable with FAI
Log roll (examiner rolls the supine leg back and forth) Patient hops on the involved leg	Groin pain recommends an intra-articular disorder; posterior pain suggests posterior muscle strain Pain can follow with strain, FAI, or other intra-articular disorder, but is concerning for hip stress fracture
Check-up of lower back, abdomen, and pelvis	Certain conditions can raise pain to the hip; check for fever or tachycardia, which suggest septic arthritis

FABER = flexion, abduction, and external rotation; FADIR = flexion, adduction, and internal rotation; FAI = femoroacetabular impingement; SI = sacroiliac.

After a patient diagnosed with all FAI symptoms mentioned earlier and also confirmed by physical and clinical examination, the patient is asked to do MRI and CT (Toomayan , et al., 2006). CT and MRI of the patient in position of 90° flexion and 20°

abductions in Dunn view¹ (Meyer , et al., 2006) are taken. If all the evidence confirms that the patient is diagnosed with FAI then patient will be send to remove the FAI by surgery (Martin , et al., 2008). Clohisy et al. claimed that FAI patients misdiagnosed with other hip diseases and delay in diagnose of FAI end up with developing OA, they accurate detection of FAI in clinical examination is important (Clohisy, et al., 2009).

3.3.1.1.1 FABER TEST

As it is shown in Table 2, FABER test is one of the experimental tests which is used to diagnose impingement. This test measures maximum flexion, maximum **abduction** in 90°flexion and maximum **external rotation** in 90°flexion. The patient's leg flexed as much as possible and the angles is reported as a flexion angle as shown in Figure 13a. The hip is flexed 90° and then abducted as much as possible as shown in Figure 13b. The hip is flexed 90° and then abducted as much as possible as shown in Figure 13d.

¹ Anteroposterior view of the hip with the patient supine and with the hips and knees flexed at 90°, the legs abducted 15°-20° from the midline

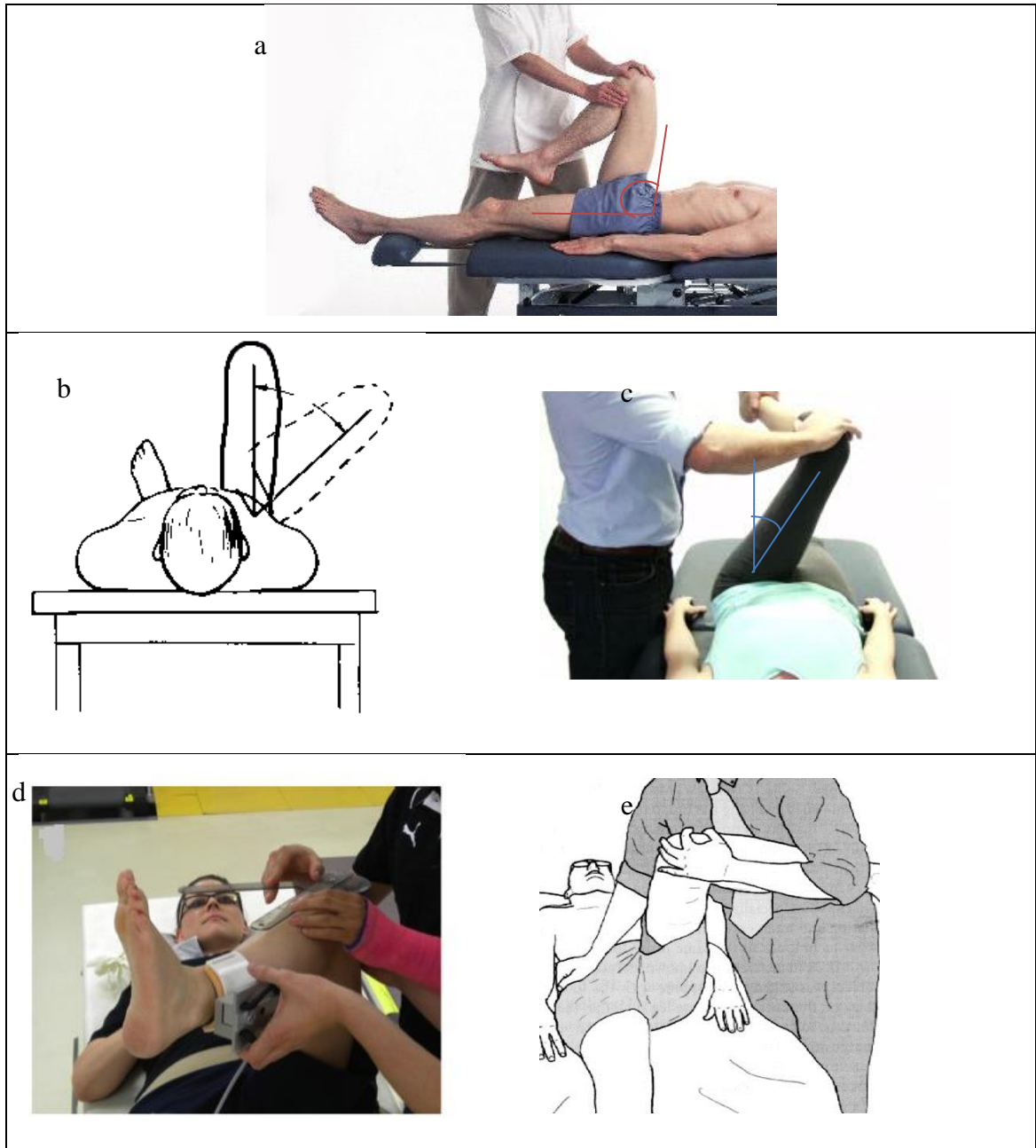


Figure 13: Angles measurement in FABER and FADIR test as two experimental tests to detect impingement a) maximum flexion, b) maximum abduction in 90°flexion, c) maximum adduction in 90°flexion, d) maximum external rotation in 90°flexion, e) maximum internal rotation (Nussbaumer, et al., 2010)

3.3.1.1.2 FADIR TEST

As shown in Table 2, FADIR test is one of the experimental tests used to diagnose impingement. This test measures maximum **flexion**, maximum **adduction** in 90°flexion and maximum **internal rotation** in 90°flexion. The FADIR testing has been taken as the most commonly used among different types of physical examination for FAI (Byrd, 2007), (Byrd & Jones , 2004). FADIR test has been used to examine FAI in

clinical and computer aided programme. A patient femur is flexed as much as possible as shown in Figure 13a. The patient femur is adducted in 90° of flexion as much as possible as shown in Figure 13c. The patient femur is internally rotated in 90° of flexion as much as possible as shown in Figure 13e (Byrd, 2007), (Kuhlman & Domb, 2009).

The hip with FAI symptoms has average of 97° flexion and 9° internal rotations in 90° flexion (Clohisy, et al., 2009). These values are lower than the 110° - 120° for flexion and 30° - 40° for internal rotation in flexion reported in normal people (Clohisy, et al., 2009).

Philippon et al. (Philippon, et al., 2007) studied the population of patients with hip pain and examine them with FADIR test. They reported that 50% of the population after MRI and CT were diagnosed to have FAI. From that 50%, 99% of them had the positive FADIR test for FAI (Philippon, et al., 2007). Also Ito et al. (Ito, et al., 2004) claimed that 90% of patients, who have positive FADIR test, diagnosed with FAI. They claimed that FADIR test can be one of the reliable and accurate methods to use in order to detect FAI (Ito, et al., 2004).

3.3.1.2 Radiographic Parameters Examinations

The sound knowledge of FAI biomechanics can provide help to physicians in designing interventions which reduces the progression risk to osteoarthritis. But future research studies must focus on two points like etiological study of disorders and nature of motions of impinging joints which gives rise to degeneration of tissues. There are several parameters defined for recognising impingements:

CEA (centre edge angle): The CEA can be estimated on AP (anterior posterior) hip radiograph. It is an angle between the line sketched from the edge of acetabulum to the central part of head of femur as shown in Figure 14a and vertical lines, as shown in Figure 14b (Marti & Tashman, 2010), (Lever & O'Hara, 2008).

An increased depth of acetabulum has been found as the major reason for pincer type of impingement. Depth of acetabulum are largely linked with the over coverage area of acetabulum and it can be measured through extremity of lateral CEA or decreased level of adults acetabulum index. The lateral CEA of a female patient as

shown in Figure 14 has been measured by using anteroposterior X-rays. Wiberg (Wiberg , 1940) gave report that central edge angle within normal adults is about 40° and below this angle, the body shown symptoms of OA and over coverage of acetabulum (Marti & Tashman, 2010), (Wiberg , 1940). Figure 14b shows the radiography sample of CEA angle.

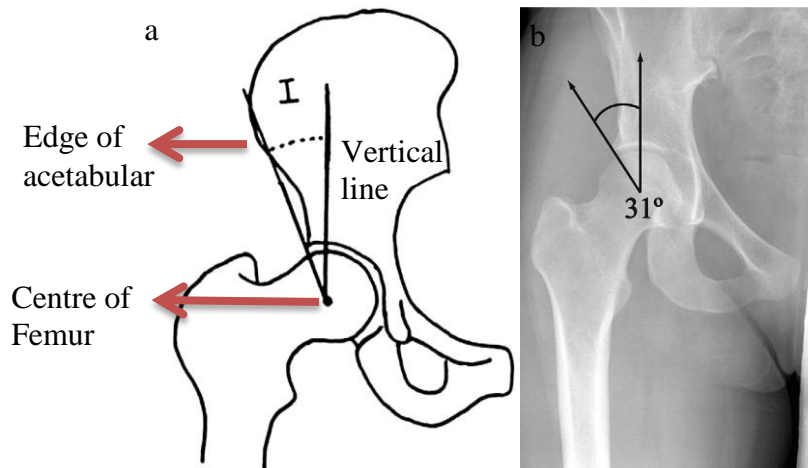


Figure 14: Measurement of Centre Edge Angle (Lever & O'Hara, 2008) b)AP radiograph of a 23-year-old female patient (anterior view of hip weight bearing) (Marti & Tashman, 2010)

Acetabular index: The acetabular index in adults has been termed as an angle between the horizontal line and tendency of sourcil which is the part of sclerosis within superior view of acetabulum, as shown in Figure 15 in the supine position (Lever & O'Hara, 2008).

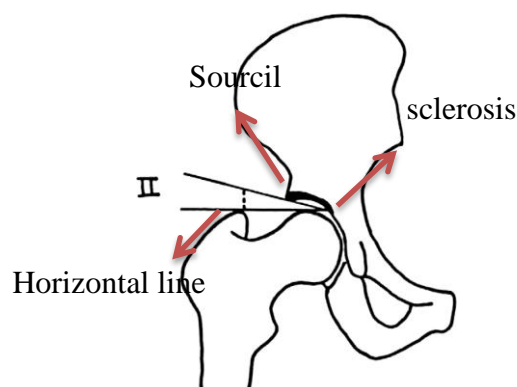


Figure 15: Measurement of adult Acetabular Index of supine position (anterior view of hip) (Lever & O'Hara, 2008)

The alpha angle: This angle presents any deformity of head-neck junction compared to the normal hip. This angle lies between the axis of neck of femur as shown in Figure 16 and line from the central part of femur head as shown in Figure 16. This can also be found from using axial MRI-cut (Marti & Tashman, 2010), (Lever & O'Hara, 2008).

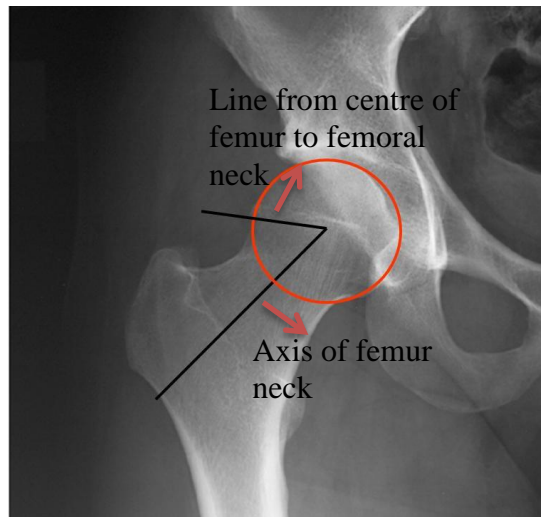


Figure 16: Measurement of alpha angle in supine position (Taunton , 2011)

In normal hip, the head of femur is sphere but in hip with impingement is not completely sphere (Marti & Tashman, 2010). One of the parameter to check whether femur is sphere is pistol grip deformity. Pistol grip deformity can be seen in MRI of hip in supine position as shown in Figure 17. However, alpha angle is used more common to check whether femur is sphere (Marti & Tashman, 2010).



Figure 17: X-ray of typical pistol grip deformity (anterior view of hip weight bearing) (Lever & O'Hara, 2008)

Femoral head-neck offset: In Figure 18a, line 1 has been drawn with the axis of neck of femur. Line 2 has been drawn just similar to line one but it lies alongside with the margin of head of femur. Line three has been drawn similar to both line 1 and 2 but it transects the asphericity point, especially for measuring alpha angle. The offset of line head shown as “OS” in Figure 18a and neck is found as a tangential space between line 2 & 3. The maximised alpha angle as well as decreased offset of head and neck within the case of cam impingement has been shown in Figure 18b (Hossain & Andrew, 2008).

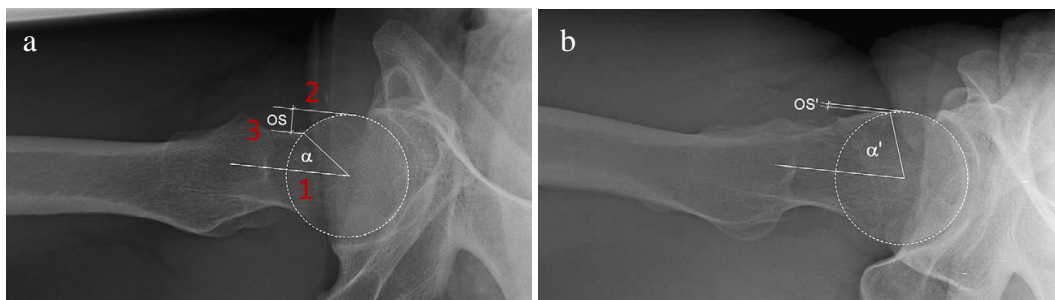


Figure 18: Alpha angle and normal head-neck offset in the lateral view a) normal hip b) Cam impingement (anterior view of hip weight bearing) (Hossain & Andrew, 2008)

Table 3 shows parameters radiography to detect hip impingement in summary. These parameters are measured within the case of impingement and normal hip (control group). Although one of these parameters (α angle, head neck offset, CEA angle, acetabular index) are enough to detect impingement (Ochoa, et al., 2010), some studies claimed that the patients' position at the time of radiography may create errors in measuring such numbers (Hossain & Andrew, 2008).

Ochoa et al. (Ochoa, et al., 2010) studied prevalence of patients who had positive sign of impingement. 87% of patients with hip pain had at least one of the impingement sign (α angle, head neck offset, CEA angle, acetabular index) (Ochoa, et al., 2010). Kapro et al. (Kapron, et al., 2011) also studied on 67 male football players who complained about hip pain. They reported that 72% of this population had an abnormal alpha angle, 64% had decreased head neck offset (Kapron, et al., 2011).

Table 3: Radiographic parameters which are used to indicate the impingement (Hossain & Andrew, 2008)

<i>Radiographic Parameters</i>	<i>Control group</i>	<i>Impingement group</i>
α angle	42°_47°	65°_74°
Head neck offset	11.6±0.7mm	7.2±0.7mm(<8mm for cam impingement)
Acetabular index	30°	Above 35°
CEA angle	40°	Less than normal group

3.3.2 Previous researche on FAI

The clinical research on this concept specify that FAI takes place when cam and pincer impingement give rise to an early contact, then it causes damages within substantial labrum and prearthrotic chondral in active young adults (Ganz, et al., 2003), (Eijer , et al., 2001), (Jäger , et al., 2004), (Murphy , et al., 2004), (Siebenrock , et al., 2003), (Strehl & Ganz , 2005).

There are numerous research papers for clinical reviews on types of impingement and some have addressed more on assessment and etiological part of FAI (Leunig, et al., 2009). The sound understanding of FAI biomechanics help physicians in designing interventions which minimises the progression risk to OA. FAI leads abnormal contact at anterior and superior part of acetabulum (Lamontagne, et al., 2009). This abnormal contact causes reduction in range of motion (Lamontagne, et al., 2009).

FAI has been found as the main reason of OA (Chegini, et al., 2009). The clinical observations have been generated for giving support to such hypothesis and various research studies have been generated for investigating the mechanism (Chegini, et al., 2009). The concepts related to distribution of stress within hip joints are not clearly understood (Bachtar, et al., 2006).

Many common daily activities, such as prolonged sitting, squatting, stair climbing, and athletic activities requiring a large ROM, produce hip pain in people with FAI (Kennedy , et al., 2009), (Adams, et al., 1999), (Lamontagne, et al., 2009). The mean time from the start of symptoms to final diagnosis is 3 years (Clohisy, et al., 2009). Early diagnosis is very challenging since many of FAI patients have insidious onset of symptoms which are the same as other muscle dysfunction diseases (Clohisy,

et al., 2009). Many of the FAI patients experience delay in diagnosis, incorrect diagnosis and ineffective treatment recommendation. Late diagnosis of FAI causes OA and damage to soft tissue (Clohisy, et al., 2009). As FAI happens in young active adults who need the full range of motion, there is a requirement to detect FAI early (Clohisy, et al., 2009). There is a major need to investigate reliable, valid and easy impingement detection framework. 74% of the FAI patients have reported significant reduction in flexion and internal rotation in flexion (Clohisy, et al., 2009). Early detection of FAI can help patients get back to their normal activity and avoid damaging the soft tissue.

Previous research on FAI in this section are divided into two types: experimental and computational research.

3.3.2.1 Experimental Research

The goniometer is the simplest and most commonly used clinical device for detecting impingement. The advantages of the goniometer are its simplicity for assessing ROM, direct measurement of joint angles without any data reduction process being required, and the low cost of the instrument. The two-arm goniometer is still the most commonly used, economical and portable device for the evaluation of ROM (Lea & Gerhardt, 1995).

However, major drawbacks of goniometry are that the starting position, the centre of rotation, the long axis of the limb and the true vertical and horizontal positions can only be visually estimated (Nussbaumer, et al., 2010); moreover, conventional goniometers must be held with two hands, leaving neither hand free for stabilization of the body or the proximal part of the joint (Nussbaumer, et al., 2010). There are also difficulties in monitoring joints that are surrounded by large amounts of soft tissue, such as the hip. In addition, manual goniometers assess joint flexibility only in two dimensions; however, as most of the hip ROM measured in clinical practice are practically in-plane movements, this limitation is minor (Nussbaumer, et al., 2010). There are also difficulties in monitoring joints that are surrounded by large amounts of soft tissue, such as the hip (Allard, et al., 1994). In addition, manual goniometers assess joint flexibility only in two dimensions. Also goniometer overestimate the majority of passive hip motion patterns by measuring intersegment angles (e.g., thigh flexion on

trunk for hip flexion) rather than true hip ROM; it is indeed difficult to reproduce true hip ROM by placing the goniometer properly and performing the anatomically correct ROM (Nussbaumer, et al., 2010). Several authors reported the restriction in measuring the internal rotation and flexion (Tannast, et al., 2007), (Jäger , et al., 2004), (Ganz, et al., 2003), (Nussbaumer, et al., 2010). Substantial errors in clinical measurements can occur if the examiner fails to recognize individual tilt or pelvic rotation (Kubiak-Langer, et al., 2007). Tilt and rotation are difficult to know or control during an examination and can vary considerably when the patient is in the supine position (Greene & Heckman, 1994), (Tannast , et al., 2005).

In light of these problems some studies started to use the electromagnetic tracking system (ETS) to measure ROM (Nussbaumer, et al., 2010) but some major findings of previous studies have reported that goniometric measurements of passive hip motion provided greater ROM value than the ETS (Nussbaumer, et al., 2010). The ETS device has several limitations. First, those relating to instrument errors, second, errors concerning the anatomical land mark and finally skin movement may cause some further errors. ETS can be used as the standard device for hip ROM assessment. Fluoroscopy and bone-pins would be more accurate, although potential errors are the same.

Previously Motion Capture lab was used during squatting and walking for patients with FAI (Kennedy , et al., 2009), (Lamontagne & Kennedy, 2009). The results indicate that the ROM decreases for cases with hip impingement when compared to normal hip cases (Kennedy , et al., 2009), (Lamontagne & Kennedy, 2009). However, there are some limitations inherent to joint kinematic studies resulting from: generic calculations, marker misplacements, and joint centre determination and skin or clothing artefacts (Leardini , et al., 2005), (Della Croce , et al., 2005) , (Reinschmidt , et al., 1997). Gait is not affected but the ROM of the hip may be restricted, particularly regarding flexion, internal rotation and adduction (Kennedy , et al., 2009). The speed of walking and ROM during normal walking is the same in both hip with FAI and hip without FAI (Kennedy , et al., 2009).

3.3.2.2 Computational Research

Various studies have reported ROM preoperatively and postoperatively using 3D model of hip (Tannast, et al., 2007), (Kubiak-Langer, et al., 2007), (Bedi, et al., 2011), (Bedi, et al., 2012), (Beaulé, et al., 2005). Results showed that range of motion can be improved by using computer simulation and arthroscopic osteoplasty (Tannast, et al., 2007), (Kubiak-Langer, et al., 2007), (Bedi, et al., 2011), (Bedi, et al., 2012). The measurement of only alpha angle is not alone enough for detecting the benefits of arthroscopy (Bedi, et al., 2011), (Bedi, et al., 2012). The identification of impingements and preoperative assessment can assist surgeons in making decisions to ascertain operative treatments (Kubiak-Langer, et al., 2007). Entire dislocation for observing patho-mechanism is not necessary, as the causes of impingement can be found preoperatively (Lavigne , et al., 2004). Some invasive approaches like arthroscopy can be used for carrying out surgical procedure of FAI, only if amount of bone to be removed is established preoperatively (Kubiak-Langer, et al., 2007).

Some research articles have shown bespoke software can be an effective tool in identifying impingement diseases preoperatively (Kubiak-Langer, et al., 2007), (Hu , et al., 2001), (Kang , et al., 2002).

The CT based models can assist surgeons to detect the impingement zone accurately and in less invasive method (Tannast , et al., 2005), (Brunner , et al., 2009), (Monahan & Shimada , 2008), (Pearle, et al., 2009), (Rivkin & Liebergall , 2009). The collision detection algorithms based on CT was able to calculate the range of motion, establish volume of resection and offered right information on pre and post-operative locations of FAI as well as impingement angle (Bedi, et al., 2011), (Bedi, et al., 2012). It has been found that surgical measures for treating FAI are more beneficial to patients and surgeons both. Hip joint's dislocation is surgically not essential for observing patho-mechanicsm of hip joint's diseases (Kubiak-Langer, et al., 2007).

The lesions on impingements and damaging in soft tissues reduce range of motion. CT based computer models can identify the regions of impingements within symptomatic-patients (Bedi, et al., 2011), (Bedi, et al., 2012). The osteoplasty surgery in impingement regions enhance range of motion and reduce the intermittent collisions and chondral injuries in FAI zone (Bedi, et al., 2011), (Bedi, et al., 2012). On the basis of some clinical research, it was reported that FAI limits adduction, internal-rotation and flexion (Jäger , et al., 2004), (Leunig, et al., 2004), (Siebenrock , et al., 2003).

Table 4 presents ROM which has been shown by some researchers with the use of computer based programmes.

Table 4: Range of motion for normal hip, hip with impingement and hip with impingement after reshaping (Kubiak-Langer, et al., 2007)

Parameter	Normal hip	FAI (preoperative)	FAI (after reshaping)
Flexion	122°±16.3°	105.2°±12.2°	125.4°±9.7°
Extension	56.5°±20.1°	61.1°±31.8°	71.1°±26.4°
Abduction	63.3°±10.9°	51.7°±12.2°	63.6°±7.5°
Adduction	32.7°±12.3°	34.6°±12.3°	35.8°±15.3°
Internal rotation in 90° flexion	35.2°±6.9°	11.1°±6.9°	35.8°±15.3°
External rotation in 90° flexion	102.5°±14.2°	83°±33.7°	93.9°±32.7°

The non-invasive type of assessment is necessary for recommendation of suitable treatments and detecting impingement (Tannast, et al., 2007). Reliable and correct simulation is quite important (Tannast, et al., 2007). The computer based analysis is matched with the clinical analysis data on range of motion in impingement (Eijer , et al., 2001), (Jäger , et al., 2004), (Leunig, et al., 2004), (Siebenrock , et al., 2003), (Strehl & Ganz , 2005), (Wettstein & Dienst , 2006).

FAI decreases internal rotation, adduction and abduction using an “analytical coordinate” system (Kubiak-Langer, et al., 2007). Such approach can be the basis for future methods in which the instruments can facilitate intraoperative implementation of osteoplasty. It can be mixed with some invasive methods like arthroscopy of hip, methods with smaller incisions needing no hip dislocation surgically (Kubiak-Langer, et al., 2007).

Tannast et al. (Tannast, et al., 2007) developed non-invasive 3D assessment of FAI called “Hip Motion” (Tannast, et al., 2007). This computer simulation detects impingement angle and impingement zone and also measures ROM of hip joint (Tannast, et al., 2007). They had two groups of 3D model; normal and impingement (Tannast, et al., 2007). They validated their computer simulation method with cadaver samples. The bespoke program overestimated ROM compared to the cadaver samples (Tannast, et al., 2007). One of the main limitations of his method “Hip Motion” program is not applicable for largely dysplastic hips with a shallow acetabulum where an unambiguous centre of rotation cannot be found (Tannast, et al., 2007). In addition, it cannot be used for hips with advanced osteoarthritis because joint space narrowing

leads to a change in the femoral head centre relative to the acetabulum, resulting in a nonconcentric joint morphology” (Tannast, et al., 2007).

Kiubic Langer et al. (Kubiak-Langer, et al., 2007) used “Hip Motion” program to measure ROM of normal, FAI after and before operation. They claimed that there is significant reduction of flexion, adduction and internal rotation in hip diagnosed with FAI (Kubiak-Langer, et al., 2007). Also their findings showed that there is 5°-8° improvement in internal rotation, 15°-20° improvement in flexion and 1°-4° improvement in adduction after operation. However impingement zone remained the same (Kubiak-Langer, et al., 2007). They claimed that information obtained by using “Hip Motion” program combined with arthroscopy can replace hip dislocation which is a major hip operation (Kubiak-Langer, et al., 2007).

Tannast et al. (Tannast, et al., 2008) used “Hip Motion” program to find impingement locations for several patients and compared the results with hip dislocation (Tannast, et al., 2008). Their results showed that the hip impingement zone is the same for FAI hips in both methods: computer simulation and hip dislocation surgery (Tannast, et al., 2008).

Chegini et al. (Chegini, et al., 2009) studied the effect of hip morphology on stress distribution on hip cartilage during daily activities in patients with hip impingement. They used CAD program to make 3D model of hip with different CE angle and then they analysed stress distribution in FEA (Chegini, et al., 2009). Their finding showed that higher CE angles cause higher contact peak pressure. However, the place of peak pressure remains the same for all CE angles (Chegini, et al., 2009). They also found that stress in hip cartilage are higher when walking than standing also stress level on hip cartilage are higher when seating than walking. The stress in seating is higher as needed to have higher rotation (Chegini, et al., 2009). They concluded that stress and peak pressure on hip cartilage depends on joint geometry, motion and load (Chegini, et al., 2009).

Asheesh bedi et al. (Bedi, et al., 2011), (Bedi, et al., 2012) developed computer-assisted 3D modelling of hip to measure ROM of hip. Their computer-assisted model did not have centre of rotation and that small load on head of the femur controls hip rotation. Their finding showed that ROM improved in FAI patients after surgery (Bedi, et al., 2011), (Bedi, et al., 2012).

It follows, therefore, there are many limitations which can be specified for previous studies;

a) Soft tissues were not used in the hip models studied computationally for impingement detection (Hu , et al., 2001), (Kang , et al., 2002), (Kubiak-Langer, et al., 2007), (Bedi, et al., 2011), (Bedi, et al., 2012). Soft tissue affects surgical interventions and even post-surgical muscular reconditioning. The impingement has been found as a bone to bone contact.

b) Effects of rotation centres are not validated by these previous researchers and they thought that rotation centres are fixed and these are at the centre part of femur (Kubiak-Langer, et al., 2007).

c) Previous researchers do not provide enough information on the measurement technique deployed and the accuracy of current methods are not considered (Kennedy , et al., 2009).

3.4 Conclusions

Previous studies have experimentally and numerically modelled hip. Most of them studied the stress and strain on hip joints. Researchers have also tried to understand the stress distribution in hip joint with disorders and diseases.

As discussed in Chapter 2, early detection and treating FAI can eliminate the risk of OA in people with hip impingement. To date there is no agreement among researchers on how the FAI is diagnosed. Currently hip modelling has been developed to be used to detect FAI by measuring ROM especially simulating FADIR test.

It is assumed that FAI is solely a bone to bone contact and also effect of soft tissue is ignored. There is a need to examine whether or not soft tissues and centre of rotation play important role on FAI detection. Also having reliable and valid impingement detection method is expected to help surgeons to treat impingement.

Chapter 4

Research Methods

4.1 Introduction

As discussed in the previous chapter, having reliable framework for detecting impingement avoids damage to joint soft tissues. Previous studies investigated to find reliable methods to measure impingement zone and angle.

In this research the objective is to develop a reliable framework for studying impingement. What is proposed in the framework is a collection of systematic procedures and methods to conduct the investigation of finding impingement location and impingement angles. The framework analyse impingement conditions and reliability of methods to detect them.

This is a short chapter which presents the structure of research to be conducted in order to achieve the objective of the thesis. The first part of the proposed investigation involves the use of FEA. The data for FEA came from Epsom hospital that provided CT and MRI data for two individuals, one with FAI condition and one without. The individual with FAI condition was operated and the excessive bone causing FAI was shaved. CT and MRI data was also provided after the operation. Thus three sets of data were obtained for FEA analysis. The FEA analysis follows the FADIR test; this was done in order to compare the results with clinical measurement. Comparing FEA investigation based on FADIR test is a major contribution which

involved the study of centre of rotation of the femur head as well as the study of the effect of soft tissues on the calculation of impingement position. The second part of the thesis investigates the effectiveness of various kinematic measurement devices used in FADIR test. The study of potential kinematic measurement devices is one of the main contributions of the work presented here.

4.1.1 Impingement Angle (FADIR Test)

Angle of impingement evaluation used in this thesis is based on FADIR test. FADIR test are included with 3 different angles: **F**lexion, **A**dduction in 90° flexion and **I**nternal **R**otation in 90° flexion. These three angles are measured and reported as impingement angle.

The flexion angle is the maximum flexion that hip can have. This angle is one of the impingement angles which is measured in this study as shown in Figure 19a.

The adduction angle in 90° flexion is the maximum angle of adduction while hip is in 90° flexion. To measure the adduction in 90° flexion, first hip flexed until 90° and then adducted until maximum angle. The maximum angle is the adduction angle. The adduction angle in 90° flexion is second impingement angle which is measured in this study as shown in Figure 19b.

The internal rotation angle in 90° flexion is the maximum angle of internal rotation while hip is in 90° flexion. To measure the internal rotation in 90° flexion, first hip flexed until 90° and then rotated internally until maximum angle. The maximum angle is the internal rotation angle. The internal rotation angle in 90° flexion as shown in Figure 19c is third impingement angle which is measured in this study.

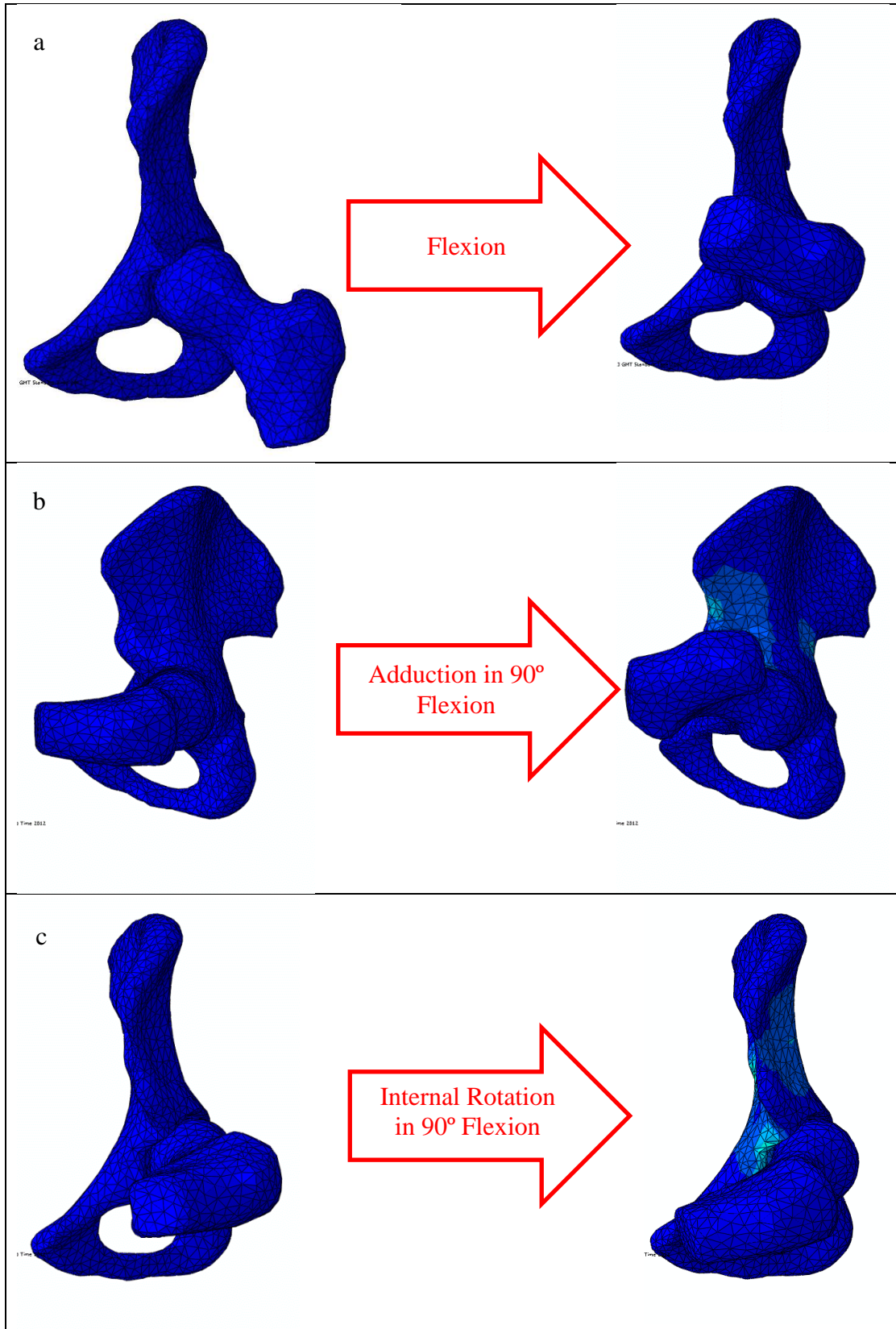


Figure 19: Impingement angle a) flexion, b) adduction in 90° flexion, c) internal rotation in 90° flexion

4.1.2 Impingement Zone (Clock Method)

The impingement zone which is used in this thesis is based on the clock method. This method is based on the place of impingement in acetabulum according to the clock as shown in Figure 20. The clock method is based on a clock fixed on acetabulum from 1 to 12 and the place of impingement is reported by the time shown in the clock. The place of impingement in acetabulum according to Ganz et al. (Ganz, et al., 2003) is the place of internal rotation in 90° flexion. This is when impingement pain in the hip is felt by the patient. The place of impingement on the acetabulum is also called impingement zone. As can be seen in Figure 20, anterior view of acetabulum shows time 3 and in the clock method and posterior view of acetabulum shows time 9 in the acetabulum. There is an arc named as “AB” in Figure 20 to indicate how the clock is set in the acetabulum. “A” shows the 11 o’clock and “B” shows the 2 o’clock.

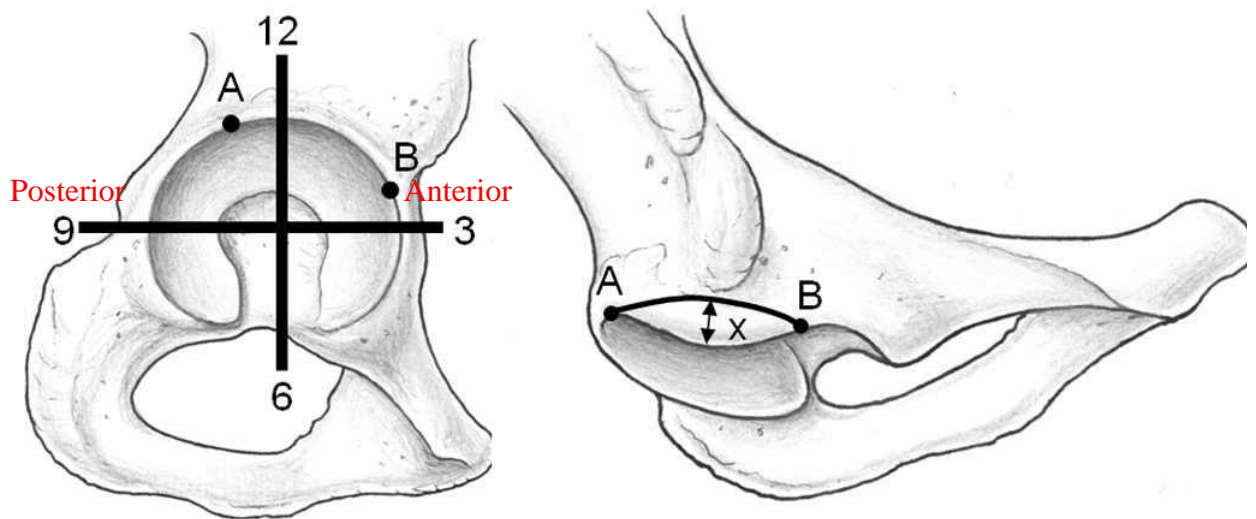


Figure 20: The clock method to measure the impingement zone (Kubiak-Langer, et al., 2007)

4.2 Finite Element Analysis (FEA)

In order to consider the effect of soft tissues and centre of rotation, FADIR test was applied to all models. Again in previous studies it was claimed that ROM improves after reshaping hip so the effect of soft tissues and centre of rotation on improvement of ROM after reshaping hip is also investigated in this section.

Two volunteers participated in our FEA investigation. The first individual was diagnosed with FAI. CT and MRI of the case with FAI were taken before and after reshaping hip. The second individual was known to have normal hip. CT and MRI of the case were also taken.

3D model of three hips were made: hip with FAI before reshaping, hip with FAI after reshaping and normal hip. All three hip models went under FADIR test in FEA and impingement zone and impingement angle was determined. Centre of rotation was changed to consider the effect of changing centre of rotation on impingement zone and impingement angle for all 3D models. Several boundary conditions were defined for all three hip models (normal hip, hip with FAI before and after reshaping). First condition, the centre of rotation was fixed as a centre of the femur head. Second condition, the centre of rotation was moved inward and outward the centre of the femur head. Third condition, a small force on head of the femur was applied instead of centre of rotation. Finally, the complete hip with soft tissues were modelled. Figure 21 shows the different cases in FEA. Figure 21 shows the procedures described above under the FEA section.

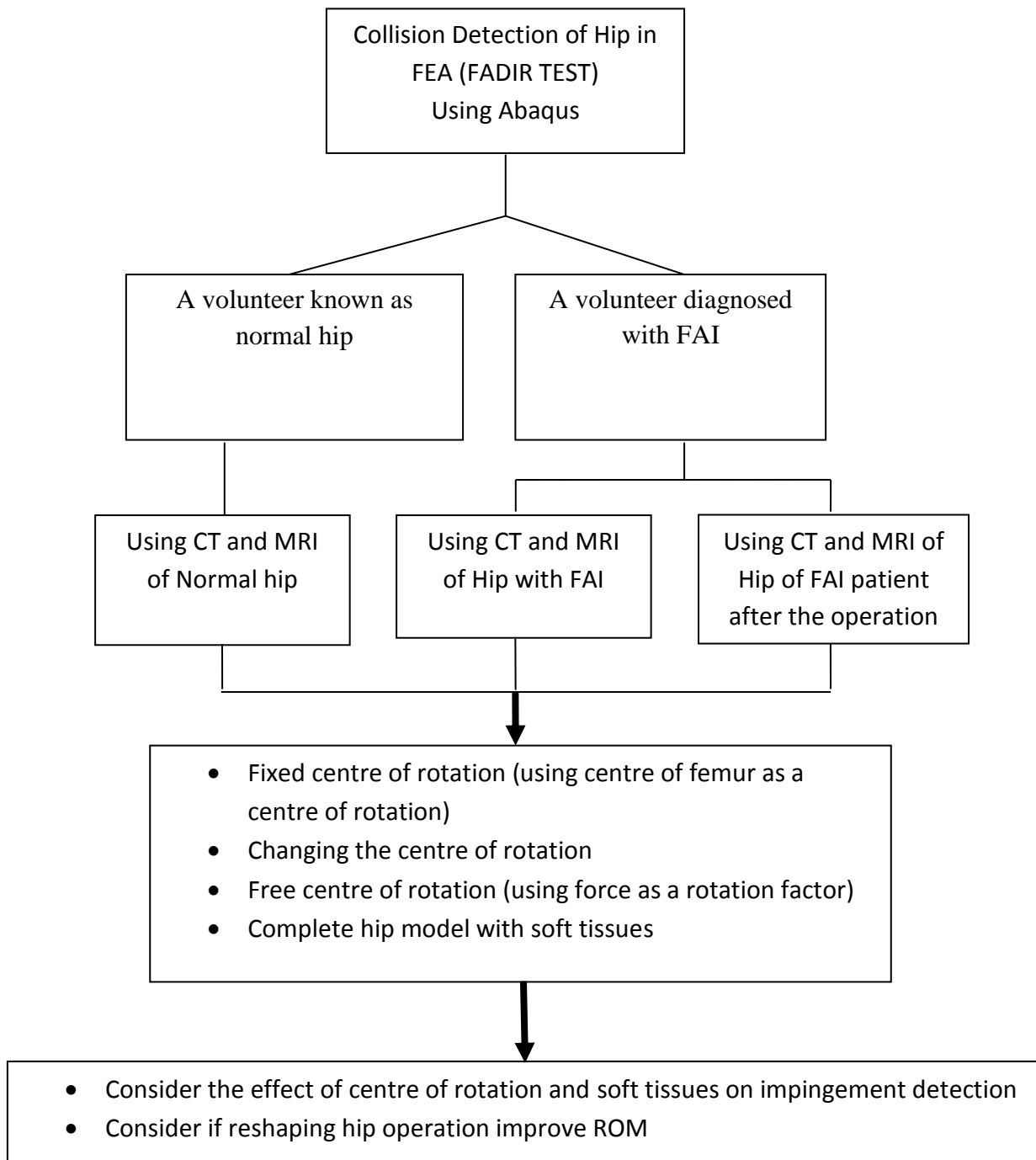


Figure 21: Outline of FEA method and results in Chapters 5 and 6

4.3 Experiments

The commonly used clinical tool to measure FADIR is goniometer. Goniometer has some errors such as fixing the centre of rotation also human errors and it is not convenient to use. Therefore an experimental investigation was conducted to find an alternative and more reliable device. In Chapter 7, four different devices are compared to check their reliability and consistency of measurement. The aim of this section is to investigate which device is suitable to be used in medical application especially in detection of hip impingement. Also it is the first time that reliability and validity of the Wiimote, MotionNode and goniometer are compared with Motion Capture to be used in medical application.

Experiments were set up to measure FADIR angles using each of four devices for each volunteer. 22 volunteers with normal hip were participated in our experiments (FADIR test). Four measurement devices (Motion Capture, Wiimote, MotionNode and goniometer) were used to measure flexion, adduction and internal rotation of the hip. Reliability of the devices were analysed to see if any one of the devices can replace goniometer in order to minimise human errors. Figure 22 shows how the experimental procedures were conducted.

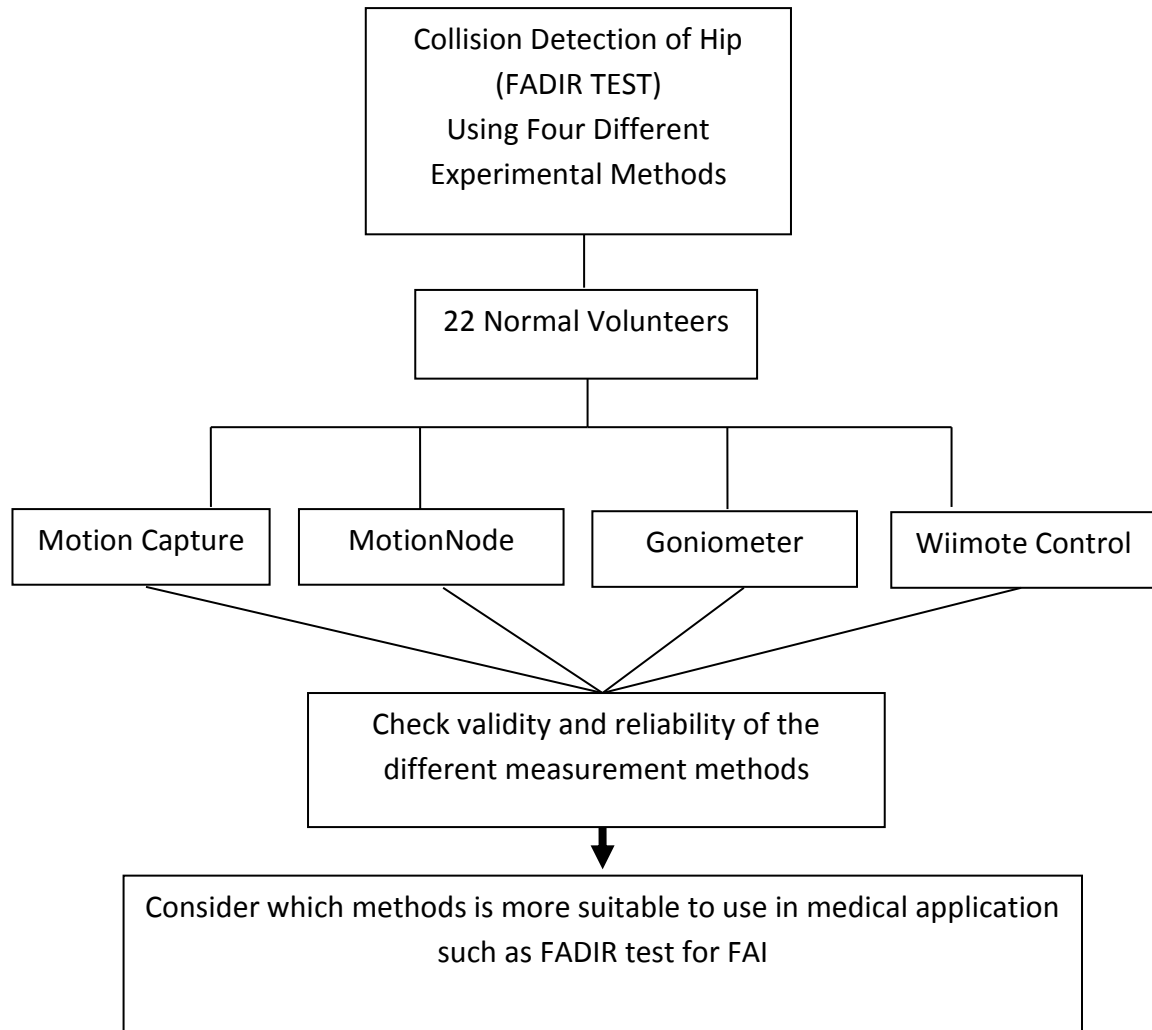


Figure 22: Outline of experimental method and results in Chapter 7

4.4 Validation of FEA with Experimental Analysis

One of the volunteers who participated in the device measurement experiments also participated in the FEA investigation providing normal data in order to compare the FEA results with the experiments. All normal hip results with different parameters and boundary conditions (such as centre of rotation of the femur head) were compared with the experimental results of the normal person. The aim of the comparison was to recognise which conditions give closer results to experiments and which hip model is more realistic. Figure 23 shows the procedure of comparing the normal volunteer results in both experiments and FEA method using FADIR test.

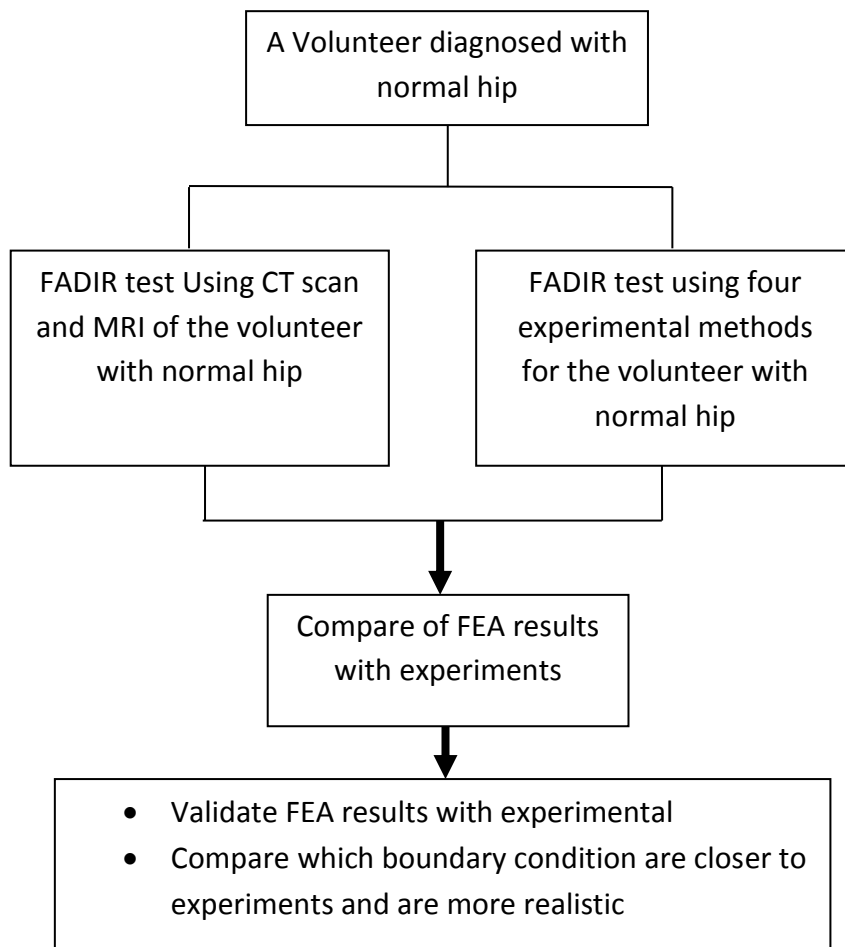


Figure 23: Outline of validating FEA with experimental results in Chapter 8

Chapter 5

Hip Modelling

5.1 Introduction

This Chapter presents the general methodology used in Chapter 6. Firstly, the methods of 3D hip model in MIMICs are described. Secondly, the mesh procedures of 3D model in 3-Matic are described. Finally, the methods of detecting hip impingement in Abaqus are explained.

In this Chapter the measurement of FADIR test are simulated in FEA. Three angles which are measured in FADIR test are measured in FEA for normal hip, hip with impingement and hip with impingement after reshaping operation. The FADIR test requires three orientations as explained in Chapter 4: maximum flexion, maximum adduction in 90° flexion and maximum internal rotation in 90° flexion. Also as explained in Chapter 4 impingement zone is measured in normal hip, hip with impingement and hip with impingement after reshaping operation.

5.2 MIMICs

Materialise' Interactive Medical Image Control System (MIMICs) interfaces between scanner data (CT, MRI, Technical scanner) and Rapid Prototyping, STL file format, CAD and Finite Element Analysis. The MIMICs software is an image-processing package with 3D visualization functions that interfaces with all common

scanner formats (MIMICs , 2014).

MIMICs software is also an interactive tool for the visualization and segmentation of CT images as well as MR images and 3D rendering of objects. Therefore, in the medical field MIMICs can be used for diagnostic, operation planning or rehearsal purposes (MIMICs , 2014).

In this study, MIMICs software was used to read the Digital Imaging and Communications in Medicine (DICOM) files of the subject patient. In this study CT data of the volunteers was obtained using GE Medical systems/Light speed VCT computed tomography scan. The DICOM images generated in the CT scan were processed using MIMICs 15 software to obtain the primary 3D model using density segmentation techniques (MIMICs , 2014).

5.2.1 Importing Medical Images

Files such as DICOM are recognised by MIMICs and can be imported automatically to MIMICs 15 (MIMICs , 2014). CT scan and MRI of patients and normal volunteers were provided by Epsom Hospital (as explained in Chapter 4). Three different CT and MRI data from two volunteers were obtained. One set of CT and MRI data from a normal person and two set of CT and MRI from a volunteer with impingement (before and after reshaping surgery) were obtained.

Indeed, the pixel size and the resolution of the image ensure the model generated is dimensionally coherent during the segmentation process (MIMICs , 2014). The image slices were then stacked and converted to be displayed in coronal, sagittal and axial views. However, the orientation of each view was defined before continuing. All the images were then displayed as shown in Figure 24.

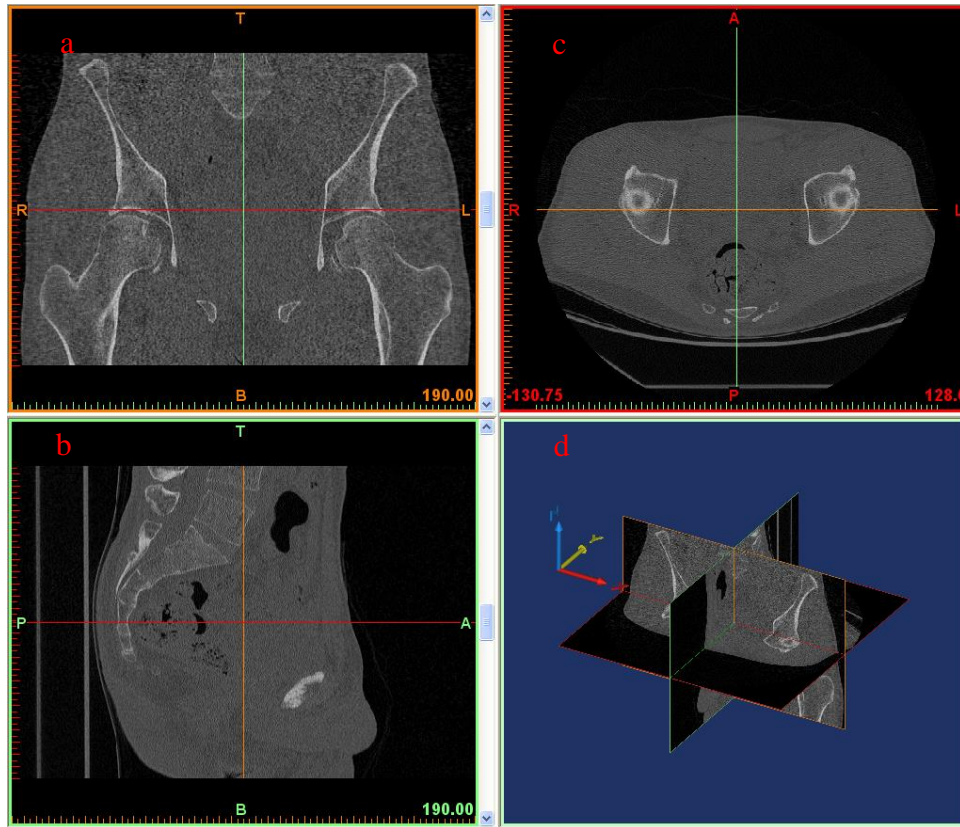


Figure 24: Different views in MIMICs program a) axial b) sagittal c) coronal d) 3D views of the pathological left hip joint

The CT scan and MR images were imported to MIMICs using automatic import wizard, since MIMICs can recognise the format of the files that were used for this project. “File -> Import Images” was used to start the import wizard. The images can be seen in different views as shown in Figure 24.

The CT and MR images loaded into MIMICs can be processed to enhance the quality of the images to enable user to create a 3D model more accurately. The tools available for image processing are thresholding and region growing. CT images were used for creating the bones (femur and acetabulum). MR images were used for soft tissues such as cartilage and ligaments. MRI is more versatile than X-ray and is used to examine a large variety of medical conditions. MRI provides optimum contrast and high spatial resolution to visualise cartilage, bone, synovial fluid, ligaments, menisci, muscle and other soft tissues.

5.2.2 Thresholding of Medical Images

Thresholding based on the Hounsfield scale was used to separate both the cortical bone of the femur and the acetabulum from the surrounding muscles and tissues. Thresholding (thresholding is a value in image processing and is different for different material to separate the boundary conditions of different materials in CT and MRI from each other) was used to create segmentation for an object. CT images are a pixel map of the linear X-ray attenuation coefficient² of tissue (MIMICs , 2014). The pixel values are scaled so that the linear X-ray attenuation coefficient of air equals to -1024 barns/atom and that of water equals to 0. This attenuation coefficient in MIMICs is called Hounsfield Unit³ (HU). HU value is different for different materials and tissues. Using this scale, fat is around -110, muscle is around 40, trabecular bone is in the range of 100 to 300 and cortical bone extends above trabecular bone to about 2000, cartilage is about 500 to 700 and ligament is about 280 to 600 (MIMICs , 2014).

The thresholding window has the ability to choose range of different body materials. It is possible by adjusting the slider in the “Thresholding” dialogue box as shown by the red circle in Figure 25. As the slider is adjusted, different types of materials on the CT scan and MR image can be highlighted by a brighter colour. This is to separate the area from rest of the body to create 3D of that area.

By selecting a specific HU value, the area of bone or muscle or cartilage will appear. After that HU value can be adjusted manually to make the CT and MR images clearer.

An intensity profile was generated as shown in Figure 25 in red circle. This profile has higher and lower thresholding value for bones. Thresholding value is between lower and higher value for each object (bones and soft tissues) and can be changed manually. However, MIMICs 15 allows changing the predefined threshold to the required threshold by choosing compact bone of an adult from a drop down menu. Therefore, a lower limit of 662 HU and upper limit of 1992 HU were defined in order to select only the cortical bones from the surrounding tissues as shown in Figure 25.

² Quantity that characterizes how easily a material can be penetrated

³ Quantitative scale for describing radio density

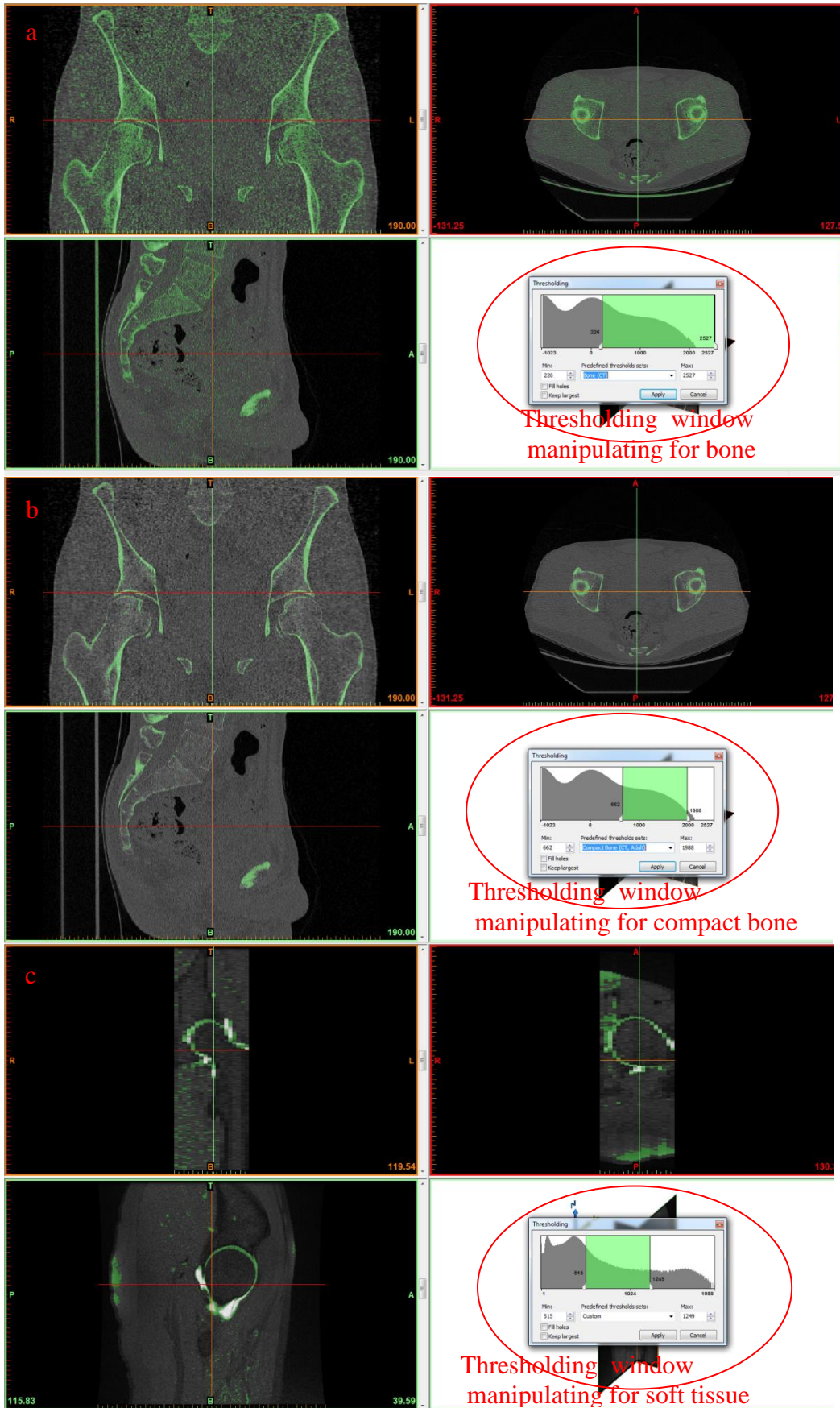


Figure 25: Segmentation of the cortical bones from the soft tissues and soft tissues from bone. a) Threshold value and segmentation of bone from soft tissues b) Threshold value and segmentation of compact bone c) Threshold value and segmentation of soft tissues

5.2.3 Region Growing

Mask is the profile, a closed region of a segment (such as bone) in a MRI and CT images slice. Region growing is a procedure to complete thresholding. The thresholding tool makes it possible to split the segmentation created by thresholding into several objects and to remove floating pixels (MIMICs, 2014). The femur, the pelvic girdle, three ligaments (iliofemoral, ischiofemoral, and pubofemoral) and two cartilage (articular cartilage) were selected separately and assigned different masks.

5.2.4 Segmentation Density Mask

The region growing splits the segmentation into separate entities. This enables to generate separate geometrical files and subsequently 3D models in the next step. Noisy pixels and artefacts were eliminated manually. Cavity filling operation was performed in order to eliminate some existing voids within the density masks. This operation was done manually using the multiple slice editors. This was a delicate process where each and every slice related to the femur, the pelvic girdle, three ligaments (iliofemoral, ischiofemoral, and pubofemoral) and two cartilage (articular cartilage) was filled completely. The following approach was adopted in order to make sure the accuracy and coherency of the original slices were not affected. In fact, the slice was initially filled and then all the excess filling was removed by intersecting a circle with the inner boundary of the cortical bone.

Afterwards, the filling operation was applied to all the filled slices for all (femur, pelvic girdle, three ligaments (iliofemoral, ischiofemoral, and pubofemoral) and two cartilage).

The proper mask of the 2D model was chosen for femur, pelvic girdle, three ligaments and two cartilage after thresholding and region growing. After the region growing inside of the region maybe empty, as shown in Figure 26a, and in some cases it may be necessary to fill that region as shown in Figure 26 b. At this stage this process is done on 2D slices. This process is known as cavity filling. Figure 26 shows the stages of cavity filling of femur for one slice of medical images.

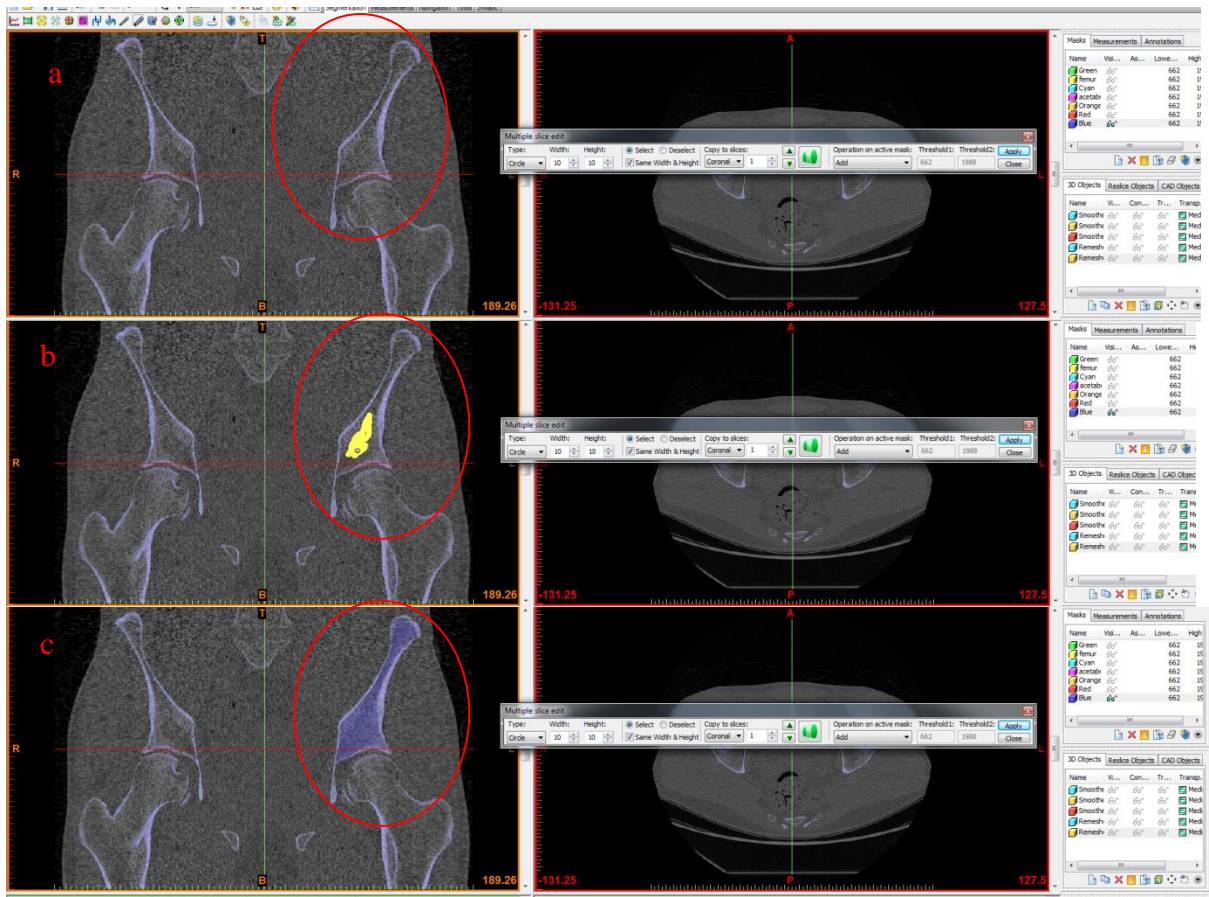


Figure 26: Filling pelvic mask manually a) a slide of pelvic mask was chosen b) pelvic mask was filled manually (yellow area) c) all of the pelvic was filled in the mask

5.2.5 Generating 3D Model

To obtain the objects in 3D, slices are collected and collection of these masks were stacked up to produce the 3D model. In This way, femur, pelvic girdle, three ligaments and two cartilage were obtained. All the 2D masks which were previously filled from each slides were collected and made a 3D model. After creating 3D models further processing were performed to improve the objects. Smoothing is one of them run by the “smooth” icon. All the 3D models were created and conservatively smoothed to have a good surface topography. Figure 27 indicates the 3D model of the hips with and without soft tissues.



Figure 27: 3D model of the pathological hip joint of the volunteer after filling cavity in MIMICs a) with soft tissues b) without soft tissues

5.2.6 Smoothing and Reduce Triangle Reduction

By applying the smoothing operation, existing artifacts in the active model are removed and consequently the surface quality of the calculated 3D objects is improved. As separation of bone from soft tissues might leave some sharp edge, smoothing makes the model smoother and reduces the sharp edges. However, smoothing the model change the real size of the model. Iteration and smoothing factor are two main parameters that used to smooth the objects. Smoothing factor is a factor that makes 3D model smoother. High smoothing factor makes 3D model smoother but it changes the size of mask. Iteration is the number of times that the smoothing operation is repeated. High iteration with same smoothing factors enhances model more times.

After constructing the 3D model, femur and acetabulum were smoothed. Smoothing factor of 0.5 with 4 times iteration was used. Triangle reduction was used to reduce sharp angles with tolerance of 0.1 and edge angle of 15° (according to MIMICs manual recommendation (MIMICs , 2014)) with 4 times iteration as shown in Figure 28.

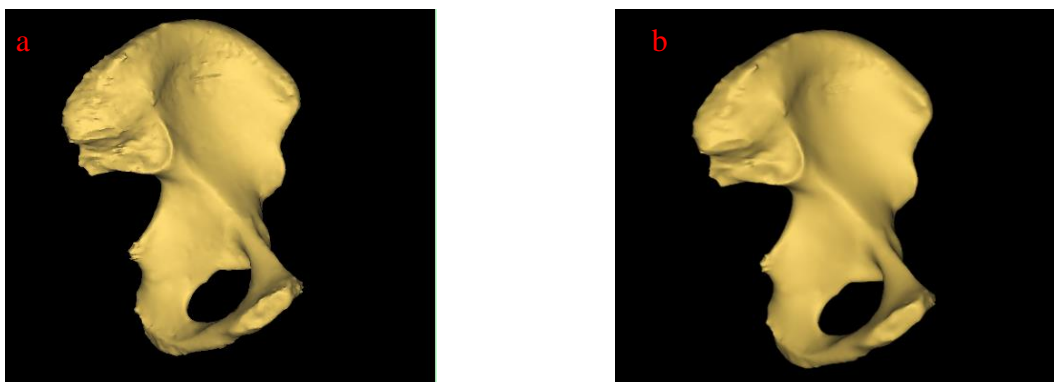


Figure 28: Smoothing a) acetabulum before smoothing b) acetabulum after smoothing

The same procedure was applied to soft tissues model such as cartilage and hip ligaments from MRI. All three ligaments and two cartilage were smoothed and their sharp edge was reduced to avoid problems in meshing.

5.3 3-Matic

3-Matic is the software that combines CAD tools with pre-processing (meshing) capabilities. To do so, it works on triangulated files (STL) and as such it is suitable for organic/freeform 3D data, like the anatomical data coming from MIMICs. 3-Matic is used to prepare the mesh for finite element modelling.

One must decide first whether to describe the system using a 1D, 2D or 3D representation. This dictates the types of elements which can be used to discretise the problem domain. All structures in the real world are three-dimensional. However, approximation can be made to facilitate simple stress analysis of a part. Indeed, the physics of the problem determine which type of element is most appropriate (3-Matic, 2014). In biomechanics, the representation of structures with 1D element is rarely enough but a 2D representation may be perfectly acceptable. For instance, a plane stress or plane strain analysis is particularly useful when the important deformation of a structure occurs primarily in one plane. Axisymmetric problems are of 2D, where the geometry has rotational symmetry about one axis even though these conditions in biomechanics are rarely met in a strict sense (3-Matic, 2014). In this study 3-Matic 7 was used.

5.3.1 Element Type

Meshing is referred to the process of defining a structure in term of nodes and elements. These elements may have two or more nodes along each side of the elements. Linear elements are commonly referred as elements having two nodes per side whereas quadratic elements are referred to as elements having three nodes per side (3-Matic, 2014). Indeed as the order of the interpolation function increases, the number of calculations necessary to evaluate the model also increases, and more closely the real variation is modelled (3-Matic, 2014). Elements are normally categorised with respect to their interpolating function into simplex, complex and multiplex.

Simplex elements have polynomials with constant and linear terms only, and the nodes are located at the corners of the elements. Complex elements use quadratic, cubic and higher order interpolation polynomials. They have triangular shape with curved edges having additional nodes. Multiplex elements also use high order interpolation polynomials but with the sides of the multiplex elements parallel to the coordinate system (Fagan, 1992). Besides the most common 3D elements are the linear eight-node brick and the quadratic twenty-node brick (3-Matic, 2014).

Indeed the finite element works by approximating the distribution of an unknown variable in a precise manner across the body to be analysed (Fagan, 1992). But these distributions are only reliably produced if the shapes of the elements are not excessively distorted. One measure of element distortion is the aspect ratio. This is the ratio of the longest side of an element to the shortest side. The measure of skew and taper can also be used to quantify element distortion illustrating two rectangular elements with the same aspect ratio but different behaviours (Fagan, 1992). 3-Matic program use simplex triangular element to do surface meshing of the 3D model imported from MIMICs.

5.3.2 Remesh

Remesh is intended to optimize the STL models for FEA/CFD purposes. The remesh operations transforms badly shaped triangles into more equilateral triangles. The more geometrically ‘regular’ the triangles are, the better and more reliable the results of the FEA/CFD calculations will be. Apart from the automatic remeshing operation, different techniques are available to further improve the quality of the triangles manually.

There are different ways to express the quality of a mesh. Depending on the chosen measure, each triangle have a certain quality value. The global triangle quality is visualized via a histogram as shown in Figure 29, but can also be visualized by colouring the bad quality triangles.

The 3D model was selected separately to make it optimal for FEA purposes. The remesher capability of MIMICs was used to generate surface meshes for both models. The 3D models were imported to 3-Matic automatically by using the “remesh” in MIMICs. The models were divided into triangular elements and nodes. However,

the quality of the triangles was measured and subsequently changed to respect a given minimum and maximum quality threshold. In fact, there are several shape parameters available to measure the quality of the triangle. The height/base parameter was used to measure the ratio between the height and the base of a triangle. A perfect triangle has a quality of 2 and a bad triangle has a quality of 0. The minimum and maximum quality threshold was defined as 0 and 2 respectively.

5.3.3 Quality of Mesh

In this section the interrogation of quality of mesh is to be discussed. The quality is summarised by quality of mesh histogram as shown in Figure 29 on the 3-Matic screen. The blue circle in Figure 29 shows the quality threshold. Quality threshold should be 0.4 according to MIMICs manual (MIMICs , 2014). This quality histogram shows the amount of triangles that have a certain quality. Three numbers summarise the histogram, the first number shown as “a” in Figure 29 stands for triangles that have quality less than minimum threshold. Second number shown as “b” in Figure 29 is number of triangles that have quality between maximum and minimum threshold. Third number shown as “c” in Figure 29 stands for triangles that have maximum threshold. In a good mesh, all mesh elements are expected to be in the third group.

The group “c” triangles may be increased by the following steps:

1. Reduce the amount of triangles of the model
2. Improve the quality of triangles of the model
3. Reduce the amount of triangles while preserving the quality

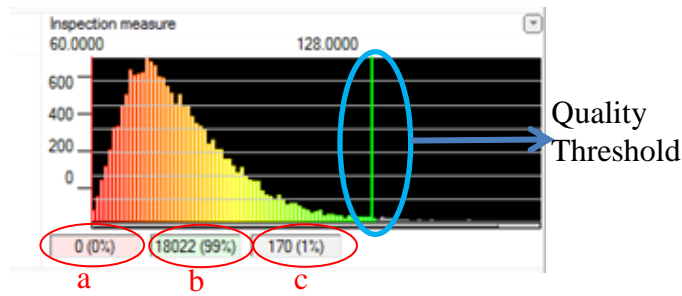


Figure 29: Quality mesh histogram that shows the amount of triangle that have certain quality according to the threshold value. Tool bar under the histogram shows the number of elements a) with minimum quality b) between minimum and maximum quality c) with maximum quality

One of the ways to reduce the group “a” triangle is to reduce the amount of all triangles. To reduce the number of triangles, inspection measure (inspection measure is one of the quality parameter which can be changed to improve the quality of mesh) was changed from largest angle to smallest edge length. As shown in Figure 30a, the histogram was changed after changing inspection measure and the amount of mesh element was reduced as shown in Figure 30b. The mesh quality can be improved by changing the maximum geometrical errors (geometrical error is a parameter controlling surface accuracy) and shape quality thresholding as shown in Figure 30c. Figure 30 shows how the quality of mesh was improved after reducing triangles. Table 5 also indicates the results of the femur to obtain the best mesh quality. Number of elements was reduced by using fix toolbar to save timing in FEA.

Basically, the same procedures were repeated for the pelvic girdle, femur, three ligaments and two cartilage.

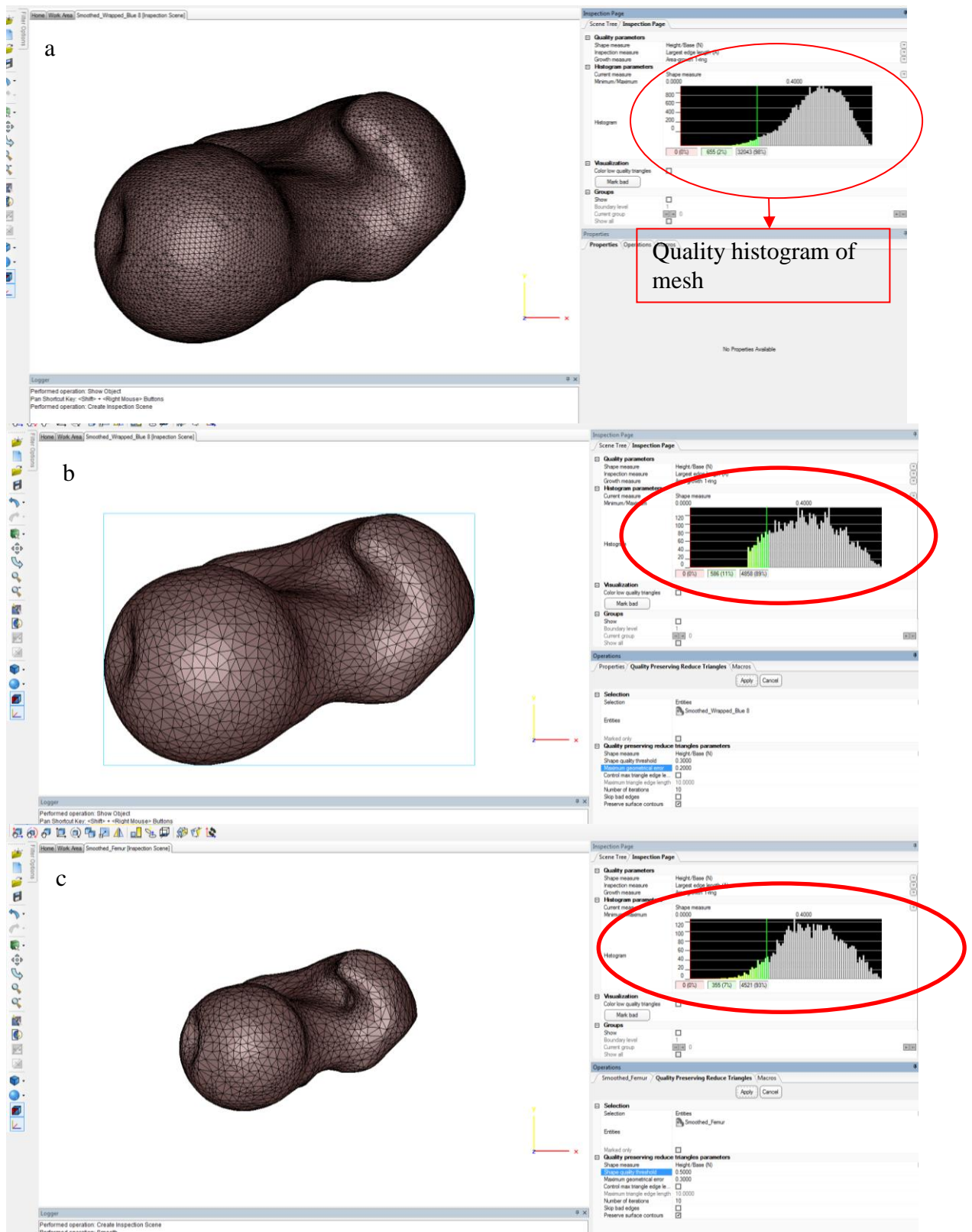


Figure 30: Changing the quality of mesh by changing the parameters such as shape measure, inspection measure, geometric errors, and maximum triangle edge length

For all these bones and soft tissues initial meshing contained too many triangles for an FE analysis. Thus, the amount of triangles was reduced as explained above.

Geometrical error of 0.1 and 5 iterations were chosen. Geometrical error was chosen as small as possible because the lower geometrical errors keep close to the initial model.

Table 5: Number of elements for femur in 3-Matic by changing the mesh parameters such as inspection measure and Max triangle edge length, the red line is the changes while the black one remain constant

Changes	Quality and type of element	Number of triangle that have quality between max and min threshold	Number of triangles that have maximum threshold
Before changes	Shape measure: Height/Base Inspection measure: Largest angle	956	4462
After changes	Shape measure: Height/Base Inspection measure: Smallest edge length	554	4899
Before changes	Shape quality threshold=0.3 Max geometric error=0.1 Max triangle edge length=5	267	5705
After changes	Shape quality threshold=0.3 Max geometric error=0.1 Max triangle edge length=10	21	6658

All the parts of the model such as femur, acetabulum, cartilage and ligaments followed the same quality mesh procedure.

5.4 Abaqus

Abaqus/CAE is an environment that provides a simple, consistent interface for creating, submitting, monitoring, and evaluating results for a wide range of FEA problems. For solid mechanics, Abaqus gives two analysis platform; Abaqus/Standard and Abaqus/Explicit simulations (Abaqus, 2014). The standard uses simple solver to obtain the response under loading by solving simultaneous equations related to the problem. The explicit on the other hand is an iterative solution and this allows the solver to deal more effectively with non- linear and contact problems.

Abaqus/Explicit has several advantages such as: ease of use, reliability, and efficiency are key ingredients in its architecture. Abaqus/Explicit is supported within the Abaqus/CAE modeling environment for all common pre- and postprocessing needs.

The results at any point within an Abaqus/Explicit run can be used as the starting conditions for continuation in Abaqus/Standard. Similarly, an analysis that starts in Abaqus/Standard can be continued in Abaqus/Explicit. The flexibility provided by this integration allows Abaqus/Explicit to be applied to those portions of the analysis where high-speed, nonlinear, transient response dominates the solution; while Abaqus/Standard can be applied to those portions of the analysis that are well-suited to an implicit solution technique, such as static, low-speed dynamic, or steady-state transport analyses.

5.4.1 Volumetric Mesh

In order to perform analysis in Abaqus, it requires volumetric mesh. The surface mesh of the femur, pelvic girdle, hip cartilage and hip ligaments have satisfactorily passed the mesh quality test. They were saved as an 'inp' file format and exported to Abaqus separately. There, the surface mesh, which was created in 3-Matic, were converted from triangular to tetrahedral elements. Indeed, the volumetric mesh of each part were verified against some defined parameters and an analysis check was carried out to determine whether the mesh passed the quality tests. Number of mesh increased after changing each part from surface mesh to volumetric mesh. Figure 31 demonstrations the volumetric meshes for each part.

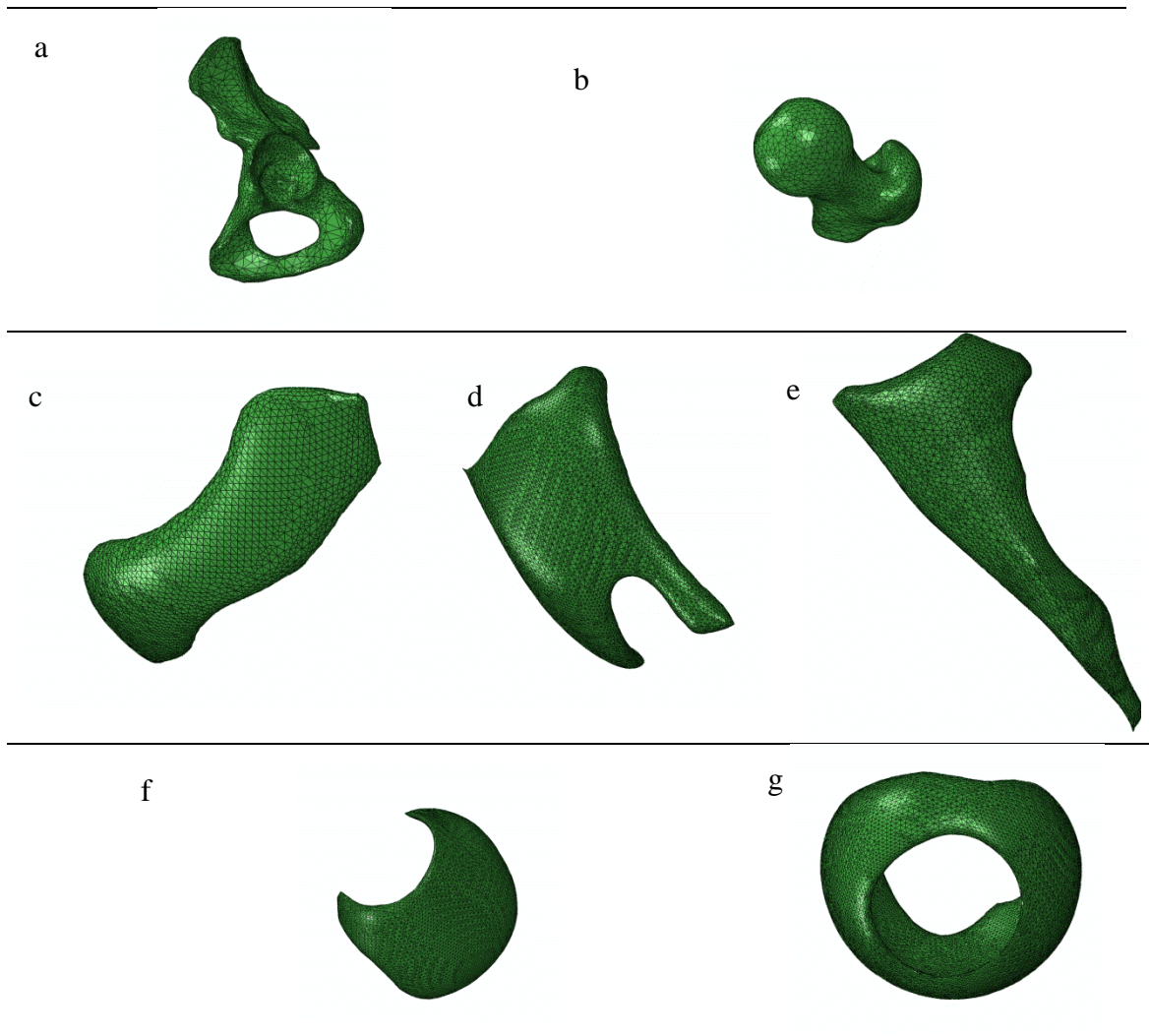


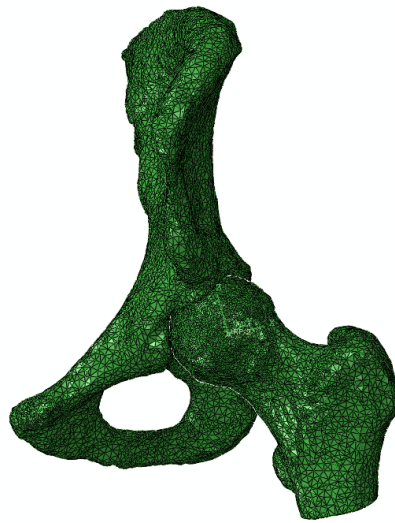
Figure 31: Volumetric mesh of a) femur b) acetabulum c, d, e) hip Ligaments f, g) hip cartilage in Abaqus

5.4.2 Assemble

All meshed parts were assembled at the locations compatible with their original position obtained from MIMICs.

The femur was imported in 'inp' file format to Abaqus software 6.11-1 (Simulia Dassault Systems). Therefore the acetabulum was imported and also copied with a different model name. The tool "copy object" was used to copy each part to similar predefined model named as "hip model". Therefore, this model was selected and assembly was chosen from the drop down menu of the module. Subsequently, both the femur and the acetabulum was separately chosen and defined as instances for the model without soft tissues as shown in Figure 32a. All parts of the model with soft tissues were assembled as shown in Figure 32b. Femure, acetabulum, three ligaments and two articular cartilage were assembled in one model named as "hip model with soft tissues".

a



b

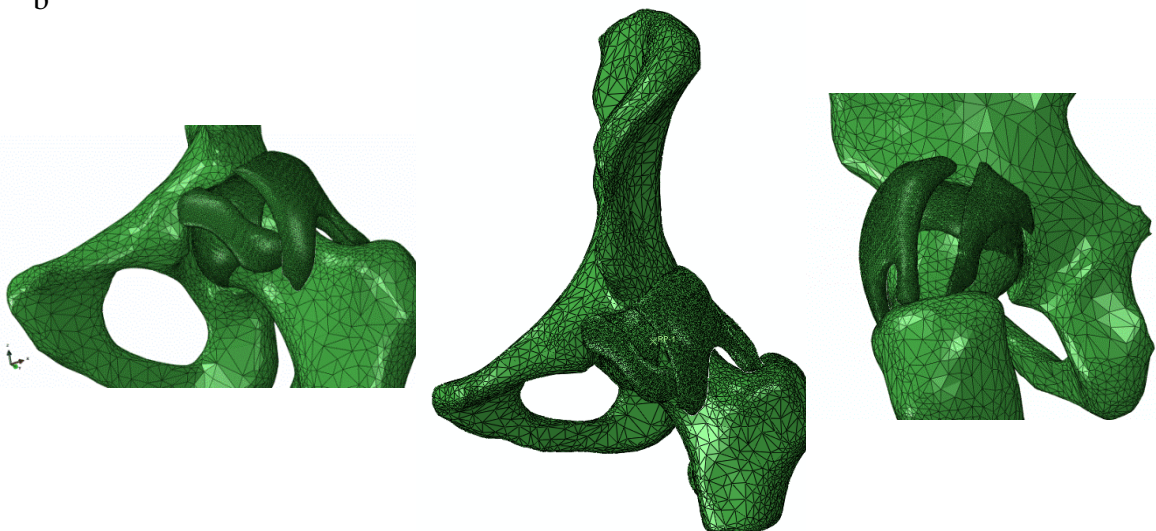


Figure 32: Assemble of hip model a) Without soft tissues b) with soft tissues

5.4.3 Material Properties

Material properties must frequently be approximated in finite element analyses. Material property approximations are particularly common for orthotropic and anisotropic materials, where a material's performance depends on its orientation (Fagan, 1992). Material properties should be defined for each part. In this study three different materials were used: bone, ligament and cartilage.

Bone is used as an isotropic material in most of the FEA application (Currey , 2009). There are a different properties for cortical and trabecular bone. Currey claimed that most articles consider the bone as cortical (Currey , 2009). He also claimed that

bone properties depend on age and bone density (Currey , 2009). In this study material properties of bone were used according to the previous articles (Peña, et al., 2006), (Beillas, et al., 2004).

Some articles assumed that ligaments and cartilage are hyper elastics (Anderson, et al., 2008), (Shirazi, et al., 2008), (Dong, et al., 2011). However a lot of other researches (Beillas, et al., 2004), (Guo, et al., 2009), (Papaioannou, et al., 2010), (Wawro & Fathi-Torbaghan, 2004) assumed that ligaments and cartilage are isotropic elastic materials.

Material properties all of the parts are given in Table 6.

Table 6: Material property of the finite element model (Hewitt, et al., 2001), (Suppanee, et al., 2013), (Rho, et al., 1993)

Region	Elastic modulus (MPa)	Poisson's ratio	Density (Kg/m ³)	Material Type
Bone	17000	0.3	1281	Elastic/Isotropic
Ligaments	146	0.5	1100.1	Elastic/Isotropic
Cartilage	500	0.3	1000.1	Elastic/Isotropic

5.4.4 Location of Hip Joint Centre

The Hip Joint Centre (HJC) is the point of the femoral head that remains fixed during motion of the joint for a restricted range of motions (Kang, et al., 2002). The HJC has been located previously by predictive methods or functional methods (Kang, et al., 2002). A predictive method is estimating a hip joint centre as the relative position of anatomical landmarks (Kang, et al., 2002). A weak point of this method comes from the fact that the position of anatomical landmarks varies depending on expert opinion. A functional method consists of locating the centre of rotation by fitting a sphere to the head of femur (Kang, et al., 2002). The centre of this sphere is the HJC (Kang, et al., 2002). In this thesis, a sphere was wrapped around and fitted on the femur to locate the hip joint centre. Figure 33a shows the fixed sphere top of the femur head to select centre of rotation.

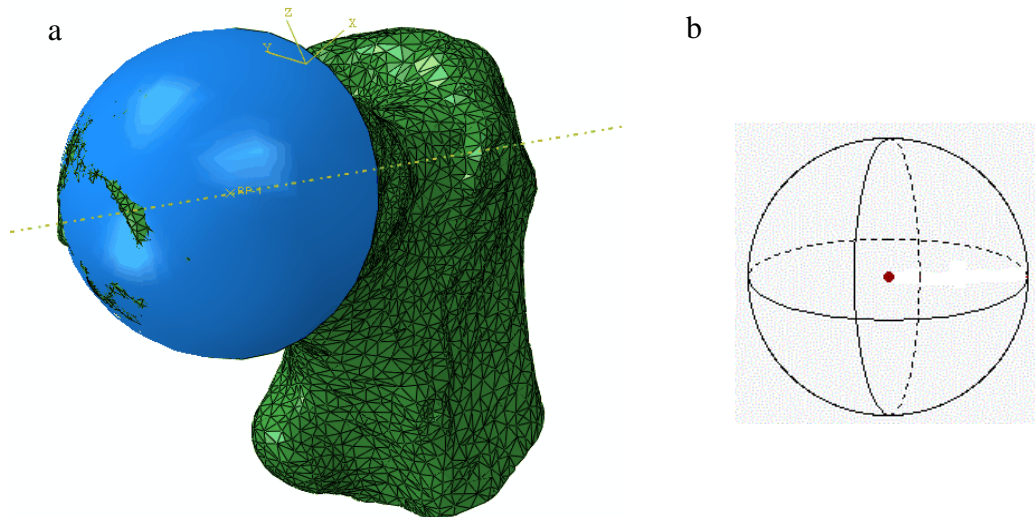


Figure 33: Fixed sphere top of the femur head to select centre of rotation. The centre of sphere is the centre of rotation

The following methods were applied in order to approximately calculate the centre of rotation of the femur:

1. Eight points from head of the femur were chosen.
2. The coordinates of the eight points were read in Abaqus. The eight point was chosen from eight different zone in the top of the femur as shown in Figure 33b.
3. According to these eight points centre and radius of sphere was calculated by using the sphere 3D equation.
4. The sphere was made using 'part' option and the sphere was fixed to the top of the femur.
5. Finally, the centre of the sphere was chosen as a centre of femur and reference point. The centre of rotation was selected to be the centre of coordinate.

5.4.5 Contact Algorithm

The general aim of contact simulation is to identify the areas on the surfaces that are in contact and subsequently calculate the contact pressures generated (Abaqus, 2014). In a finite element analysis contact conditions are a special class of discontinuous constraint. The analysis has to be able to apply the constraint when the two surfaces are in contact and similarly remove the constraint when they are separate (Abaqus, 2014). In this study, Abaqus Explicit was used to carry out the contact simulations.

Abaqus Explicit provides two algorithms for modelling contact interactions. The general automatic contact algorithm which provides very simple definitions of contact with few restrictions on the types of surfaces involved (Abaqus, 2014). On the other hand, the contact pair algorithm has more restrictions on the types of surfaces where contact must be carefully defined.

Furthermore, the interaction between contacting surfaces consists of two components, normal to the surfaces and tangential to the surfaces. The tangential component consists of the relative motion (sliding) of the surfaces and frictional shear stresses. In this study, the contact between the acetabulum and the femur was assumed to be ideally frictionless with no bonding (Abaqus, 2014). Besides, it is possible for a node on one contact surface to contact any of the facets on the opposite contact surface. Abaqus Explicit uses sophisticated search algorithms for tracking the motions of the contact surfaces. The general contact algorithm uses a more sophisticated global search or local tracking approach that does not require user control. Abaqus Explicit automatically adjusts the un-deformed coordinates of nodes on contact surfaces to remove any initial over closures. Indeed the general contact algorithm stores any unresolved initial penetrations as offsets to avoid large initial accelerations (Abaqus, 2014).

5.4.6 Boundary Condition

Specification of loads, boundary and interface conditions are the last task in the model creation. For instance, when modelling parts of the skeletal system, the loads are typically joint forces, muscular forces and ligament forces that exist during gait. Boundary conditions in finite element models consist of displacement constraints which

are required in any static FEA to prevent rigid body motion of the model (Biewener, 1992). These constraints are simply prescription of nodal displacements taken to be zero. The displacements are typically applied at sections of the model far removed from the primary area of interest (Biewener, 1992).

The general boundary conditions which were applied for all the hip models are discussed as follow. The boundary conditions were applied according to the previous articles (Philips , et al., 2007). However, the specific boundary conditions for each model are discussed in Chapter 6.

Femur was coupled to the hip joint centre of rotation shown in Figure 34. It was used to impose kinematics between reference node (centre of rotation) and the femur.

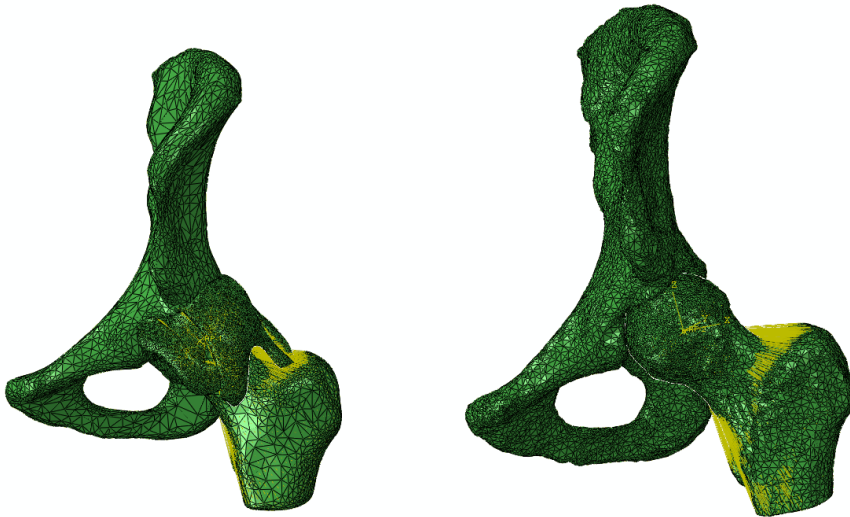


Figure 34: Coupling femur to centre of rotation

For the model with soft tissues, an extra step was defined in the boundary condition. The surfaces of ligaments were tied to the surface of femur and acetabulum. Also articular cartilage was tied to the femur and acetabulum, shown in Figure 35.

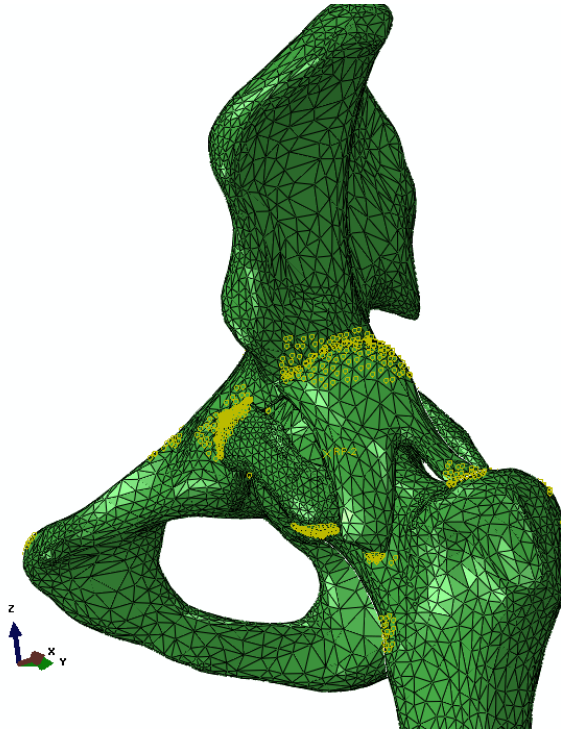


Figure 35: Ligaments and articular cartilage were tied to the femur and acetabulum

The medial pelvic wall was pinned in the X , Y and Z directions as shown in yellow in Figure 36. The pelvic bone support of the acetabulum was non-rigid. This is important in order to make the pelvic bone compliant and thus facilitating attainment of continuous horseshoe shaped contact of a normal hip articulation (Russell, et al., 2006), (Philips, et al., 2007).

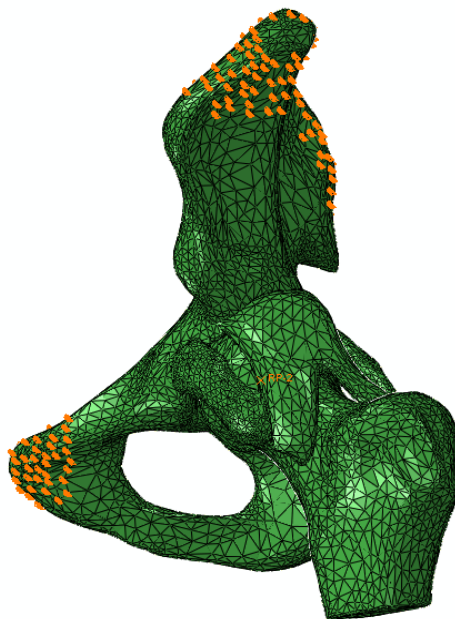


Figure 36: Pinned area in hip model

The centre of rotation of the femur was coupled with the whole section of the femur. During application of load, the centre of rotation was chosen and different physiological values were defined. Thus, this enabled the femur to move in the predefined directions. The UR_1 , UR_2 , UR_3 were defined for rotation around each direction (as is discussed in the Section 5.4.7).

5.4.7 Impingement Angle and Impingement Zone

In this thesis calculation of impingement angle and impingement zone are two important objectives and factors of the investigation. Therefore, these terms need to be explained. Several tasks were done in each hip model before choosing the impingement angles and impingement zone. The hip joint centre was chosen as a centre of coordinate. The Z axis was chosen parallel to the femur shaft. The X axis was chosen parallel to the horizontal hip line shown in Figure 15. The Y axis was automatically changed perpendicular to the X and Z axis.

Impingement Angle: Impingement angle is an important angle to diagnose the impingement in early stage. Impingement angle which is presented in this study is comprised of three angles. The impingement angles are the angles measured in FADIR test. FADIR test was simulated in this study. The first angle was maximum flexion which was the rotation of femur around X axis called UR_1 in Abaqus. The femur was rotated around X direction to obtain the first angle of impingement. The second angle was the maximum adduction in 90° flexion which was the rotation of femur around Y axis called UR_2 in Abaqus. The femur was rotated around X axis 90° then was rotated around Y direction to obtain the second angle of impingement. The third angle was the maximum internal rotation in 90° flexion which was the rotation of femur around Z axis called UR_3 in Abaqus. The femur was rotated around X axis 90° then was rotated around Z direction to obtain the third angle of impingement.

Impingement Zone: Impingement zone used in this study shows the place of impingement in acetabulum according to the clock method. A round clock was assumed to be placed in the acetabulum. 12 o'clock was placed in the superior part of acetabulum. 6 o'clock was placed in the inferior part of acetabulum. 3 o'clock was placed in the anterior part of acetabulum. 9 o'clock was placed in the posterior part of

acetabulum. The impingement zone was reported according to the clock time. This was explained in greater detail in Chapter 4 and shown in Figure 20.

In order to detect impingement angle and impingement zone the following boundary conditions were applied to all models.

5.4.8 Collision Detection of Impingement

One simple way of studying the location of impingement is to perform collision detection by applying joint motion and extending it until it collides. Many articles (Hu , et al., 2001), (Kubiak-Langer, et al., 2007), (Bedi, et al., 2011), (Bedi, et al., 2012), (Tannast, et al., 2007) studied the range of motion for hip with impingement to help surgeons using collision detection methods. Collision detection involves determining when one object penetrates another. It is clearly an expensive proposition as this is performed in an incremental fashion, particularly when large numbers of objects are involved and objects have complex shape (Moore & Wilhelms, 1988).

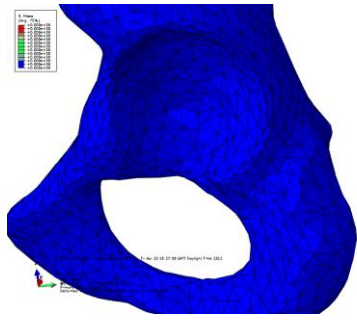
The goal of collision detection in a FEA software (also known as interference detection, contact determination, or impingement detection) is to automatically report a geometric contact when it is about to occur or has actually occurred (Lin & Manocha, 1995). There are two classes of collision detection methods. The first kind determines whether the surfaces of objects intersect (Moore & Wilhelms, 1988). In the first model, surfaces are modelled as a grid of points connected to form triangles. Collision between surface are detected by testing for penetration of each vertex point through the planes of any triangle not including that vertex. The surface are assumed to be initially separate. For each time step of animation, the positions of points at the beginning and the end of the time step must be compared to see if any point went through a triangle during that time step. If so a collision has occurred (Moore & Wilhelms, 1988). The second is based on the calculation of distances between objects, because two objects are separate if they have a positive distance from each other (Lin & Manocha, 1995). The heart of their collision detection algorithm is a simple and fast incremental method to compute the distance between two polyhedral. It utilizes convexity to establish some local applicability criteria for verifying the closest feature to constant size and thus guarantee expected constant running time for each test (Lin & Manocha, 1995).

The method developed in this thesis for collision detection is based on the stress-impingement angle diagram. When two objects in the space have not impinged, the contact stress between them is zero. As soon as two objectives are impinged, the contact stress starts to increase. In the diagram of stress-impingement angle the point where stress starts to increase from 0, is the impingement angle.

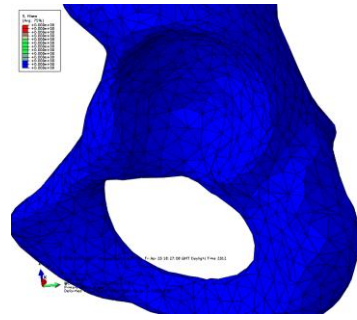
Abaqus was used to detect impingement angle and impingement area. Flexion, adduction, and internal rotation were defined for each model. Femur rotates around fixed centre and hit the acetabular in the certain impingement angle. Flexion is defined to vary between 0-180 which 0 is when femur is in position of 0° of flexion 180 was the maximum flexion. Figure 37 shows an example of the stress distribution in the acetabulum between 0°-180°. As it is shown at 126°, the femur starts to hit the acetabulum and stress appears. From 0° to 125° stress is 0 which shows that acetabulum and femur do not contact with each other. The contact between femur and acetabulum starts at 126° as can be seen in Figure 37 stress contour is not zero any more. Figure 37 illustrates the acetabulum every 9° as a sample but the impingement angle was checked every 1°. Stress-impingement angle diagram is shown in Figure 38 for the all elements in impinged zone. The stress-angle diagram is used to detect impingement angle. There is an increase point from 0 in the diagram that shows the femur hits acetabulum at that point as shown in Figure 38.

The first point that stress is not zero after which point the impinged angle, is shown.

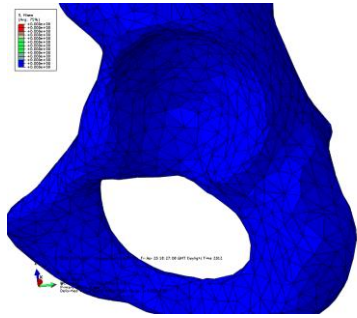
(More information is provided in Appendix B.)



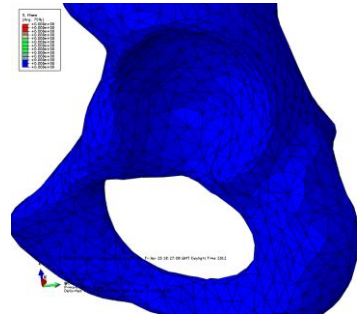
0°



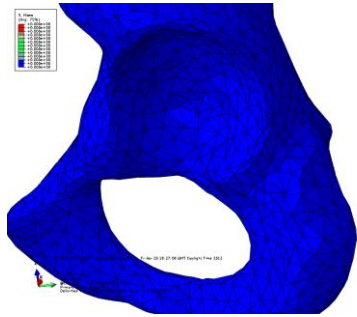
9°



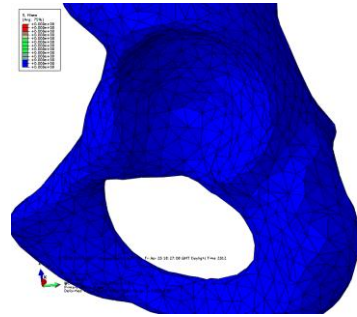
36°



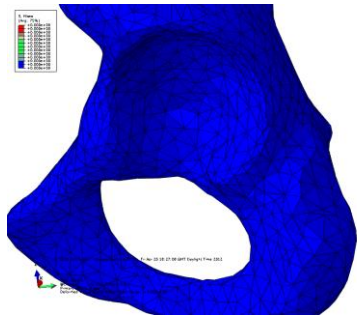
45°



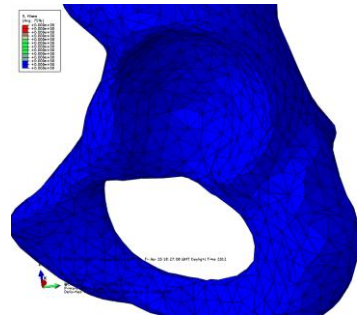
54°



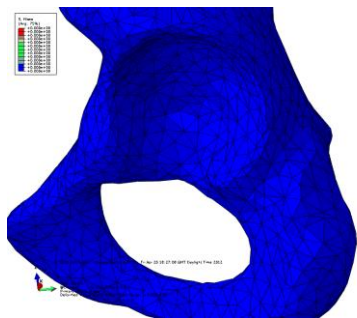
63°



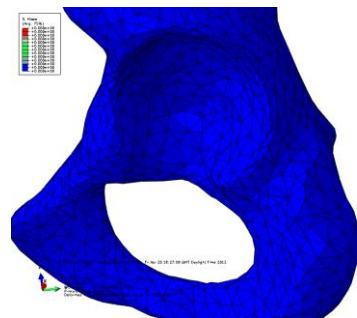
72°



81°



90°



99°

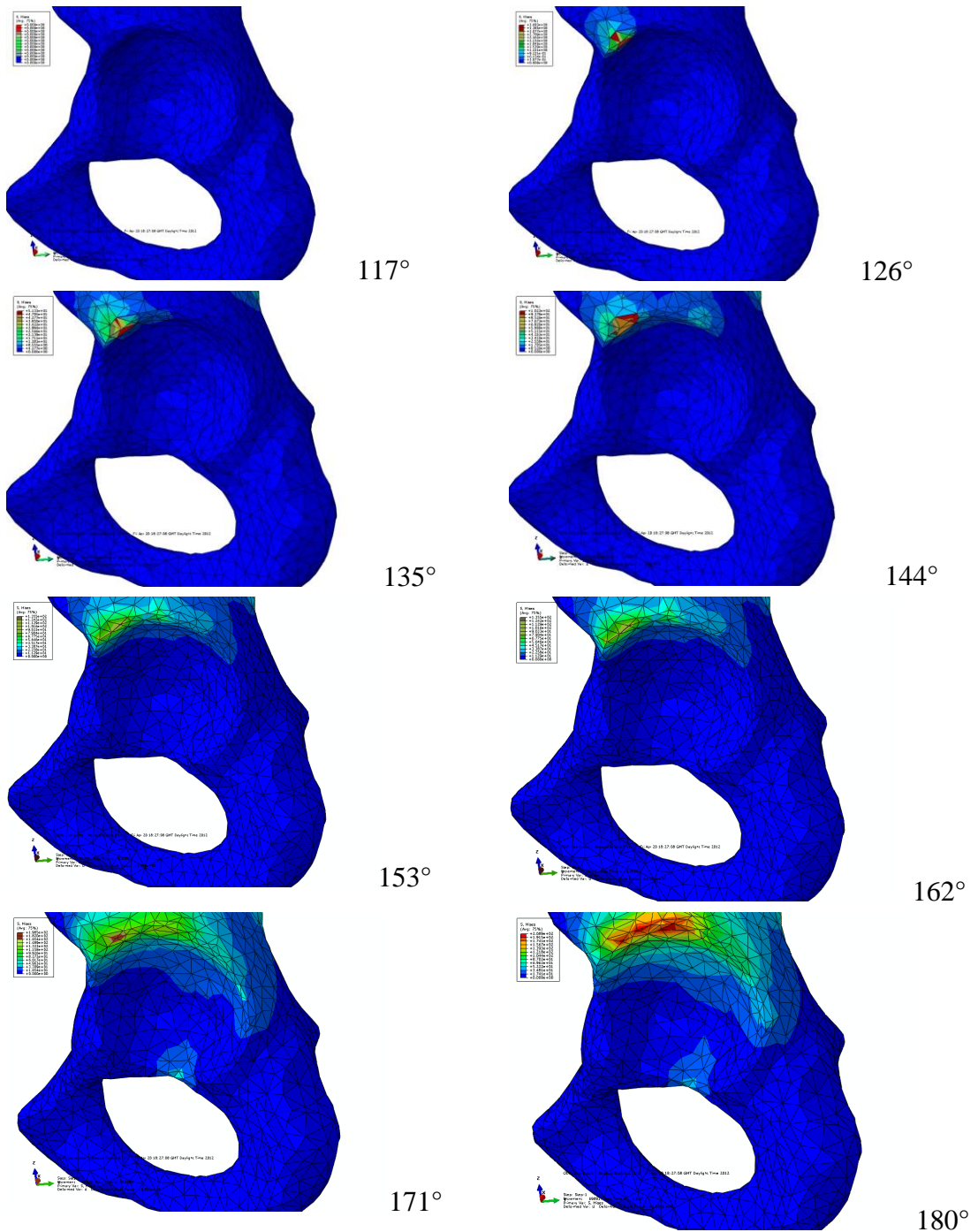


Figure 37: Schematic of acetabulum before and after impingement happens (sagittal view of left hip)

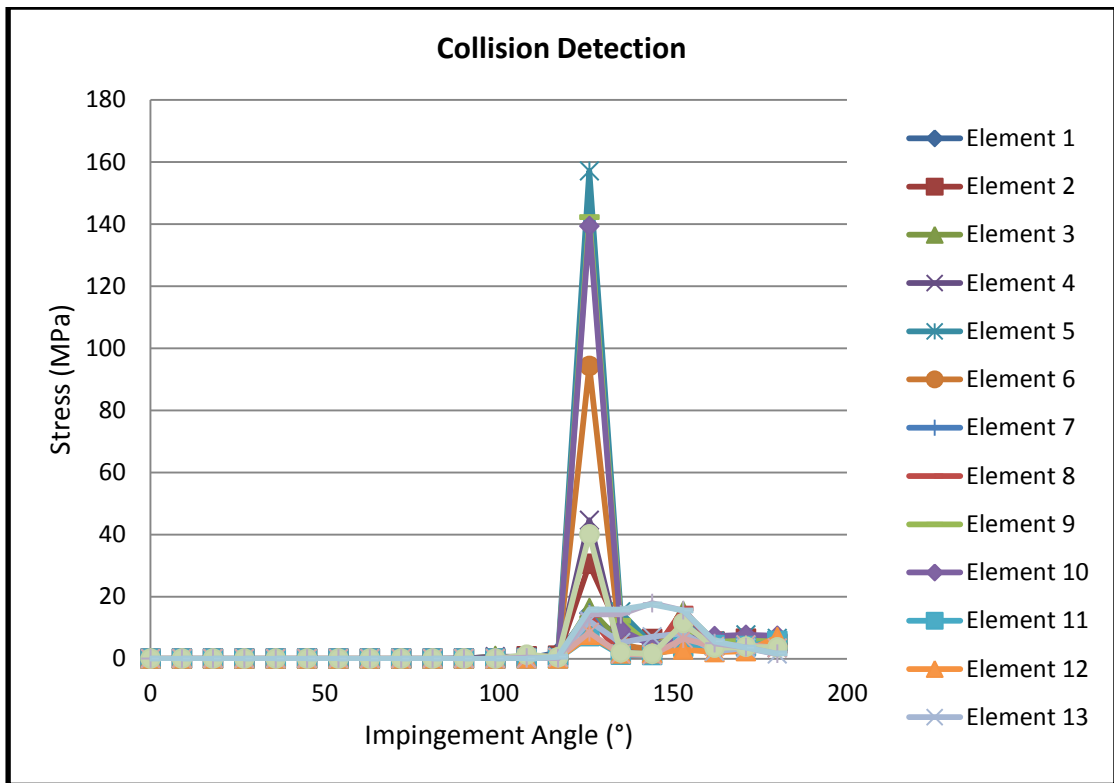


Figure 38: Stress-Impingement angle diagram of impinged area

5.5 Conclusion

In conclusion, the computer-aided programme which were used in this work, are based on 3D hip model of patients. Our collision detection of measured impingement angle is based on stress-impingement angle. This is the first time that a complete hip model with soft tissues are developed to inform surgeons about hip biomechanics. Although our hip model is mainly developed to detect hip impingement, it can also be extended to be used in some other hip disorders such as OA.

Chapter 6

Hip Modelling Results

6.1 Introduction

In this chapter the effect of the kinematics of the hip joint are described regarding femoral acetabular impingement with the centre of rotation and boundary condition being the main kinematic considerations for hip modelling. The FADIR test was described in Chapter 3. Measuring the flexion, adduction in 90° and internal rotation in 90° of flexion (called FADIR test) is one example of impingement tests. This test is applied to all three models (normal hip, hip with impingement and hip with impingement after reshaping) as explained in Chapter 4.

In this chapter the influence of the centre of rotation and boundary condition on flexion, adduction in 90° flexion and internal rotation in 90° flexion on FAI are addressed. To this end Chapter is divided into four parts.

In the first part flexion, adduction in 90° flexion and the internal rotation in 90° flexion of FAI for all 3 hip models are calculated with a centre of rotation that is fixed in line with the recommendations of previous articles (Tannast, et al., 2007), (Kubiak-Langer, et al., 2007).

In the second part, the centre of rotation is changed for all 3 hip models so as to determine the outcomes of changing the joint kinematics on flexion, adduction in 90° flexion and internal rotation in 90° flexion of the FAI. This experiment is repeated each time the centre of rotation is changed.

In the third part the centre of rotation is not prescribed and the models are defined as a free centre of rotation. These conditions are applied for all hip models.

Finally, the complete model of hip with soft tissues for all three hip models is modelled. It is the first time that a complete hip model with soft tissues has been designed and used in a computer-aided programme. All the cases are analysed with tissues attached.

6.2 Case Studies

As explained in Chapter 4, the CT and MRI of 2 cases were provided by Epsom hospital.

Case 1: A male with age of 42 and diagnosed with Cam impingement on his left hip. The height of 1.75m and weight of 74Kg were reported. The CT and MR images were taken after and before reshaping operation so two sets of data were available for this volunteer.

Case 2: A male with age of 38 and diagnosed with normal hip. The height of 1.8m and weight of 78Kg were reported. The CT and MR images were taken.

These two cases had 3 CT and MRI data, and case 1 had two CT and MRI data before and after surgery.

6.3 Methodology

MIMICs: As explained early in Chapter 5, MIMICs software was used to model the femur and the acetabular.

3-Matic: As clarified early in Chapter 5, 3-Matic software was used to mesh the femur and acetabular which are modelled in MIMICs.

Abaqus: All the steps such as assembly, material properties, boundary conditions were remained the same as explained in Chapter 5. The boundary conditions were changed as follow.

6.3.1 Fixed centre of Rotation

In the models with fixed centre of rotation, the centre of rotation was the centre of the femur as explained in Chapter 5.

The 3D model of hip (hip with impingement, normal hip and reshaped hip) which were made in MIMICs, then converted to Abaqus. The 3D of hip with fixed centre of rotation were flexed, adducted and rotated internally to detect impingement area and angles. Centre of rotation was fixed according to the centre of femur. Femur displacement was fixed at X, Y, Z direction that means $U_1=U_2=U_3=0$. Rotations around X, Y, Z direction were applied. UR_1 (flexion), UR_2 (adduction) and UR_3 (internal rotation) was applied for all 3 models (normal hip, hip with impingement, reshaped hip). UR_1, UR_2, UR_3 were explained in Chapter 5.

A centre of rotation was fixed as the centre of the femur and rotation was applied according to the centre (as it explained in Chapter 5).

6.3.2 Changing the Centre of Rotation

Nine different cases were identified in order to examine the effect of kinematics on the FAI as shown in Table 7. Case 5 was fixed as a control case in which the centre of rotation was set as the centre of the femur. As shown in Figure 39, the centre of rotation was varied in order to consider the effect of the change of the centre of rotation on hip impingement angle and zone. Cases 1, 2, 3 and 4 represented the situation when the centre of rotation was moved towards the acetabulum, whereas in cases 6, 7, 8 and 9 the centre of rotation was moved outwards from the acetabulum as shown in Figure 39.

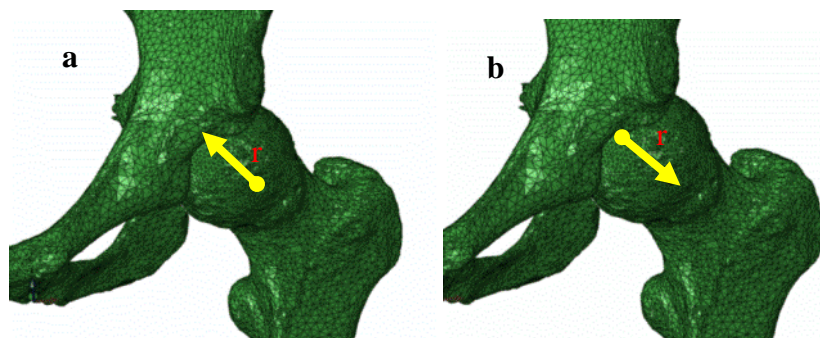


Figure 39: Schematic centre of rotation displacement a) toward (-) and b) outward (+) the acetabulum

Table 7 shows how much (mm) the centre of rotation was moved inward and outward of the acetabulum. The centre of rotation was moved in a radius of sphere which was fixed on top of the femur (as explained in Section 5.4.4)

Table 7: Nine different location of centre of rotation were introduced between femur and acetabulum to examine the effect of kinematic on the FAI

Cases	r (- means toward acetabulum and + means outward acetabulum)
1	-1 mm
2	-2 mm
3	-3 mm
4	-4mm
5	0 mm (centre of rotation fixed as a centre of the femur)
6	+1 mm
7	+2 mm
8	+3 mm
9	+4mm

The coordinate of the centre of rotation (x,y,z) are obtained according to Figure 40 and Eqn. 1. It was assumed that the centre of rotation was changed according to the radius of a sphere on top of the femur as shown in Figure 40. It was assumed that $x=y=z$ (x,y,z coordinate of centre of rotation) to calculate x,y,z . It means that the centre of rotation was changed in x,y,z direction at the same amount. x,y,z can be calculated by knowing r as shown in Eqn. 2. The control case when $r=0$ is the case that centre of rotation is fixed as a centre of the femur. The centre of femur was chosen as a centre of coordinate so $x=y=z = 0$.

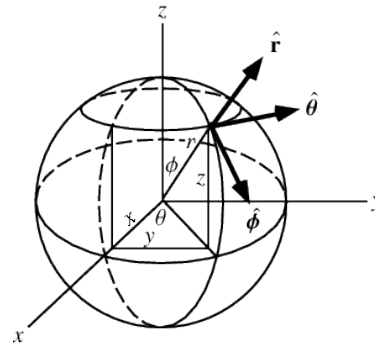
$$r = \sqrt[3]{x^2 + y^2 + z^2} \quad (1)$$

When $x = y = z$ and by knowing r according to Table 7.

$$r = \sqrt[3]{3x^2} \quad (2)$$

By changing r then x, y, z can be calculated as follows:

$r=-4$	$x=y=z= -2.31$
$r=-3$	$x=y=z= -1.73$
$r=-2$	$x=y=z = -1.15$
$r=-1$	$x=y=z = -0.58$
$r=0$	$x=y=z = 0$
$r=+1$	$x=y=z = 0.58$
$r=+2$	$x=y=z = 1.15$
$r=+3$	$x=y=z = 1.73$
$r=+4$	$x=y=z= +2.31$



$$\begin{aligned}
 r=1\text{mm} & \quad x=y=z = \sqrt[2]{3}/3 \\
 r=2\text{mm} & \quad x=y=z = 2\sqrt[2]{3}/3 \\
 r=3\text{mm} & \quad x=y=z = \sqrt[2]{3} \\
 r=4\text{mm} & \quad x=y=z = 4\sqrt[2]{3}/4
 \end{aligned}$$

Figure 40: Calculation of the coordinate of the centre of rotation

6.3.3 Free Centre of Rotation

For all the models (normal hip, hip with impingement, hip after reshaping), a small force was applied to the head of the femur, in this case no assumption was made with respect to the centre of rotation used. The proposed force is the same as that of Asheesh Bedi and his colleagues (Bedi, et al., 2011) (Bedi, et al., 2012). They applied the force, in the anterosuperior direction, on the femur head, to measure the flexion, adduction, and the internal rotation (Bedi, et al., 2011) (Bedi, et al., 2012). A small posteriorly and superiorly directed force was applied to the femur to rotate femur in different direction as shown in Figure 41. This simulation was validated previously by Tannast et al. (Tannast, et al., 2007) and Kubiak-Langer et al. (Kubiak-Langer, et al., 2007). In the simulation given by these researchers, the pelvis was fixed in space, and the femur was free to translate and rotate in all directions. They measured the location of contact between the neck of the femur and the acetabular by using the clock method (as explained in Section 5.4.7) and the location of the contact between the cam and rim lesion was defined (Bedi, et al., 2011) (Bedi, et al., 2012). Furthermore, in this model, the load of about 655N ($F_x = -300$; $F_y = 300$; $F_z = 500$) was applied in an anterosuperior direction to measure the impingement angle.

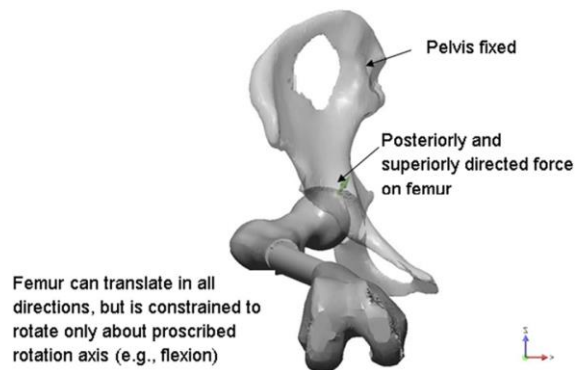


Figure 41: The hip model with the free centre of rotation (Bedi, et al., 2011), (Bedi, et al., 2012)

6.3.4 Hip Models with Soft Tissues

A hip model containing all ligaments and cartilage was made. These were modelled in MIMICs by using MR images (as explained in Chapter 5). UR_1 , UR_2 , UR_3 were defined and U_1 , U_2 , U_3 were not 0. The hip model could freely rotate and the ligaments keep the femur attached to the acetabulum.

6.4 Results

In this section all experiments conducted on the model with and without tissues are repeated with tissues attached. The simulation results of FEA for fixed centre of rotation hip models, different centre of rotation hip models, free centre of rotation hip models and hip models with soft tissues are presented for all three hip models (normal hip, hip with impingement and hip with impingement after reshaping). Figure 42 shows simulation of the flexion angles for the normal volunteer as a sample. Figure 42a shows the normal volunteer hip model flexion when the centre of rotation is fixed. Figure 42b presents the normal volunteer hip model flexion when centre of rotation is free. Figure 42c shows the normal volunteer hip model flexion when the soft tissues are included in the hip model.

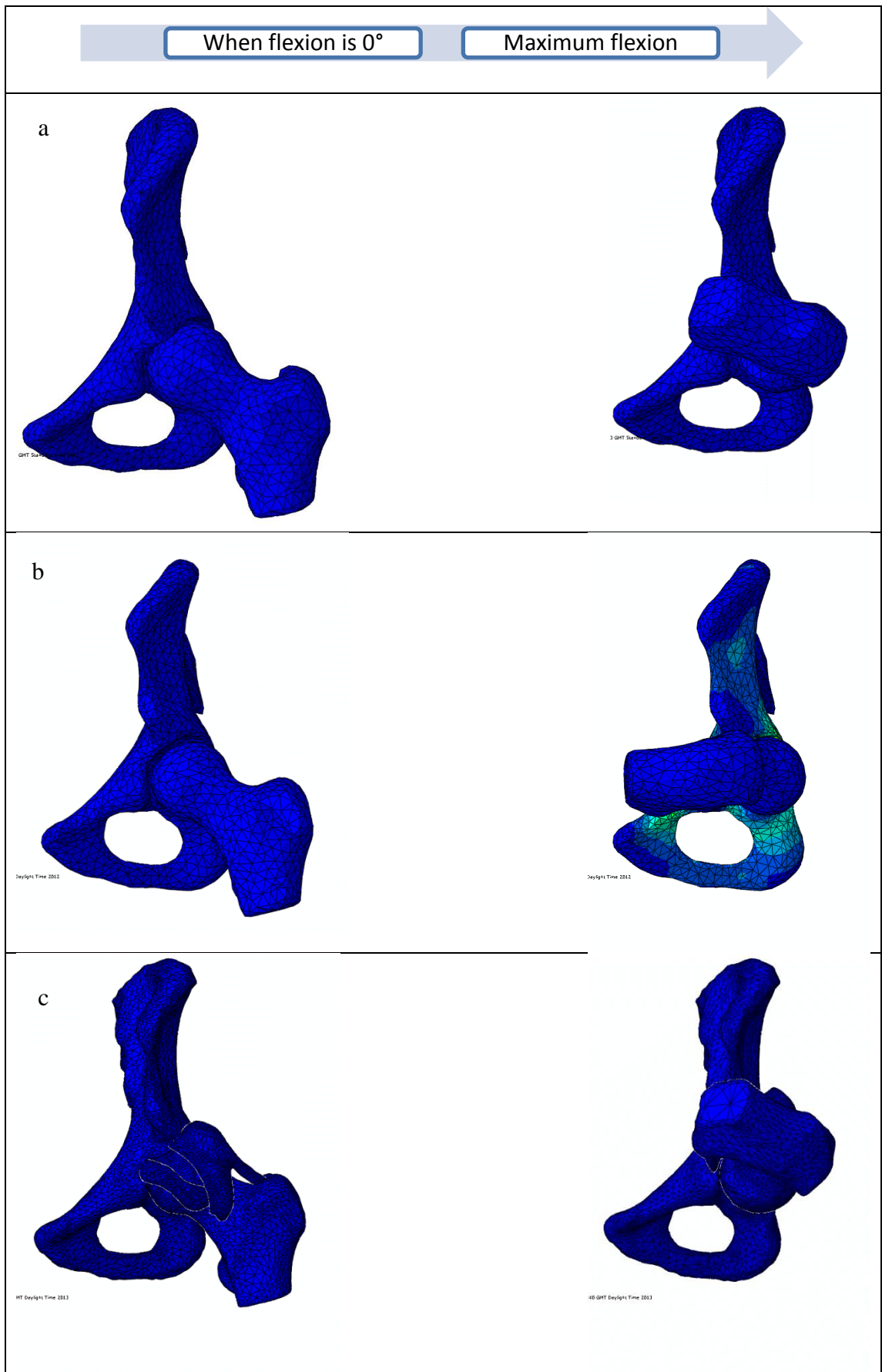


Figure 42: Flexion angles of normal volunteer for a) hip model with fixed centre of rotation, b) hip model with free centre of rotation, c) hip model with soft tissues

Figure 43 shows simulation of the adduction angles in 90° flexion for normal volunteer as a sample. Figure 43a shows the normal volunteer hip model adduction when centre of rotation is fixed. Figure 43b indicates the normal volunteer hip model adduction when centre of rotation is free. Figure 43c demonstrates the normal volunteer hip model adduction when soft tissues are included in the hip model.

Figure 43a indicates the adduction angle in 90° flexion for femur and acetabulum with fixed centre of rotation. Figure 43b indicates the adduction angle in 90° flexion for femur and acetabulum when centre of rotation is not defined and load applied instead of centre of rotation. Figure 43c indicates the adduction angle in 90° flexion for femur and acetabulum with soft tissues.

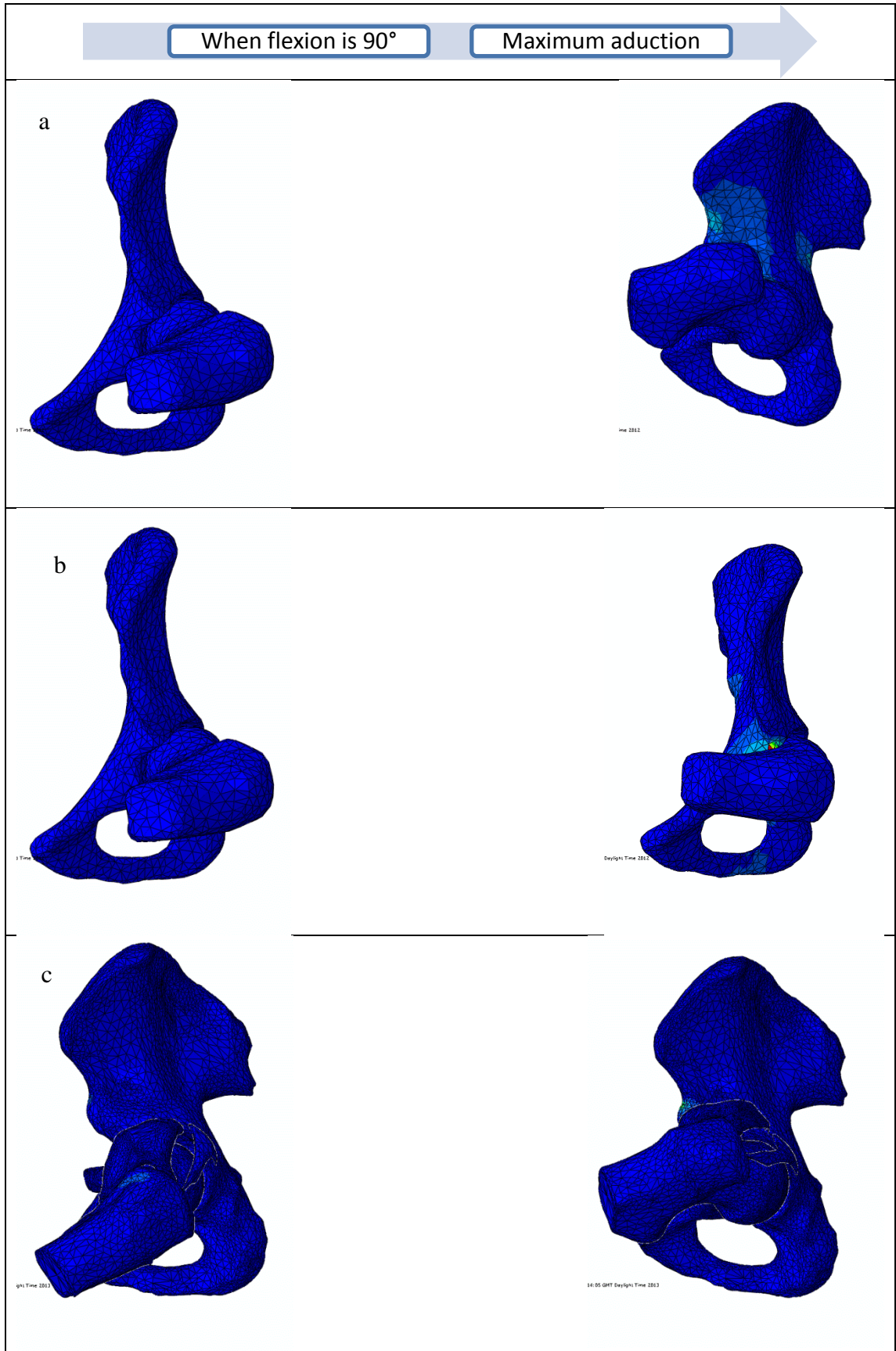


Figure 43: Adduction in 90° flexion a) hip model with fixed centre of rotation, b) hip model with free centre of rotation, c) hip model with soft tissues

Figure 44 shows simulation of the internal rotation angles for normal volunteer as a sample. Figure 44a shows the normal volunteer hip model internal rotation when centre of rotation is fixed. Figure 44b indicates the normal volunteer hip model internal rotation when centre of rotation is free. Figure 44c demonstrates the normal volunteer hip model internal rotation when soft tissues are included in the hip model.

Figure 44a indicates the internal rotation angle in 90° flexion for femur and acetabulum with fixed centre of rotation. Figure 44b indicates the internal rotation angle in 90° flexion for femur and acetabulum when centre of rotation is not defined and load applied instead of centre of rotation. Figure 44c indicates the internal rotation angle in 90° flexion for femur and acetabulum with soft tissues

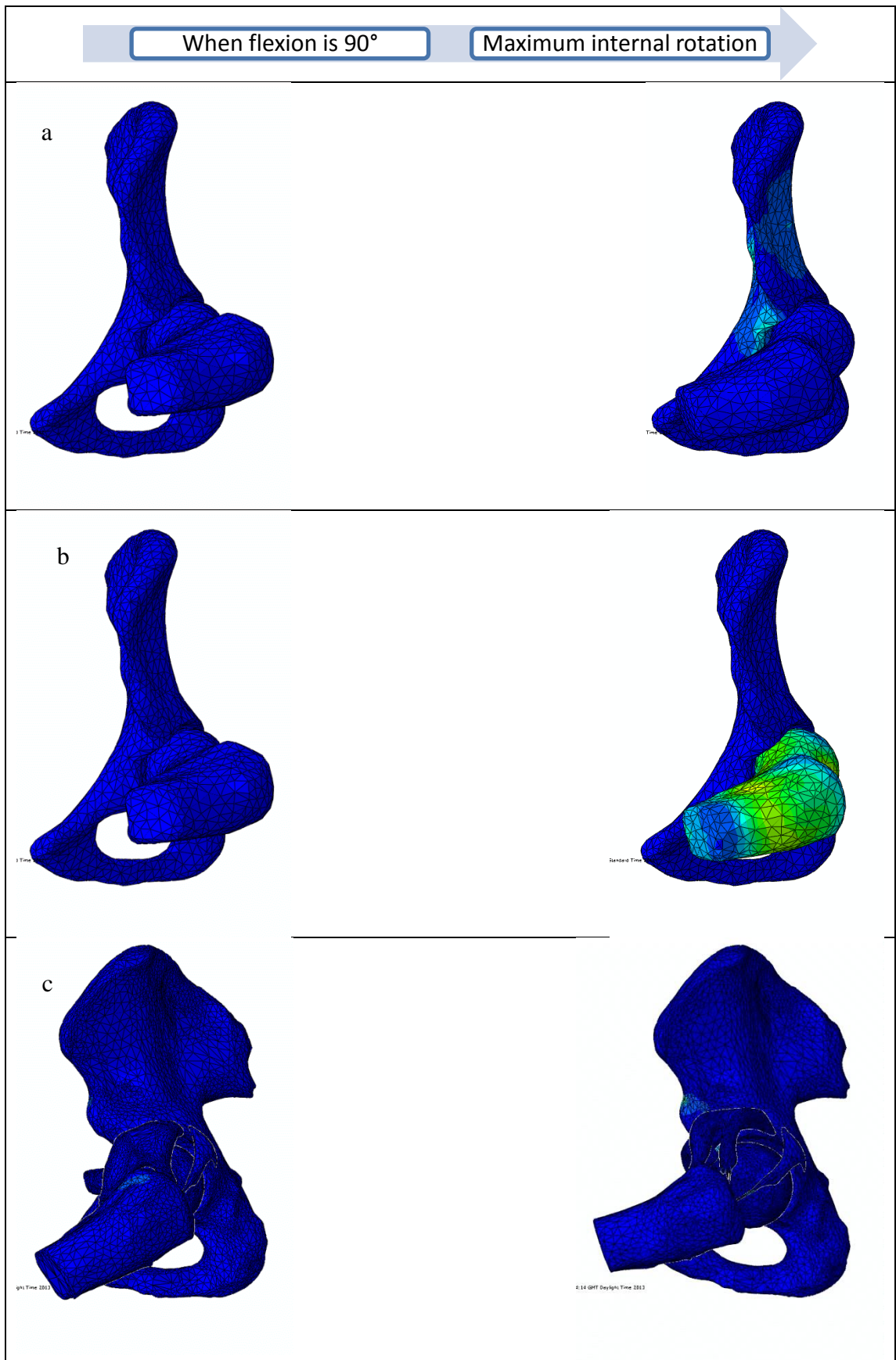


Figure 44: Internal rotation in 90° flexion a) hip model with fixed centre of rotation, b) hip model with free centre of rotation, c) hip model with soft tissues

The results of impingement angle (FADIR test) and impingement zone (clock method) as explained in Chapter 4, are presented for all conditions (fixed centre of rotation, free centre of rotation, different centre of rotation and hip models with soft tissues) and for all of the hip models (normal hip, hip with impingement and hip with impingement after reshaping) in the following sections (Sections 6.4.1, 6.4.2, 6.4.3, 6.4.4)

6.4.1 Fixed Centre of Rotation

The centre of rotation was defined as the centre of the sphere for the normal hip, the hip with impingement and the reshaped hip. Figure 45 shows the stress-flexion angle graphs for all these three hip models. The graph indicates that before impingement happens, stress is 0 and at the impingement angle stress is not 0. Also the graph indicates that stress in impingement zone increases after impingement occurred. In addition, Figures 46 and 47 show the collision detection graphs of adduction and internal rotation for these models. The impingement angle in three different cases for normal, reshaped and patient with impingement are shown in Figure 48.

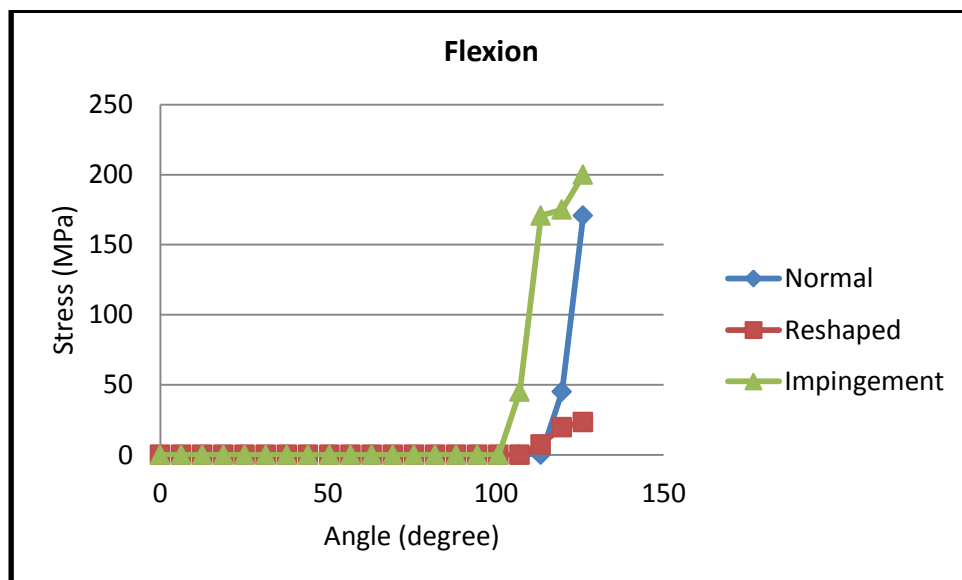


Figure 45: Collision detection for flexion angle of the hip model with fixed centre of rotation

Figure 46 shows the stress-adduction angle graphs for all these three hip models. The graph indicates that before impingement happens, stress is 0 and at the

impingement angle stress is not 0. Also the graph indicates that stress in impingement zone increases after impingement occurred.

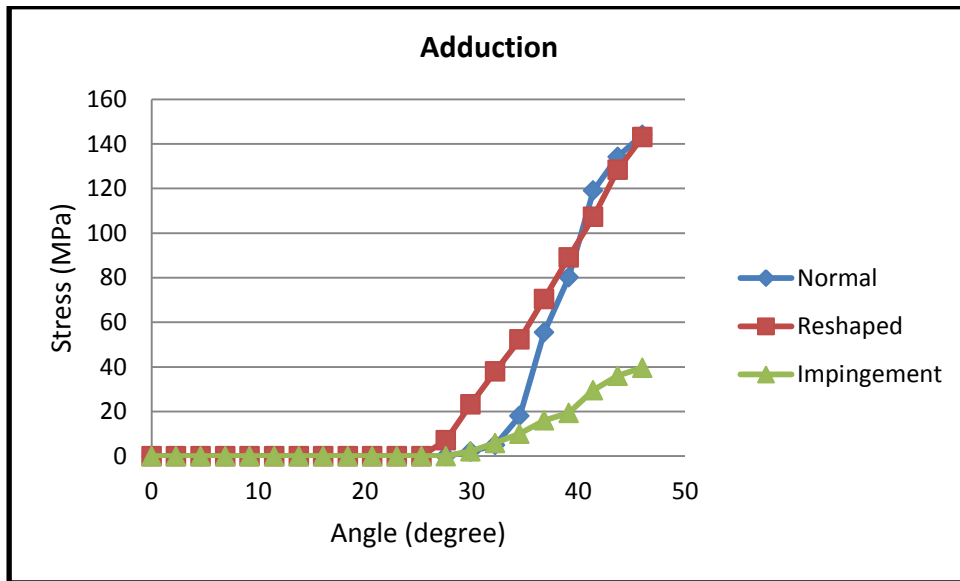


Figure 46: Collision detection for adduction angle of the hip model with fixed centre of rotation

Figure 47 shows the stress-internal rotation angle graphs for all these three hip models. The graph indicates that before impingement happens, stress is 0 and at the impingement angle stress is not 0. Also the graph indicates that stress in impingement zone increases after impingement occurred.

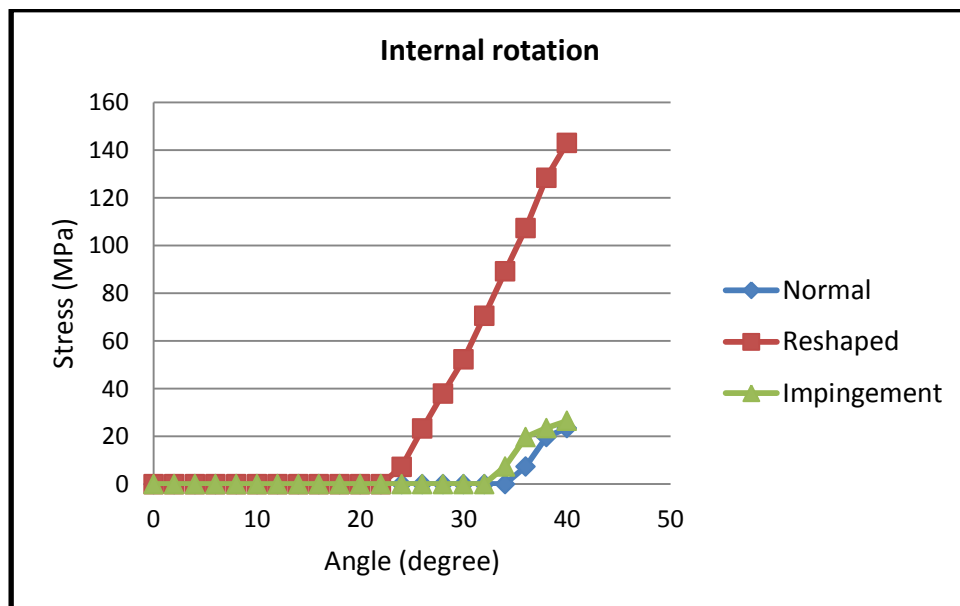


Figure 47: Collision detection for internal rotation angle of the hip model with fixed centre of rotation

Figure 48 presents the range of motion regarding flexion, adduction and internal rotation after reshaping, and compared to the impinged hip. The results are consistent with the findings of Kubiak-Langer et al. (Kubiak-Langer, et al., 2007) who stated that the range of motion improves after a surgical operation. Figure 49 compares the results of our collision detection findings and previous work (Kubiak-Langer, et al., 2007) and our results are similar to those found in these articles ($p \leq 0.001$). This outcome confirms that our results are in line with previously published literature. Figure 48 indicates that ROM improves after reshaping.

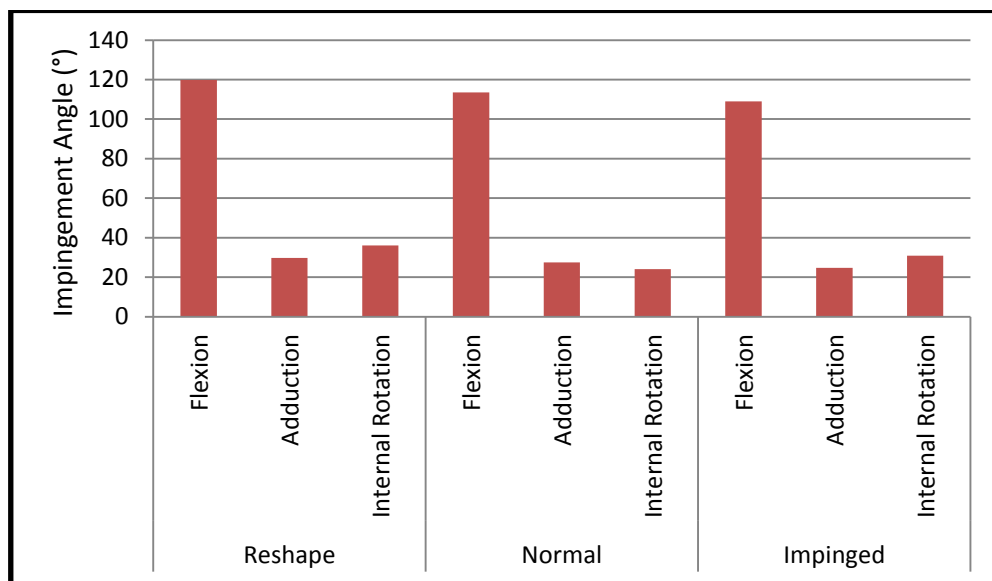


Figure 48: Flexion, adduction, internal rotation for normal, reshaped and impinged model with fixed centre of rotation

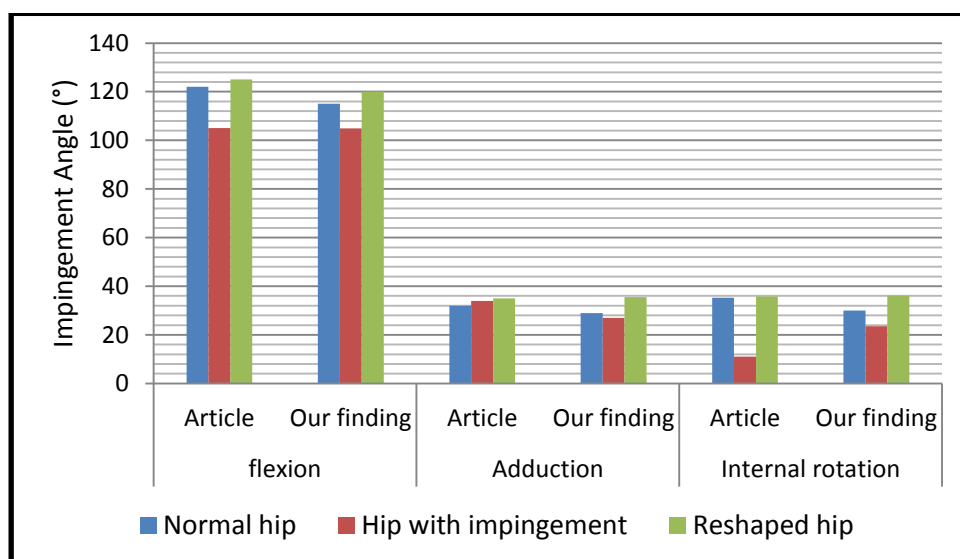


Figure 49: Comparison of our results with previous articles (Kubiak-Langer, et al., 2007) when centre of rotation is fixed to the centre of the femur

6.4.2 Changing the Centre of Rotation

Figure 50 shows the effects of centre of rotation on the range of motion (FADIR test) for a hip with impingement. The centre of rotation was changed in order to measure the changes in the range of motion.

As can be seen from Figures 50, 51 and 52 the range of motion was changed by changing the centre of rotation. That is, changing the centre of rotation inwards and outwards from the acetabulum changes the range of motion, and ROM increases when the centre of rotation shifts inwards and outwards from the centre of the femur.

Figure 50 indicates the effect of centre of rotation on hip flexion angle. As it was explained in Section 6.3.2, the centre of rotation was moved inward and outward of acetabulum. The flexion angle increases by changing the centre of rotation inward and outward of the acetabulum according to the original centre of rotation (centre of fixed sphere on top of the femur). Figure 50 indicates that the flexion angle increase by moving the centre of rotation from original position in hip with impingement, normal hip and hip with impingement after reshaping.

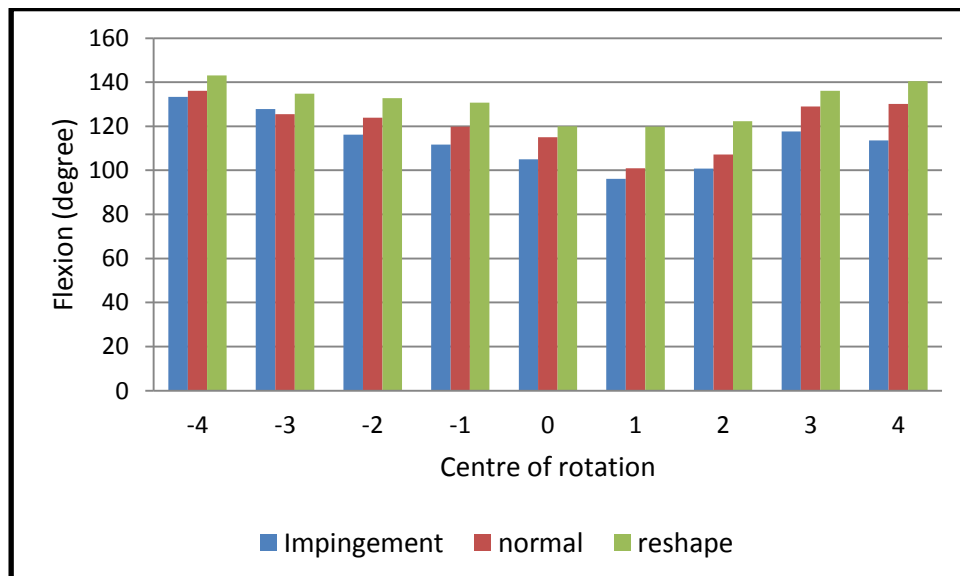


Figure 50: Flexion angle in terms of centre of rotation for the normal, impingement and reshaped hip

Figure 51 indicates the effect of centre of rotation on adduction angle in 90° flexion angle. As it was explained in Section 6.3.2, the centre of rotation was moved inward and outward of acetabulum. The adduction angle in 90° flexion

increases by changing the centre of rotation inward and outward of the acetabulum according to the original centre of rotation (centre of fixed sphere on top of the femur). Figure 51 indicates that the adduction angle in 90° flexion angle increase by moving the centre of rotation from original position in hip with impingement, normal hip and hip with impingement after reshaping.

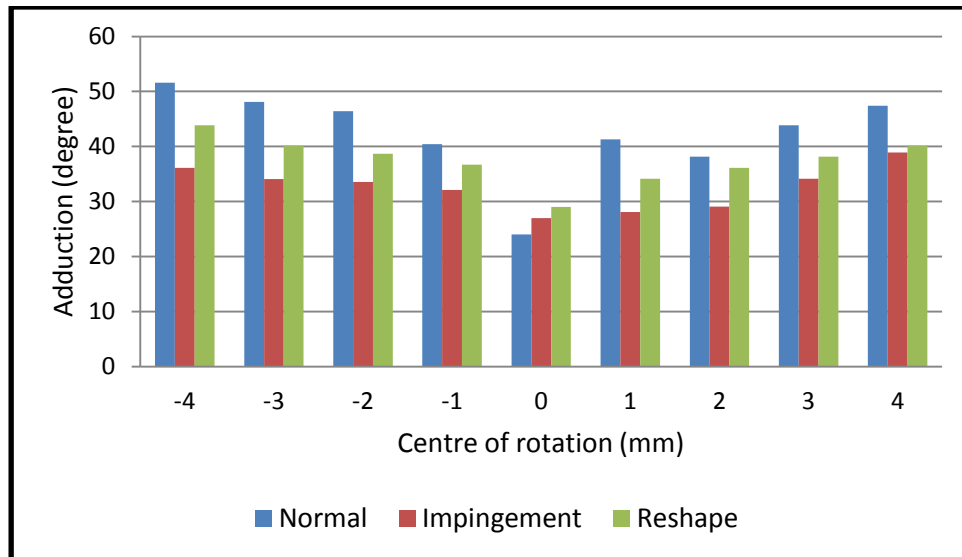


Figure 51: Adduction angle in terms of centre of rotation for the normal, impingement and reshaped hip

Figure 52 indicates the effect of centre of rotation on internal rotation angle in 90° flexion angle. As it was explained in Section 6.3.2, the centre of rotation was moved inward and outward of acetabulum. The internal rotation angle in 90° flexion increases by changing the centre of rotation inward and outward of the acetabulum according to the original centre of rotation (centre of fixed sphere on top of the femur). Figure 52 indicates that the internal rotation angle in 90° flexion angle increase by moving the centre of rotation from original position in hip with impingement, normal hip and hip with impingement after reshaping.

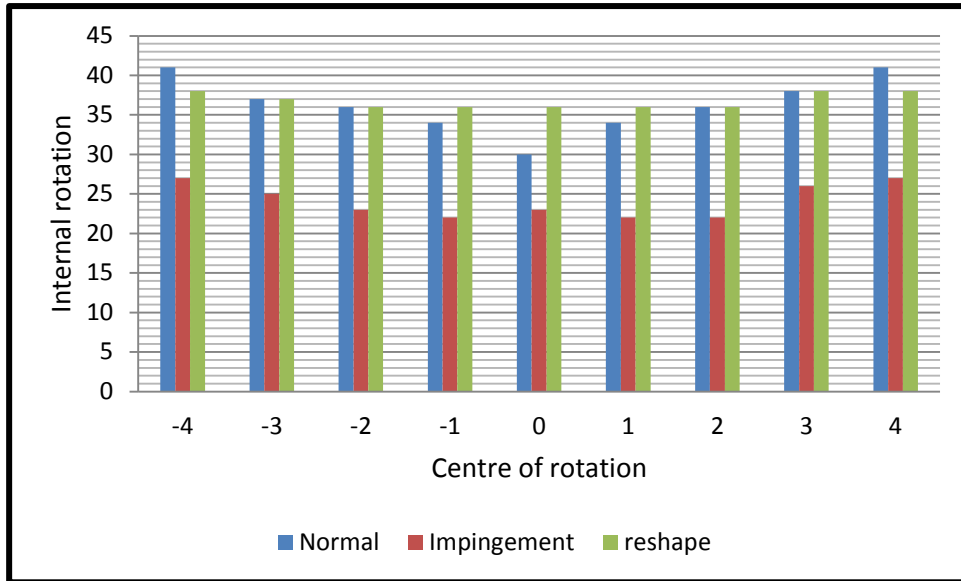
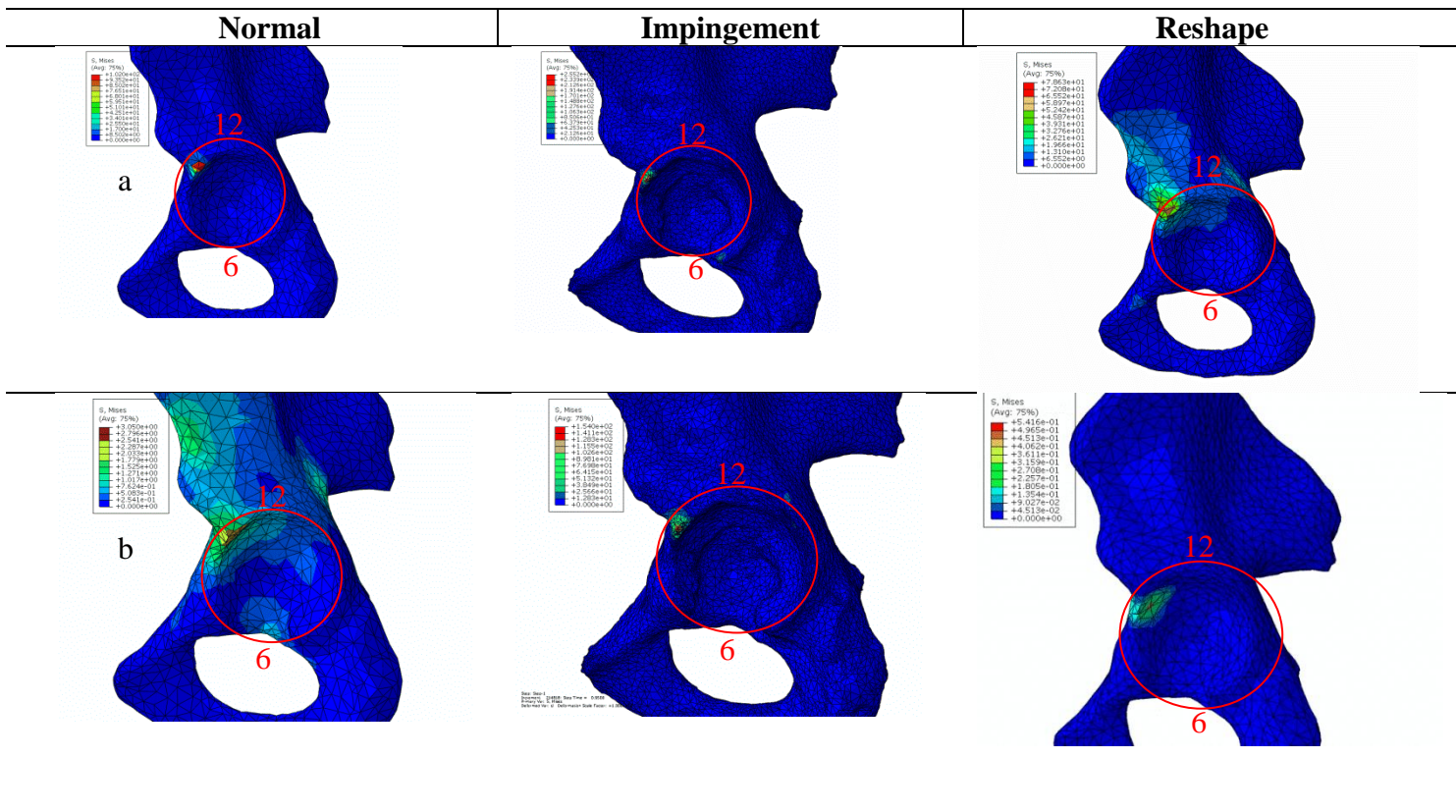
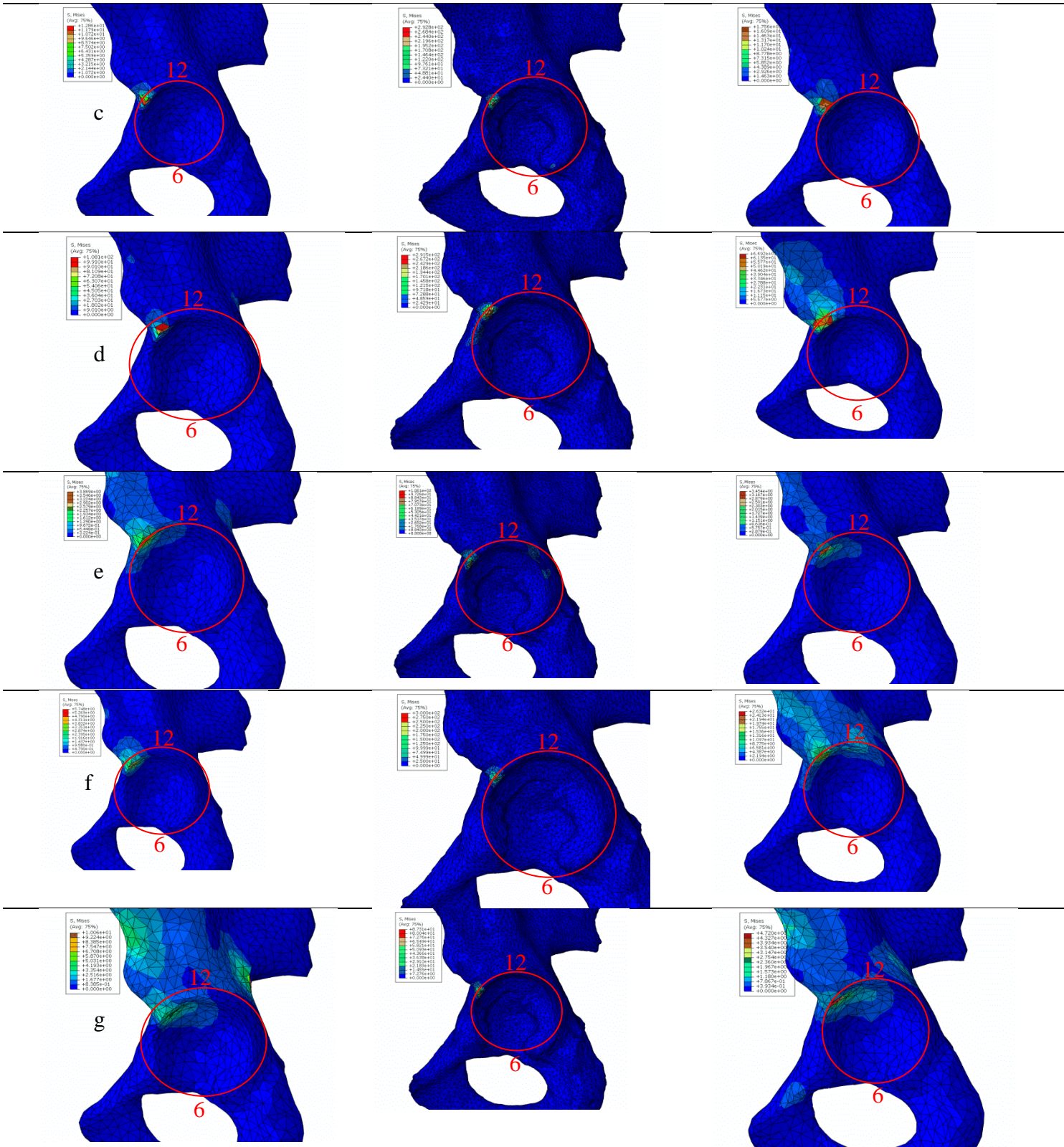


Figure 52: Internal rotation angle in terms of centre of rotation for the normal, impingement and reshaped hip

Figure 53 shows the impingement zone for different centres of rotation. As can be seen, impingement happens at the 11 o'clock point but these are not significant changes in the impingement zone. By changing the centre of rotation (inward and outward at the fixed centre of rotation), the impingement zone becomes wider.





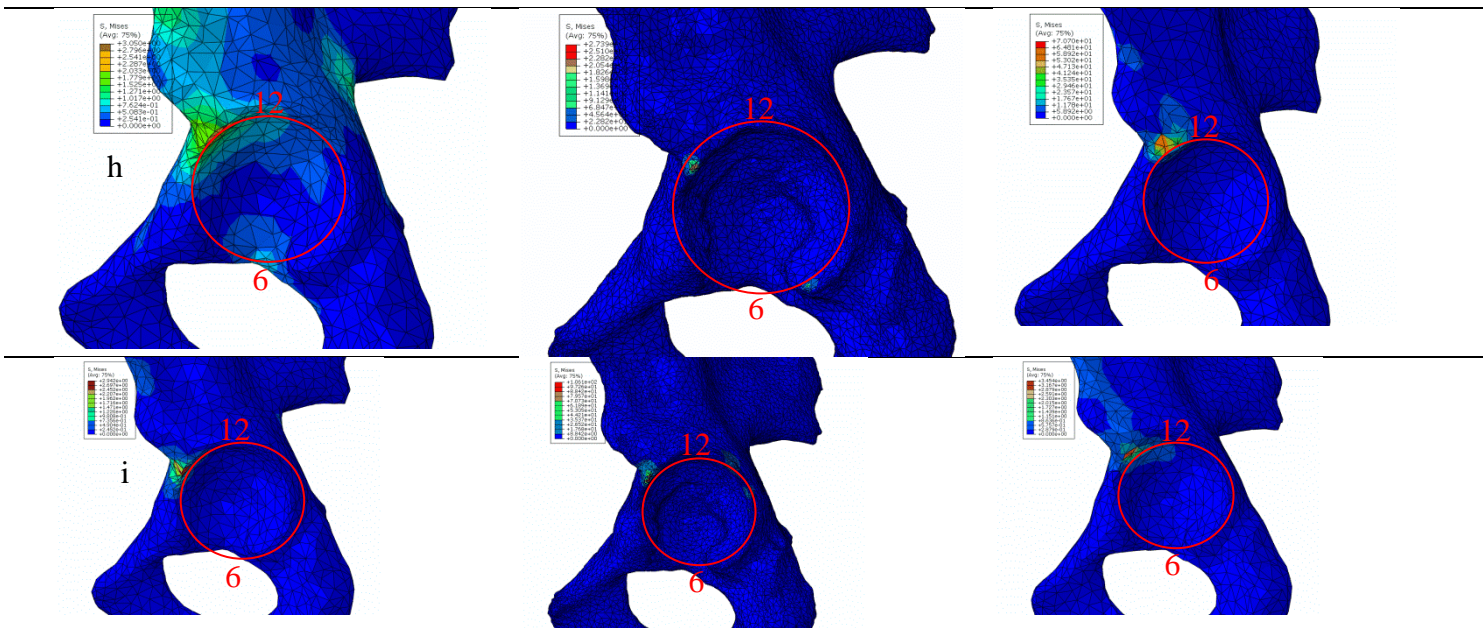


Figure 53: Impingement zone for normal, impingement and reshaped hip with different centre of rotations a) -4mm b)-3mm c) -2mm d)-1mm e) 0mm f) 1mm g) 2mm h) 3mm i) 4mm away from centre of the femur (lateral view of left hip)

6.4.3 Free centre of rotation

Table 8 gives the range of motion for normal, impingement and reshaped hip when the centre of rotation is free. Table 8 indicates the results of impingement angle when the centre of rotation is not defined for normal, impingement and reshaped hip. Table 9 shows the comparison of our free centre of rotation results with previous studies (Bedi, et al., 2011) (Bedi, et al., 2012).

Table 8: Range of motion in free centre of rotation models

	Flexion	Adduction	Internal Rotation
Normal hip	105.194	32	8.61
Hip with impingement	91.37	36.31	10
Reshaped hip	126	47.84	15.97

Table 9: Range of motion in free centre of rotation models according to the previous articles (Bedi, et al., 2011) (Bedi, et al., 2012)

	Flexion	Internal Rotation
Hip with impingement	107±11	19±13
Reshaped hip	111±11	28.4±12

Figure 54 also confirms that impingement zone is at 11 o'clock for free and fixed centre of rotation. However, for the free centre of rotation there is also

impingement at 6 o'clock. This may occur because of free motion of the femur in all direction.

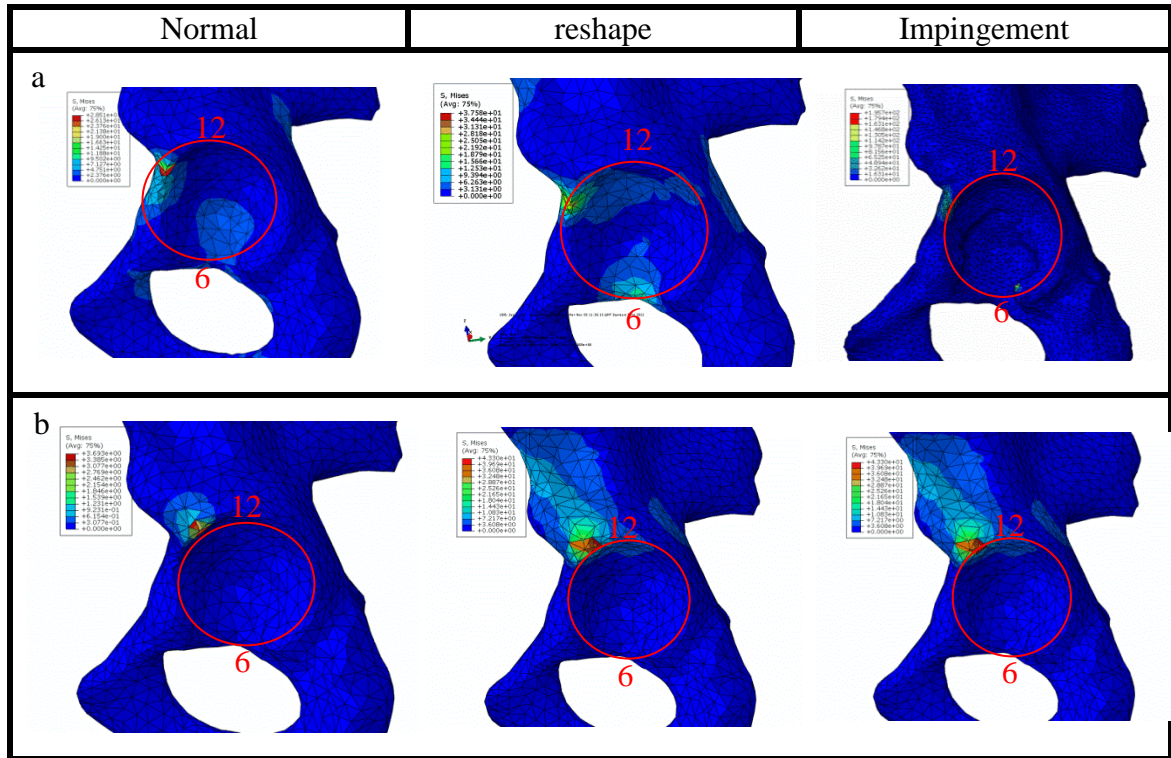


Figure 54: Comparison of impingement zone for normal, impingement and reshaped hip with free and fixed centre of rotation a) free centre of rotation b) fixed centre of rotation (lateral view of left hip)

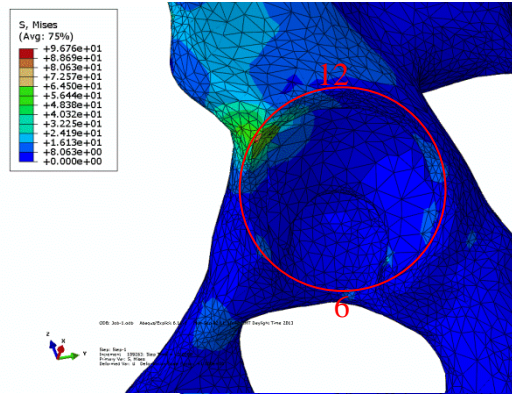
6.4.4 Hip Models with Soft Tissues

Boundary conditions are important in computer-aided programmes. The closer the boundary conditions are to the real hip, the more accurate are the results and the information is closer to the reality. Furthermore, there is a need for computer aided programme for a hip model without simplifications. Table 10 presents the results of flexion, adduction and internal rotation of the hip model with soft tissues. Table 10 presents the impingement angle when soft tissue was added to hip models. Further, Figure 55 shows that impingement happens at the 11 o'clock position for both hip models, with and without the soft tissues.

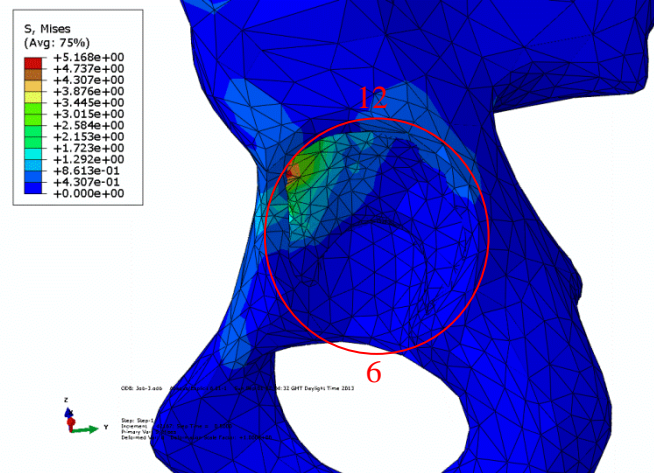
Table 10: Flexion, adduction and internal rotation for hip model with soft tissues

	Flexion	Adduction	Internal Rotation
Normal hip	139	40	30
Hip with impingement	120	23	19
Reshaped hip	146	45	33

Normal



Reshape



Impingement

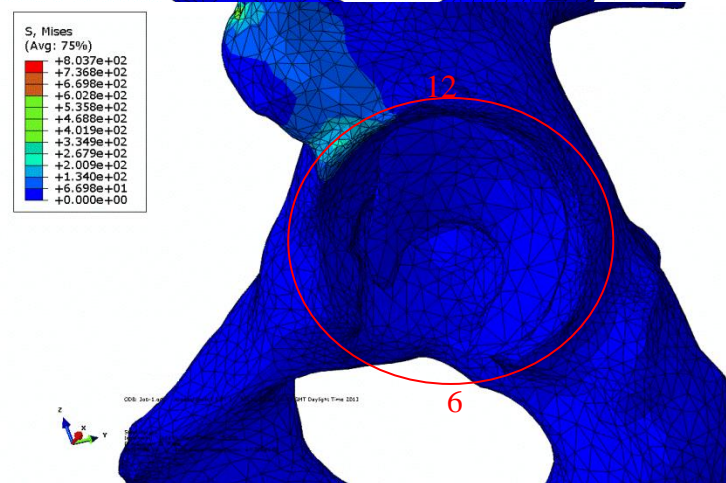


Figure 55: Impingement zone for hip model with soft tissues (lateral view of left hip)

6.5 Discussion

The boundary condition of the hip model is very important when studying the biomechanics of the hip. Moreover, as shown above in Figures 50, 51 and 52, the centre of rotation is an important parameter in hip mechanics. Previously (Kubiak-Langer, et al., 2007) the centre of rotation was fixed at the centre of the femur in computer aided programs in order to detect impingement. The method used in this work to find the impingement angle (flexion, adduction in 90° flexion and the internal rotation in 90° flexion), is quite similar to that adopted in previous studies (Kubiak-Langer, et al., 2007) where the centre of rotation is fixed as shown in Figure 49. According to our findings, hip arthroscopy can help patients with impingement and increase their ROM.

Boundary conditions are one of the main factors in hip modelling. As seen from the results in Section 6.4, flexion, adduction and internal rotation are changed by shifting the centre of rotation, in particular, the impingement angle increases by changing the centre of rotation. Changing the centre of rotation in both directions, i.e. inwards and outwards from the acetabulum increases the impingement angle. Slight changes in the centre of rotation about 4mm significantly change the impingement angle about 20° in flexion, about 20° in adduction and about 10° in internal rotation. The impingement zone is not changed significantly and remains at the 11 o'clock point (impingement zone remains between 10-11 o'clock) for the normal hip, the hip with impingement and the reshaped hip.

Our results for the free centre of rotation, as shown in Table 8, are the same as those found in previous articles (Bedi, et al., 2011), (Bedi, et al., 2012) and Tables 8 and 9 show that the impingement angles are similar to previously reported findings. The results in this instance are slightly lower (about 10° in flexion, about 10° in internal rotation) than for the fixed centre of rotation. The adduction remains the same for the both models. The impingement zone remains the same, being positioned at 11 o'clock. However in this case there is also an impingement at the 6 o'clock point, which may appear to be the consequence of the free centre of rotation, as the hip moves freely in any directions.

The complete model of the hip with soft tissues is closer to the real biological counterpart. This model with cartilage and ligaments is a complete model obtained from a specific patient. In this model, the impingement angles are higher (about 20° in

flexion, about 10° in adduction) than the model without soft tissues. The internal rotation remains the same for both models. The impingement zone remains at the 11 o'clock point.

The important message in this study is that the centre of rotation is an important factor when attempting to detect the impingement angle. As the results of this work, it becomes clear that the soft tissues play an important role in kinematics and this might affect the impingement angle. All previous studies (Kubiak-Langer, et al., 2007), (Tannast, et al., 2007), (Bedi, et al., 2011) (Bedi, et al., 2012), assumed that the centre of rotation was fixed with the centre of femur and in addition these studies (Kubiak-Langer, et al., 2007), (Tannast, et al., 2007), (Bedi, et al., 2011) (Bedi, et al., 2012), did not consider the complete hip model with cartilage, ligaments and muscles, for impingement evaluation. Some researchers claimed that the method chosen regarding fixing the centre of rotation affects the results of the computational modelling of the hip (Arbabi, et al., 2012). Our results show that the point selected for the centre of rotation can change the impingement angle for the hip. Moreover, having a fixed centre or free centre of rotation has an important impact on the impingement angle.

Many computer-based simulations are used to speed up and improve the accuracy of the detection of diseases and to cure them (Arbabi, et al., 2012). But it should be noted that when different methods are applied to selecting the centre of rotation in hip models different values for the same hip model can be obtained (Arbabi, et al., 2012). Some researchers have also obtained range of values for motion when the centre of rotation is changed (Arbabi, et al., 2012).

6.6 Conclusion

Most of the computational models have assumed that the centre of rotation is fixed. The finding of this chapter demonstrates that the centre of rotation can have a considerable effect on impingement angle. The need in clinical study is a complete hip model without simplification and the geometry of the hip. The model should be as faithful to the true geometry as possible.

Changing the boundary conditions, changes the simulation results. One of the main boundary conditions is the centre of rotation which changes the angles obtained in the FADIR test.

Our complete hip model with soft tissues and with free centre of rotation shows slight differences in hip impingement angle in comparison to the hip model with fixed centre of rotation. However, in all cases the impingement zone remains the same. The soft tissues have an impact on impingement angle.

Chapter 7

Experiments on FADIR Test

7.1 Introduction

In this chapter the flexion, adduction in 90° flexion and internal rotation in 90° flexion (three angles in FADIR test) were measured experimentally in order to compare and confirm the results with finite element analysis. Four different measurement devices (Motion Capture, Wiimote control, MotionNode and goniometer) were used to measure FADIR test in volunteers. All devices were calibrated before the main experiments. Validity and reliability all of the experimental measurements were compared.

The Motion Capture lab deploys seven cameras to record six degrees of freedom of special markers that are stack on the body. The Wiimote control and MotionNode record movement by using the gyroscope, accelerometer and magnetometer and both convey information to the computer via Bluetooth (MotionNode Manual, 2013), (Tseklevs, et al., 2012).

Motion Capture is often used in the fields of media, medical sciences, business intelligence and robotics. It is applied for medical purposes to improve the performance of athletes, or to carry out analysis of a patient's gait to assess the condition of their joints and bones. In general, video tracking has been increasingly used in medical systems to aid diagnosis, to speed up the operator's task and to study biomechanic of human body (Maggio & Cavallaro, 2011), (Charbonnier, et al., 2009), (Yahia-Cherif, et al., 2004).

The Wii Remote, also known as the Wiimote, has motion sensing capability, which allows the user to interact with and manipulate items on a screen via gesture recognition and pointing which is achieved through the use of an accelerometer and optical sensor technology. Another feature is its expandability through the use of attachments. Currently Wiimote has been used as rehabilitation device in medical application to help patient with disability (Tseklevs, et al., 2012).

The MotionNode is small, easy to use, and yields accurate orientation tracking results. It is designed for tracking human motion and can be used in motion research, virtual reality, animation and biomechanics as well (MotionNode Manual, 2013).

The hip joint range of motion (ROM) is a basic clinical parameter for diagnosing hip diseases, such as OA (Arokoski , et al., 2004), (Holm , et al., 2000), FAI (Tannast, et al., 2007), (Leunig, et al., 2009), and is relied on for monitoring the efficacy of a treatment (Bierma-Zeinstra, et al., 1998). Hip joint ROM is widely assessed using low-technology tools such as manual goniometers or inclinometers. Goniometric measurements are used by physical therapists to quantify baseline limitations of motion, decide on appropriate therapeutic interventions, and document the effectiveness of these interventions (Gajdosik & Bohannon, 1987).

7.2 Methodology

7.2.1 Subjects

A total of 22 healthy volunteers (12 male and 10 female) were evaluated and assessed under the FADIR test. The three angles of FADIR test (maximum flexion, maximum adduction in 90° flexion and maximum internal rotation in 90° flexion) were measured by all the above measurement methods (Motion capture, Wiimote, MotionNode and goniometer). The information on volunteers is shown in Table 11. All volunteers were provided with a written form for obtaining their informed consent and an information sheet prior to data collection. Ethical approval for the study was received from the ethics committee of Brunel University (Ethical approval and concept form are provided in Appendix F). A physical therapist with 5 years experiences applied FADIR test on each volunteers. Temperature of the lab was controlled and fixed on 10° C. The volunteer were asked to lie down in supine position and flex their

hip 5-10 times before starting the experiments. Each motion for each volunteers were taken three times and one out of three was chosen. There was a five minutes gap between each motions, for example after finishing three times flexion continuously and before starting three times adduction, there was five minutes gap. Start and end takes for each device was announced by the physical therapist. The volunteers were chosen from the same age and same BMI (body mass index) to keep the effect of age and BMI as low as possible. However, reliability and validity of each volunteer was compared with each other.

Table 11: General information of all volunteers

Volunteer Information	Gender	Number	Age	BMI(Kg/m ²)
	Female & Male	22	30±2	23.61±3.463

7.2.2 Motion Capture

The Motion Capture lab used in this work had 7 cameras (model 141 RC Manfrotto) to monitor motion. Vicon Blad 1.7.0 software was used to define the 3D space in relation to physical boundaries of the room. Figure 56 shows the Motion Capture lab. According to the Motion Capture manual the maximum error in Motion Capture is sub millimetre (Motion Capture Manual , 2013).

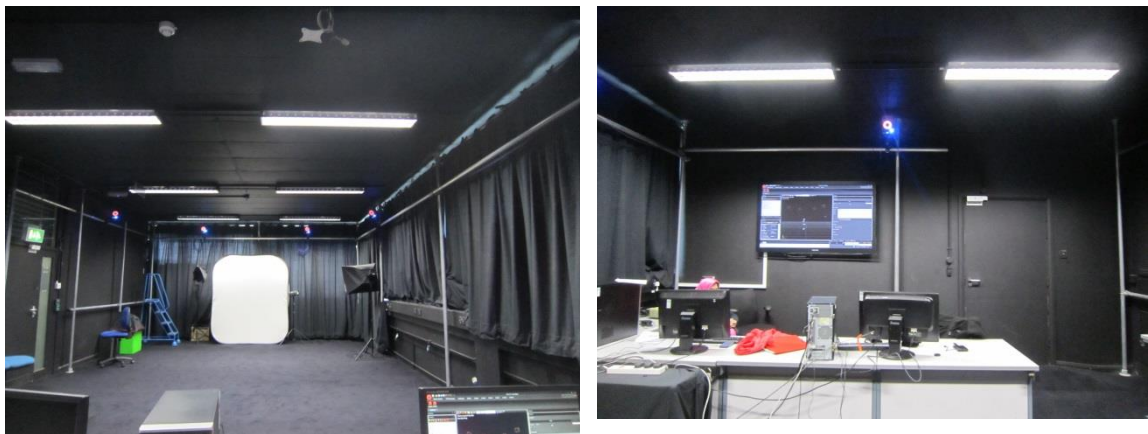


Figure 56: General view of the Motion Capture lab with seven cameras and large screen to show human motion

The Vicon switch was turned on and left for 2 minutes to complete the booting up process. If connecting key is pressed too soon, markers and some cameras may be missed on Vicon blade software.

The Vicon switch connects all cameras to the computer and it supplies power to them. Then MOCAP and Blade software should be started. “Connect” button on top left window of the Blade software was clicked as shown in Figure 57.

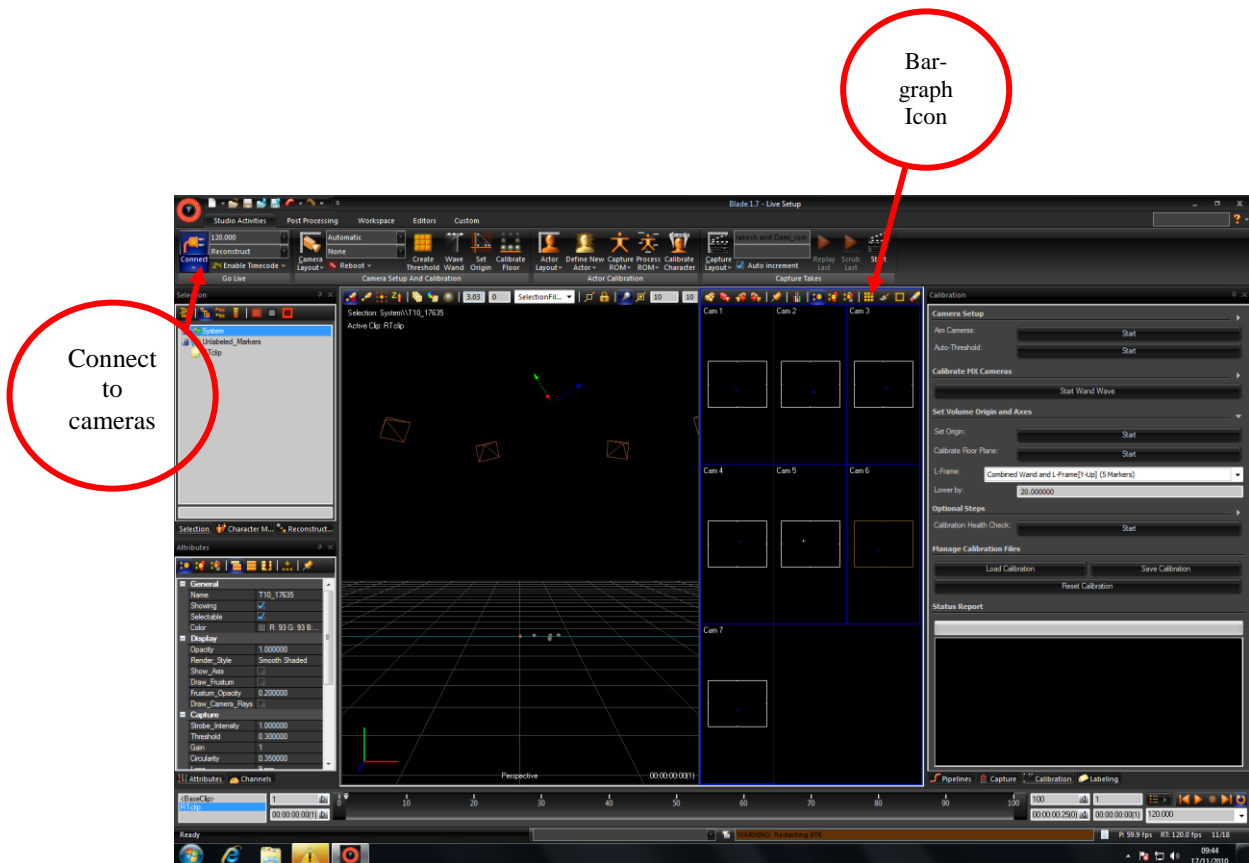


Figure 57: Vicon Blade software window start-up

After connecting to all cameras, it is important to check the camera hardware settings to reduce the noise. To do this, the following steps were applied;

1. Dual viewport () should be selected as shown in Figure 58.
2. By choosing dual view port the bar-graph icon as shown in Figure 58 in red rectangle appears for each camera. This shows bar graph of individual camera such as strobe, gain and so on as shown in Figure 58. There are recommended settings for the capture lab (recommended setting are the highest value on each parameter). Therefore

all cameras must be reset to these settings before use. If this is not done, it may affect the camera sensitivity and affect the Motion Capture footage.

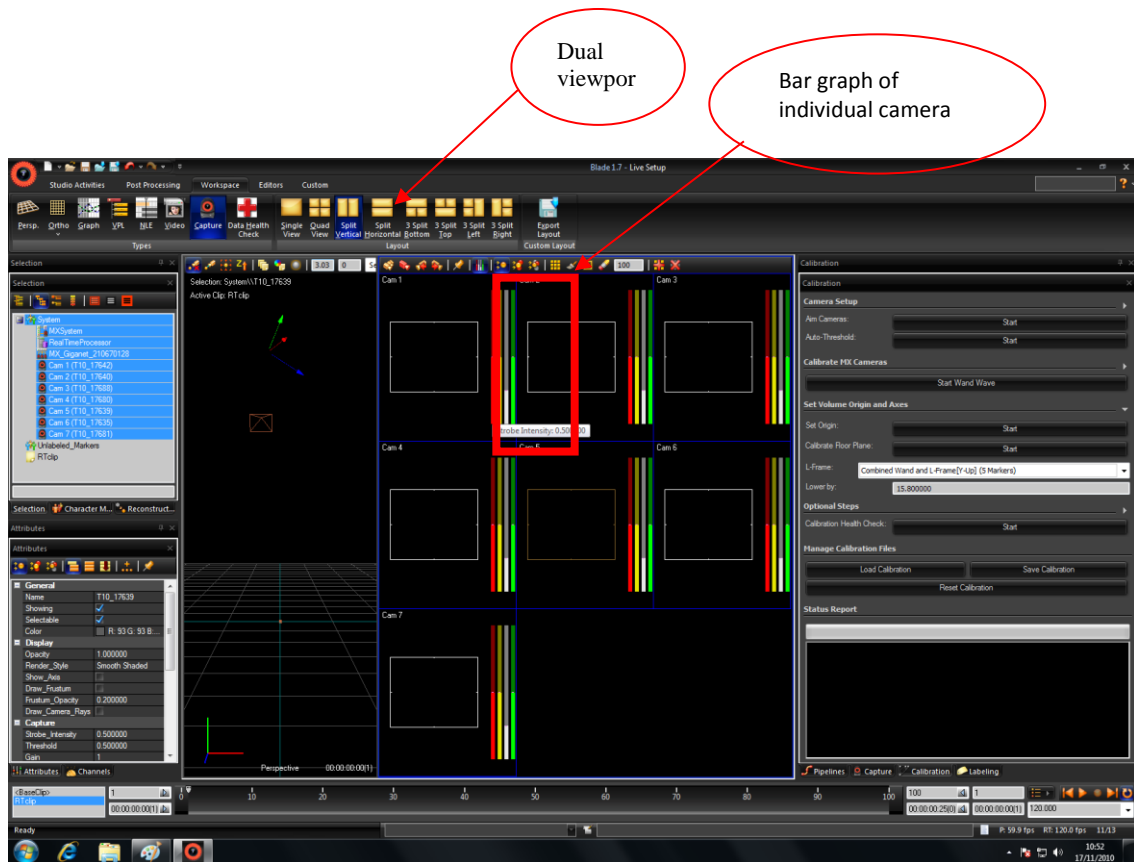


Figure 58: Camera hardware reset

7.2.2.1 Calibration

Calibration of the system must be taken before taking any Motion Capture footage; otherwise the system will not have any references to work with. Also the system cannot correlate the real marker position to that of 3D space in the software.

Three calibration parameters have to be specified;

1. 3D Space
2. Origin
3. Floor Plane

The calibration is typically done in the above order. A good calibration data will lead to achieving accurate Motion Capture data.

3D Space Calibration

The 3D space calibration was performed using the 5 marker T-shape wand. The wand should be placed in the middle floor of the Motion Capture area. The “calibration” icon as shown in Figure 59 started and then stopped the calibration. The wand was moved around the lab room to define the minimum and maximum 3D space area. The software processes all the marker reference points in the 3D workspace automatically after clicking on “stop calibration” icon. Also the Vicon Blade software informs user if the calibration is poor then these steps need to be repeated.

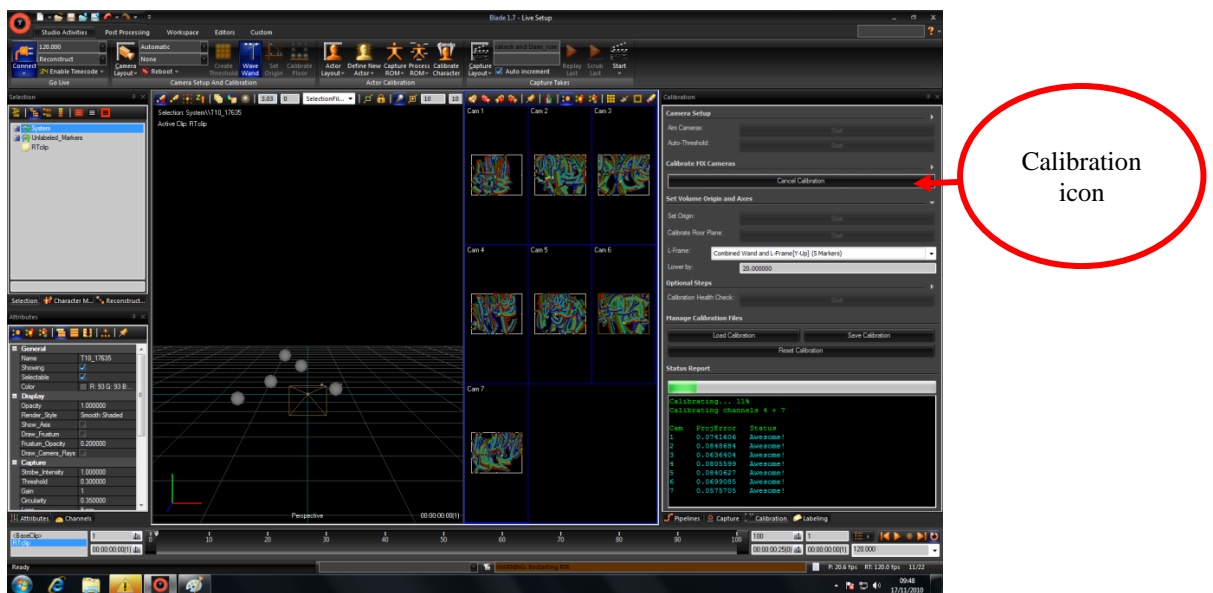


Figure 59: 3D space calibration window

Origin Calibration

To define the origin, the wand must be placed somewhere in the middle of the room (it does not have to be perfectly central). The direction of the handle piece defined the positive and negative X and Y axis. The wand’s handle points to the negative direction.

The “origin calibration” icon was selected and left for 30s to calibrate origin. All cameras should be above the floor plane on the screen and become located as set up in Motion Capture lab.

Floor Plane Calibration

Either the wand or markers can be used to calibrate the floor plane. Placing markers around the floor gives better representation of the lab floor since it is not perfectly levelled as in the software domain. The “floor plan calibration” icon was used to calibrate floor. The floor offset value should be adjusted until the markers touching the floor as shown in Figure 60.

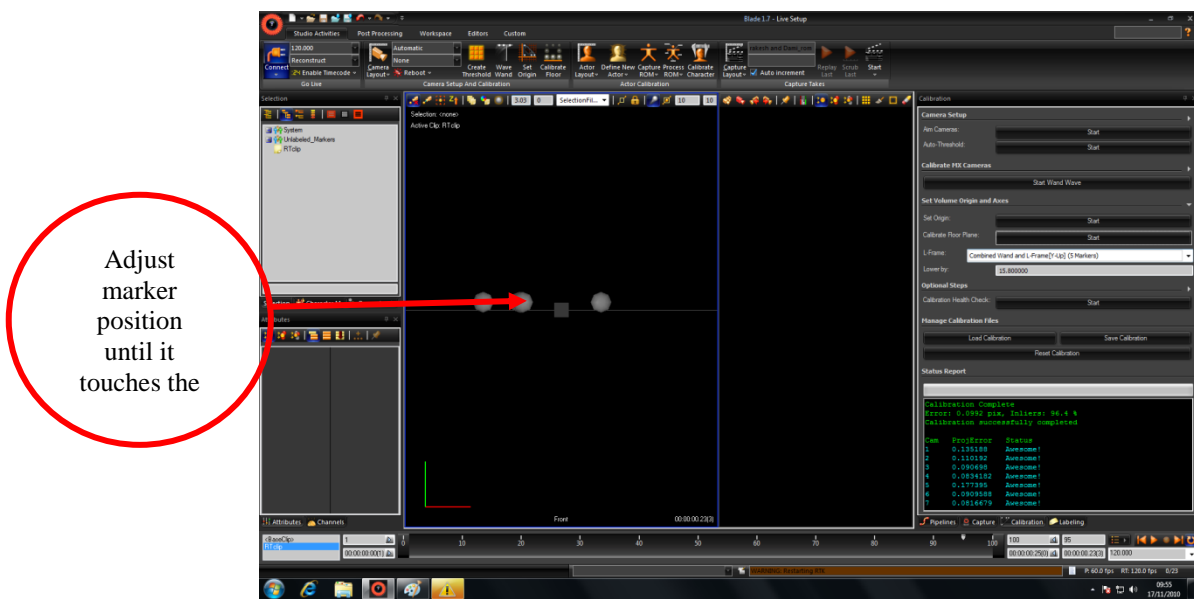


Figure 60: Floor calibration marker view

7.2.2.2 Accuracy of Motion Capture

After calibration, a simple test was done to calculate the accuracy of Motion Capture. The Motion Capture was used as a reference method in our experimental to compare the validity of the other devices. Movement of hand as shown in Figure 61 was measured by Motion Capture and a simple ruler (a simple ruler has accuracy of 0.1 cm). The simple distance was measured by ruler and Motion Capture. Both results were compared to obtain the accuracy of Motion Capture. Figure 61 shows the sensors and hand movement to measure a distance from position 1 to position 2 by ruler and Motion Capture. Table 12 compares the results of both methods.

Accuracy of Motion Captured was measured by a simple test.

Distance of marker ‘a’ as shown in Figure 61 from position 1 to 2 is equal to $\sqrt{(x_1 - x_2)^2 + (y_1 - y_2)^2 + (z_1 - z_2)^2}$. x_1, y_1, z_1 are coordinate of marker “a” at position 1 and x_2, y_2, z_2 are coordinates of marker “a” at position 2.

Table 12: Comparison of Motion Capture and ruler measurement (n=10)

Measured by ruler	Measured by Motion Capture
Mean value \pm SD	Mean value \pm SD
25.7 \pm 2 cm	25.874 \pm 0.827 cm

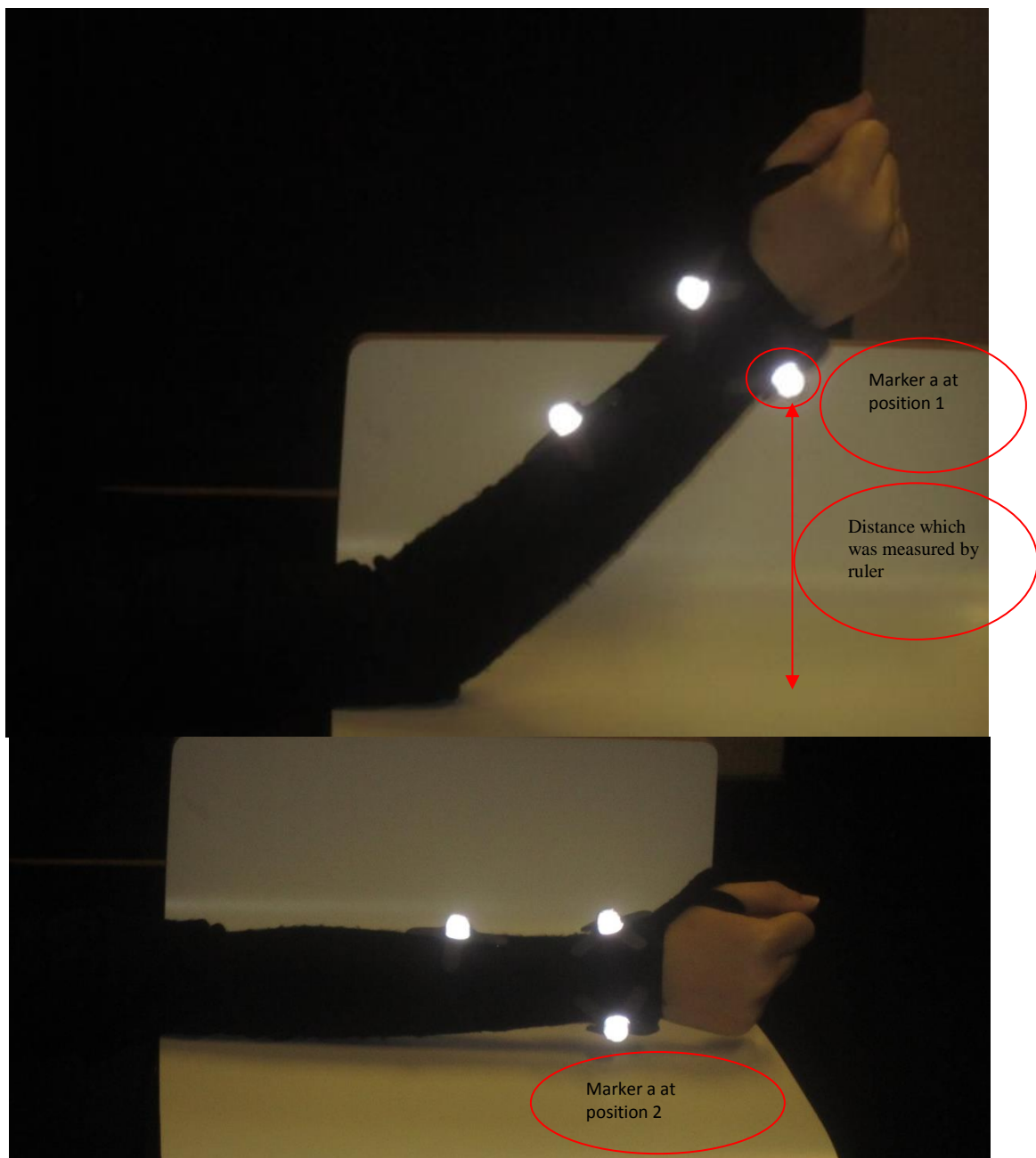


Figure 61: Measuring the accuracy of the Motion Capture and movement of the hand was measured by ruler

7.2.2.3 Data Recording

According to the anatomy palpation (anatomy palpation shows places of the bone on the skin) and surface markings, places of marker were chosen on the skin (Field & Hutchinson, 2006) (more information is provided in Appendix C). Six markers (Appendix C) were used to capture the motion of hip as shown in Figure 62. Two markers were placed on the ankle joint. One of them was placed anteriorly and the other one laterally. Two markers were placed on the knee joint. One of them was placed anteriorly and the other one laterally. One of the markers was placed at the middle of the femur laterally and the last marker was placed on the iliac crest laterally.

The result of each marker was demonstrated according to their 3D coordinate in the space. The coordinate of the markers were sampled at equal time intervals.

Three angles of FADIR test was measured for each volunteer. The volunteer hip was first flexed to measure flexion and to measure first angle. The volunteer hip was first flexed 90° and then adducted to the maximum range and to measure adduction to measure second angle. The volunteer hip was first flexed 90° and then internally rotated to the maximum range and to measure internal rotation to measure third angle.

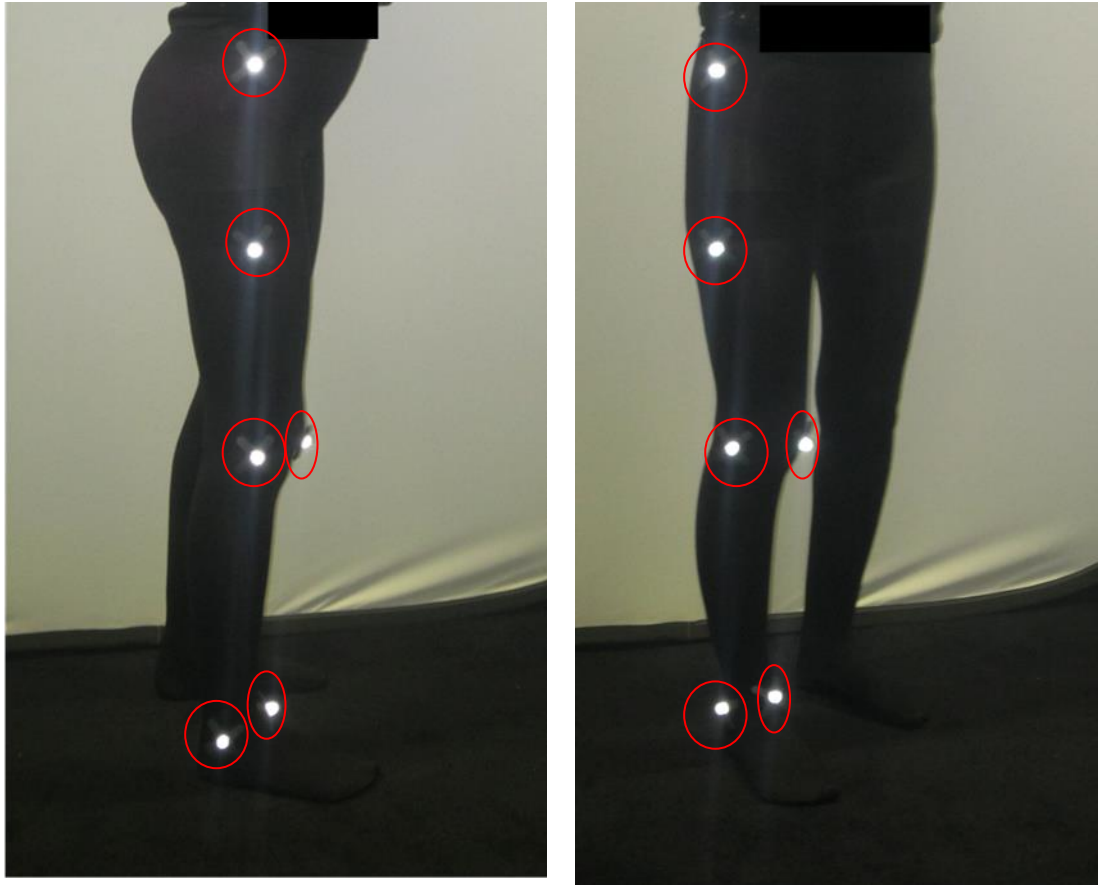


Figure 62: Marker places on leg to measure flexion, adduction and internal rotation of hip

The volunteer was asked to lie down in the supine position as shown in Figure 63c. The physical therapist flexed the volunteer hip until maximum degree as shown in Figure 63d. The maximum flexion degree varies between individuals. The take was started when the volunteer was in the supine position and stopped when the volunteer hip was flexed until maximum degree. Marker “a” was placed in the lateral view of knee joint. Marker “a” at the maximum flexion was called “a’”. The reference marker which was placed on the iliac crest at the lateral view was called “b”. Motion Capture lab recorded the coordinate of markers from the start of the take to the end of the take. (A sample of raw data is provided in Appendix D.1)

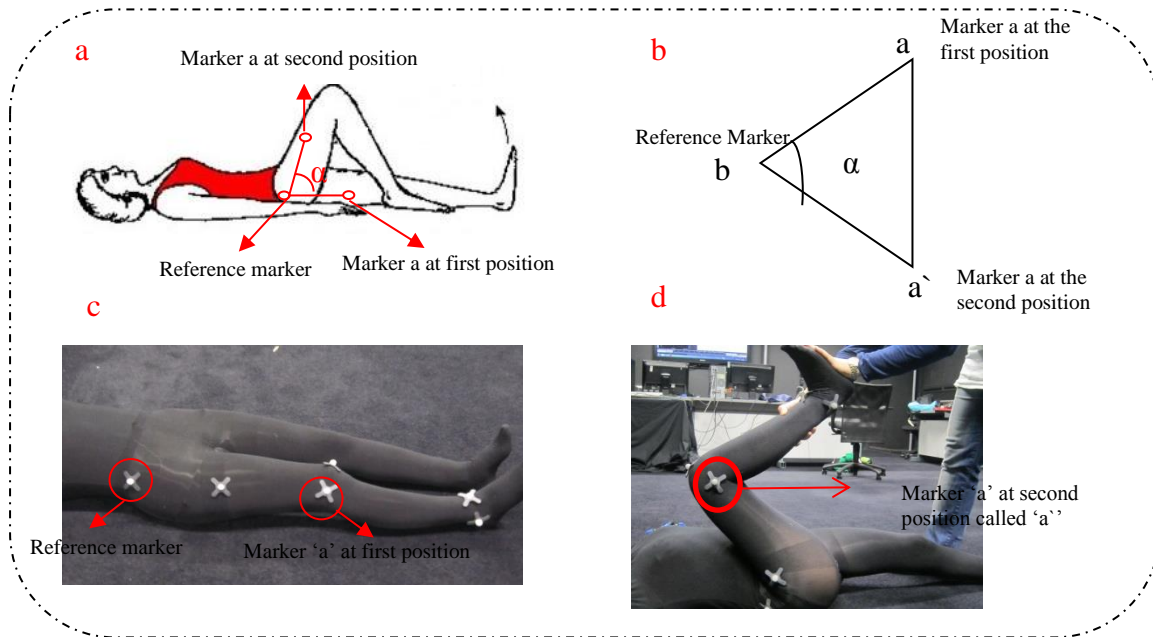


Figure 63: Measurement of flexion angle in the Motion Capture lab

Figures 63a and 63b show how flexion was measured in hip by measuring the angle of a triangle which is made from 3 points (marker “a”, marker “a`” and marker “b”). Equations 3, 4, 5 and 6 (Sobel & Lerner, 1991) show consequently how the angle of flexion was calculated by knowing the coordinate of markers “b”, “a” and “a`”. Equations 3, 4 and 5 demonstrate how to calculate triangle sides ($|ba|$, $|ba`|$ and $|aa`|$) by knowing the coordinates of “a”, “b” and “c”. Eqn. 6 shows how to calculate the maximum flexion angle by knowing the sides of triangle which is made by marker “a”, “b” and “c”.

$$|ba| = \sqrt{(x_a - x_b)^2 + (y_a - y_b)^2 + (z_a - z_b)^2} \quad (3)$$

$$|ba`| = \sqrt{(x_{a`} - x_b)^2 + (y_{a`} - y_b)^2 + (z_{a`} - z_b)^2} \quad (4)$$

$$|aa`| = \sqrt{(x_{a`} - x_a)^2 + (y_{a`} - y_a)^2 + (z_{a`} - z_a)^2} \quad (5)$$

$$\cos \alpha = \frac{(|ba|^2 + |ba`|^2 - |aa`|^2)}{2 |ba| |ba`} \quad (6)$$

Same procedure as mentioned for flexion was applied for adduction as shown in Figure 64. Maximum adduction angle in 90° of flexion was measured. The volunteer was asked to lie down in the supine position as shown in Figure 63c. The physical therapist flexed the volunteer hip until 90° as shown in Figure 64b then adducted the volunteer hip until maximum degree as shown in Figure 64c. The maximum adduction degree varied between individuals. The take was started when the volunteer's hip was in the 90° flexion and stopped when the volunteer's hip was adducted until maximum degree. Marker "a" was placed in the lateral view of knee joint. Marker "a" at the maximum adduction was called "a'". The reference marker which was located on the iliac crest at the lateral view was called "b". Motion Capture lab recorded the coordinate of markers from start of the take to the end of the take. Maximum adduction in 90° flexion was calculated by knowing the coordinate of "a'", "a", "b" and using Equations 3, 4, 5 and 6.

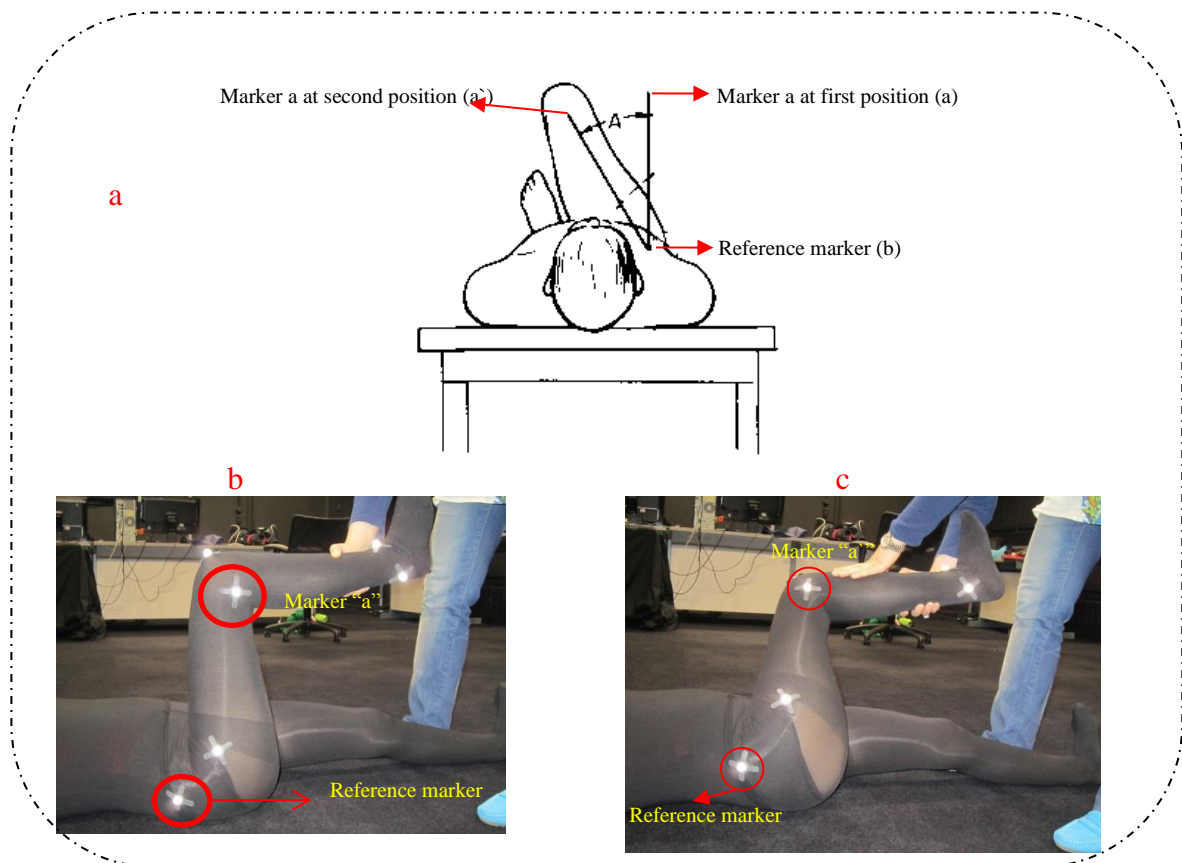


Figure 64: Measurement of adduction in 90° flexion angle in the Motion Capture lab

Same procedure as mentioned for flexion was applied for internal rotation in 90° flexion as shown in Figure 65. Maximum internal rotation angle in 90° of flexion was measured. The volunteer was asked to lie down in the supine position as shown in Figure 63c. The physical therapist flexed the volunteer hip until 90° as shown in Figure 65b then internally rotated the volunteer's hip until maximum degree as shown in Figure 65c. The maximum internal rotation degree varies between individuals. The take was started when the volunteer's hip was in the 90° flexion and stopped when the volunteer hip was internally rotated until maximum degree. Marker "a" was placed in the anterior view of ankle joint. Marker "a" at the maximum internal rotation was called "a'". The reference marker which was placed on the knee joint at the anterior view was called "b". Motion Capture lab recorded the coordinate of markers from start of the take to the end of the take. Maximum internal rotation in 90° flexion was calculated by knowing the coordinate of "a", "a'", "b" and using Equations 3, 4, 5 and 6.

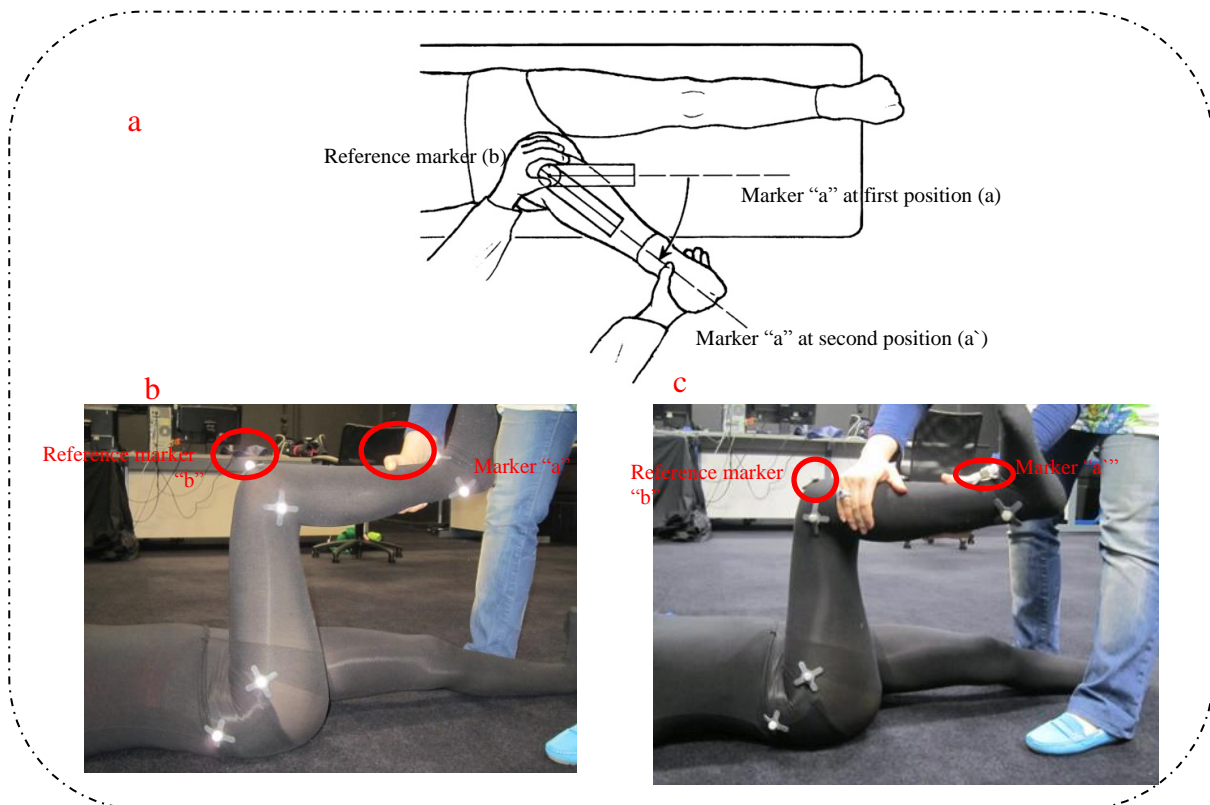


Figure 65: Measurement of internal rotation in 90° flexion angle in the Motion Capture lab

7.2.3 Wii-Remote

Nintendon Wiimote was used to measure flexion, adduction in 90° flexion and internal rotation in 90° flexion in 22 normal volunteers.

The developed Wiimote system as represented in Figure 66 include three parts: data collection, data fusion and motion tracking algorithm and 3D visualization. The data access operation mainly contains functions that allow the application to obtain sensor data sent from multiple Wiimote plus to personal computer by Bluetooth communication. In the middle part, the received information from Wiimote sensors undergo a process of smoothing and multiplexing using a data fusion algorithm in order to achieve higher accuracy and precision. The end results are mapped into quaternion forms that translate the orientation of a constructed 3D body model and also from the data structure. The top part in Figure 66 embraces the dynamic physical simulation of a 3D animation in real-time (Warland, et al., 2012), (Tsekleves, et al., 2012). The obtained data is in quaternion orientation. Quaternion value was converted to the Euler angles (Madgwick, 2010).

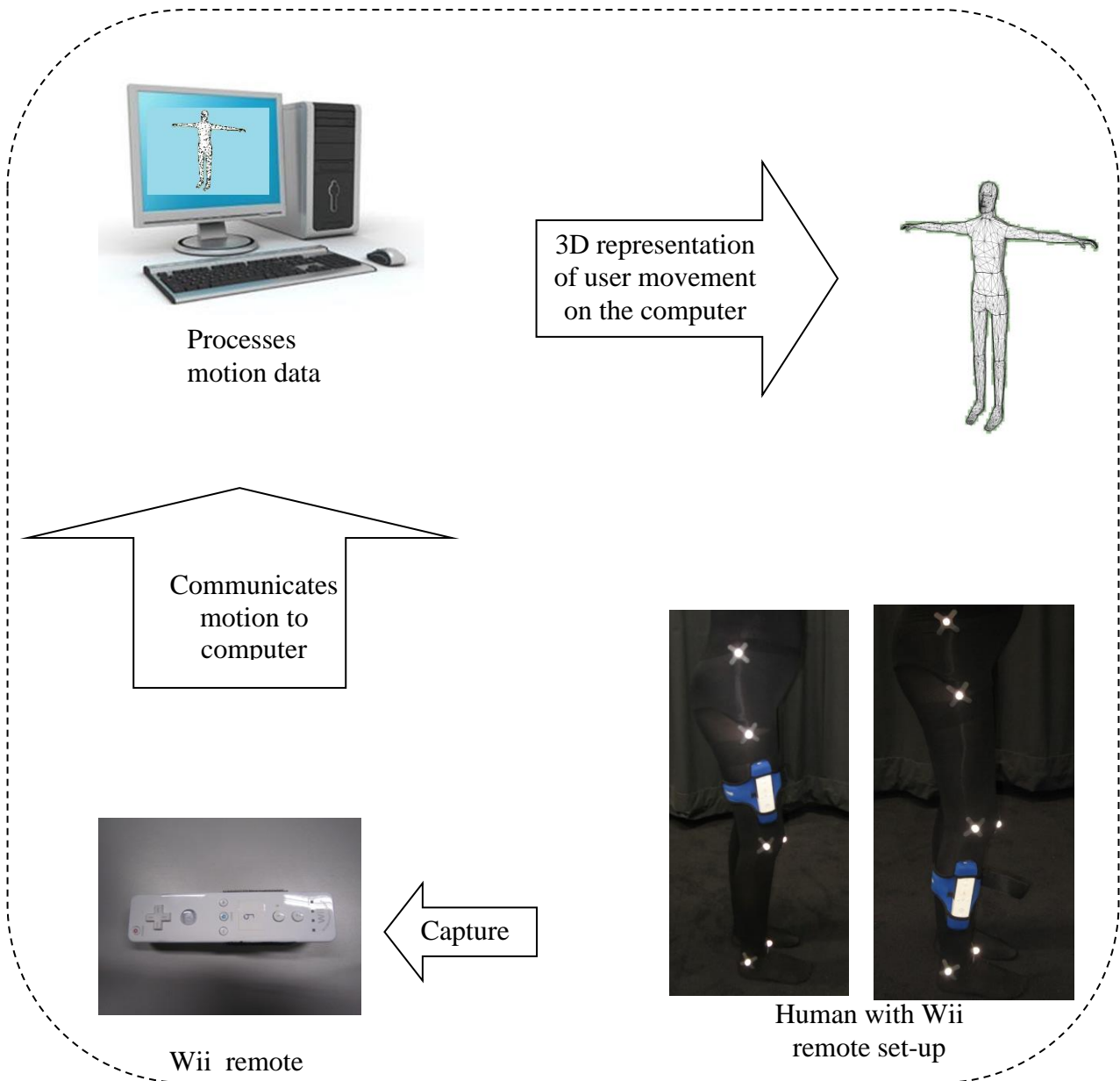


Figure 66: Schematic procedure of Wii-remote control to get motion data of human

Figure 67 shows how Wiimote was attached to the body. Figure 67a shows the place of Wiimote during measuring flexion and adduction. Wiimote was placed at the middle of femur in the lateral view of hip during flexion and adduction. Figure 67b shows the place of Wiimote during measuring internal rotation. The Wiimote was placed at the middle of fibula in the lateral view during internal rotation.



Figure 67: Place of Wiimote on the body a) measuring flexion and adduction, b) measuring internal rotation

7.2.3.1 Calibration

Calibration of the Wiimote was done by using the “WiiRemote Active” windows as shown in Figure 68. To calibrate the Wiimote as shown in Figure 68 by red circle the “Enable Cursor” was selected and the Wiimote was rotated in all the directions for 30 sec to 1 minute. Then ‘Cursor Ended’ was selected as shown in Figure 68 by black circle. Faster movement of the Wiimote in the space give better calibration results. After this stage new window was opened as can be seen in Figure 69.

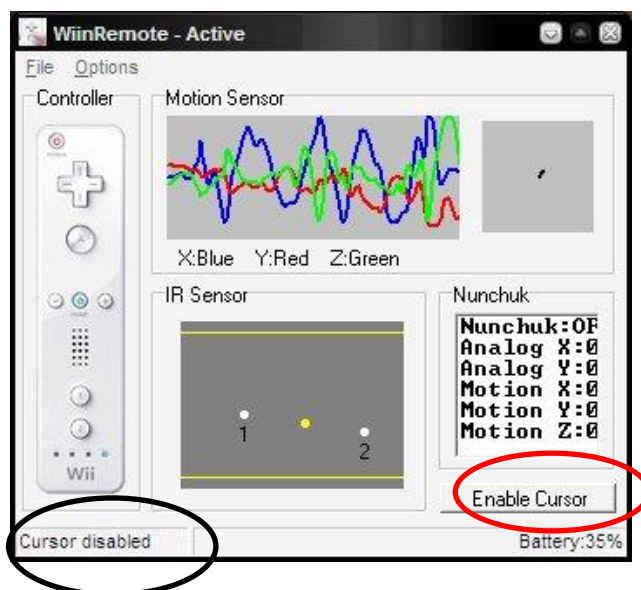


Figure 68: The calibration window of Wiimote

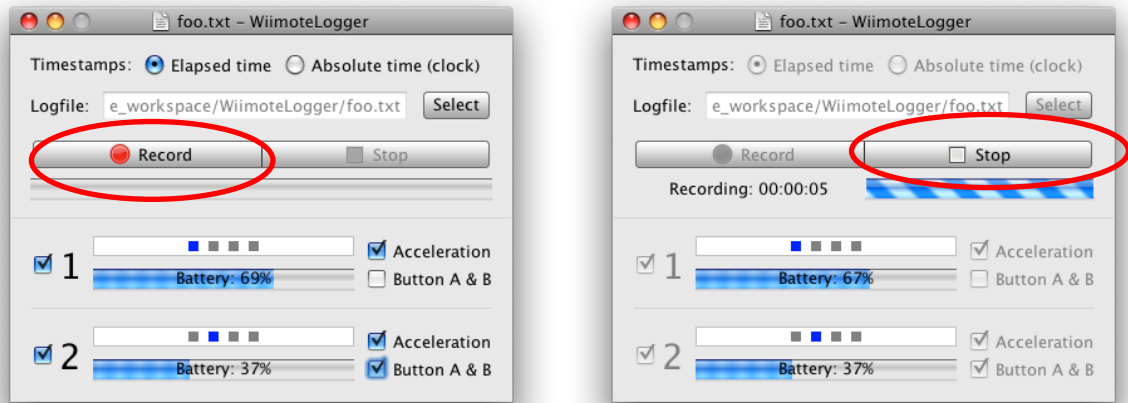


Figure 69: The take window of Wiimote

7.2.3.2 Data Recording

After calibration, “WiimoteLogger” window as shown in Figure 69 was opened. The “Record” command was used to start taking motion record and the “Stop” command was used to stop taking motion record.

Flexion, adduction in 90° of flexion and internal rotation in 90° of flexion were recorded for all 22 volunteers. The data were saved in an excel file. The Wiimote provided 3 angles per take. The two angles which were reported per take were close to the zero. For example for flexion: the two first angles were the rotation angle around the X and Z axis which were close to the zero from starting the take to the end of the take as shown in Figure 70. The third angle was the rotation angle around the Y axis which was the flexion angle (A sample of raw data is provided in appendix D). By starting the take if the two other angles moved more than 5° , the take was repeated. It was tried to keep the two other angles as close as possible to zero.

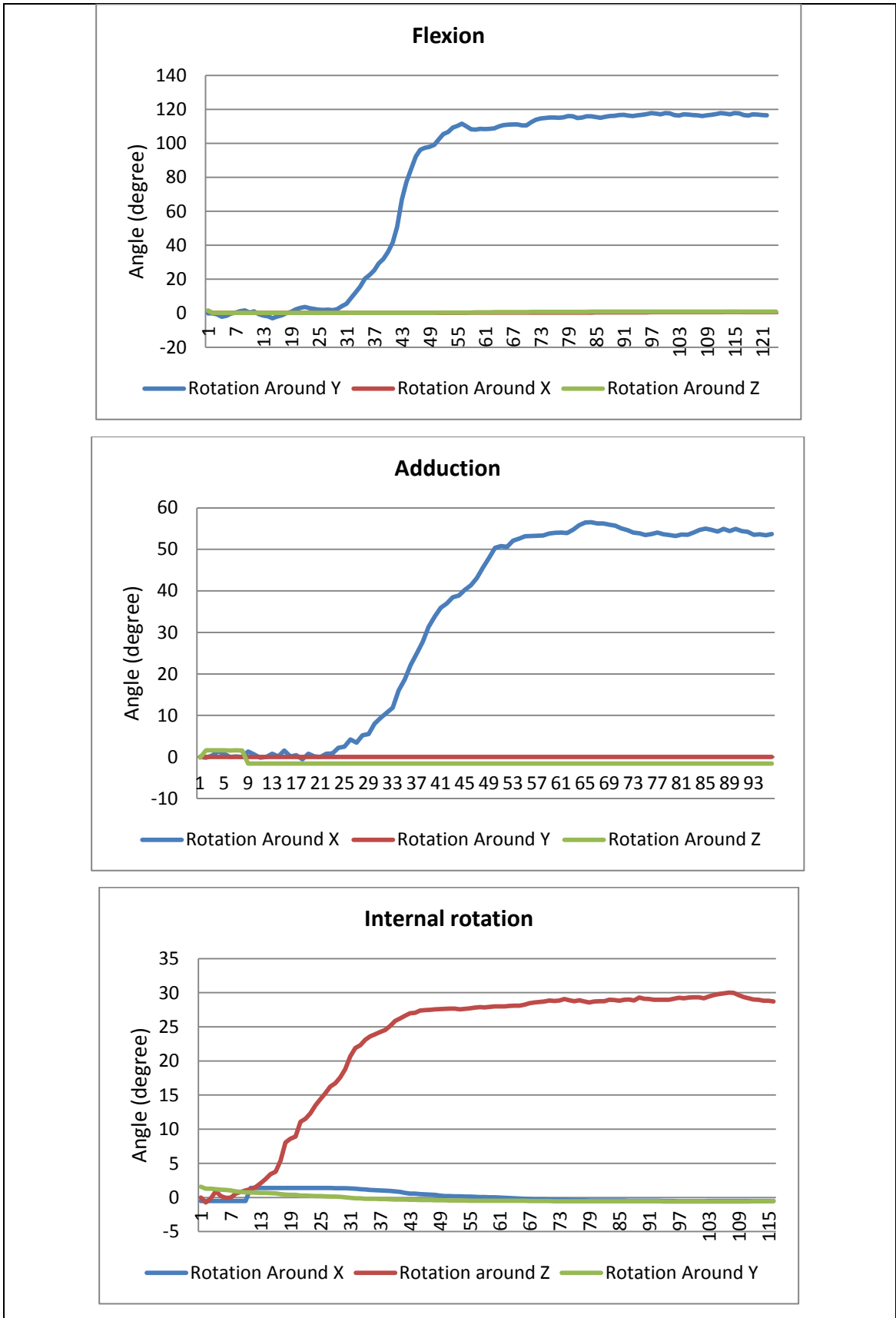


Figure 70: Sample of data recording for Wiimote in terms of time

The flexion angles started from the supine position as shown in Figure 71a and ended in maximum flexion as shown in Figure 71b. The data for flexion angle was set to start from zero (supine position) to the maximum flexion angle. The same procedure was followed for adduction and internal rotation. Figure 71c shows zero degree for adduction in 90° flexion and Figure 71d shows maximum angle for adduction in 90° flexion. Figure 71e shows zero angles for internal rotation in 90° flexion and Figure 71f shows maximum angle of internal rotation in 90° flexion.

Figure 71 shows how Wiimote measured the flexion, adduction in 90° flexion and internal rotation in 90° flexion.

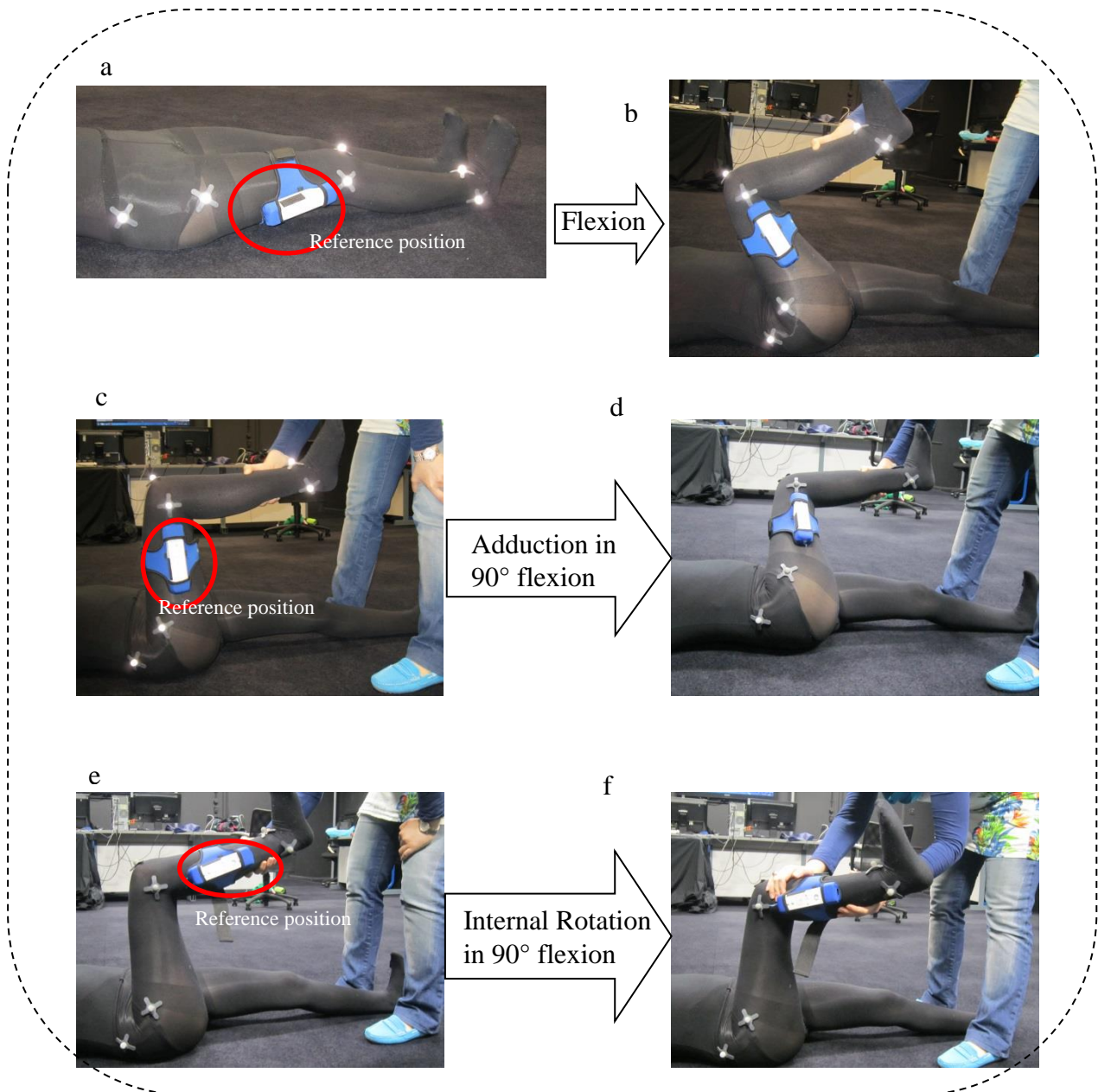


Figure 71: Measurement of flexion, adduction in 90° of flexion and internal rotation 90° of flexion by Wiimote and Motion Capture at the same time

7.2.4 MotionNode

MotionNode is small as shown in Figure 72a, easy to use, and accurate. MotionNode provides orientation, acceleration, and angular rate data in real-time, making it perfect for almost any biomechanics research application. The small form of the device allows for easy attachment to the body. MotionNode is designed to

measure in three degree of freedom. Figure 72b shows the MotionNode sensor, motion software display screen and also X, Y, Z axis (MotionNode Manual, 2013).

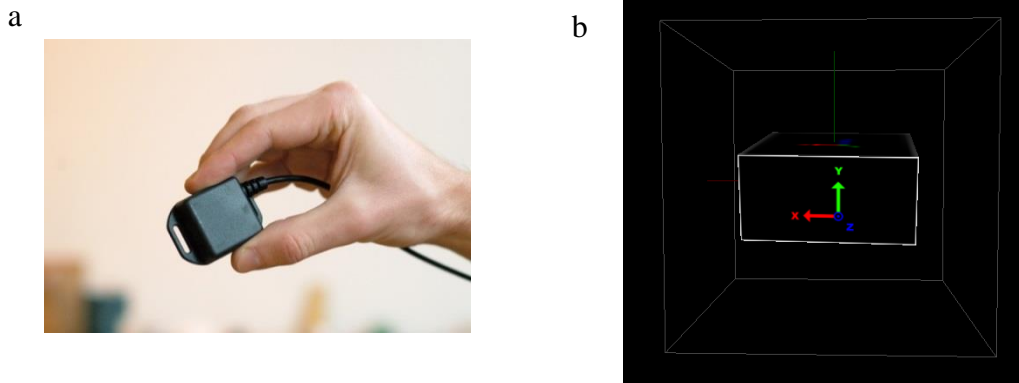


Figure 72: a) MotionNode device which is as small as a pound coin, b) X, Y, Z axis in MotionNode software

7.4.2.1 Calibration

Calibration of the MotionNode was done by using the “calibration” window as shown in Figure 73. To calibrate the MotionNode as shown in Figure 73 by red circle the “Start Take” icon was selected and the MotionNode was rotated in all the directions for 30 sec to 1 minute. Then “Stop Take” icon was selected as shown in Figure 73 by red circle. Faster movement of the MotionNode in the space have better calibration results. After calibration stage, capturing the motion by MotionNode can be started. Data and graph of three rotations is shown on the left side of Figure 74.

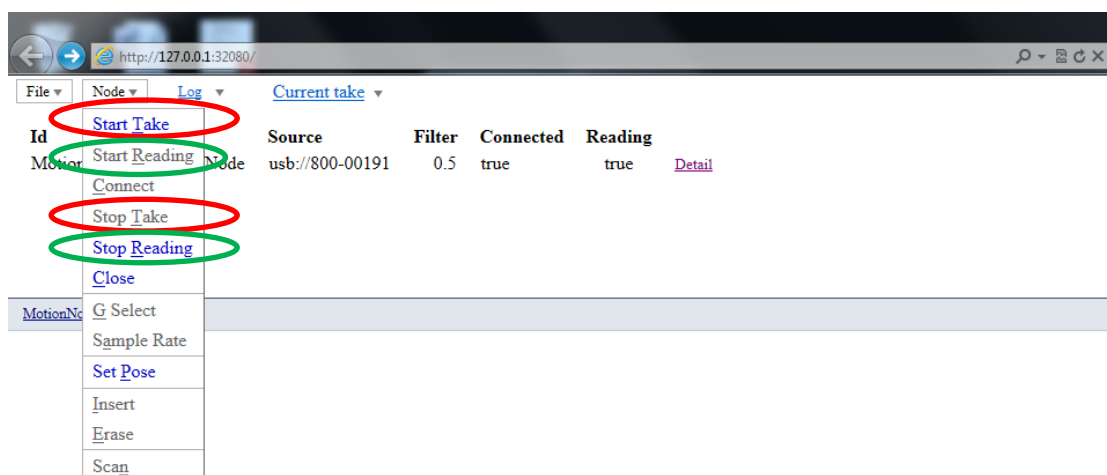


Figure 73: Calibration window in MotionNode software

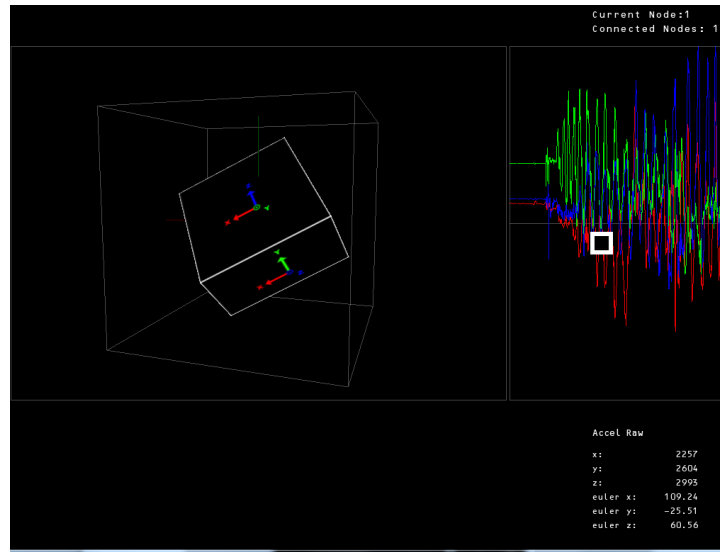


Figure 74: MotionNode device view in MotionNode software, right hand side of the software shows the rotation changes around X, Y, Z axis during each take

7.2.4.2 Data Recording

After calibration, capturing the motion can be started. The “Start Reading” command as shown in Figure 73 by green circle was used to start taking motion record and the “Stop Reading” command as shown in Figure 73 by green circle was used to stop taking motion record.

Figure 76a shows the place of MotionNode during measuring flexion and adduction. MotionNode was placed at the middle of femur in the lateral view of hip during flexion and adduction. Figure 76e shows the place of MotionNode during measuring internal rotation. The MotionNode was placed at the middle of fibula in the lateral view during internal rotation.

Flexion, adduction in 90° of flexion and internal rotation in 90° of flexion were recorded for all of 22 volunteers. The data were saved in an excel file. The MotionNode provides three rotational angles per take. The Two angles which were reported per take were close to the zero. For example, for flexion: the two first angles were the rotation angle around the X and Z axis which were close to zero from starting the take to the end of the take. The third angle is the rotation angle around the Y axis

which was the flexion angle as shown in Figure 75 (A sample of raw data is provided in Appendix D). By starting the take, if the two other angles moved more than 5°, the take was repeated. It was tried to keep the two other angles as close as possible to zero.

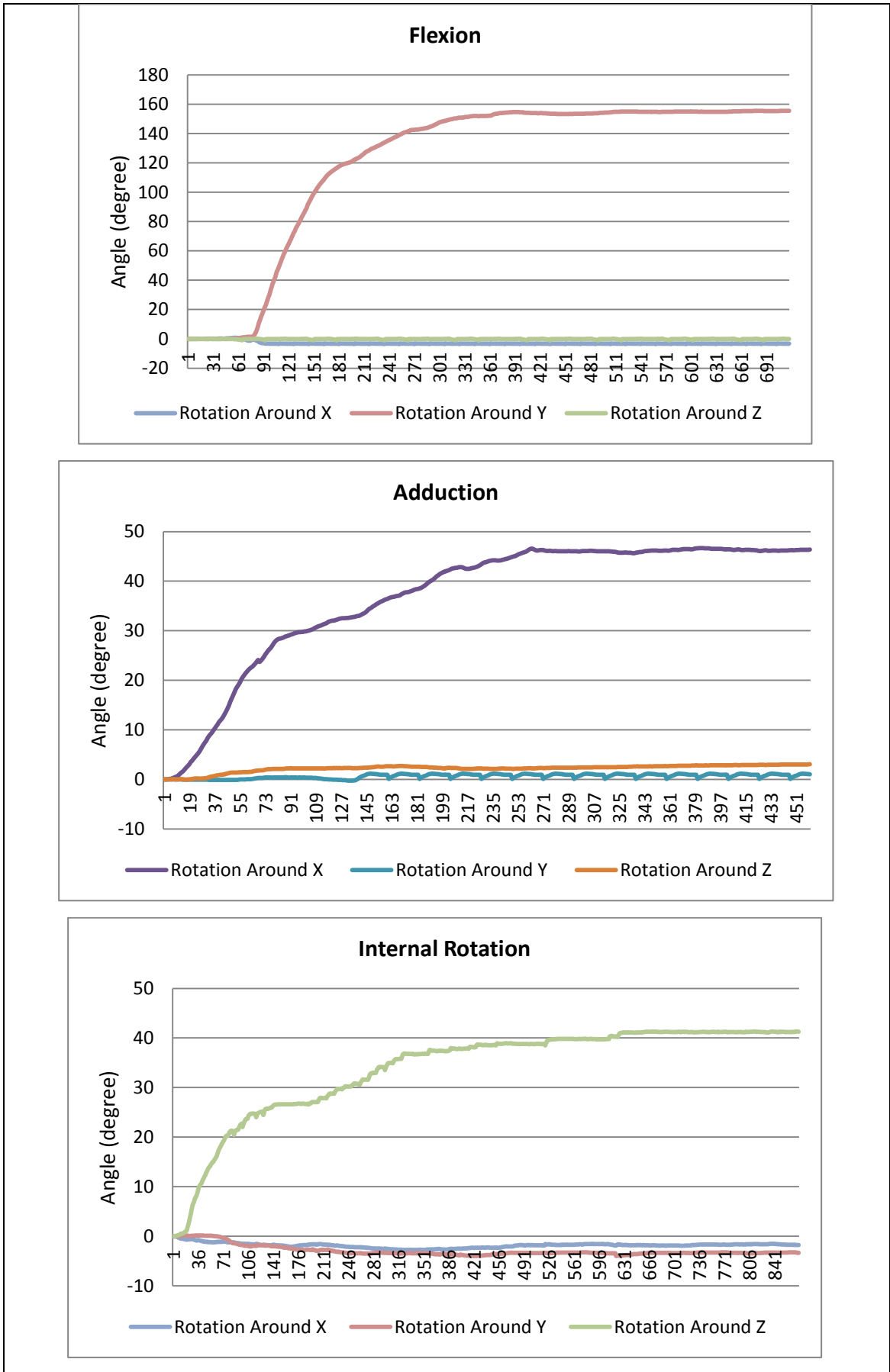


Figure 75: Sample of data recording for MotionNode interms of time

The flexion angles started from the supine position as shown in Figure 76a and ended in maximum flexion as shown in Figure 76b. The data for flexion angle was normalized to start from zero (supine position) to the maximum flexion angle. The same procedure was followed for adduction and internal rotation. Figure 76c shows zero degree for adduction in 90° flexion and Figure 76d shows maximum angle for adduction in 90° flexion. Figure 76e shows zero degree for internal rotation in 90° flexion and Figure 76f shows maximum angle of internal rotation in 90° flexion.

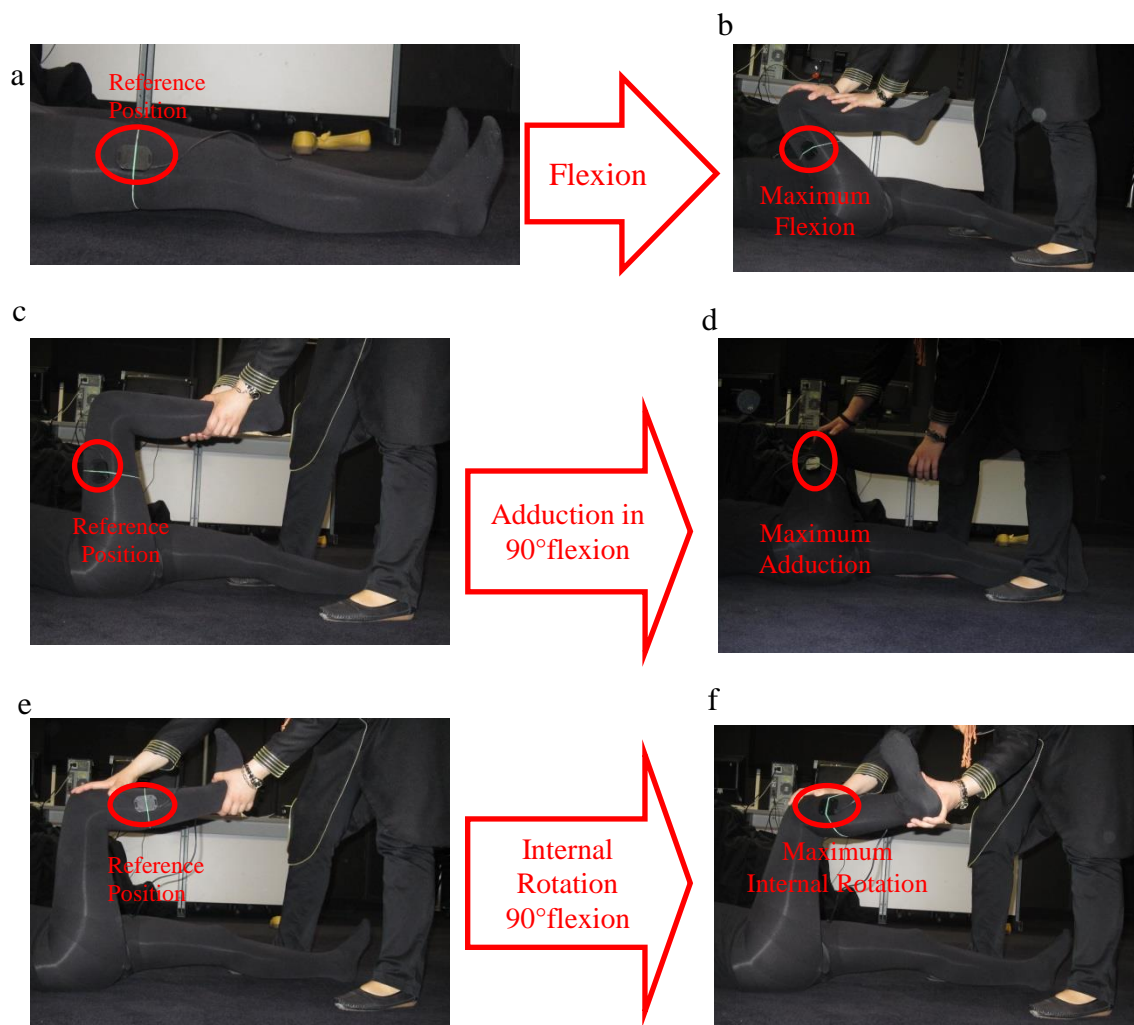


Figure 76: Measurement of flexion, adduction in 90° of flexion and internal rotation 90° of flexion by MotionNode

7.2.5 Adjustable goniometer

The ROM test (Flexion, adduction in 90° of flexion, internal rotation in 90° of flexion) was measured by adjustable goniometer as shown in Figure 77 for volunteers without impingement. A simple long-arm goniometer with 360° scale was used in this

study. The volunteers go under the same procedure as shown in Figures 63, 64 and 65 (FADIR test) to measure flexion, adduction in 90° of flexion and internal rotation in 90° of flexion. Figure 78a shows how flexion was measured by goniometer. One arm of the goniometer was aligned with femur in the supine position in the lateral view and the other one was fixed in the maximum flexion as shown in Figure 78a. Figure 78b shows how adduction was measured by goniometer. One arm of the goniometer was aligned with femur in 90° of flexion in the anterior view and the other one was fixed in the maximum adduction in 90° of flexion as shown in Figure 78b. Figure 78c shows how internal rotation was measured by goniometer. One arm of the goniometer was aligned with fibula in the 90° of flexion in the anterior view and the other one was fixed in the maximum internal rotation in 90° of flexion as shown in Figure 78c.



Figure 77: Adjustable goniometer used in the experiments

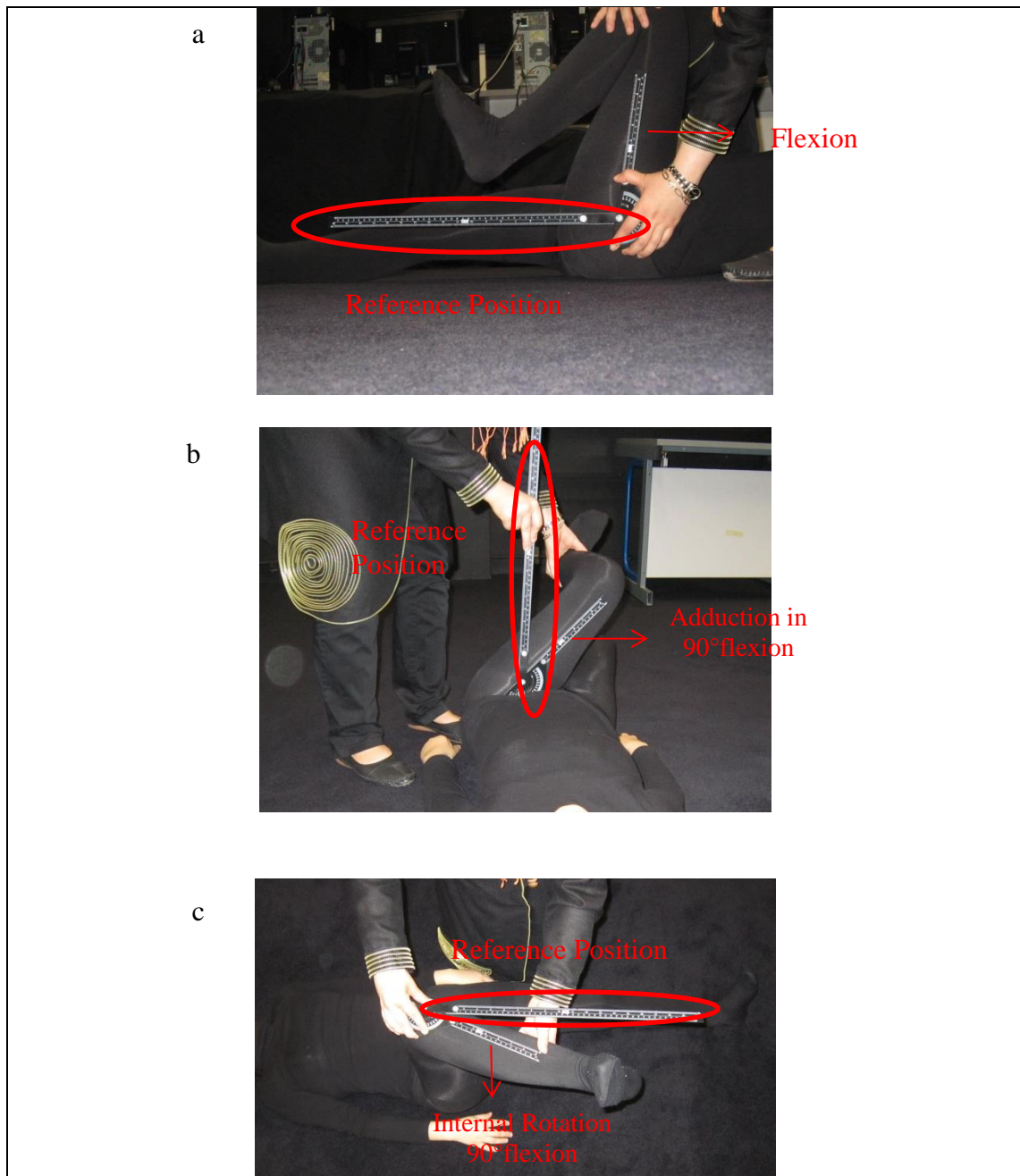


Figure 78: Measurement of a) flexion, b) adduction in 90° of flexion, c) internal rotation 90° of flexion by goniometer

7.2.6 Statistical Analysis

Normality and homogeneity of data variance were tested. Data were then checked for t-test. The mean values and standard deviation were evaluated for each instrument for each movement.

The concurrent validity of data was measured to determine the validity of measuring techniques, by comparing them with established system (Motion Capture). Concurrent validity between each measurement device and Motion Capture were analysed using Intraclass Correlation Coefficient (ICC). ICC describes how strongly units in the same group resemble each other and limit of agreement (LOA^o). LOA is expected 95% of differences between the two measurement methods. Motion Capture was used as a reference and the validity of the other devices compared with Motion Capture. ICC value is between 0-1. The higher ICC value for a device means the device has higher validity. LOA means how much the members of a group differ from the reference value for the group. Lower LOA means higher reliability.

The reliability of data was calculated to check whether the data were reliable or not. The reliability was assessed by using interclass correlation (ICC), coefficient of variation (CV%) and standard errors of measurement (SEM) and limit of agreement (LOA^o). As a general rule, an ICC value over 0.75 was considered as good. The higher ICC value for a device means the device has higher reliability. CV% is defined as a ratio of standard deviation to the mean. The less CV% means more reliability. SEM shows how repeated measures of a device on the same person tend to be distributed around the reference device value. The less SEM means the value obtained by a device is more reliable. LOA means how much the members of a group differ from the mean value for the group. Lower LOA means higher validity.

7.3 Results and Discussion

The results of mean and standard deviation are presented in Table 13 for all the measurement instruments. The standard deviation for the data do not show significant changes for each motion according to the different devices and data compression results are more or less the same across all the movements. However, the mean values are very different regarding flexion. As mentioned above the Motion Capture was used as a reference and the other three devices reported approximately the same mean value with five degree of difference from it. The mean values for adduction (around 49^o) and internal rotation (around 38^o) are almost the same for all the devices.

Table 13: Mean± SD volunteers ROM for each measurement device (n=44)

	Flexion	Adduction	Internal Rotation
Goniometer	130.3863±18.0557	51.2128±6.6494	38.8043±6.6820
Wiimote	134.2709±18.40615	47.8438±6.8154	38.3059±7.9653
Motion Capture	128.83607±20.4503	50.0925±6.7569	39.0853±6.7135
MotionNode	136.1447±17.7193	49.2167±7.7908	37.4912±7.0176

Figure 79 indicates the angle of flexion in terms of time for Motion Capture, MotionNode and Wiimote. The angle starts from zero which is the supine position of the volunteer Figure 71a. Then the angle increases to its maximum amount as the leg is flexed as shown in Figure 71b.

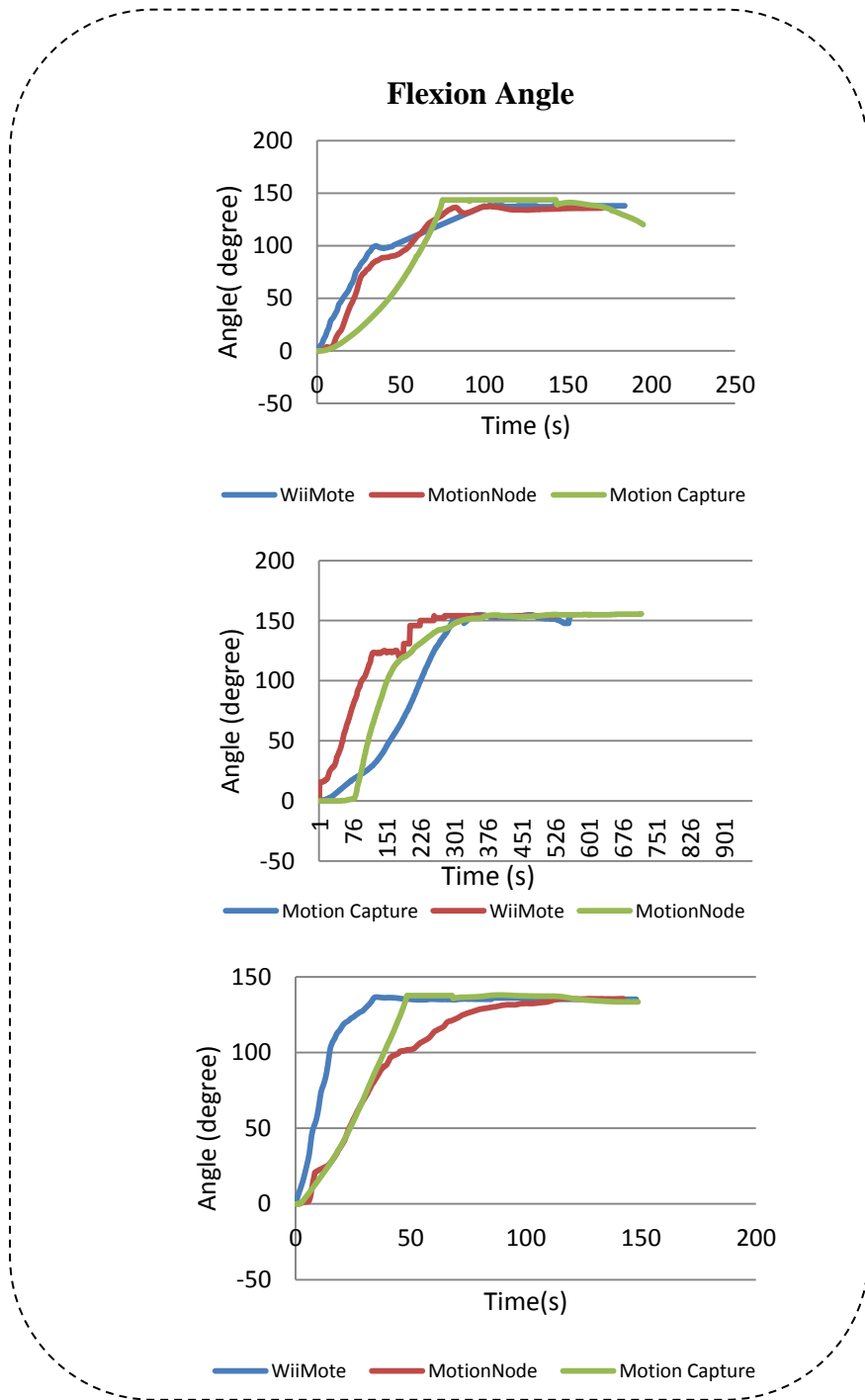


Figure 79: Angle of flexion in terms of time for three volunteers as a sample

Figure 80 indicates the angle of adduction in 90° flexion, in terms of time for Motion Capture, MotionNode and Wiimote. The angle starts from zero, which is the supine position of the volunteer in the 90° hip flexion shown in Figure 71c. Then the angle increases to its maximum amount as the leg is adducted as shown in Figure 71d. The maximum angle shows the adduction in 90° flexion.

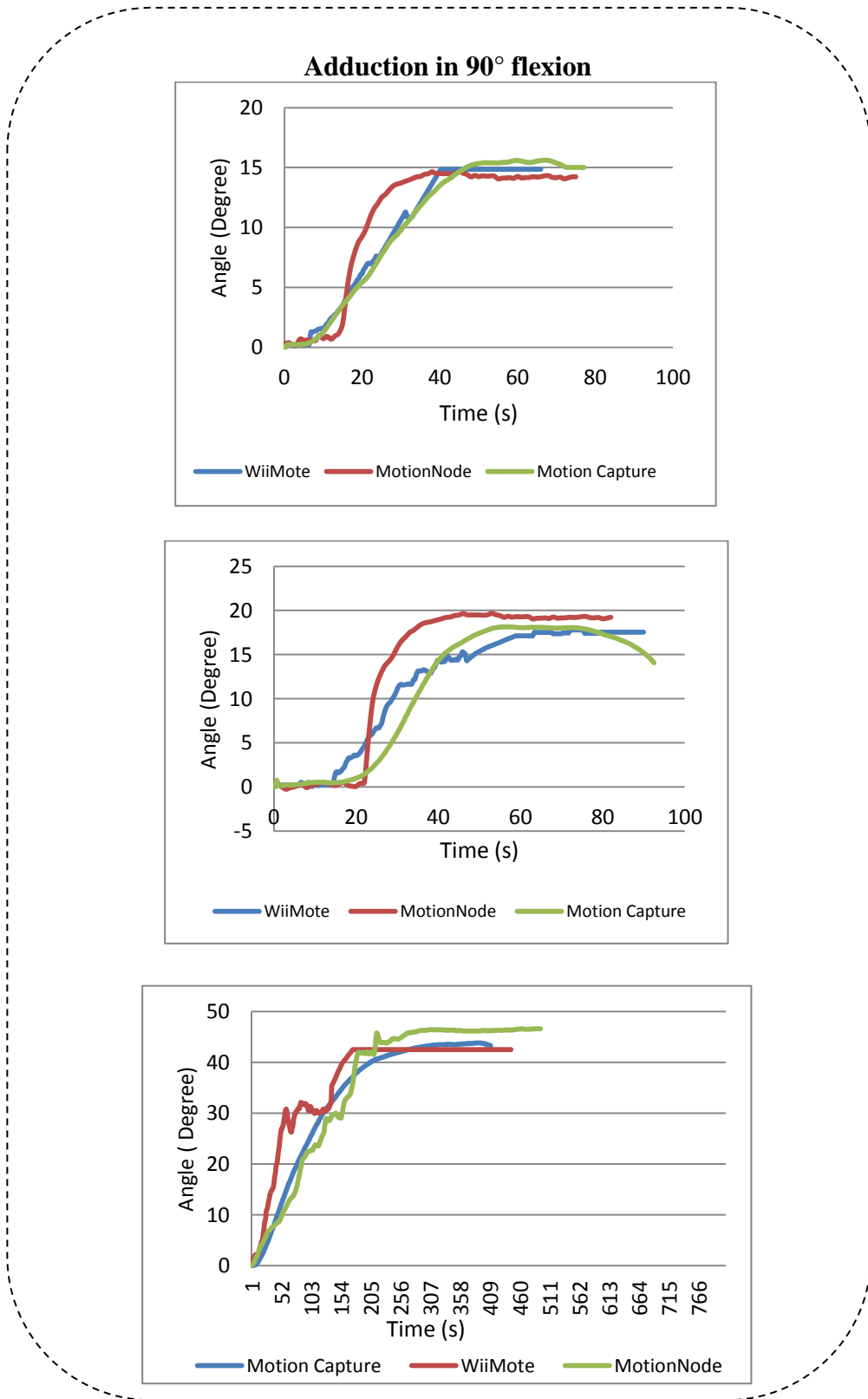


Figure 80: Angle of adduction in 90° flexion in terms of time for three volunteers as a sample

Figure 81 indicates the angle of internal rotation in 90° flexion in terms of time for Motion Capture, MotionNode and Wiimote. The angle starts from zero, which is

the supine position of the volunteers in 90° of hip flexion shown in Figure 71e. Then the angle increases to its maximum amount as the leg is internally rotated, Figure 71f. The maximum angle shows the internal rotation in 90° flexion.

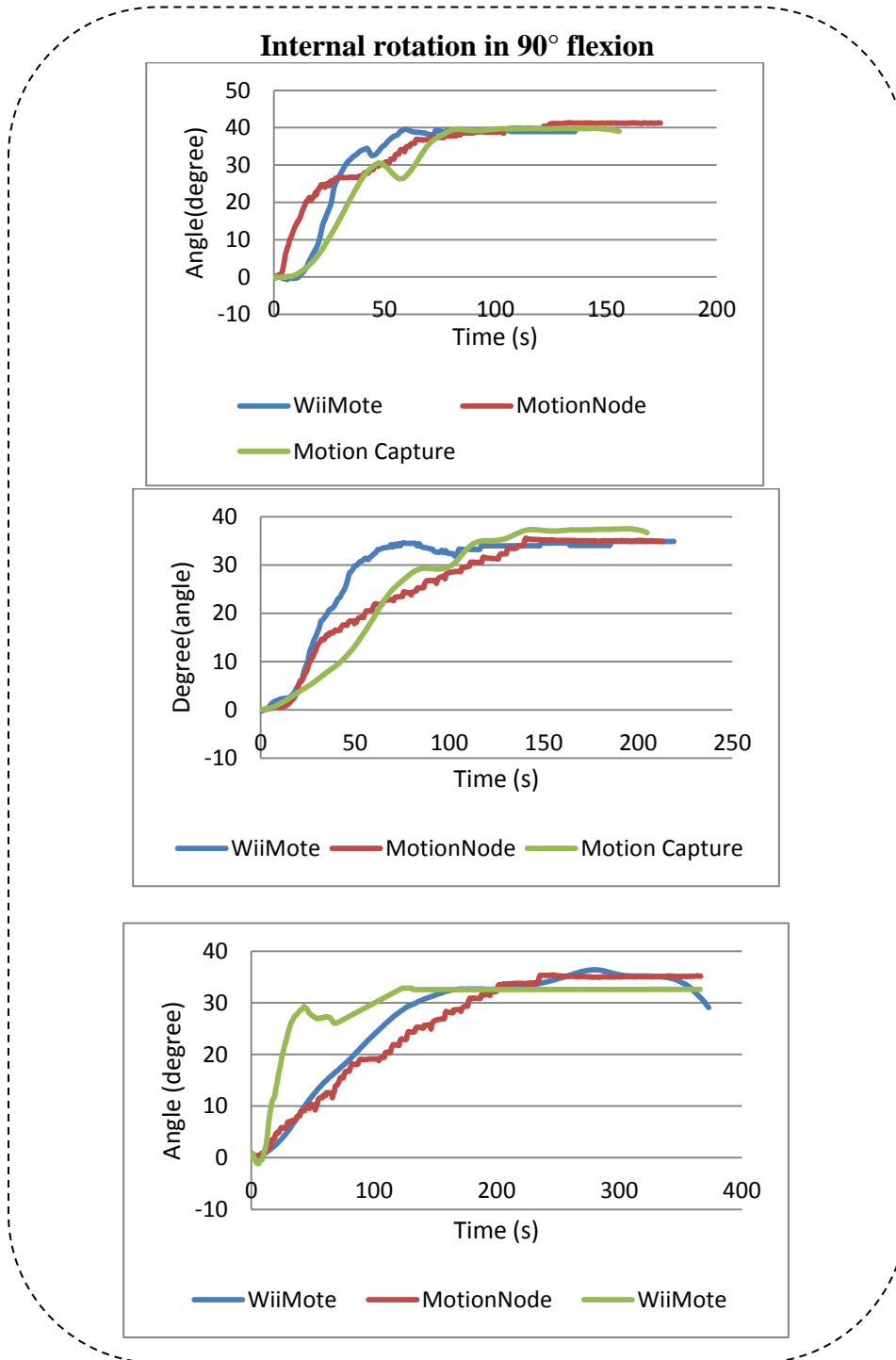


Figure 81: Angle of internal rotation in 90° flexion in terms of time for three volunteers as a sample

7.3.1 Validity

Concurrent validity method was used to determine the validity of the new measuring techniques by comparing them with the established technique. That is, the validity of the goniometer, Wiimote and MotionNode are compared to the Motion Capture. According to the company information for Motion Capture, the error is sub millimetre (Motion Capture Manual , 2013) and Motion Capture calibrated each time before test so the Motion Capture was used as a reference method to compare the other methods validity. Table 14 shows the parameter of validity for these three measurement techniques. The ICC of all the techniques is quite similar; however the MotionNode value is higher than the others.

LOA is the limitation of agreement. LOA was quite similar between the goniometer, Wiimote and the MotionNode. LOA was higher for flexion for all the three techniques for adduction and internal rotation. Gajdosik and his colleague (Gajdosik & Bohannon, 1987) reported that the reliability of measuring ROM of the extremities is affected by the complexity of the actions measured and by the inherent structural and functional differences of the action, for example the rotation is more complicated than flexion and extension (Gajdosik & Bohannon, 1987). Results of Gajdosik and his colleague (Gajdosik & Bohannon, 1987) suggested that reliability of measuring ROM is specific to the action measured and to regional structure and function for example, measurements of the elbow, generally considered a simple hinge joint, show less day-to-day variation in ROM than measurements of the wrist (Gajdosik & Bohannon, 1987).

Passive ROM is more difficult to measure reliably than active ROM (Gajdosik & Bohannon, 1987). Passive movements are extremely difficult to reproduce, because the stretching of soft tissues at the limits of motion depends on the force applied to the limb, which must, therefore, be carefully controlled. The variability of passive flexibility generally was higher than the variability of active flexibility (Gajdosik & Bohannon, 1987).

The force exerted by the therapist during the passive movement may be the variable that caused the goniometric discrepancy (Gajdosik & Bohannon, 1987). Obtaining high reliability among different examiners for measurements of complex passive movements is more difficult than for measurements of simple passive movements (Gajdosik & Bohannon, 1987).

Table 14: Validity of the Wiimot, goniometer and MotionNode (MotionCapture was used as a reference device) for hip ROM (n=22)

		Wiimote	Goniometer	MotionNode
Flexion	ICC	0.926548	0.965541	0.975148
	LOA (°)	±3.809262	±4.010515	±3.758019
Adduction	ICC	0.861613	0.89891	0.904045
	LOA (°)	±1.456102	±1.441152	±1.452687
Internal Rotation	ICC	0.893894	0.888904	0.907411
	LOA (°)	±1.495262	±1.339096	±1.402239

Table 15 shows that our results are much more valid as the limit of agreement (LOA) is significantly ($p \leq 0.001$) less than that of previous findings (Nussbaumer, et al., 2010). The hip ROM measured by goniometer, Wiimote and MotionNode give results that are more valid than the results given previously (Nussbaumer, et al., 2010) when ETS devices was used. The LOA is about $\pm 8^\circ$ less than the previous research (Nussbaumer, et al., 2010) for flexion and about $\pm 6^\circ$ less than the previous research (Nussbaumer, et al., 2010) for adduction and internal rotation. Also the ICC value for Wiimote, MotionNode and goniometer (0.92-0.97) are higher than the previous research (0.4).

Table 15: Comparison of our finding (n=22) with the previous articles (Nussbaumer, et al., 2010)

		Previous articles (Nussbaumer, et al., 2010)		Our Finding		
		ETS devices		Wiimote	Goniometer	MotionNode
Flexion	ICC	0.4	0.92	0.96	0.97	
	LOA (°)	± 12	±4	±4	±4	
Adduction	ICC	0.5	0.86	0.89	0.90	
	LOA (°)	±7	±1.4	±1.4	±1.4	
Internal Rotation	ICC	0.8	0.89	0.88	0.90	
	LOA (°)	±8	±1.5	±1.3	±1.4	

The validity diagram of Wiimote, goniometer and MotionNode was plotted. This diagram represents the data against reference device (Motion Capture). The data distribution in the diagram should be close to the line $x=y$. The closer data is to the line, the higher the reliability is for the device.

Figure 82 shows the plot of the reference method (Motion Capture) against the test methods (goniometer, Wiimote and MotionNode) for all the hip ROM measures. R is the gradient of the closest line to the obtained data. As the R value is closer to 1, there is higher reliability. All the methods have a similar R values (between 0.8-0.9). However, the MotionNod method has the highest R value.

Figure 82 indicates distributions of data in terms of reference method (Motion Capture) for impingement angle (flexion, adduction in 90° flexion and internal rotation in 90° flexion). The data are valid as they are similar to the reference method. Figure 82 also confirms that MotionNode and Wiimote are valid enough to measure ROM.

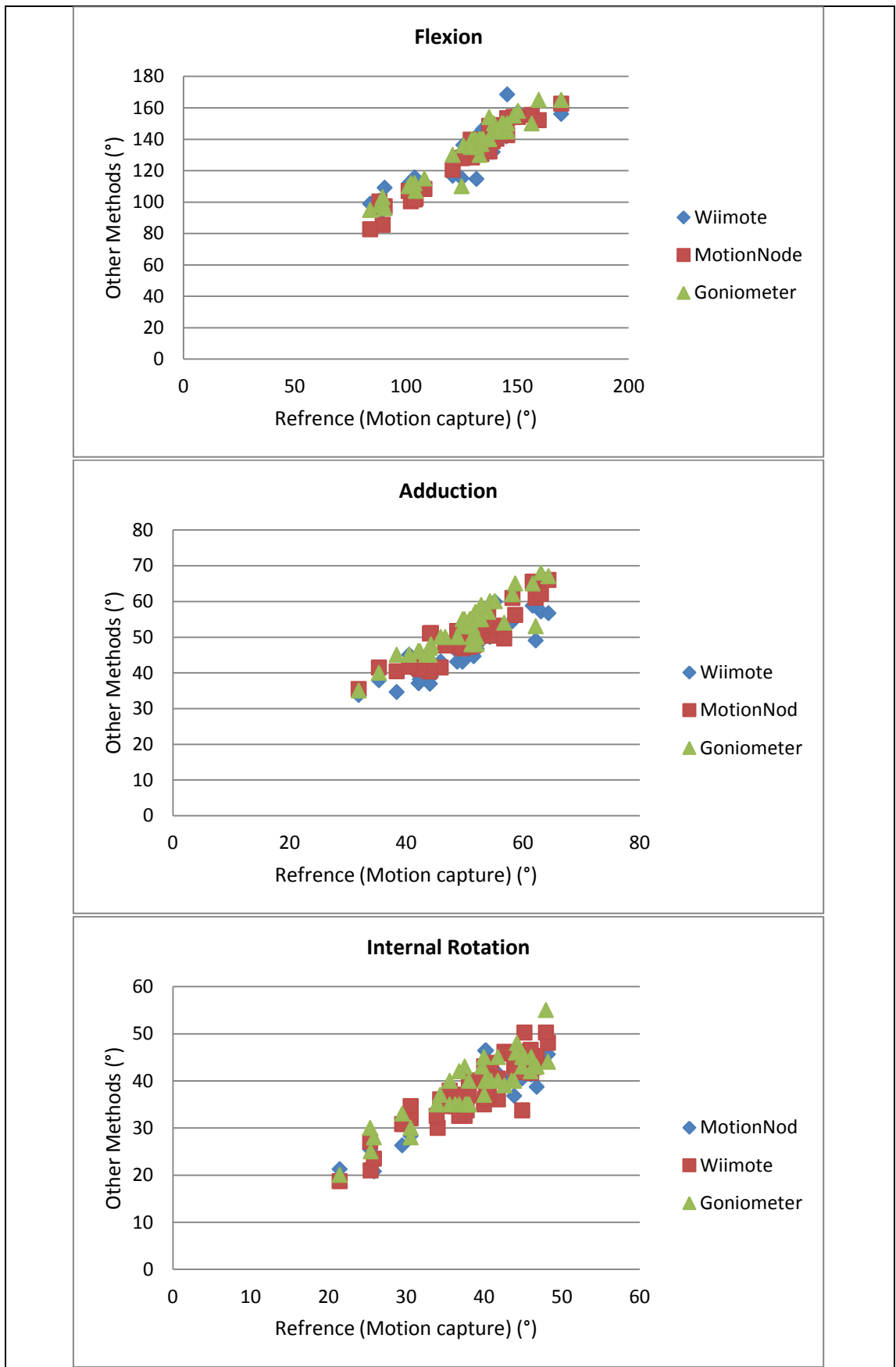


Figure 82: Graph of reference method (Motion Capture) against the test methods (Goniometer, MotionNode, Wiimote) (correlation plot)

7.3.2 Reliability

Reliability tests were taken to elicit whether the same reading occurs every time the measurement is taken for the same parameter. Table 16 shows the reliability information for the goniometer, Motion Capture, Wiimote and MotionNode.

The ICCs were above 0.9 which is good enough for reliability with the goniometer and Motion Capture having slightly higher reliability as compared with others about 0.07. SEM is the standard error measurement and higher SEM presents lower reliability. CV% is the coefficient of variance and a lower CV% indicates higher reliability. SEM, CV% and LOA are more or less the same for all of the motions for all the measurement methods.

Table 16: Reliability of Goniometer, Wiimote, Motion Capture and MotionNode for hip ROM

		Goniometer	Wiimote	Motion Capture	MotionNode
Flexion	ICC	0.90735	0.958321	0.976517	0.922248
	CV%	0.136243	0.129832	0.144488	0.130151
	SEM	2.658148	2.598986	2.785836	2.612574
	LOA(°)	±5	±5	±5	±5
Adduction	ICC	0.915439	0.903412	0.947541	0.901111
	CV%	0.134974	0.125928	0.127439	0.15682
	SEM	1.010182	0.872965	0.953969	1.140304
	LOA(°)	±1.9	±1.7	±1.8	±2
Internal Rotation	ICC	0.92002	0.919579	0.919101	0.95673
	CV%	0.18026	0.20794	0.156177	0.186754
	SEM	1.019784	1.174423	0.910031	1.047149
	LOA(°)	±2	±2.3	±1.7	±2

Table 17 confirms that our findings are more valid than those presented in the previous articles (Nussbaumer, et al., 2010). The SEM and CV% of our findings are less than previously reported which indicates higher reliability. Also the LOA degree for all the hip motion is significantly ($p \leq 0.001$) less than those reported for ETS device by Nussbaumer data (Nussbaumer, et al., 2010). Previous articles reported the CVs % of 3.1- 7.7 % (Nussbaumer, et al., 2010).

Our results are better than previous article (Nussbaumer, et al., 2010) because they used ETS and we used bespoke Wiimote and MotionNode. The results confirm that Wiimote and MotionNode can be used medical application.

Table 17: Comparison of our finding with previous articles (Nussbaumer, et al., 2010)

		Previous Findings (Nussbaumer, et al., 2010)		Our Findings			
		Gonio	ETS	Gonio	Wiimote	Motion Capture	Motion Node
Flexion	ICC	0.9	0.9	0.91	0.96	0.98	0.92
	CV%	3.1	2.6	0.1	0.1	0.1	0.1
	SEM	3.49	2.9	2.6	2.5	2.7	2.6
	LOA	±11	±8	±5	±5	±5	±5
Adduction	ICC	0.8	0.8	0.91	0.90	0.95	0.90
	CV%	6.7	2.3	0.1	0.1	0.1	0.1
	SEM	2.3	1.6	1.01	0.8	0.9	1.1
	LOA	±7	±4	±1.9	±1.7	±1.8	±2
Internal Rotation	ICC	0.9	0.9	0.92	0.92	0.92	0.96
	CV%	7.7	10.2	0.1	0.2	0.1	0.1
	SEM	2.4	2.9	1.0	1.1	0.9	1.0
	LOA	±6.9	±7.9	±2	±2.3	±1.7	±2

The Bland-Altman plot is used to show the reliability of methods in measurements including two repeated tests for two different times. This plot shows the distribution of data around the mean value and between $\pm 1.96SD$.

Figure 83 presents Bland-Altman plots, showing the deviation of data for all the devices. The plots show that the deviation of data is between $\pm 1.96SD$. As can be seen in these plots, the data are distributed near the central line (bias) for all the measurement methods (More explanation about Bland-Altman plot and also statistical analysis and data are given in Appendix E). The more close the data to the central line, the more reliable the method.

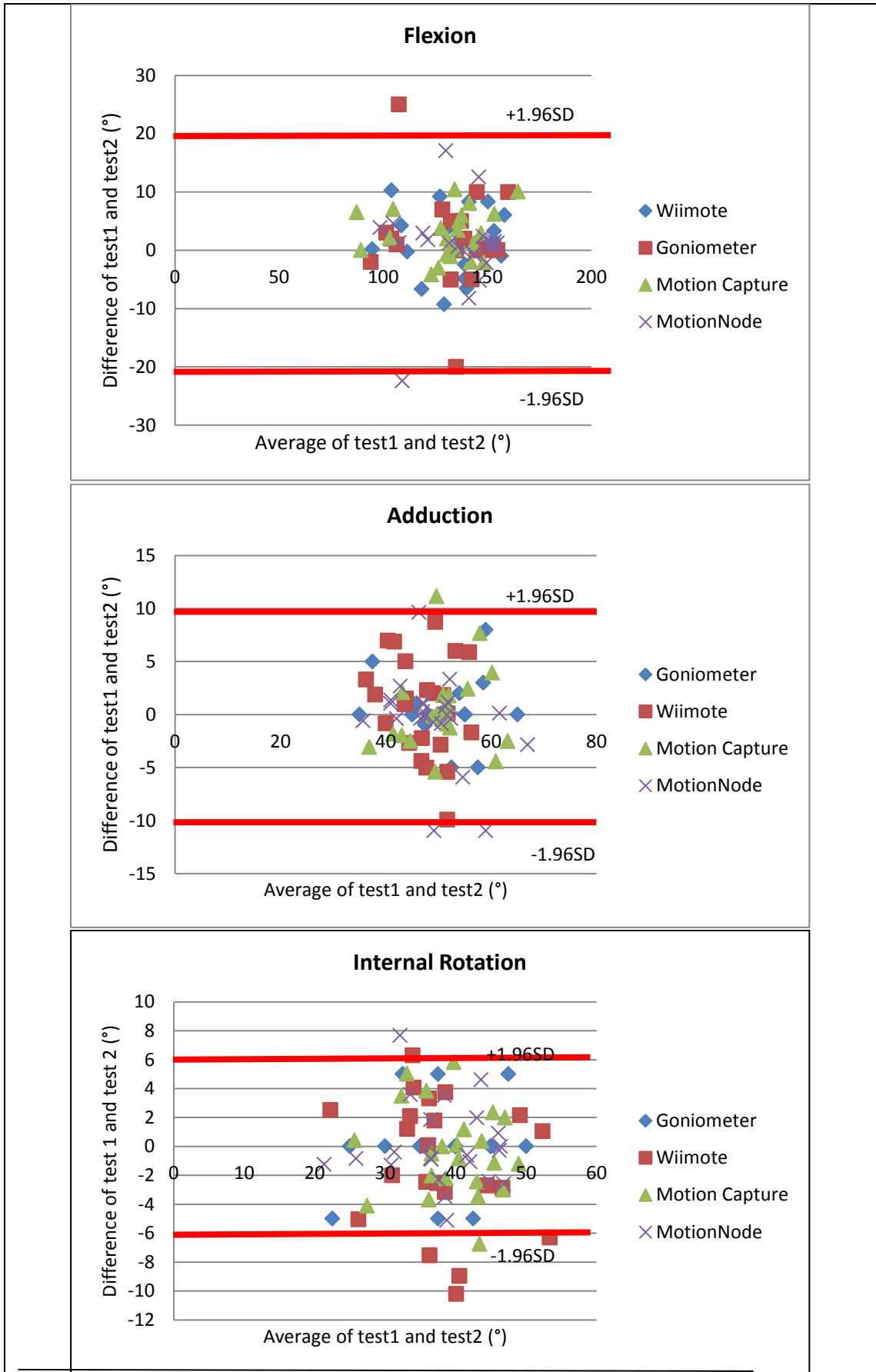


Figure 83: Bland-Altman plot for goniometer, Motion Capture, MotionNode and Wiimote

7.4 Conclusion

Three different experimental techniques were used to measure the flexion, adduction and internal rotation to validate the computer program methods. All three experimental approaches have advantages and disadvantages which were previously explained in Chapter 3. The outcomes show that they have more or less similar validity and test-retest reliability for each volunteer. The goniometer is not convenient to use and surgeons need to have a free hand in order to avoid pelvis movement. The Motion Capture method has the highest reliability and validity amongst other methods. MotionNode, Wiimote Control and goniometer have quite similar validity and reliability as compared to the Motion Capture but MotionNode, Wiimote Control are easy to use, leaving surgeons with both hand free to measure the ROM. As a result goniometer can be replaced by MotionNode, Wiimote to avoid the human error. These two methods do not have any wire which makes them even easier for a surgeon to use in order to measure ROM. Further, when compared to the results given in previous studies, they have higher reliability and validity than the previous ETS method. Flexion has the highest reliability and validity among the other motions. Also MotionNode, Wiimote can be used in physical therapy measurement. The main advantages of MotionNode and Wiimote is that they don't need initializing and positioning.

Chapter 8

Summary and Conclusion

8.1 Summary

The objective of this project is to develop a framework with which impingement angles and locations can be identified accurately. Identification of impingement involves determining the angles of the joint and the location. The impingement angles are measured by using FADIR test. Impingement zone are measured by using clock method.

The initial diagnostics for impingement location in medical practice is done by using goniometer. This was the state of art at the beginning of this project. The test protocol followed is known as FADIR test. Any suspicion of the condition is referred to X-ray where suspected joint is X rayed and investigated.

The clinical methods have either misdiagnosed impingement with the other hip diseases or either diagnosed late. Late diagnosis of impingement leads to OA. The computer based programmes are developed to help surgeons to measure impingement zone and angles to avoid misdiagnosing impingement.

To our knowledge and up to current investigation is carried out evaluating the effectiveness of goniometer. This project focuses on, evaluating the current practise and finding alternative methods to evaluate their effectiveness. The following objectives has been considered in this project:

- A valid and reliable framework has been developed to diagnose the FAI in early stages.
- A complete and real hip model with soft tissues has been developed. The hip model is based on CT and MRI of a specific person.
- A collision detection of FAI based on stress to detect the impingement angle has been developed. The collision detection has been designed to detect FAI based on stress- impingement angle diagram.
- The effect of centre of rotation and boundary condition on hip modelling has been considered to detect FAI.
- The validity and reliability of current clinical methods has been compared with Motion Capture experimental studies.
- Replacing goniometer with a valid, reliable, easy to use and without human errors devices.

In this research joint surface model obtained from patients using MIMICs and FEA for studying joint kinematics and loading. Joint kinematics was studied experimentally using motion lab, Wiimote and MotionNode. These are various devices capable of measuring the kinematics of the gait.

The modelling was carried out using MRI data from two individuals. A normal individual, an individual diagnosed with FAI before reshaping operation and the individual diagnosed with FAI after reshaping operation for which CT and MRI data were collected.

Experimental kinematics studies were carried out using goniometer, Motion lab, Wiimote and MotionNode. For these experiments twenty two volunteered individuals were participated. Validity of all methods was measured and compared with Motion Capture lab. Reliability of the methods were measured and compared with each other.

The normal volunteers, who went through CT and MRI, were asked to participate on experimental work and his results of experiment and modelling were compared with each other.

Results obtained for different centre of rotations are presented in Table 18. Slight change in moving the centre of rotation inward and outward the acetabulum, changes the angles of impingement. The fixed centre of rotation according to the previous articles (Kubiak-Langer, et al., 2007), (Tannast, et al., 2007) was set as 0 which is centre of the femur and centre of the coordinates. The impingement angles (flexion,

adduction in 90° flexion and internal rotation in 90° flexion) increase by moving the centre of rotation inwards and outwards the 0 position. The impingement angles increase when centre of rotation moved away from 0 position in both directions (inward and outward the acetabulum).

Table 18: Results of different centre of rotations, 0 is the fixed centre of rotation (previous article (Kubiak-Langer, et al., 2007) used this centre) and -1 means that centre of rotation was moved 1 mm inward the acetabulum and +1 means that centre of rotation was moved 1 mm outward the acetabulum

	Flexion			Adduction			Internal Rotation		
	Normal	Imping	Reshape	Normal	Imping	Reshape	Normal	Imping	Reshape
-4	136	133	143	51	36	43	41	27	38
-3	125	127	134	48	34	40	37	25	37
-2	123	116	132	46	33	38	36	23	36
-1	119	111	130	40	32	36	34	22	36
0	115	105	120	24	27	29	30	23	36
1	100	96	119	41	28	34	34	22	36
2	107	100	122	38	29	36	36	22	36
3	128	117	136	43	34	38	38	26	38
4	130	113	140	47	38	40	41	27	38

Previously, many researches have worked on the impingement zone and angle (Bedi, et al., 2011), (Bedi, et al., 2012), (Kubiak-Langer, et al., 2007), (Tannast, et al., 2007). They have used the patient's CT scan to create their 3D model. However, none have included soft tissues as the researchers contended that impingement is an outcome of bone to bone contact.

As observed from the obtained results, in Table 19, having soft tissues attached to the model also has an effect on obtaining bigger angles. Because the ligaments connect the bones together and constrain the range of motion of the bone, the ligaments could act as lever arm which increase the angle. In addition, the cartilage affect the kinematics of the hip.

Table 19 presents that different boundary conditions effect the impingement angles. Free centre of rotation condition has the lowest result for impingement angles. The hip model with soft tissues has the highest impingement angle.

Table 19: Results of different boundary conditions

	Flexion			Adduction			Internal Rotation		
	Normal	Imping	Reshape	Normal	Imping	Reshape	Normal	Imping	Reshape
Fixed centre of rotation	115	105	120	27	24	29	30	24	36
Free centre of rotation	105	91	120	32	36	47	8	10	15
Hip with soft tissues	139	120	146	40	23	45	30	19	33

The results of reliability of all of the experimental methods are presented in Table 20. Reliability of all of the methods are the same and as can be seen from Table 20, Motion Capture has slightly higher ICC in flexion and adduction and also Standard Errors of Measurement (SEM) is lower in Motion Capture compared with the other methods. Wiimote and Motion Capture provide relatively high reliability and they can be replaced with the current clinical method (goniometer).

Table 20: Reliability of the different measurement techniques

		Goniometer	Wiimote	Motion Capture	MotionNode
Flexion	ICC	0.90	0.95	0.97	0.92
	CV%	0.13	0.12	0.14	0.13
	SEM	2.65	2.59	2.78	2.61
Adduction	ICC	0.91	0.90	0.94	0.90
	CV%	0.13	0.12	0.12	0.15
	SEM	1.01	0.87	0.95	1.14
Internal Rotation	ICC	0.92	0.91	0.91	0.95
	CV%	0.18	0.20	0.15	0.18
	SEM	1.01	1.17	0.91	1.04

Table 21 presents validity of different measurement technique compared with the Motion Capture. Results show that all techniques have relatively high reliability and that reliability amongst different technique are the same.

Table 21: Validity of Wiimote, goniometer and MotionNode compared to the Motion Capture

		Wiimote	Goniometer	MotionNode
Flexion	ICC	0.92	0.96	0.97
	LOA°	±4	±4	±4
Adduction	ICC	0.86	0.89	0.90
	LOA°	±1.4	±1.4	±1.4
Internal Rotation	ICC	0.89	0.88	0.90
	LOA°	±1.5	±1.3	±1.4

Table 22 contains comparisons of obtained results for both the experimental and computational hip models for the normal individual. Those obtained from the hip model with soft tissues are close to the experimental results. As can be observed from Table 22, the experimental flexion result is closer to the model with the soft tissues connected to it. In addition, it is observed that the experimental model and the hip model with soft tissues register the flexion angle as being approximately 140°. However, the model with no soft tissues has a considerably lower flexion angle, around 115°. These differences can also be seen regarding adduction and internal rotation. Moreover, adduction and internal rotation for the hip model with the soft tissues and the experimental model are approximately the same.

The results obtained from the two hip models are significantly ($p \leq 0.005$) different. This difference shows that the soft tissues could exert a massive effect with respect to the impingement angle. By including soft tissues in the model, the results are closer to the experimental results than without soft tissues and these have a large impact on the hip model. The impingement zone for both hip models is approximately the same at 11 o'clock. Soft tissues do not have effect on impingement zone.

Table 22: The comparison of the normal hip ROM for computer-aided programme and experimental results

Conditions	Flexion	Adduction	Internal Rotation
Fixed centre of rotation	115	27	30
Free centre of rotation	105	32	8
Hip with soft tissue	139	40	30
Experiments results	142	43	32

8.2 Conclusions

- The hip impingement collision detection used in this study is based on stress and it is first in its kind. The purpose of developing the collision detection is to consider the effect of different boundary conditions including soft tissues on hip impingement.
- Slight changes in centre of rotation changes the result of impingement angle and thus boundary conditions have an important role on detecting impingement.
- Changing the centre of rotation does not change the impingement zone.
- Soft tissues play an important role on detecting the impingement angles. Impingement angles change by adding ligaments and cartilage to the hip model in computational based programming detection.
- The impingement zone for the model with or without attached soft tissue is almost the same. Soft tissues do not affect the detection of the impingement zone in computational based programming.
- Computational modelling and programming are sensitive to the boundary conditions and the results can change by changing the boundary conditions.
- Goniometer which is the current clinical method to detect ROM of FAI can be replaced by Wiimote and MotionNode as they are reliable, valid, easy to use and avoiding human errors.
- Goniometer has similar reliability and validity to the Wiimote and MotionNode. Reliability and validity of goniometer are 100% on human but Wiimote and MotionNode measurement are taken by computer. Also Goniometer measures the movement in 2D but Wiimote and MotionNode measure human movement in 3D.

- The 3D hip models with soft tissues are the first hip model in its kind and it can be used for studying other hip diseases and biomechanics of hip diseases.
- The ROM of hip improves after reshaping in any boundary conditions. The ROM of impinged person is lower than the ROM of normal person in any boundary conditions.
- Computer assistant programming including FEA could not accurately mimick the human movement and human motion analysis since the results depend on boundary condition.
- It is necessary to include soft tissues on hip modelling in order to have accurate kinematic results.
- Wiimote and MotioNode do not need positioning and initializing to measure ROM.
- Wiimote and MotioNode can be used instead of computer programming for the purpose of studying human motion.
- Wiimote and MotioNode can be used in any application to measure ROM such as physical therapy application.

8.3 Future Work

There is a large scope for possible future study on the hip modelling and hip impingement.

- Ligament and cartilage material were assumed to be isotropic. Ligaments and cartilage behave as a viscoelastic model. Many articles show that the stress-strain diagram of ligaments is not linear. Ligaments show time dependent and load-history dependent mechanical behaviour. In this thesis, ligaments and cartilage were assumed to be elastic and future work towards completing and developing the hip model should focus on the material properties of ligaments and cartilage. An experiment can be set up to measure the shear relaxation modulus ratio, bulk relaxation modulus ratio and relaxation time to use this information in Abaqus.
- The hip model needs to be completed by adding muscles to it which is possible by using accurate MRI and carrying out some image processing on the MR

images. As threshold values for soft tissues are quite similar, image processing can be used to distinguish the soft tissues.

- Soft tissues such as ligaments and cartilage are simply attached by tie tool bar. However, the connection between the soft tissues and bone in the real model are stronger than in the tie tool bar. It is necessary to make our hip model as one object.
- In the experiment, different methods are used to compare and validate results with the computational hip model. However, all of them measure the range of motion on skin that can have small errors. Thus, using fluoroscopy to measure the range of motion could be a complete and error free method to validate our hip model.

Bibliography

3-Matic, 2014. *3-Matic 7 reference guide manual*, pp. 1-11.

Abaqus, 2014. *Abaqus 6.11-1 reference guide manual*, pp. 5-23.

Ackerman, M. J., Spitzer, V. M., Scherzinger, A. L. & Whitlock, D. G., 1995. The visible human data set: An image resource for anatomical visualization. *Medinfo*, 8(2), pp. 1195-1198.

Adams, D. & Swanson, S. A., 1985. Direct Measurement of Local Pressures in the Cadaveric Human Hip Joint During Simulated Level Walking. *Ann Rheum Dis*, 44(10), pp. 658-66.

Adams, M. A. et al., 1999. Experimental determination of stress distributions in articular cartilage before and after sustained loading. *Clin Biomech*, 14(2), pp. 89-96.

Afoke, N. Y., Byers, P. D. & Hutton, W. C., 1987. Contact pressures in the human hip joint. *J Bone Joint Surg Br*, 69(4), pp. 536-41.

Allard, P., Stokes, I. & Blanche, J. P., 1994. *Three-dimensional analysis of human movement, champagne: human kinetics*. First ed. USA: Braun-Brumfield.

Anderson, A. E., Ellis, B. J., Maas, S. A. & Weiss, J. A., 2010. Effects of idealized joint geometry on finite element predictions of cartilage contact stresses in the hip. *J Biomech*, 43(7), pp. 1351–1357.

Anderson, B., 2013. *Sports Injury Info*. [Online]
Available at: <http://www.sports-injury-info.com/hip-flexor-injury.html>
[Accessed 20 02 2014].

Anderson, E. et al., 2008. Validation of finite element predictions of cartilage contact pressure in the human hip joint. *Journal of Biomechanical Engineering*, 130(5), p. ID 051008.

Anon., 2012. *National joint registry*. [Online]
Available at:
<http://www.njrcentre.org.uk/njrcentre/Patients/Jointreplacementsstatistics/tabid/99/Default.aspx>
[Accessed 22 June 2014].

Arbabi, E. et al., 2012. Sensivity of hip tissues contact evaluation to the methods used for estimating the hip joint center of rotation. *Med boil eng comput*, 50(6), pp. 595-604.

- Arokoski, M. H., Haara, M., Helminen, H. J. & Arokoski, J. P., 2004. Physical function in men with and without hip osteoarthritis. *Arch Phys Med Rehabil*, 85(4), pp. 574-581.
- Bachtar, F., Chen, X. & HisadHisada, T., 2006. Finite element contact analysis of the hip joint. *Medical biological engineering computing*, 44(8), pp. 643-651.
- Beaulé, P. et al., 2005. three-dimensional computed tomography of the hip in the assessment of femoroacetabular. *J Orthop Res*, 23(6), pp. 1286-1292.
- Beck, M., Kalhor, M., Leunig, M. & Ganz, R., 2005. Hip morphology influences the pattern of damage to the acetabular cartilage: femoroacetabular impingement as a cause of early osteoarthritis of the hip. *J Bone Joint Surg*, 87(7), pp. 1012-1018.
- Beck, M. et al., 2004. Anterior femoroacetabular impingement: part II. Midterm results of surgical treatment. *Clin Orthop*, Volume 418, pp. 67-73.
- Bedi, A. et al., 2011. Surgical treatment of femoroacetabular impingement improves hip kinematics : A computer-assisted model. *The American Journal of Sports Medicine*, 39(1), pp. 42s-48s.
- Bedi, A. et al., 2012. Computer-assisted modeling of osseous impingement and resection in femoroacetabular impingement. *The Journal of Arthroscopic and Related Surgery*, 28(2), pp. 204-210.
- Beillas, P., Papaioannou, G., Tashman, S. & Yan, K. H., 2004. A new method to investigate in vivo knee behavior using a finite element model of the lower limb. *Journal of Biomechanics*, 37(7), pp. 1019–1030.
- Bergmann, G. et al., 2001. Hip contact forces and gait patterns from routine activities. *J Biomechanic*, 34(7), pp. 859-871.
- Bergmann, G., Graichen, F., Rohlmann, A. & Linke, H., 1997 Feb. Hip joint forces during load carrying. *Clin Orthop Relat Res*, Volume 335, pp. 190-201.
- Bierma-Zeinstra, S. M. et al., 1998. Comparison between two devices for measuring hip joint motions. *Clin Rehabil*, 12(6), pp. 497-505.
- Biewener, A. A., 1992. *Biomechanics – Structures and systems, a practical approach*. First ed. New York USA: Oxford University Press.
- Brown, T. D. & Shaw, D. T., 1983. In Vitro contact stress distributions in the natural human hip. *J Biomech*, 16(6), pp. 373-384.
- Brunner, A., Horisberger, M. & Herzog, R. F., 2009. Evaluation of a computed tomography-based navigation system prototype for hip arthroscopy in the treatment of femoroacetabular cam impingement. *Arthroscopy*, 25(4), pp. 382-391.

- Byrd, J. & Jones, K., 2004. Diagnostic accuracy of clinical assessment, magnetic resonance imaging, magnetic resonance arthrography, and intra-articular injection in hip arthroscopy patients. *Am J Sports Med*, 32(7), pp. 1668-1674.
- Byrd, T. J., 2007. Hip arthroscopy in the athlete. *N Am J Sports Phys Ther*, 2(4), pp. 217-230.
- Byrd, T. J. W., 2007. Evaluation of the hip: history and physical examination. *N Am J Sports Phys Ther*, 2(4), pp. 231-240.
- Charbonnier, C., Assassi, L., Volino, P. & Magnenat-Thalmann, N., 2009. Motion study of hip joint in extreme postures. *The Visual Computer*, 25(9), pp. 873-882.
- Chegini, S., Beck, M. & Ferguson, S. J., 2009. The effects of impingement and dysplasia on stress distributions in the hip joint during sitting and walking: a finite element analysis. *J Orthopaedic Research Society*, 27(2), pp. 195-201.
- Clohisey, J. C. et al., 2009. Clinical Presentation of patients with symptomatic anterior hip impingement. *Clin Orthop Relat Res*, 467(3), pp. 638-644.
- Cowin, S. C., 2001. *Bone Mechanics Handbook*. 2nd ed. USA: CRC Press LLC.
- Currey, J., 2009. Measurement of the mechanical properties of bone. *Clin Orthop Relat Res*, 476(8), pp. 1948-1954.
- Czerny, C., Hofmann, S. & Neuhold, A. A., 1996. Lesions of the acetabular labrum: accuracy of MR imaging and MR arthrography in detection and staging. *Radiology*, 200(1), pp. 225-230.
- Daenen, B. R., Ferrara, M. A., Marcelis, S. & Dondelinger, R. F., 1998. Evaluation of patellar cartilage surface lesions: comparison of CT arthrography and fat-suppressed FLASH 3D MR imaging. *Eur Radiol*, 8(6), pp. 981-985.
- Dalstra, M., Huiskes, R. & Van Erning, L., 1995. Development and validation of a three-dimensional finite element model of the pelvic bone. *J Biomech En*, 117(3), pp. 272-278.
- Della Croce, U., Leardini, A., Chiari, L. & Cappozzo, A., 2005. Human movement analysis using stereophotogrammetry. Part 4: assessment of anatomical landmark misplacement and its effects on joint kinematics. *Gait Posture*, 21(2), pp. 226-237.
- Dong, Y. F. et al., 2011. Accurate 3D reconstruction of subject-specific knee finite element model to simulate the articular cartilage defects. *Journal of Shanghai Jiaotong University*, 16(5), pp. 620-627.
- Drake, R. L., Vogl, A. W. & Mitchell, A. W. M., 2010. *Gray's anatomy for students*. second ed. Canada: Churchill Livingstone Elsevier.
- Eckstein, F. et al., 2000. Effect of gradient and section orientation on quantitative analysis of knee joint cartilage. *J Magn Reson Imaging*, 11(4), pp. 469-470.

- Eckstein, F. et al., 1998. In vivo reproducibility of threedimensional cartilage volume and thickness measurements with MR imaging. *AJR Am J Roentgenol*, 170(3), pp. 593-597.
- Eijer, H., Myers, S. R. & Ganz, R., 2001. Anterior femoroacetabular impingement after femoral neck fractures. *J Orthop Trauma*, 15(7), pp. 475-481.
- El-Khoury, G. Y. et al., 2004. Cartilage thickness in cadaveric ankles: measurement with double-contrast multi-detector row CT arthrography versus MR imaging. *Radiology*, 233(3), pp. 768-773.
- Elsayed, S., 2010. *Hip Examination*. [Online]
Available at: <http://www.hipscope.co.uk/6.html>
[Accessed 23 June 2014].
- Fagan, M. J., 1992. *Finite element analysis, theory and practice*. First ed. UK: Longman Group UK Limited.
- Fagerston, T. L., 1998. *The hip handbook*. First ed. USA: Butterworth-Heinemann.
- Ferguson, S. J., Bryant, J. T., Ganz, R. & Ito, K., 2000. The influence of the acetabular labrum on hip joint cartilage consolidation: a poroelastic finite element model. *J Biomech*, 33(3), pp. 953-960.
- Field, D. & Hutchinson, O. J., 2006. *Anatomy palpation and surface markings*. 4th ed. UK: Butterworth-Heinemann.
- Filigenzi, J. M. & Bredella, M. A., 2008. *MR imaging of femoroacetabular impingement*. [Online]
Available at: <http://www.appliedradiology.com/articles/mr-imaging-of-femoroacetabular-impingement>
[Accessed 20 09 2014].
- Finlay, J. B., Bourne, R. B., Landsberg, R. P. & Andreae, P., 1986. Pelvic stresses in vitro--I. malsizing of endoprotheses. *J Biomech*, 19(9), pp. 703-714.
- Gajdosik, R. L. & Bohannon, R. W., 1987. Clinical Measurement of Range of Motion, Review of Goniometry Emphasizing Reliability and Validity. *Journal of the American Physical Therapy*, 67(12), pp. 1867-1872.
- Ganz, R., Leunig, M., Leunig-Ganz, K. & Harris, W., 2008. The etiology of osteoarthritis of the hip: an integrated mechanical concept. *Clinical orthopaedics and related research*, 466(2), pp. 264-272.
- Ganz, R. et al., 2003. Femoroacetabular impingement: a cause for osteoarthritis of the hip. *Clinical orthopaedics and related research*, Volume 417, pp. 112-120.

- Gauresh, D., 2009. *healthHype*. [Online]
Available at: <http://www.healthhype.com/femoral-neck.html>
[Accessed 20 Jan 2014].
- Genda, E. et al., 2001. Normal hip joint contact pressure distribution in single-leg standing--effect of gender and anatomic parameters. *J Biomech*, 34(7), pp. 895-905.
- Genda, E., Konishi, N., Hasegawa, Y. & Miura, T., 1995. A computer simulation study of normal and abnormal hip joint contact pressure. *Arch Orthop Trauma Surg*, 114(4), pp. 202-206.
- Goel, V. K., Valliappan, S. & Svensson, N. L., 1978. Stresses in the normal pelvis. *Comput Biol Med*, 8(2), pp. 91-104.
- Greene, W. B. & Heckman, J. D., 1994. *The clinical measurement of joint motion*. First ed. s.l.:American Academy of Orthopaedic Surgeons.
- Griffin, D., 2007. *NHS, Surgery for femoroacetabular impingement*. [Online]
Available at:
http://www.library.nhs.uk/trauma_orthopaedics/viewResource.aspx?resID=269337
[Accessed 20 Jan 2014].
- Guo, Y., Zhang, X. & Chen, W., 2009. Three-dimensional finite element simulation of total knee joint in gait cycle. *Acta Mechanica Solida Sinica*, 22(4), pp. 347-351.
- Harris, W. H., 1986. Etiology of osteoarthritis of the hip. *Clinical Orthopaedics & Related*, Volume 213, pp. 20-33.
- Hayes, W. C., Keer, L. M., Herrmann, G. & Mockros, L. F., 1972. A mathematical analysis for indentation tests of articular cartilage. *J Biomech*, 5, pp., 5(5), pp. 541-551.
- Hewitt, J., Guilak, F., Glisson, R. & Vail, P. T., 2001. Regional material properties of the human hip joint capsule ligaments. *Journal of orthopaedic research*, 19(3), pp. 359-364.
- Hodge, W. A. et al., 1986. Contact pressures in the human hip joint measured in vivo. *Proc Natl Acad Sci U S A*, 83(9), pp. 2879-2883.
- Holm, I. et al., 2000. Reliability of goniometric measurements and visual estimates of hip ROM in patients with osteoarthrosis. *Physiother Res Int*, 5(4), pp. 241-248.
- Horisberger, M., Brunner, A. & Herzog, R. F., 2010. Arthroscopic treatment of femoroacetabular impingement of the hip. *Clin Orthop Relat Res*, 468(1), pp. 182-190.
- Hossain, M. & Andrew, J. G., 2008. Current management of femoro-acetabular Impingement. *Current Orthopaedics*, Volume 22, pp. 300-310.
- Hu, Q. et al., 2001. A fast impingement algorithm for computer-aided orthopaedic surgery. *Comput Aided Surg*, 16(2), pp. 104-110.

- Iko, K. et al., 2001. Femoroacetabular impingement and the cam-effect a MRI-based quantitative anatomical study of the Femoral head-neck offset. *J Bone Joint Surg*, 83(2), pp. 171-176.
- Ito, K., Leunig, M. & Ganz, R., 2004. Histopathologic features of the acetabula labrum in femoroacetabular impingement.. *Clinical Orthopaedics & Related Research*, Volume 429, pp. 262-271.
- Jäger , M., Wild , A., Westhoff , B. & Krauspe, R., 2004. Femoroacetabular impingement caused by a femoral osseous head-neck bump deformity: clinical, radiological, and experimental results. *J Orthop Sci*, 9(3), pp. 256–263.
- Jones, O., 2013. *TeachMeAnatomy*. [Online]
Available at: <http://teachmeanatomy.info/lower-limb/joints/the-hip-joint/>
[Accessed 20 02 2014].
- Kang , M., Sadri, H., Mocozet, L. & Magnenat-Thalmann , N., 2002. *Accurate simulation of hip joint range of motion*. CA, Proceedings of IEEE Computer Animation, pp. 215-219.
- Kang, M. et al., 2002. *Accurate simulation of hip joint range of motion*. MIRALab – University of Geneva, IEEE, Proceedings of the Computer Animation.
- Kapron, A. L. et al., 2011. Radiographic prevalence of femoroacetabular impingement in collegiate football players: AAOS exhibit selection. *Journal of Bone & Joint Surgery American*, 93(19), pp. 1-10.
- Kennedy , M. J., Lamontagne, M. & Beaulé , P. E., 2009. Femoroacetabular impingement alters hip and pelvic biomechanics during gait walking biomechanics of FAI. *Gait & Posture*, 30(1), pp. 41-44.
- Kim, Y. H., Kim, J. S. & Cho, S. H., 2001. Strain distribution in the proximal human femur. an in vitro comparison in the intact femur and after insertion of reference and experimental femoral stems. *J Bone Joint Surg Br*, 83(2), pp. 295-301.
- Kolata, G., November 2011. *Hip procedure grows popular despite doubt*. *Health section new York time*. [Online]
Available at: http://www.nytimes.com/2011/11/16/health/hip-impingement-grows-popular-but-remains-unproven.html?pagewanted=all&_r=0
[Accessed 21 Jan 2014].
- Kubiak-Langer, M. et al., 2007. Range of motion in anterior femoroacetabular impingement. *Clinical orthopaedics and related research*, Volume 458, pp. 117–124.
- Kuhlman, G. S. & Domb, B. G., 2009. Hip impingement: identifying and treating a common cause of hip pain. *American Family Physician*, 80(12), pp. 1429-1434.
- Lamontagne, M. & Kennedy, M. J., 2009. The Effect of Cam FAI on Hip and Pelvic Motion during Maximum Squat. *Clin Orthop Relat Res*, 467(3), pp. 645–650.

- Lamontagne, M., Kennedy, M. J. & Beaulé, P. E., 2009. The effect of cam FAI on hip and pelvic motion during maximum squat. *Clin Orthop Relat Res*, 476(3), pp. 645-650.
- Lavigne, M. et al., 2004. Anterior femoroacetabular impingement. Part I: techniques of joint preserving surgery. *Clin Orthop Relat Res*, Volume 418, pp. 61-66.
- Lea, R. D. & Gerhardt, J. J., 1995. Range-of-motion measurements. *J Bone Joint Surg Am*, 77(5), pp. 784-798.
- Leardini, A., Chiari, L., Della Croce, U. & Cappozzo, A., 2005. Human movement analysis using stereophotogrammetry. Part 3. Soft tissue artifact assessment and compensation. *Gait Posture*, 21(2), pp. 212-225.
- Lee, C. F. et al., 2006. Three-dimensional reconstruction and modeling of middle ear biomechanics by high-resolution computed tomography and finite element analysis. *Laryngoscope*, 116(5), pp. 711-716.
- Leunig, M., Beaulé, P. & Ganz, R., 2009. The concept of femoroacetabular impingement current status and future perspectives. *Clin Orthop Relat Res*, 476(3), pp. 616-622.
- Leunig, M., Beck, M., Dora, C. & Ganz, R., 2005. Femoroacetabular impingement: etiology and surgical concept. *Operative Techniques in Orthopaedics*, 15(3), pp. 274-255.
- Leunig, M. & Ganz, R., 2005. Femoroacetabular impingement: a common cause of hip complaints leading to arthrosis. *Unfallchirurg*, 108(1), pp. 9-17.
- Leunig, M. et al., 2004. Magnetic resonance arthrography of labral disorders in hips with dysplasia and impingement. *Clin Orthop Relat Res*, Volume 418, pp. 74-80.
- Levangie, P. K. K. & Norkin, C. C., 2001. *Joint structure and function: a comprehensive analysis*. 3rd ed. United States: Davis Company.
- Lever, C. J. & O'Hara, J. N., 2008. Young adult hip disease: hip morphology and impingement. *Current Orthopaedics*, 22(6), pp. 414-421.
- Lin, M. C. & Manocha, D., 1995. Fast interference detection between geometric models. *The Visual Computer*, 11(10), pp. 542-561.
- Macirowski, T., Tepic, S. & Mann, R. W., 1994. Cartilage stresses in the human hip joint. *J Biomech Eng*, 116(1), pp. 8-10.
- Madgwick, S. O. H., 2010. An efficient orientation filter for inertial and inertial/magnetic sensor arrays. In: pp. 15-18.
- Maggio, E. & Cavallaro, A., 2011. *Video tracking theory and practice*. First ed. Singapore: John Wiley and Sons.

- Mak, A. F. & Mow, V. C., 1987. Biphasic indentation of articular cartilage- I, theoretical analysis. *J Biomech*, 20(7), pp. 703-714.
- Mankin, H. J., 1974. The reaction of articular cartilage to injury and osteoarthritis (second of two parts). *N Engl J Med*, 291(25), pp. 1335-1340.
- Mann, R. W., 2002. Comment on quantitative determination of joint incongruity and pressure distribution during simulated gait and cartilage thickness in the human hip joint. *Journal of Orthopaedic Research*, 18(1), pp. 164-167.
- Marti, D. E. & Tashman, S., 2010. The biomechanics of femoroacetabular impingement. *Operative Techniques in Orthopaedics*, 20(4), pp. 248-254.
- Martin , R., Irrgang , J. & Sekiya , J., 2008. The diagnostic accuracy of a clinical examination in determining intra-articular hip pain for potential hip arthroscopy candidates. *Arthroscopy*, 24(9), pp. 1013-1018.
- Mavcic, B. et al., 2002. Mathematical estimation of stress distribution in normal and dysplastic hips. *Journal of Orthopaedic Research*, 20(5), pp. 1025-1030.
- Meyer , D., Beck , M., Ganz, R. & Leunig , M., 2006. Comparison of six radiographic projections to assess femoral head/neck asphericity. *Clin Orthop Relat Res*, Volume 445, pp. 181-185.
- Michaeli, D. A., Murphy, S. B. & Hipp, J. A., 1997. Comparison of predicted and measured contact pressures in normal and dysplastic hips. *Med Eng Phys*, 19(2), pp. 180-186.
- MIMICs , 2014. *Mimics 15 refrence guid manual*, pp. 1-20.
- Monahan , E. & Shimada , K., 2008. Verifying the effectiveness of a computeraided navigation system for arthroscopic hip surgery. *Stud Health Technol Inform*, Volume 132, pp. 302-307.
- Moore, M. & Wilhelms, O., 1988. Collision detection and response response for computer animation. *Computer graphics and interactive techniques*, 22(4), pp. 289 – 298.
- Motion Capture Manual , 2013. *Motion Capture manual*. [Online] [Accessed 19 07 2014].
- MotionNode Manual, 2013. *MotionNode*. [Online] Available at: <http://www.motionnode.com/> [Accessed 29 02 2014].
- Mow, V. C., Kuei, S. C., Lai, W. M. & Armstrong, C. G., 1980. Biphasic creep and stress relaxation of articular cartilage in compression: theory and experiments. *J Biomech Eng*, 102(1), pp. 73-84.

- Murphy , S. et al., 2004. Debridement of the adult hip for femoroacetabular impingement: indications and preliminary clinical results. *Clin Orthop Relat Res*, Volume 429, pp. 178–181.
- Murray, R. O., 1965. The aetiology of primary osteoarthritis of the hip. *British Journal of*, 38(455), pp. 810-824.
- Nussbaumer, S. et al., 2010. Validity and test-retest reliability of manual goniometers for measuring passive hip range of motion in femoroacetabular impingement patients. *BMC Musculoskeletal Disorders*, 11(194), pp. 2-11.
- Ochoa, L. M., Dawson, L., Patzkowski, J. C. & Hsu, J. R., 2010. Radiographic prevalence of femoroacetabular impingement in a young population with hip complaints is high. *Clinical Orthopaedics & Related Research*, 468(10), pp. 2710-2714.
- Oh, I. & Harris, W. H., 1978. Proximal strain distribution in the loaded femur. An in vitro comparison of the distributions in the intact femur and after insertion of different hip-replacement femoral components. *J Bone Joint Surg Am*, 60(1), pp. 75-85.
- Oonishi, H., Isha , H. & Hasegawa, T., 1983. Mechanical analysis of the human pelvis and its application to the artificial hip joint--by means of the three dimensional finite element method. *J Biomech*, 16(6), pp. 427-44.
- Papaoiannou, G., Demetropoulos, C. K. & Kin, Y. H., 2010. Predicting the effects of knee focal articular surface injury with a patient-specific finite element model. *Knee*, 17(1), pp. 61–68.
- Pearle, A. D., Kendoff , D. & Musahl , V., 2009. Perspectives on computer-assisted orthopaedic surgery: movement toward quantitative orthopaedic surgery. *J Bone Joint Surg Am*, 91(1), pp. 7-12.
- Peña, E., Calvo, B., Martínez, M. A. & Dobra, M., 2006. A three-dimensional finite element analysis of the combined behavior of ligaments and menisci in the healthy human knee joint. *Journal of Biomechanics*, 39(9), pp. 1686–1701.
- Philippon , M. et al., 2007. Arthroscopic management of femoroacetabular impingement: osteoplasty technique and literature review. *Am J Sports Med*, 35(9), pp. 1571-1580.
- Philippon, M. J. & Schenker, B. L., 2006. Arthroscopy for the treatment of femoroacetabular impingement in the athlete. *Clin Sports Med*, 25(2), pp. 299-308.
- Philips , A. T. M. et al., 2007. Finite element modelling of the pelvis: inclusion of muscular and ligamentous boundary conditions. *medical engineering and physics*, 29(7), pp. 739-748.
- Rapperport, D. J., Carter, D. R. & Schurman, D. J., 1985. Contact finite element stress analysis of the hip joint. *J Orthop Res*, 3(4), pp. 435-446.

- Reinschmidt , C. et al., 1997. Effect of skin movement on the analysis of skeletal knee joint motion during running. *J Biomech*, 30(7), pp. 729– 732.
- Rho, J. Y., Ashman, R. B. & Turner, C. H., 1993. Young's modulus of trabecular and cortical bone material: ultrasonic and microtensile measurements. *Journal of Biomechanic*, 26(2), pp. 111-119.
- Ries, M. et al., 1989. Normal pelvic strain pattern in vitro. *J Biomed Eng*, 11(5), pp. 398-402.
- Rivkin , G. & Liebergall , M., 2009. Challenges of technology integration and computer-assisted surgery. *J Bone Joint Surg Am*, 91(1), pp. 13-16.
- Rodrigo , M. et al., 2005. Surgical treatment of femoroacetabular impingement: evaluation of the effect of the size of the resection. *J bone & joint surgery*, 87(2), pp. 273-279.
- Ross, C. & Craig , A., 2007. *Introductory biomechanics from cells to organisms*. First ed. Canada: Cambridge University Press.
- Rushfeldt, P. D., Mann, R. W. & Harris, W. H., 1979. Influence of cartilage geometry on the pressure distribution in the human hip joint. *Science*, 204(4691), pp. 413-415.
- Rushfeldt, P. D., Mann, R. W. & Harris, W. H., 1981. Improved techniques for measuring in vitro the geometry and pressure distribution in the human acetabulum. Ii instrumented endoprosthesis measurement of articular surface pressure distribution. *J Biomech*, 14(5), pp. 315-323.
- Russell, M. E., Shivanna, K. H., Grosland, N. M. & Pedersen, D. R., 2006. Cartilage Contact Pressure Elevations in Dysplastic Hips: A Chronic Overload Model. *Journal of Orthopaedic Surgery and Research*, 1(6), pp. 5-11.
- Shirazi, R., Shirazi-Adl, A. & Hurtig, M., 2008. Role of cartilage collagen fibrils networks in knee joint biomechanics under compression. *Journal of Biomechanics*, 41(16), pp. 3340–3348.
- Siebenrock , K., Schöniger , R. & Ganz , R., 2003. Anterior femoro-acetabular impingement due to acetabular retroversion: treatment with periacetabular osteotomy. *J Bone Joint Surg Am*, 85(A(2)), pp. 278–286.
- Sitteck, H. et al., 1996. Assessment of normal patellar cartilage volume and thickness using MRI: an analysis of currently available pulse sequences. *Skeletal Radiol*, 25(1), pp. 55-62.
- Sobel, M. A. & Lerner, N., 1991. *Precalculus Mathematics*. 4th ed. Mishawaka: Prentice Hall.
- Solomon , L., Schnitzler , C. & Browett , J., 1982. Osteoarthritis of the hip: the patient behind the disease. *Ann Rheum Dis*, 41(2), pp. 118-125.

- Soltz, M. A. & Ateshian, G. A., 2000. A conewise linear elasticity mixture model for the analysis of tension-compression nonlinearity in articular cartilage. *J Biomech Eng*, 122(6), pp. 576-586.
- Strehl , A. & Ganz , R., 2005. Anterior femoroacetabular impingement after healed femoral neck fractures. *Unfallchirurg*, 108(4), pp. 263–273.
- Stulberg, S. D. & Harris, W. H., 1974. *Acetabular dysplasia and development of osteoarthritis of hip*, Proceedings of the second open scientific meeting of the hip society. St.Louis: Mosby.
- Suh, J. K. & Bai, S., 1998. Finite element formulation of biphasic poroviscoelastic model for articular cartilage. *J Biomech Eng*, 120(2), pp. 195-201.
- Suppanee, R. et al., 2013. Simulating osteoarthritis: The effect of the changing thickness of articular cartilage on the kinematics and pathological bone-to-bone contact in a hip joint with femoroacetabular impingement. *Journal of European Orthopaedics and Traumatology*, 4(2), pp. 1-9.
- Tannast , M. et al., 2005. Anatomic referencing of cup orientation in total hip arthroplasty. *Clin Orthop Relat Res*, Volume 436, pp. 144-150.
- Tannast, M. et al., 2008. Hip damage occurs at the zone of femoroacetabular impingement. *Clin Orthop Relat Res*, 466(2), pp. 273–280.
- Tannast, M. et al., 2007. Non-invasive three-dimensional assessment of femoroacetabular impingement. *Journal of orthopaedic research*, 25(1), pp. 122-131.
- Tanzer, M. & Noiseux , N., 2004. Osseous abnormalities and early osteoarthritis the role of hip impingement. *Clinical orthopaedics and related research*, Volume 429, pp. 170-177.
- Taunton , M., 2011. *Orthopedic One*. [Online]
Available at:
<http://www.orthopaedicsone.com/display/Main/Femoroacetabular+impingement>
[Accessed 24 June 2014].
- Terzaghi, K., 1943. *Theoretical soil mechanics*. New Yor, John Wiley and Sons.
- Toomayan , G. et al., 2006. Sensitivity of MR arthrography in the evaluation of acetabular labral tears. *AJR Am J Roentgenol*, 186(2), pp. 449-453.
- Tortora, G. J., 2003. *Principles of anatomy and physiology*. 10th ed. Wiley.
- Truesdell, C. & Toupin, R., 1960. *The Classical Field Theories*. Berlin, Springer-Verlag.
- Tsekleves, E. et al., 2012. *Personalised stroke rehabilitation intervention using open source 3D software and the Wii Remote Plus*. France, 9th Intl Conf in Disability, Virtual Reality & Associated Technologies.

- Van Rietbergen, B., Odgaard, A., Kabel, J. & Huiskes, R., 1996. Direct mechanics assessment of elastic symmetries and properties of trabecular bone architecture. *J Biomech*, 29(12), pp. 1653-1657.
- Wang, Z. et al., 2007. Three-dimensional reconstruction on pc-windows platform for evaluation of living donor nephrectomy. *Comput Methods Programs Biomed*, 86(1), pp. 39-44.
- Warland, A. et al., 2012. ReWiiRe (research in Wii rehabilitation): user involvement in the development of a personalised rehabilitation system for arm re-education after stroke. *International Journal of Stroke*, 7(2), pp. 79-83.
- Wawro, M. & Fathi-Torbaghan, M., 2004. A parallel framework for the FE-based simulation of knee joint motion. *IEEE Transactions on Biomedical Engineering*, 51(8), pp. 1490–1494.
- Wettstein, M. & Dienst, M., 2006. Hip arthroscopy for femoroacetabular impingement. *Orthopad*, 35(1), pp. 85-93.
- Wiberg, G., 1940. Studies on dysplastic acetabula and congenital subluxation of the hip joint with special reference to the complication of osteoarthritis. *The Journal of the American Medical Association*, 115(1), pp. 7-38.
- Yahia-Cherif, L., Gilles, B., Molet, T. & Magnenat-Thalmann, N., 2004. Motion capture and visualization of the hip joint with dynamic MRI and optical systems. *Computer Animation and Virtual Worlds*, 15(3-4), pp. 377–385.
- Yoshida, H. et al., 2006. Three-dimensional dynamic hip contact area and pressure distribution during activities of daily living. *J Biomech*, 39(11), pp. 1996-2004.

Appendix A: Surgical Procedure

A.1 Surgical procedure of FAI

Hip arthroscopy is the correction surgery for someone who has hip impingement and knowing the biomechanics of hip allow better understanding of the hip operation. Hip arthroscopy procedure is followed as:

1. The lower limb was placed in slight flexion (10° - 20°), with the foot maintained in neutral to slight external rotation.
2. The patient was put in the lateral position. Figure A.1 shows the patient's position before arthroscopy. The lower limb was placed in slight flexion (10-20), with the foot maintained in neutral to slight external rotation.



Figure A.1: Preparation of patient in the lateral position under arthroscopy surgery

3. Figure A.2 shows the surgery procedure and how the arthroscopy needle and wire was inserted into the patient hip.

Start of surgery



Adjusting the position of the needle by the aid of x-ray images



Tracing the labral tears



Camera system at the location of operation

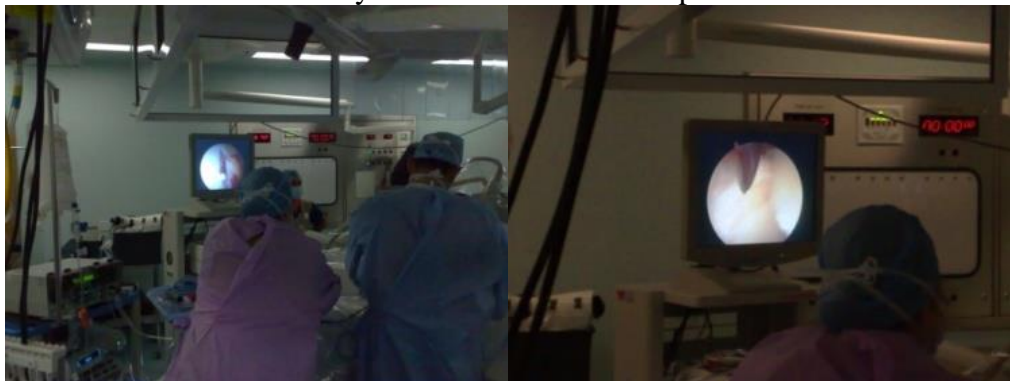


Figure A.2: Procedure of arthroscopy surgery

4. A chondral split was detected during the arthroscopy which was sealed using a radio frequency probe as shown in Figure A.3. Then, the osseous bump at the head-neck region of the femur was resected.

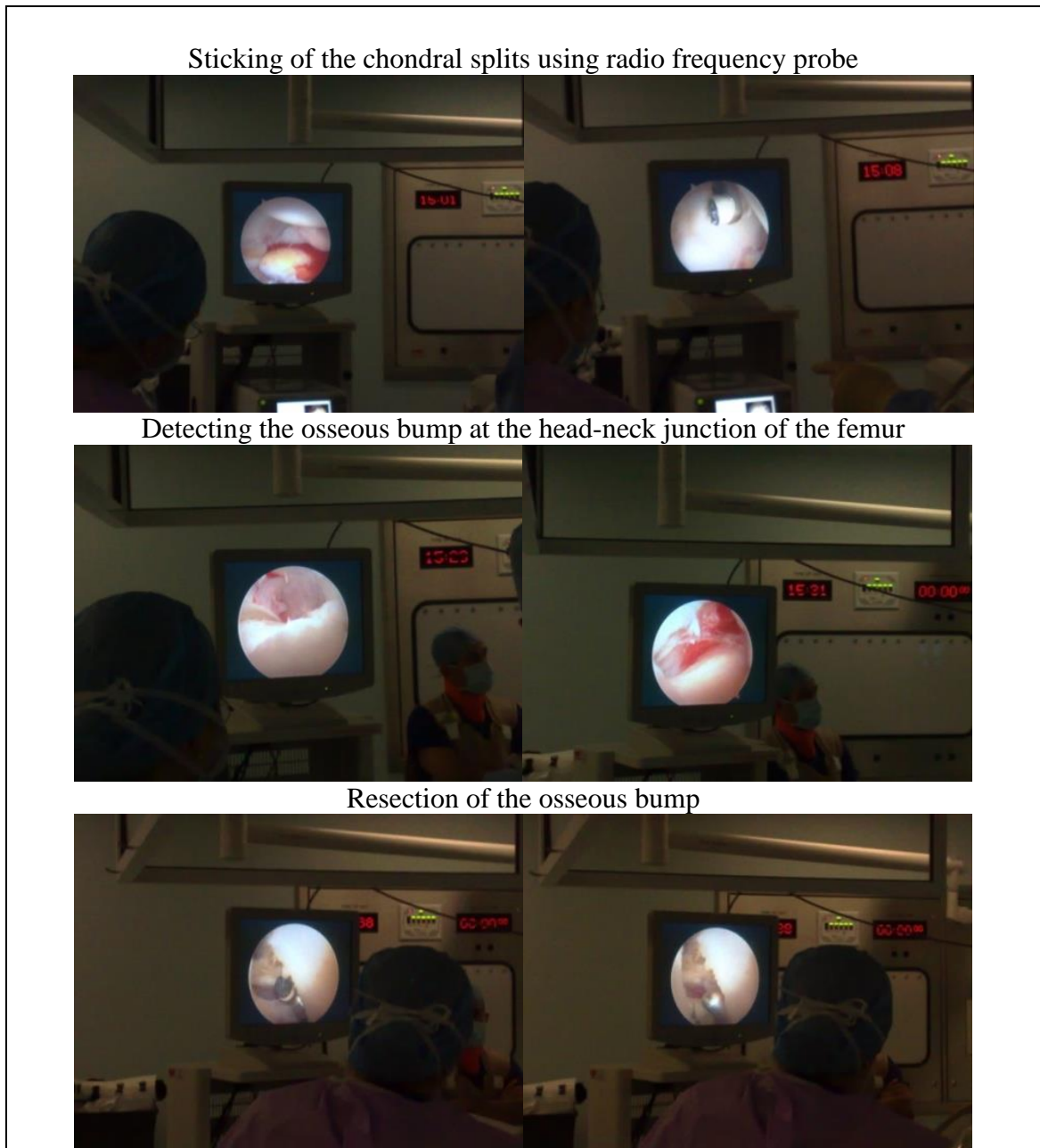


Figure A.3: Sealing of the chondral splits and resection of the bony growth

5. After completion of the surgery, the needle and the probe was removed from the body and the body tissues were held together by a surgical suture as shown in Figure A.4.

Removing the needle and probe from the body



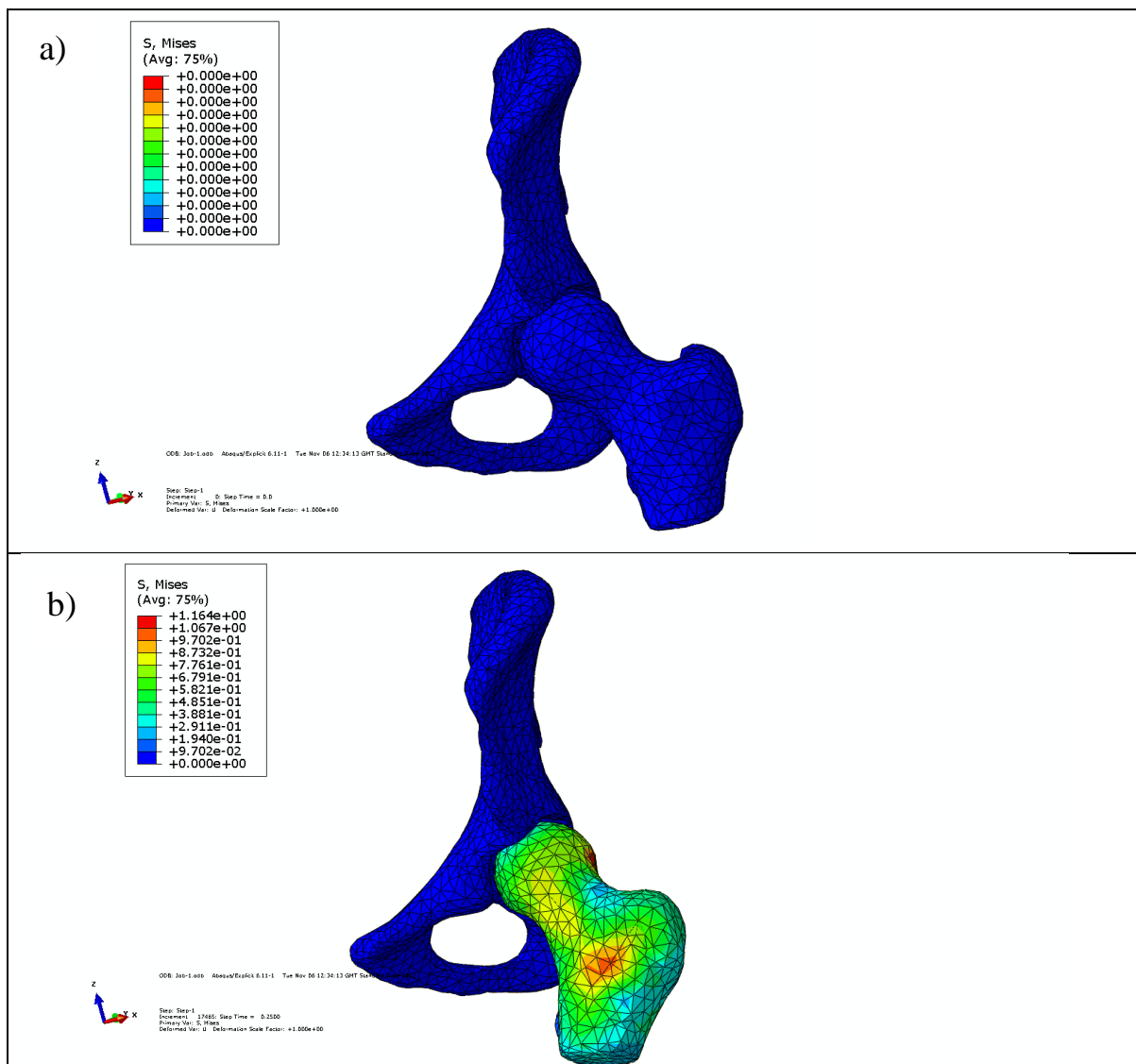
Surgical Suture

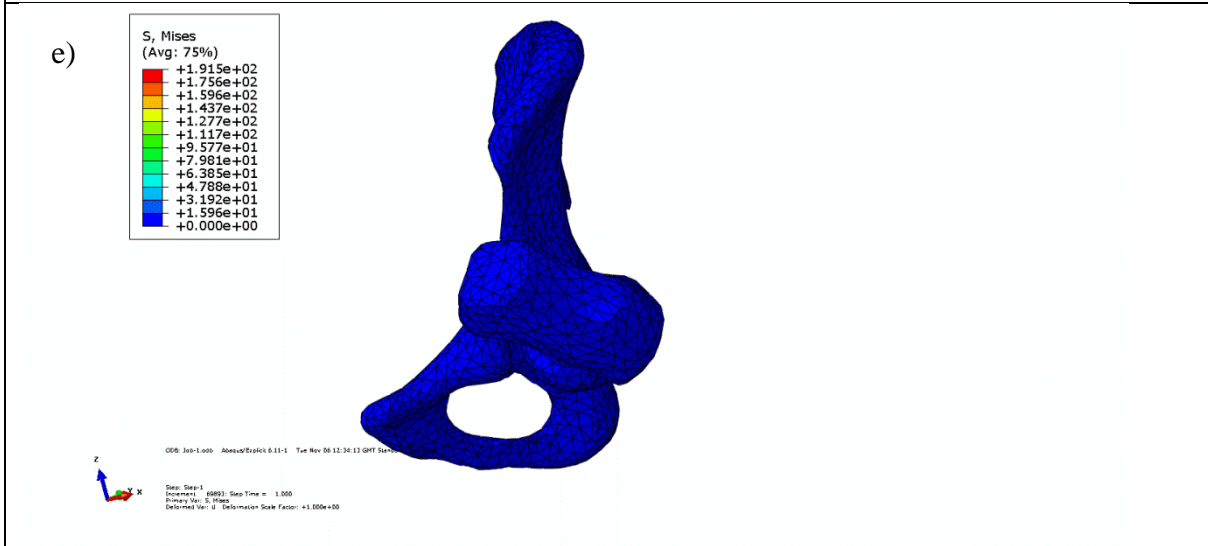
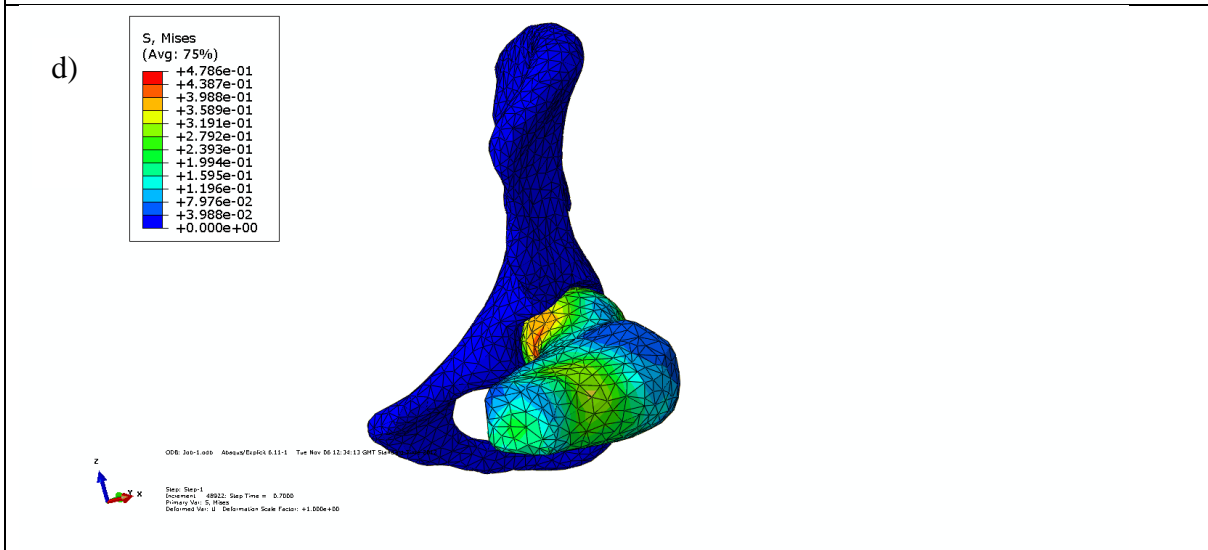
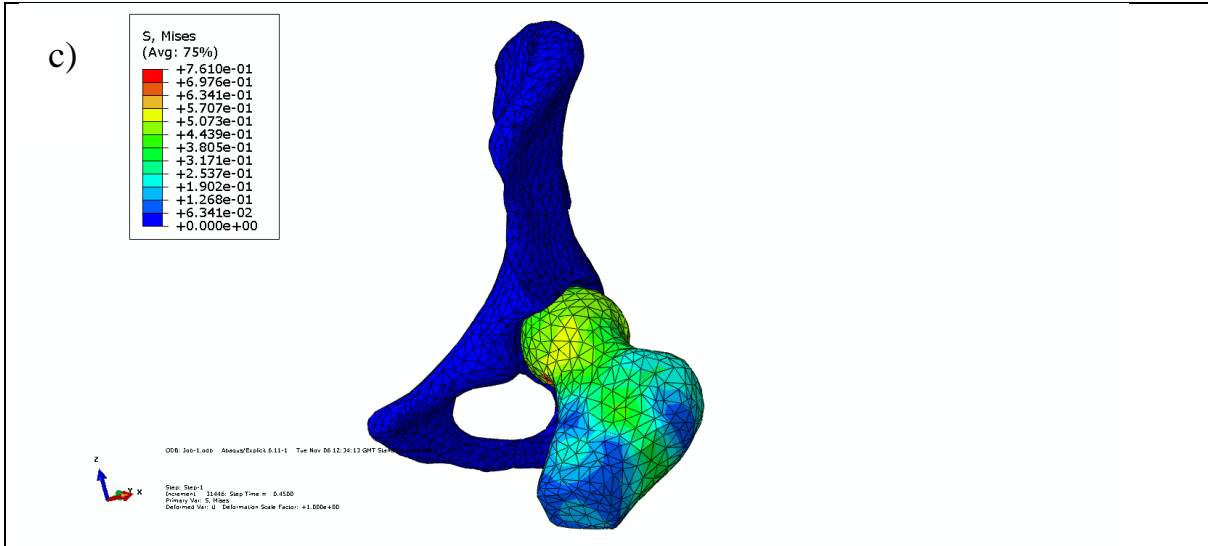


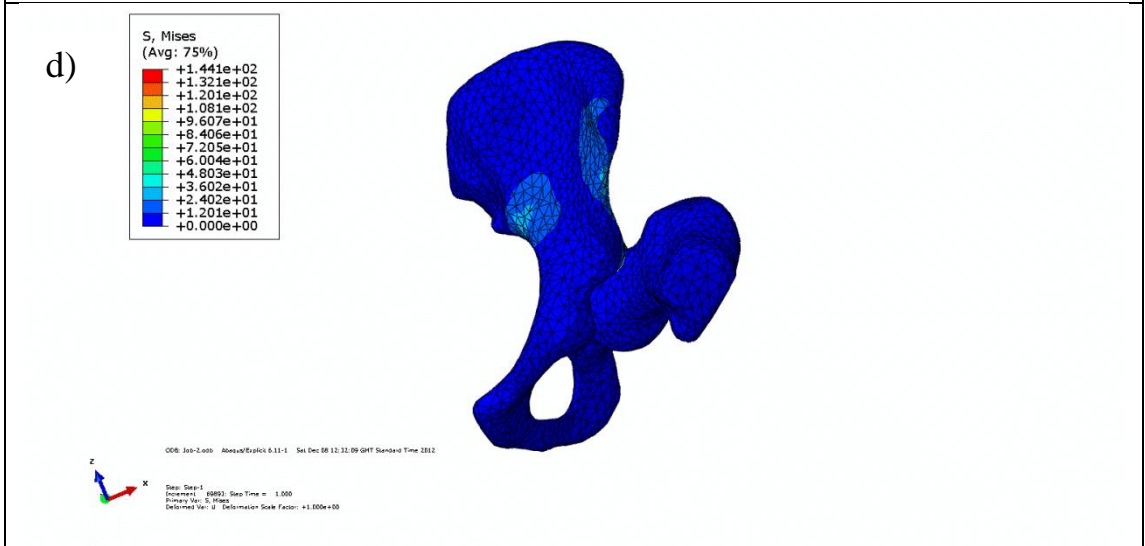
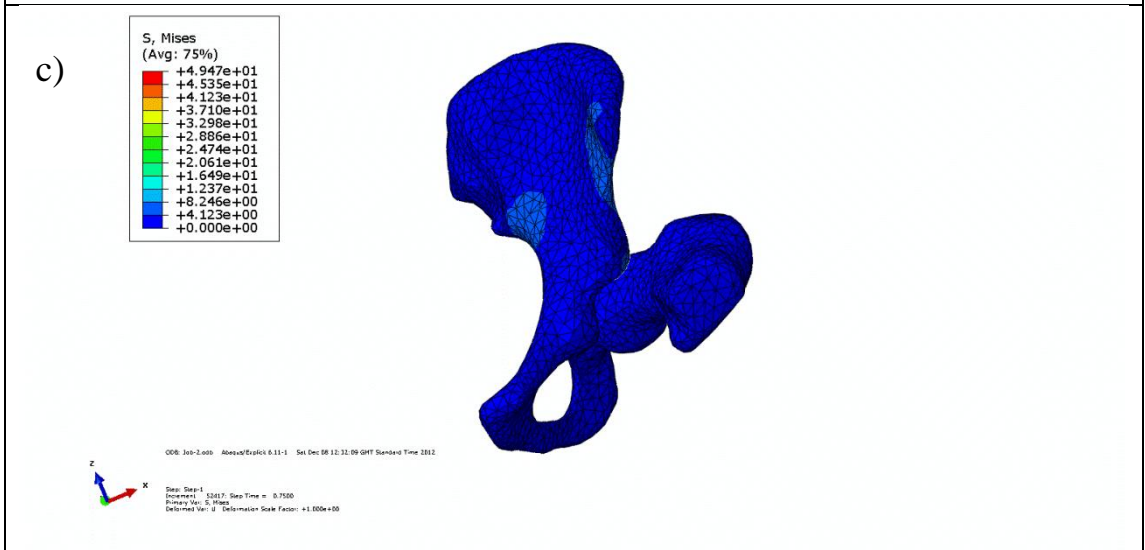
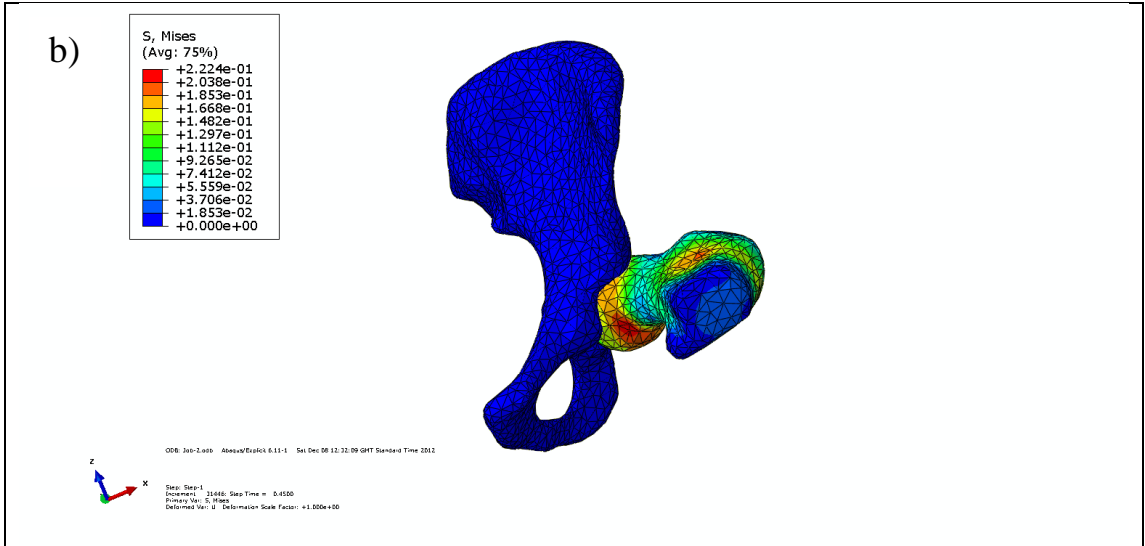
Figure A.4: End of the surgery

Appendix B: Collision Detection of Hip

B.1 Fixed Centre of Rotation







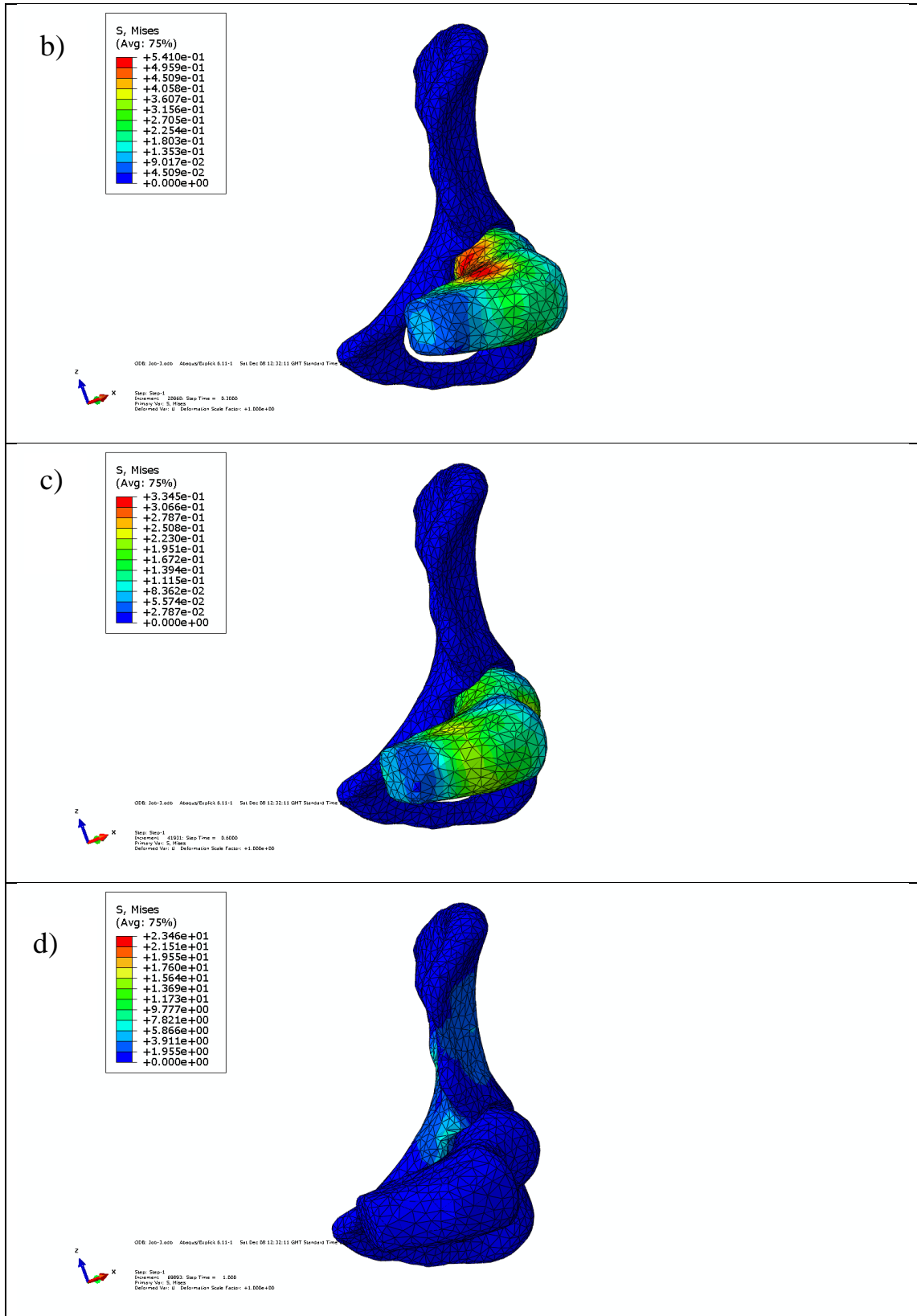
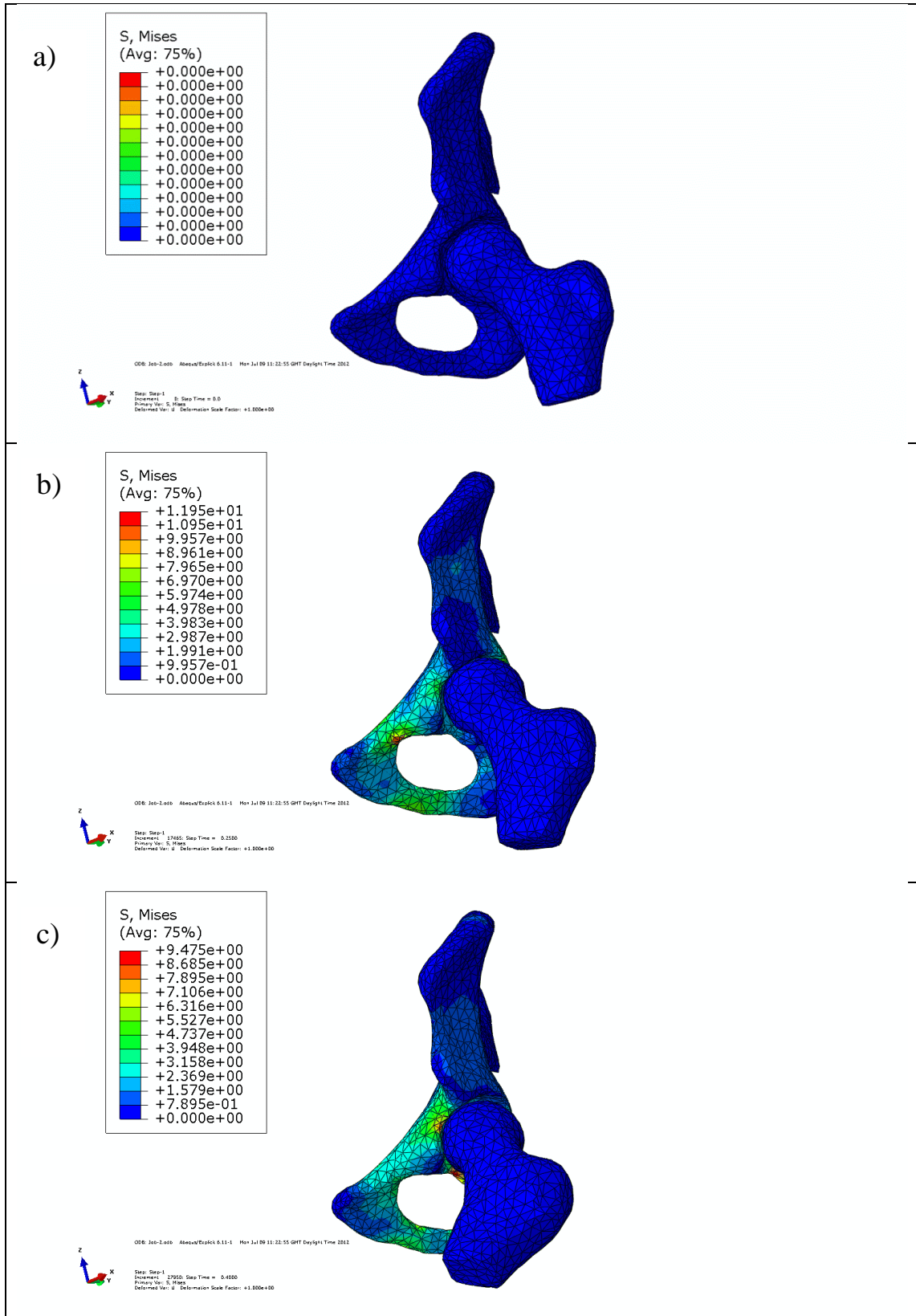
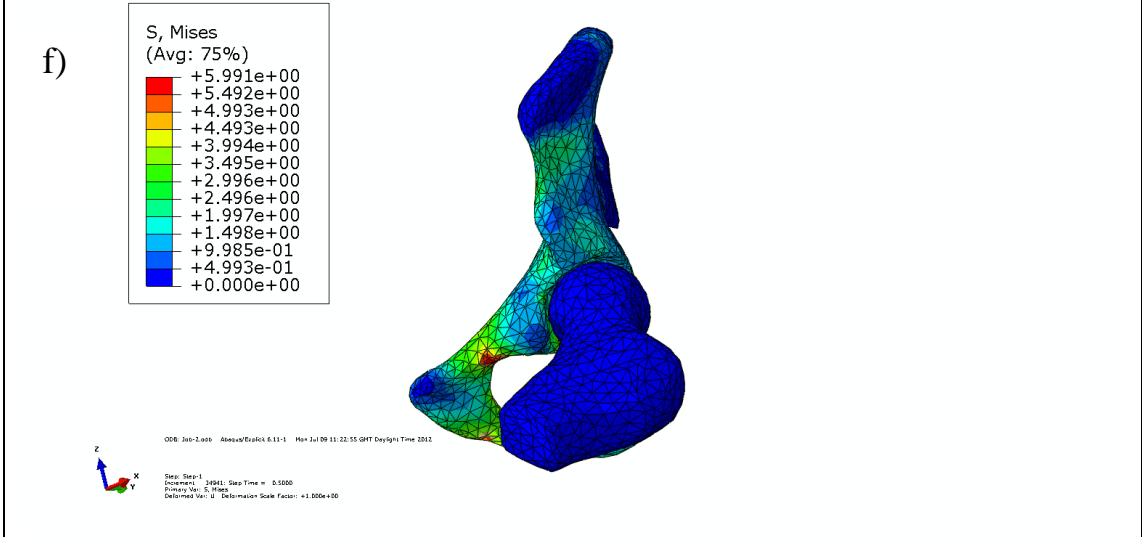
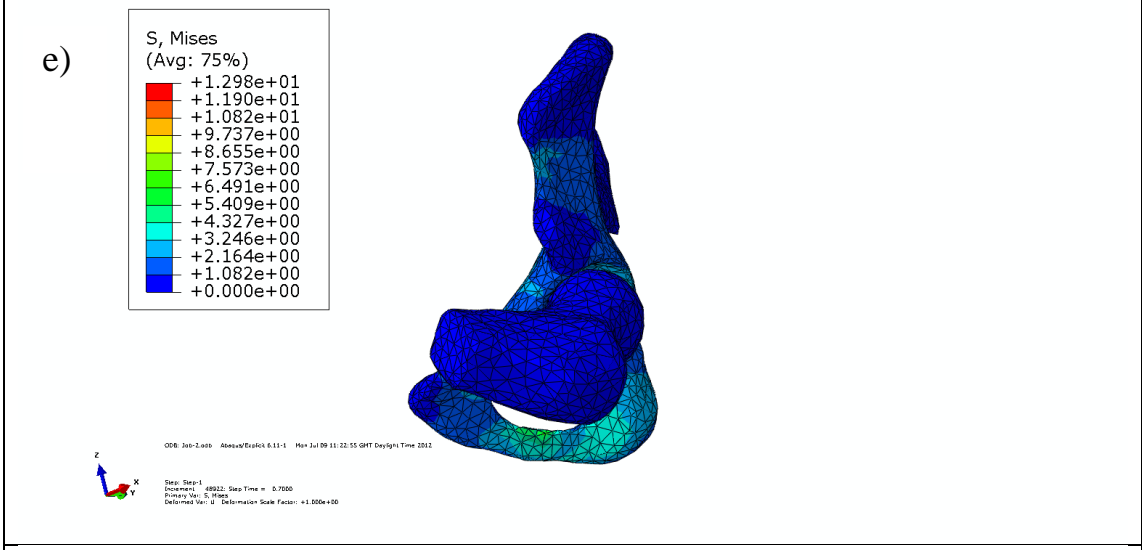
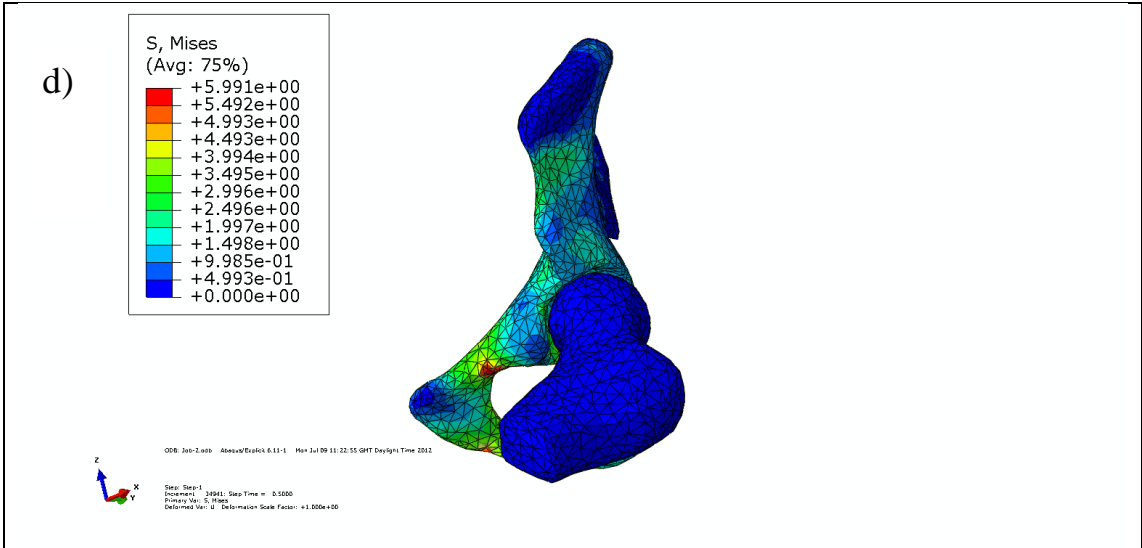


Figure B.3: Internal rotation of the femur around the fixed centres of rotation in 90° flexion (left hip) a- d) femur and acetabulum from 90° flexion position until impingement happens (left hip)

B.2 Free Centre of Rotation





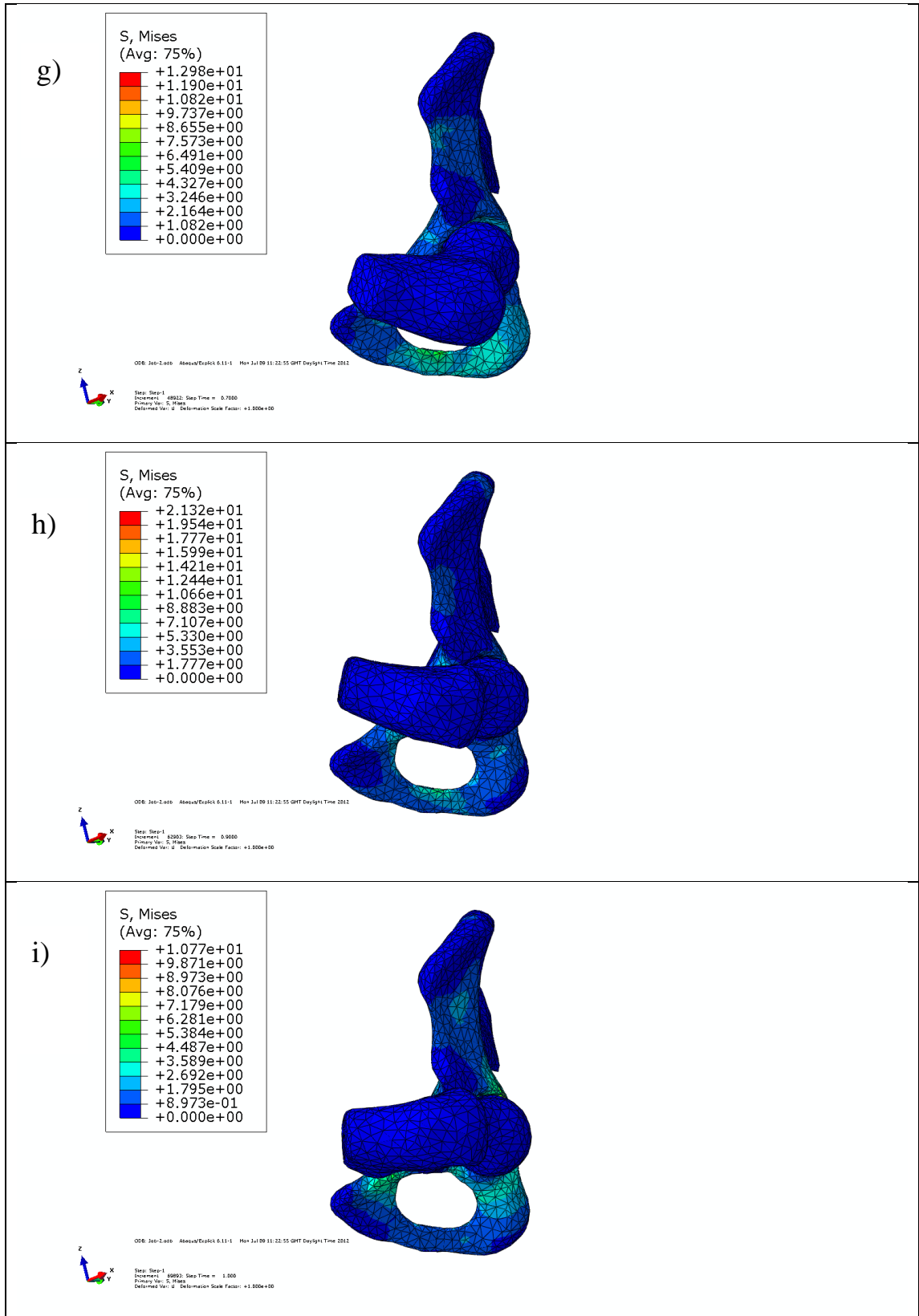
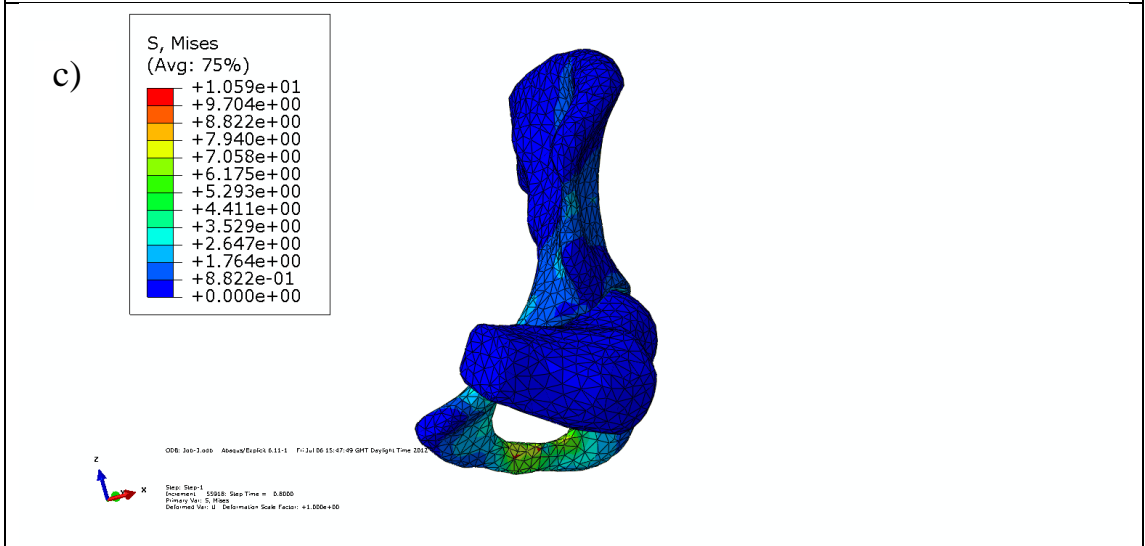
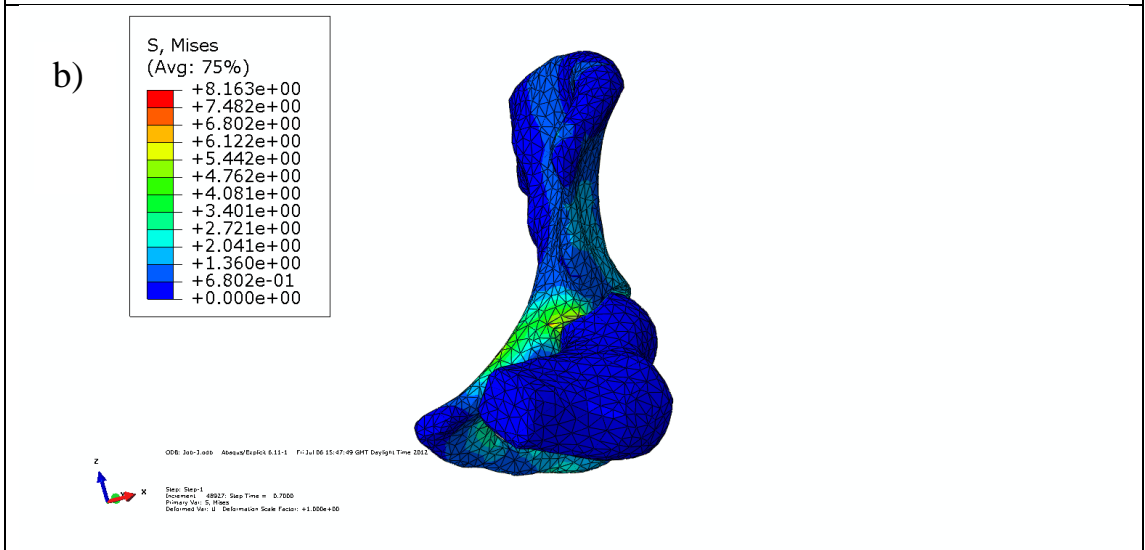
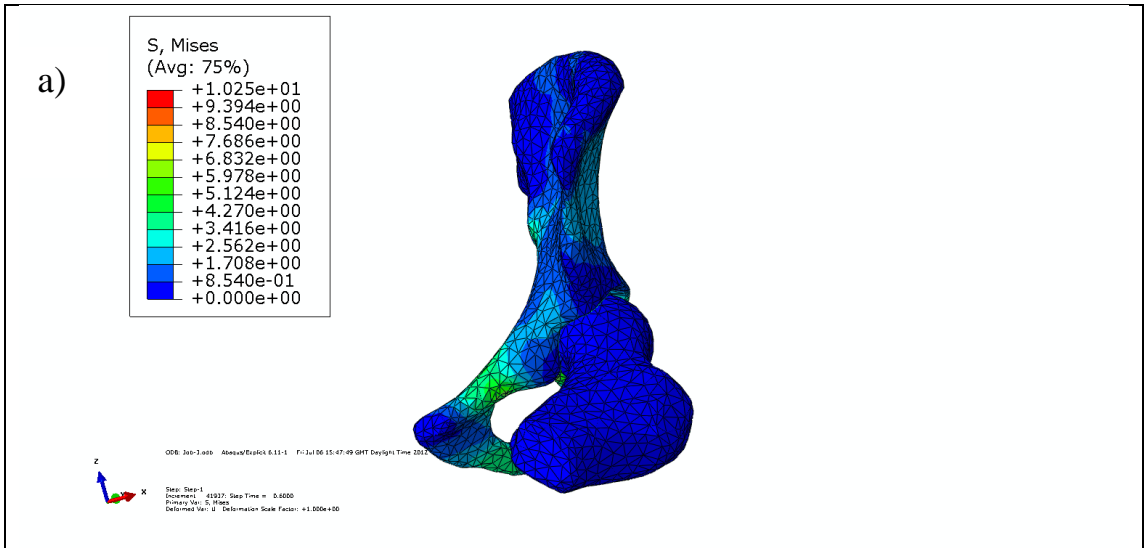


Figure B.4: Flexion of the femur by applying the flexion force a- i) femur and acetabulum from supine position until impingement happens (left hip)



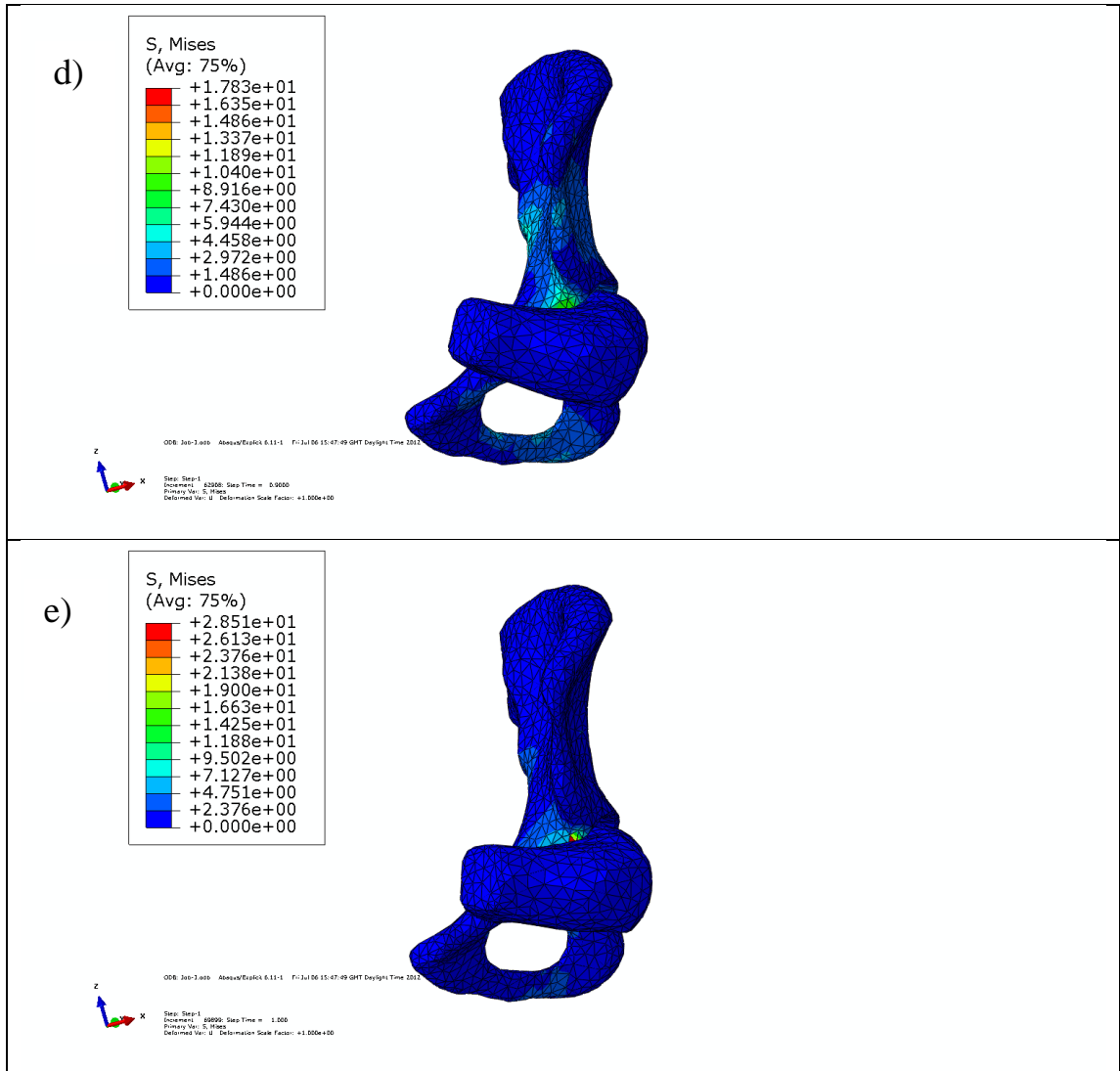
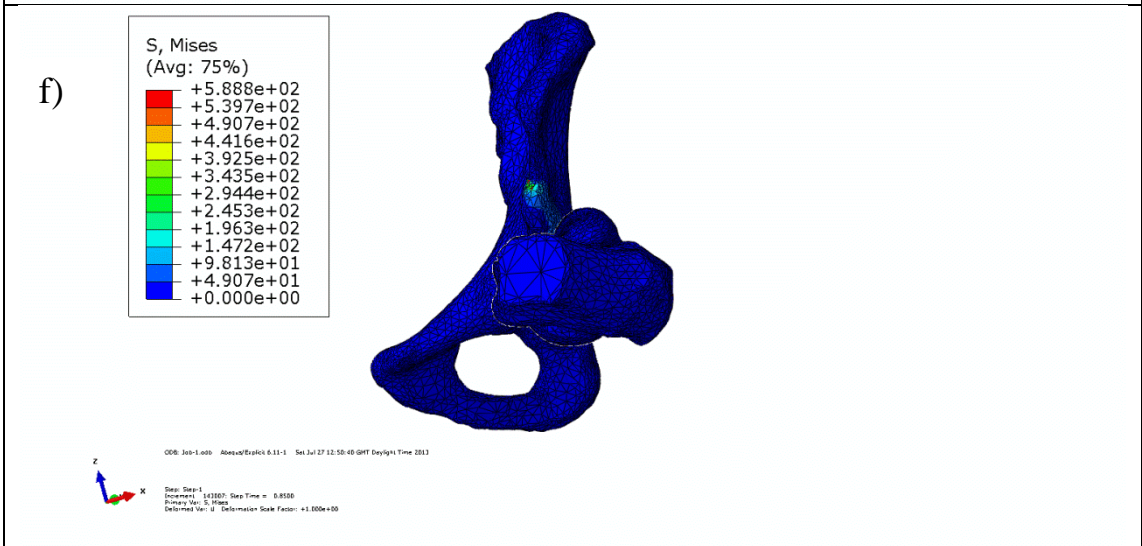
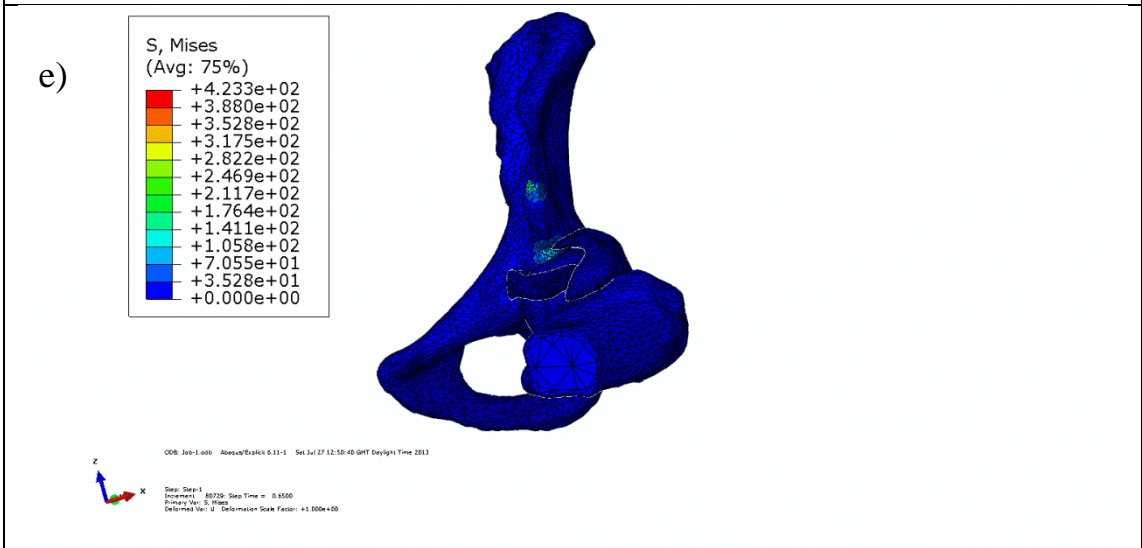
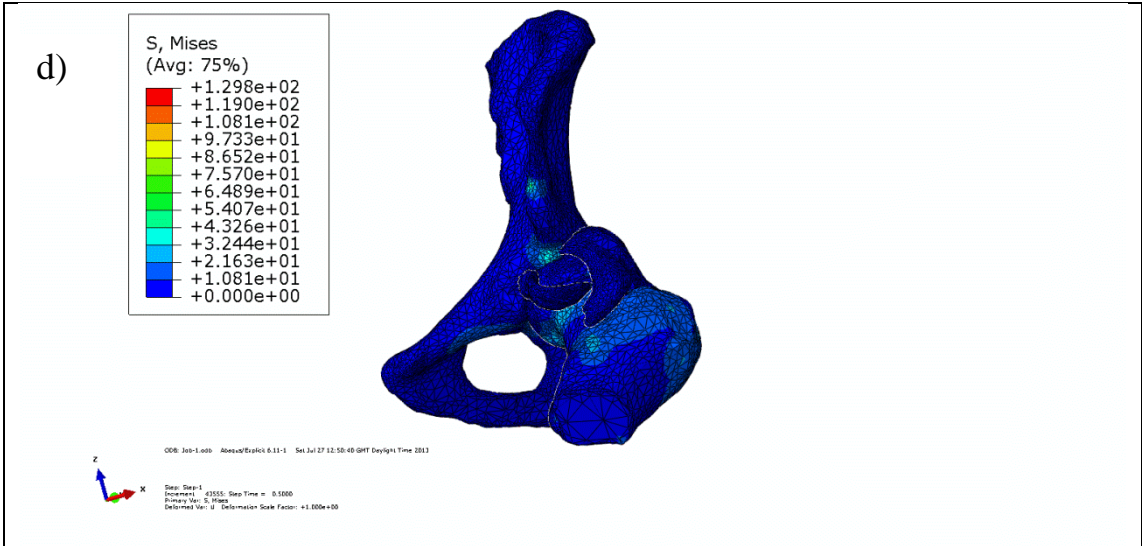


Figure B.5: Adduction of the femur by applying the adductor force in 90° of flexion a- e) femur and acetabulum from supine position until impingement happens (left hip)



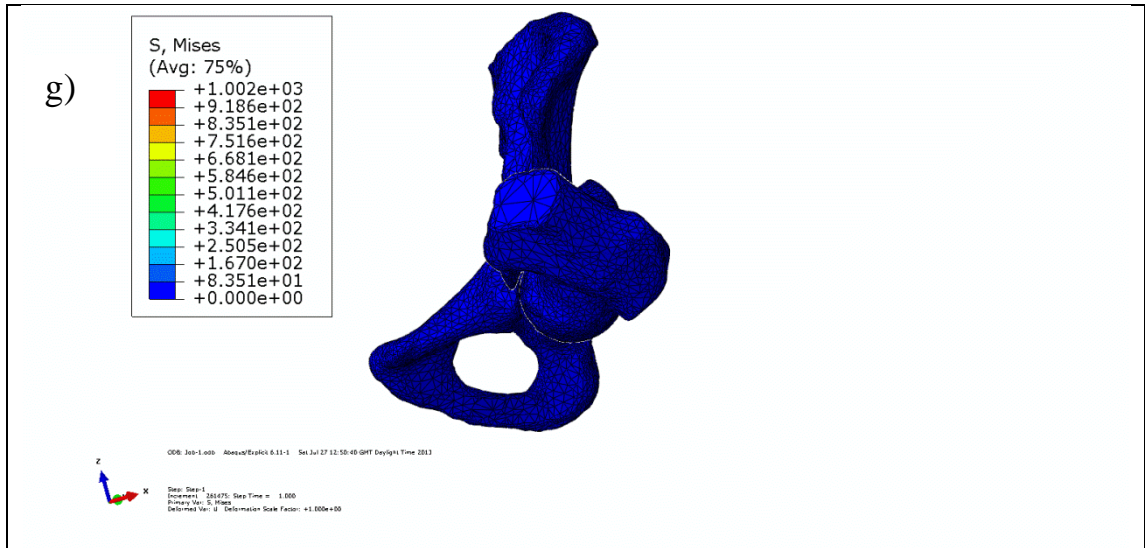
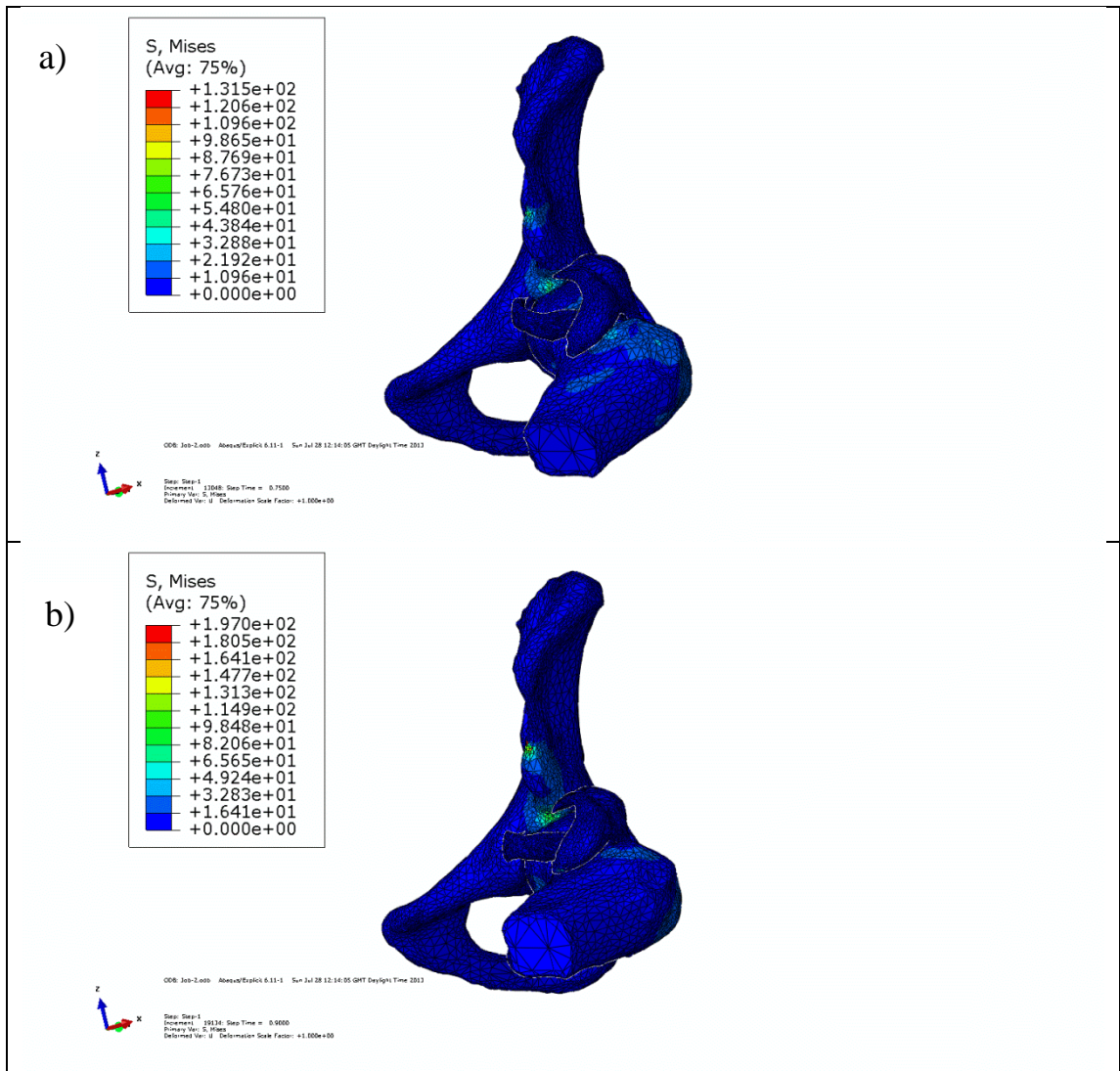
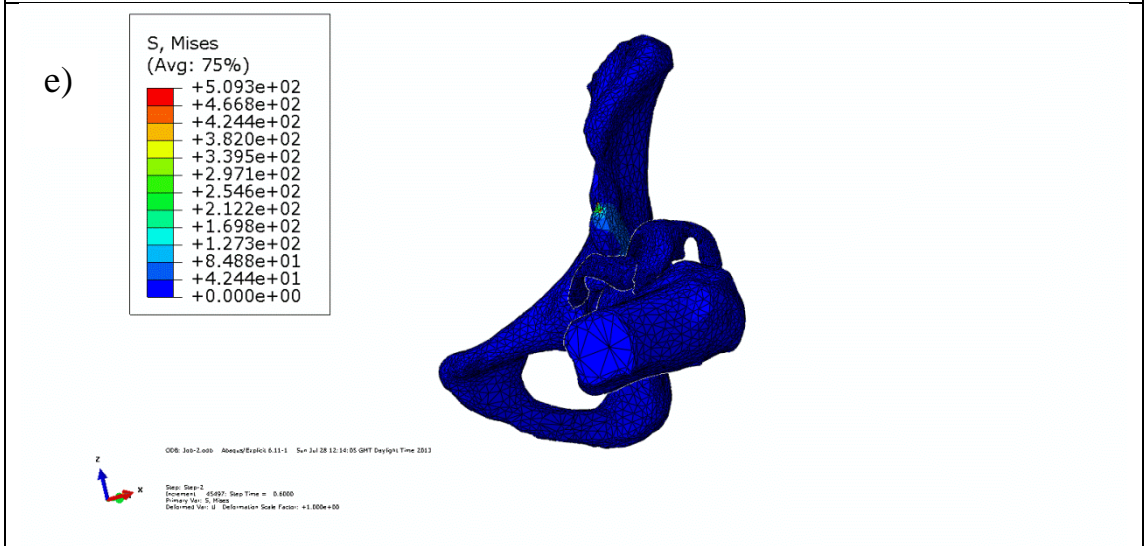
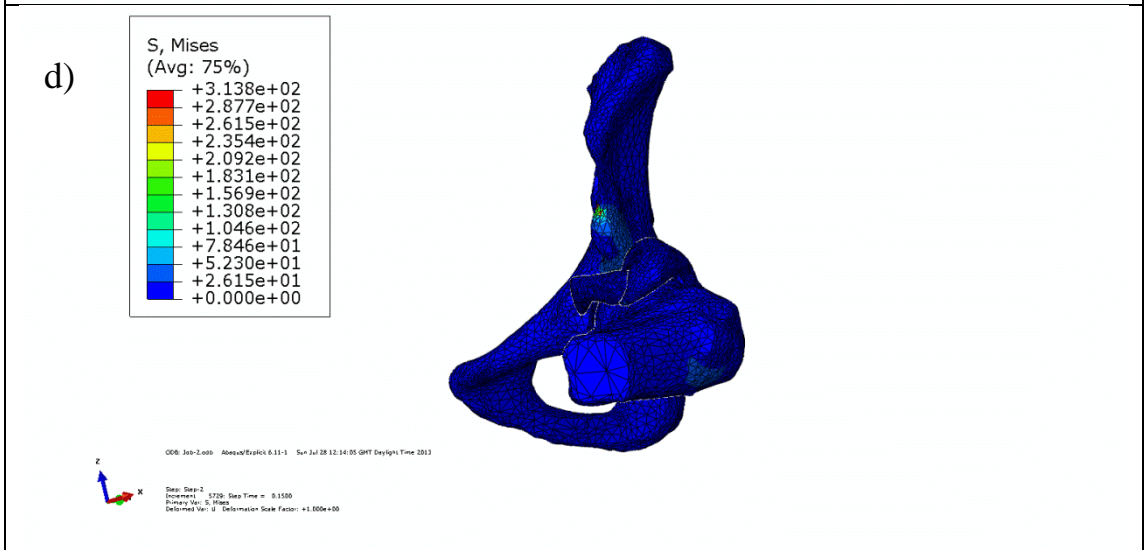
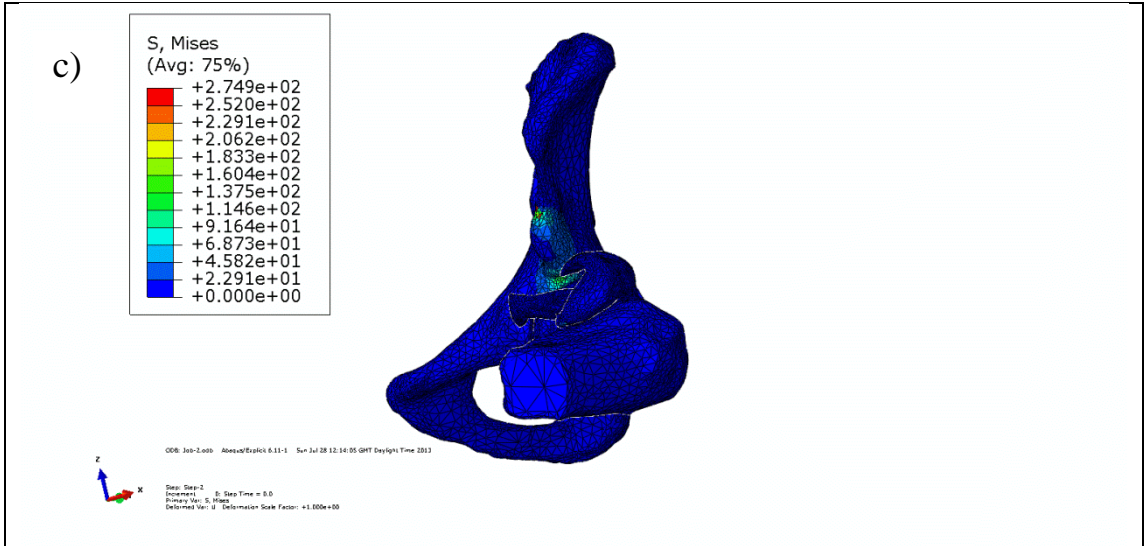
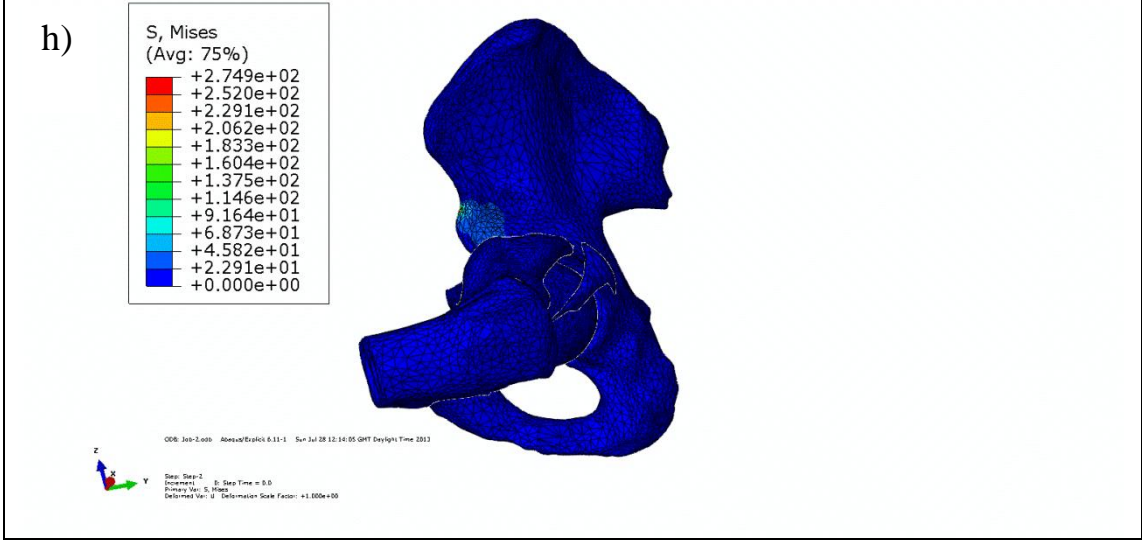
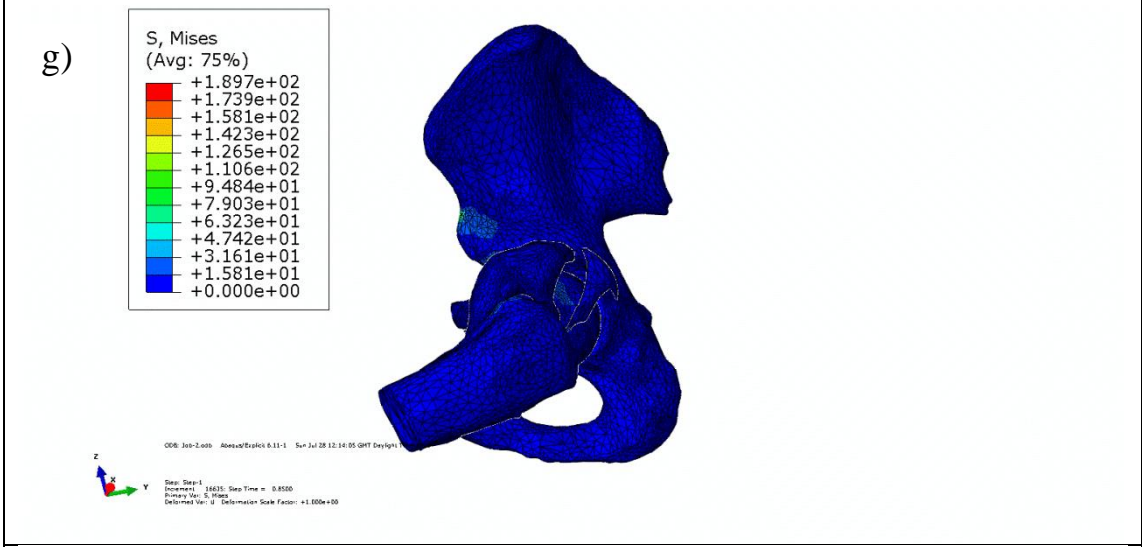
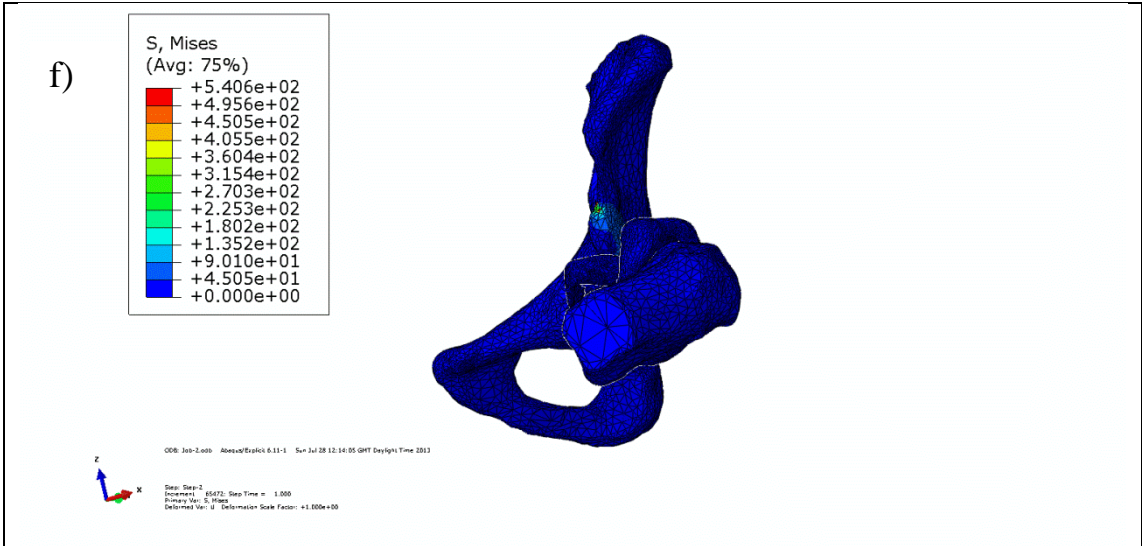


Figure B.6: Flexion of the femur in hip model with soft tissues a- g) femur and acetabulum from supine position until impingement happens (left hip)







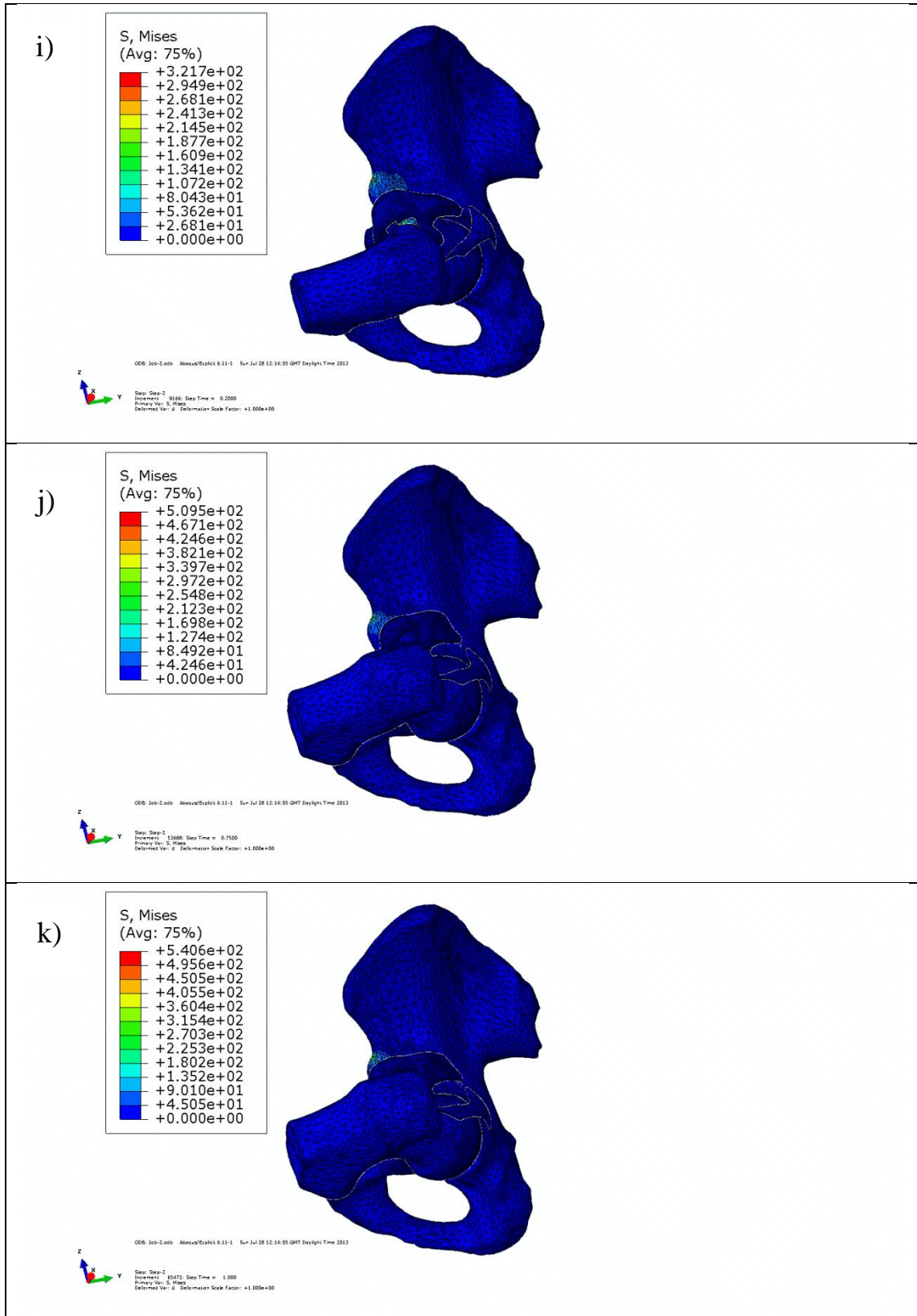
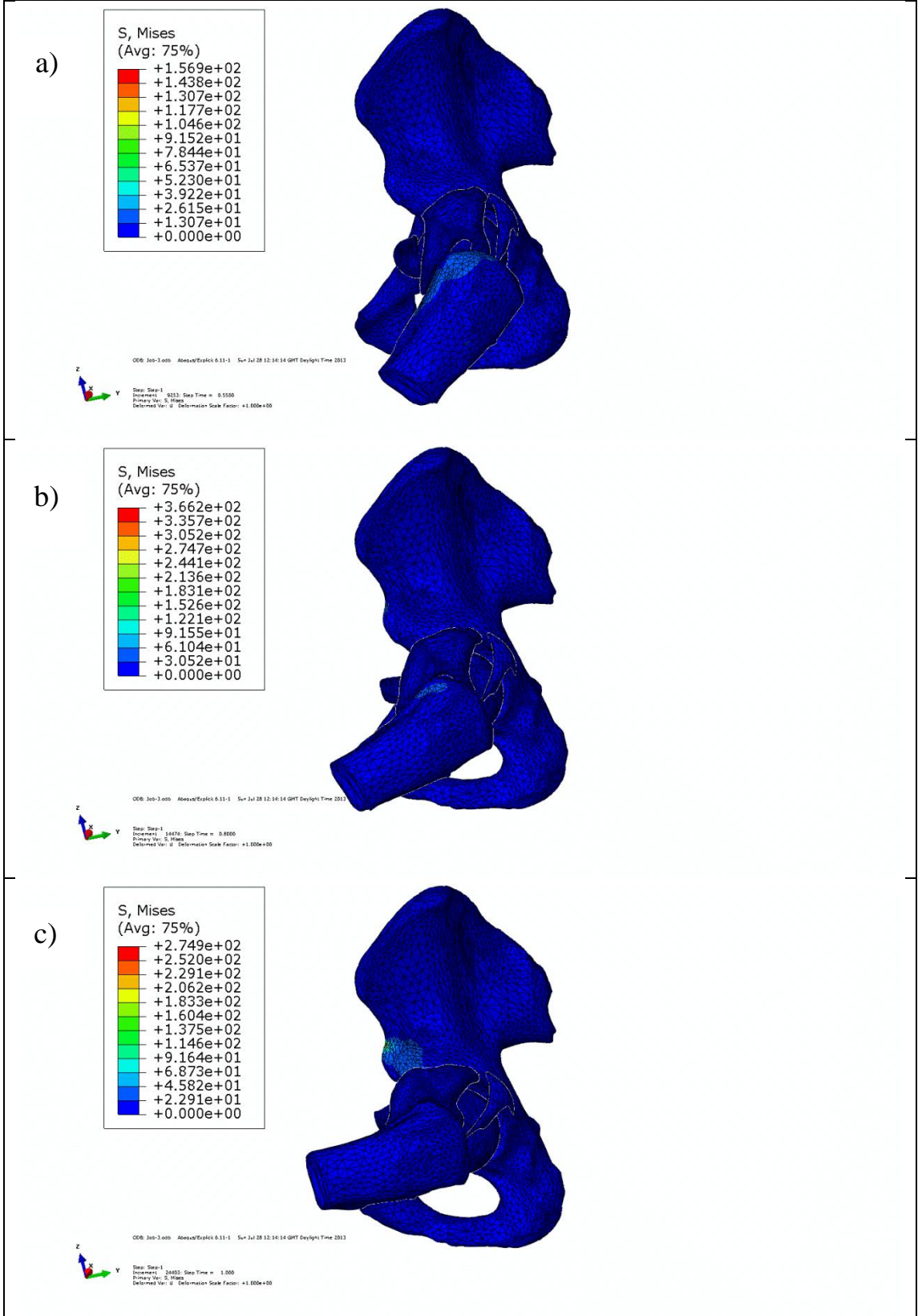
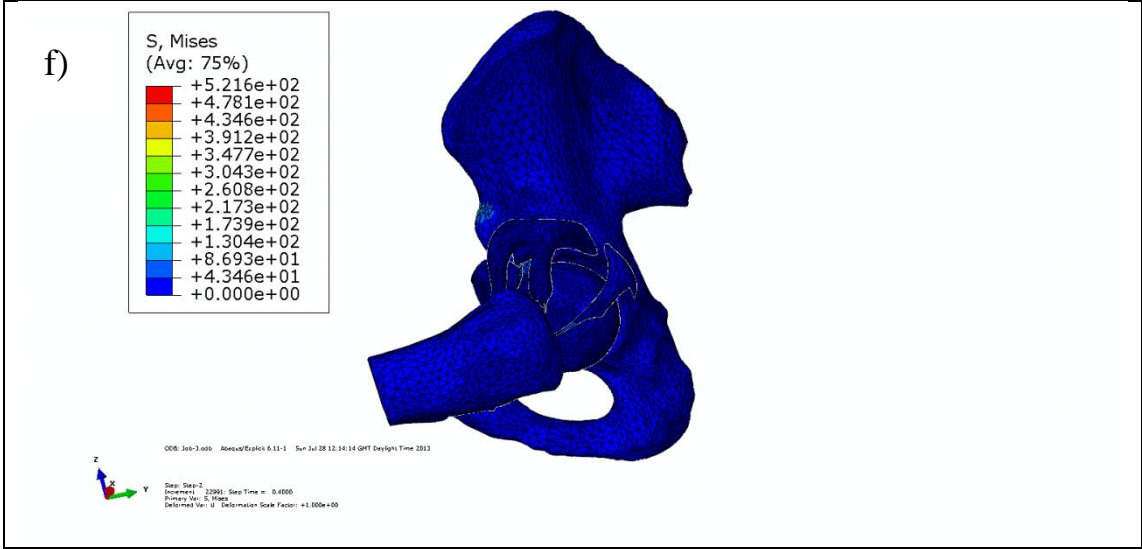
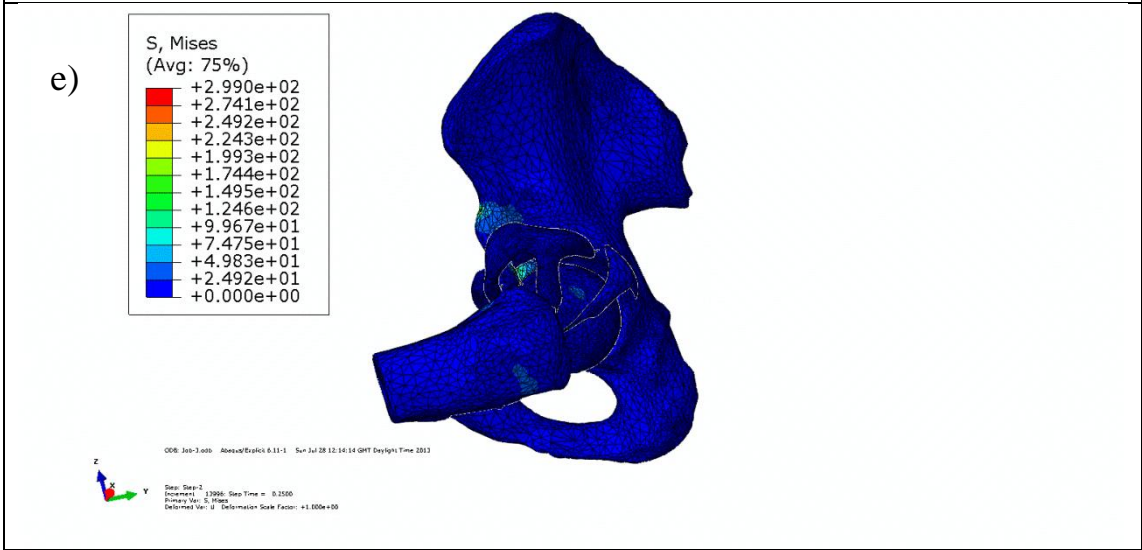
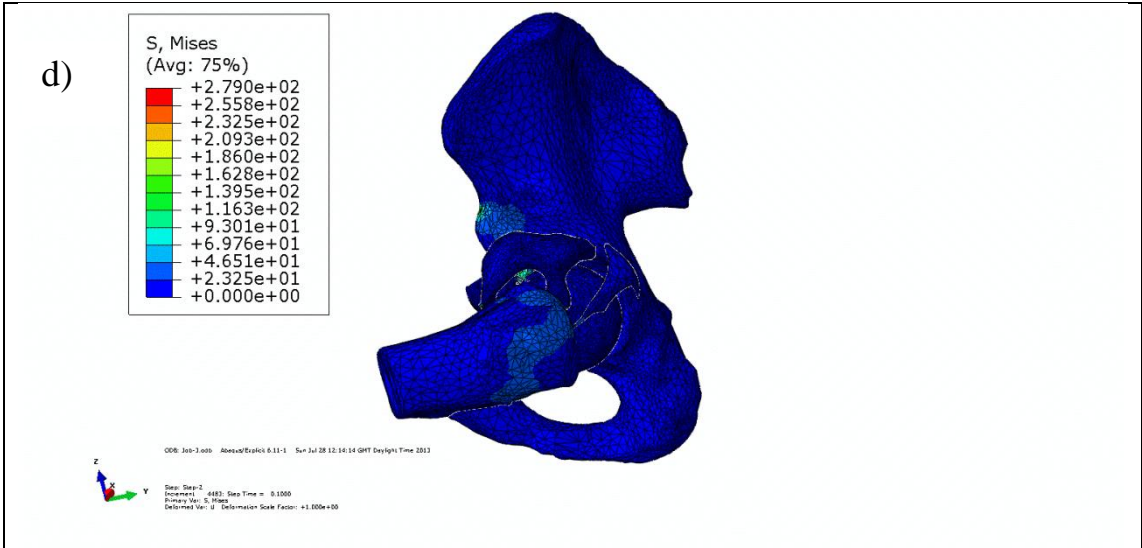


Figure B.7: Adduction of the femur in hip model with soft tissues in 90° of flexion a- f) femur and acetabulum from 90° flexion position until impingement happens (left hip), g- k) femur and acetabulum from 90° flexion position until impingement happens (left hip)





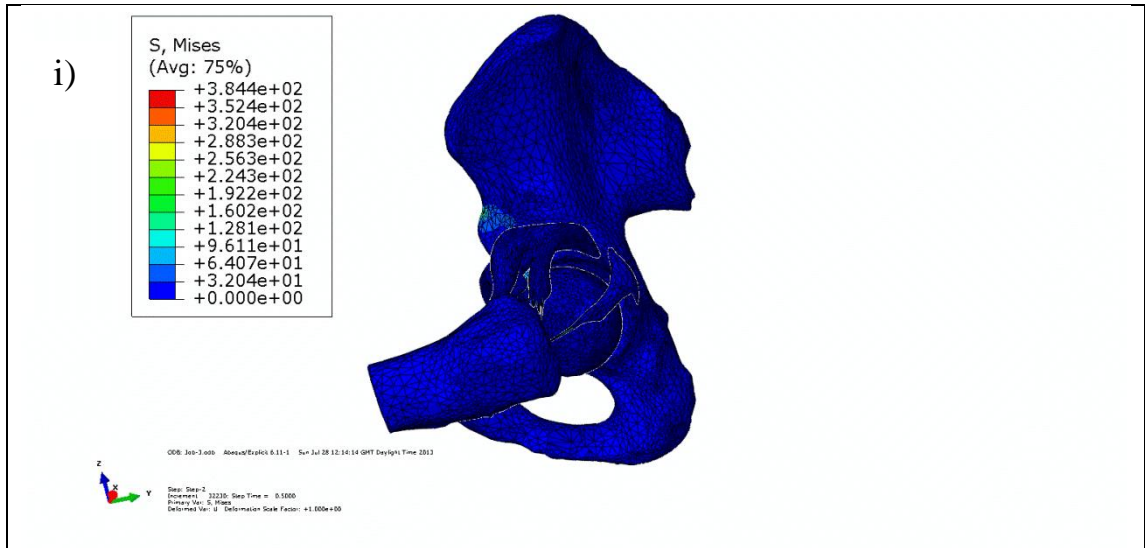


Figure B.8: Internal rotation of the femur in the hip model with soft tissues in 90° of flexion a- i) femur and acetabulum from 90° flexion to impingement happens (left hip)

Appendix C: Anatomical Landmarks

C.1: Anatomical land mark of hip bones and muscles

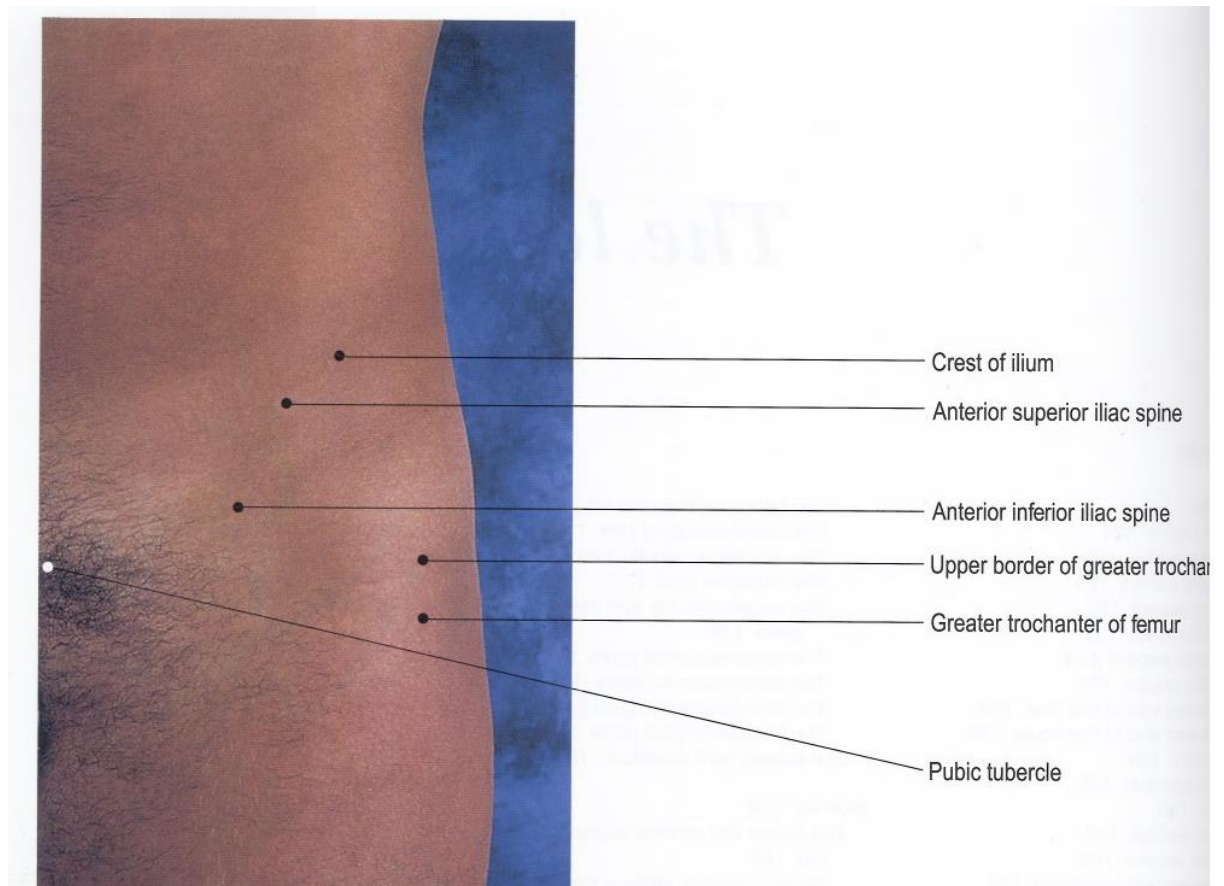


Figure C.1: Anterior view of hip joint landmark on the hip skin. The places of markers on the hip skin to measure the ROM of hip (Field & Hutchinson, 2006)

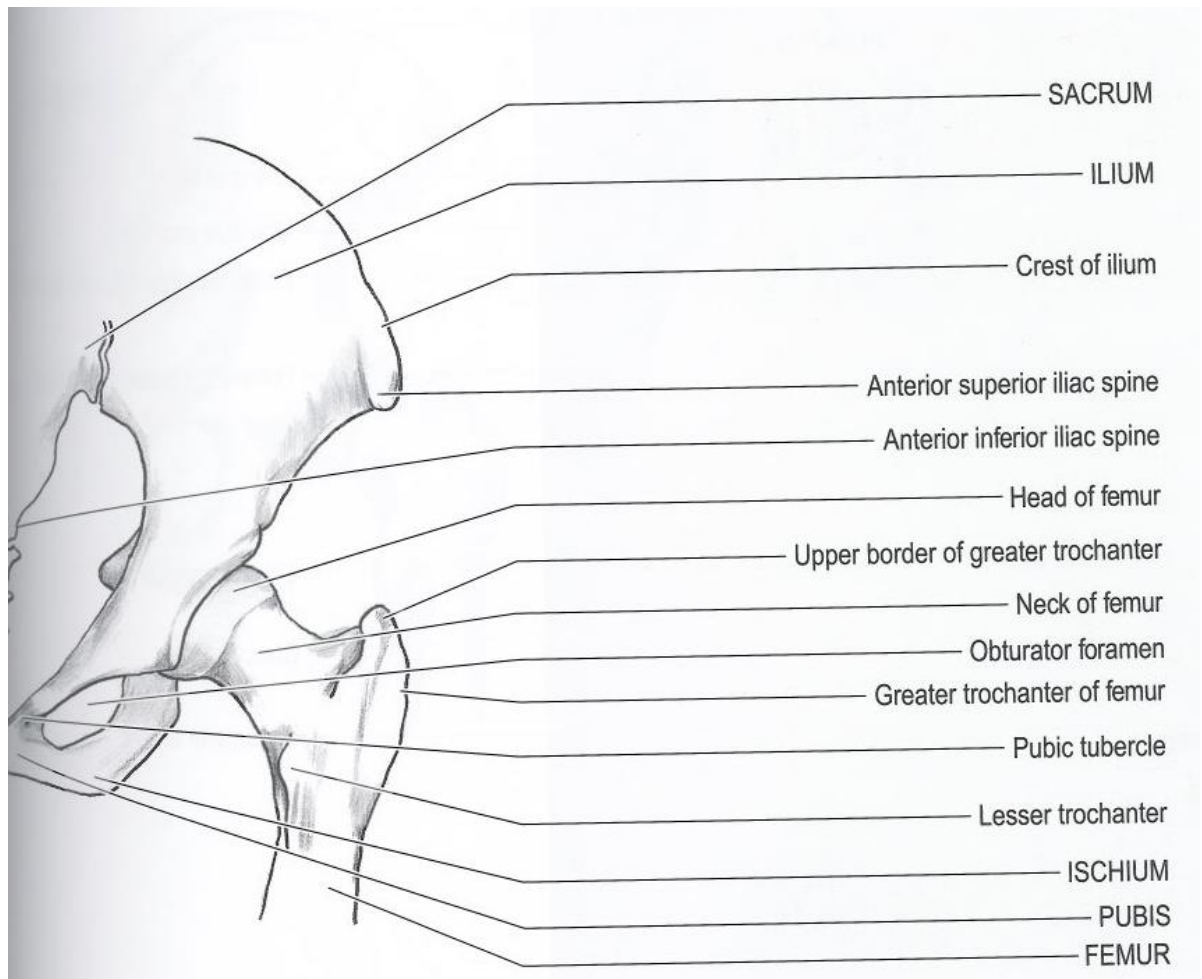


Figure C.2: Anterior view of hip joint bones (Field & Hutchinson, 2006)

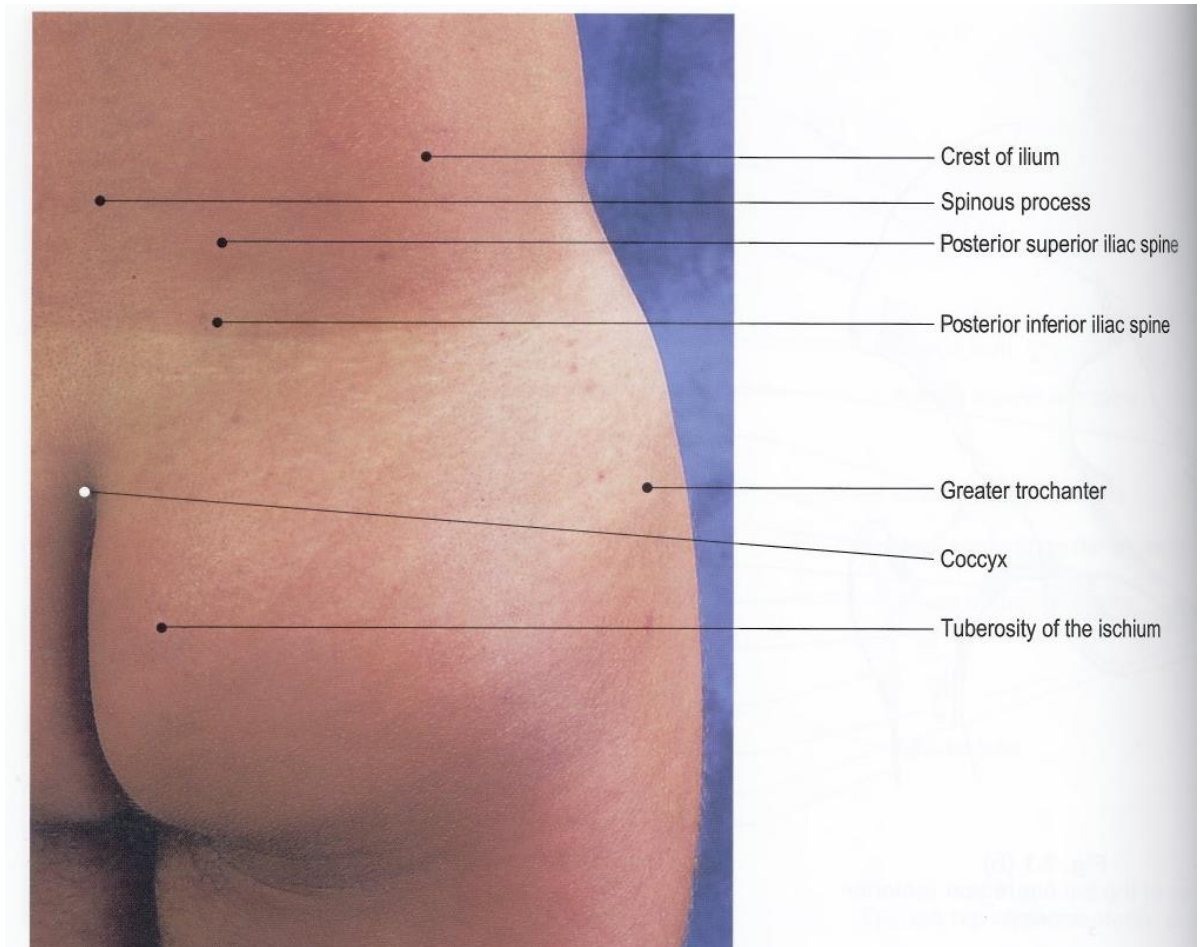


Figure C.3: Posterior view of hip joint landmark on the hip skin. The places of markers on the hip skin to measure the ROM of hip (Field & Hutchinson, 2006)

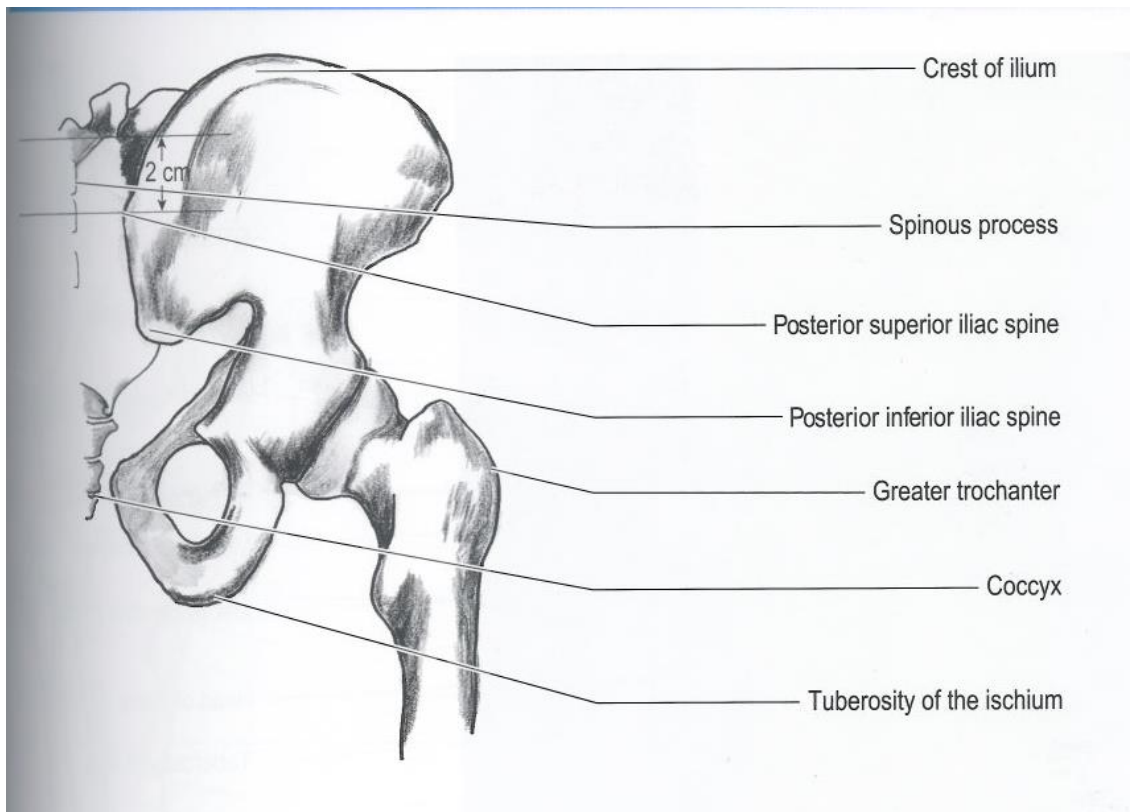


Figure C.4: Posterior view of hip joint bones (Field & Hutchinson, 2006)

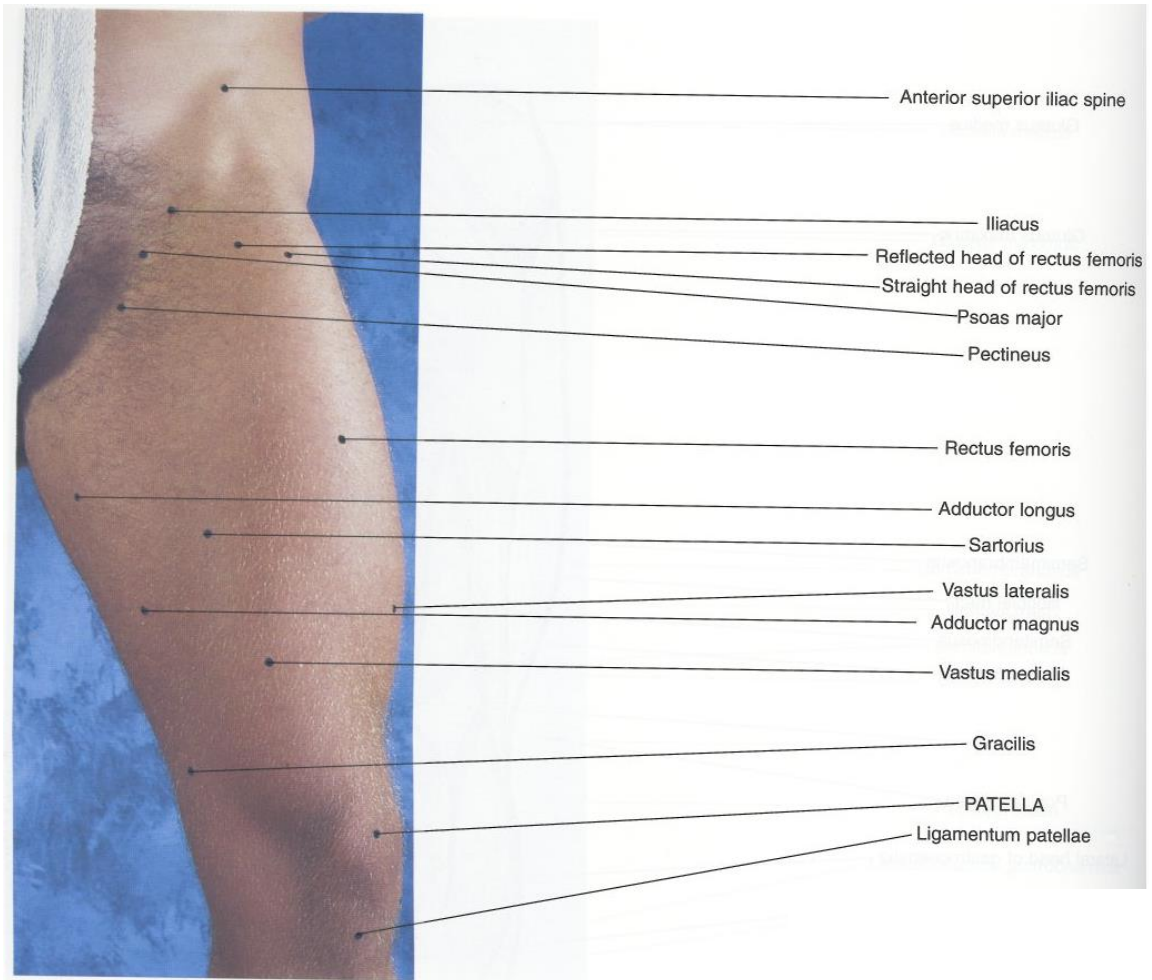


Figure C.5: Anterior view of hip joint muscle landmark on the hip skins (Field & Hutchinson, 2006)

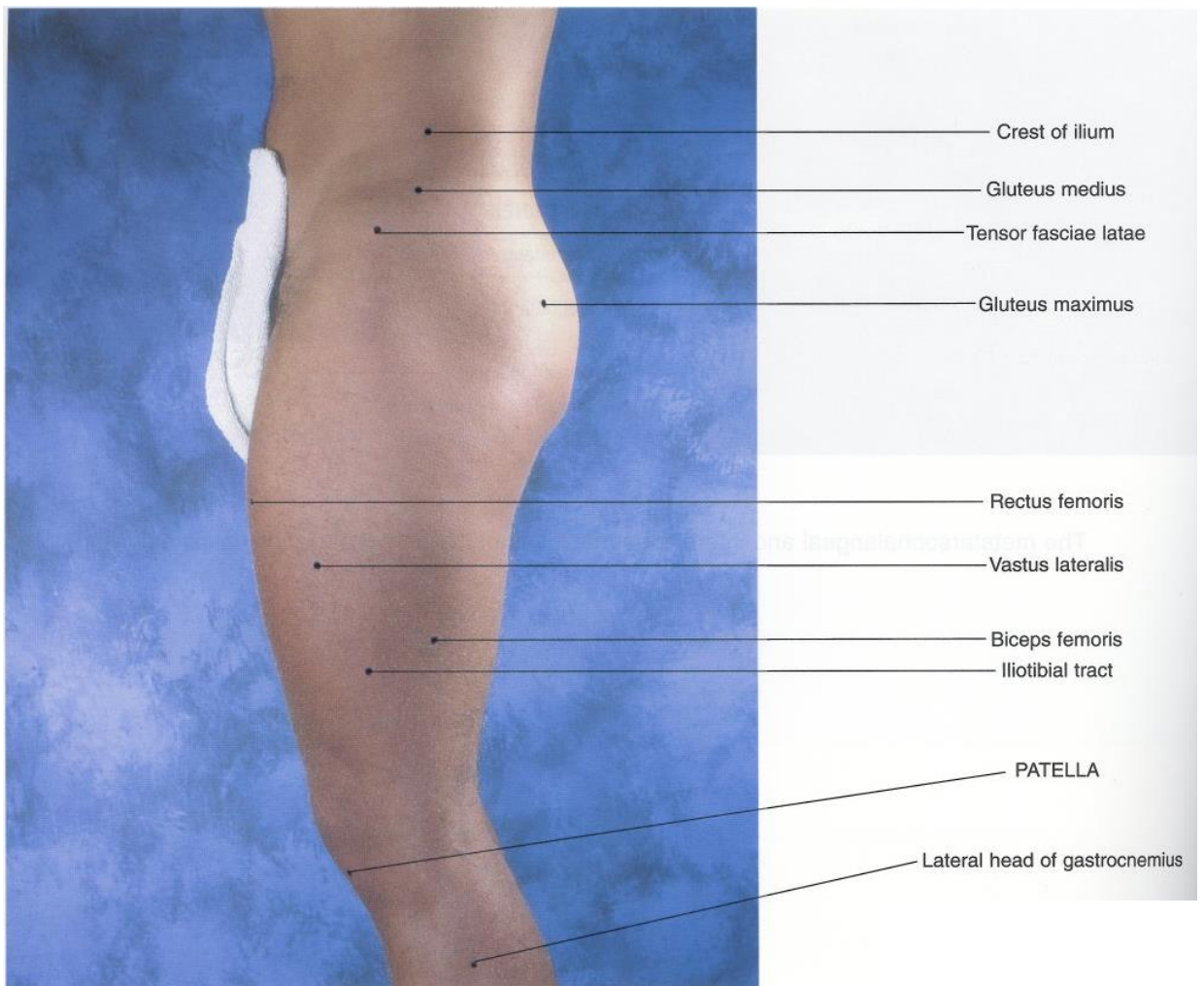


Figure C.6: Posterior view of hip joint muscle landmark on skin (Field & Hutchinson, 2006)

Appendix D: Data Recording

D.1 Motion Capture

Table D.1: Sample of measuring flexion by Motion Capture (raw data)

Time	Reference Marker "b"			Marker "a"		
	x	y	z	x	y	z
0.008333	489.4068	9.876471	-1389.79	-105.296	84.07485	-1443.32
0.016667	489.4068	9.876471	-1389.79	-105.292	84.0139	-1443.22
0.025	489.3964	9.940467	-1389.78	-105.269	84.09641	-1443.22
0.033333	489.3835	9.979069	-1389.78	-105.028	84.50856	-1443.51
0.041667	489.3941	9.946383	-1389.79	-104.717	84.90119	-1444.05
0.05	489.4062	9.878266	-1389.79	-105.107	84.38837	-1443.69
0.058333	489.3064	9.996029	-1389.85	-105.265	84.18081	-1443.36
0.066667	489.3031	10.07958	-1389.83	-105.319	84.08867	-1443.2
0.075	489.2878	10.0467	-1389.85	-105.312	84.12943	-1443.18
0.083333	489.2882	10.04193	-1389.85	-105.316	84.21089	-1443.17
0.091667	489.2886	10.04215	-1389.85	-105.208	84.30791	-1443.17
0.1	489.2998	10.00912	-1389.86	-105.207	84.49111	-1443.14
0.108333	489.2896	10.03985	-1389.85	-105.159	84.67569	-1443.19
0.116667	489.2993	10.01011	-1389.86	-105.076	84.69981	-1443.12
0.125	489.3112	9.942822	-1389.87	-105.022	84.93112	-1443.2
0.133333	489.3022	10.00222	-1389.85	-104.86	85.08775	-1443.18
0.141667	489.2997	10.00974	-1389.86	-104.808	85.2879	-1443.22
0.15	489.1979	10.09989	-1389.92	-104.725	85.52135	-1443.24
0.158333	489.2005	10.0798	-1389.94	-104.646	85.67661	-1443.22
0.166667	489.1997	10.03665	-1390.06	-104.512	85.90313	-1443.31
0.175	489.2132	10.0125	-1389.95	-104.405	86.05508	-1443.42
0.183333	489.1704	9.956147	-1389.94	-104.318	86.25217	-1443.49
0.191667	489.2001	10.02926	-1390.06	-104.21	86.43741	-1443.58
0.2	489.1782	9.997027	-1390.07	-104.065	86.47563	-1443.63
0.208333	489.1792	9.98889	-1390.06	-104.036	86.51038	-1443.66
0.216667	489.1702	9.833879	-1389.98	-103.897	86.50366	-1443.69
0.225	489.1667	9.940536	-1390.06	-103.834	86.56122	-1443.77
0.233333	489.1485	9.996593	-1390.07	-103.725	86.48791	-1443.77
0.241667	489.1699	9.898259	-1390.09	-103.585	86.52524	-1443.84
0.25	489.1741	9.887135	-1390.08	-103.467	86.43411	-1443.88
0.258333	489.1733	9.889658	-1390.08	-103.401	86.51798	-1443.96
0.266667	489.1512	9.988167	-1390.07	-103.279	86.57397	-1444.09
0.275	489.1483	9.996096	-1390.07	-103.235	86.47034	-1444.11
0.283333	489.1673	10.02437	-1390.05	-103.132	86.35113	-1444.19

0.291667	489.1684	10.02451	-1390.05	-103.114	86.24152	-1444.19
0.3	489.1981	10.03803	-1390.07	-103.059	86.1815	-1444.25
0.308333	489.1884	10.10407	-1390.06	-103.061	86.07343	-1444.27
0.316667	489.1561	10.09456	-1390.04	-103.059	85.9479	-1444.26
0.325	489.1664	10.02669	-1390.05	-103.07	85.9059	-1444.2
0.333333	489.1886	10.09972	-1390.06	-103.079	85.90913	-1444.13
0.341667	489.1568	10.09458	-1390.04	-103.422	85.49051	-1443.5
0.35	489.054	10.18269	-1390.1	-103.405	85.5144	-1443.47
0.358333	489.057	10.16284	-1390.12	-103.406	85.59882	-1443.49
0.366667	489.1626	10.03348	-1390.06	-103.353	85.62483	-1443.51
0.375	489.082	10.07449	-1390.11	-103.373	85.71943	-1443.62
0.383333	489.0601	10.15561	-1390.12	-103.352	85.85967	-1443.63
0.391667	489.06	10.15958	-1390.12	-103.37	85.86488	-1443.61
0.4	489.0615	10.15596	-1390.12	-103.361	85.91244	-1443.73
0.408333	489.0723	10.09122	-1390.12	-103.354	85.92513	-1443.74
0.416667	489.0635	10.15006	-1390.11	-103.462	85.84399	-1443.68
0.425	489.0909	10.17149	-1390.14	-103.474	85.82626	-1443.66
0.433333	489.0808	10.20481	-1390.13	-103.472	85.76123	-1443.78
0.441667	489.0609	10.15901	-1390.12	-103.52	85.57948	-1443.76
0.45	489.0617	10.15365	-1390.11	-103.6	85.31792	-1443.71
0.458333	489.0917	10.16905	-1390.13	-103.684	85.11812	-1443.69
0.466667	489.1017	10.29528	-1390.21	-103.708	84.88959	-1443.68
0.475	489.0946	10.24989	-1390.12	-103.761	84.69511	-1443.65
0.483333	489.1109	10.20006	-1390.11	-103.844	84.41116	-1443.61
0.491667	489.1212	10.32387	-1390.18	-103.964	84.24067	-1443.65
0.5	489.0847	10.31418	-1390.11	-104.017	84.05506	-1443.63
0.508333	489.0938	10.367	-1390.07	-104.111	83.85976	-1443.6
0.516667	489.0942	10.37078	-1390.07	-104.087	83.68186	-1443.52
0.525	489.1051	10.33712	-1390.08	-104.189	83.50891	-1443.45
0.533333	489.1062	10.33439	-1390.08	-104.187	83.40157	-1443.46
0.541667	489.0841	10.43282	-1390.06	-104.24	83.345	-1443.42
0.55	489.0811	10.44102	-1390.07	-104.251	83.30716	-1443.41
0.558333	489.1001	10.46931	-1390.04	-104.269	83.25095	-1443.41
0.566667	489.1013	10.46943	-1390.04	-104.32	83.22895	-1443.4
0.575	489.101	10.46898	-1390.04	-104.274	83.24461	-1443.4
0.583333	489.0904	10.53306	-1390.04	-104.317	83.23381	-1443.4
0.591667	489.0955	10.60307	-1390.01	-104.297	83.16065	-1443.43
0.6	489.0994	10.47598	-1390.05	-104.274	83.17279	-1443.52
0.608333	489.1018	10.46506	-1390.04	-104.261	83.05897	-1443.56
0.616667	489.0796	10.56577	-1390.03	-104.3	83.01508	-1443.66
0.625	489.0763	10.57465	-1390.03	-104.293	82.98222	-1443.79
0.633333	489.0773	10.57171	-1390.03	-104.241	82.93414	-1443.92
0.641667	489.0994	10.47315	-1390.05	-104.345	82.79018	-1443.99
0.65	489.1022	10.4653	-1390.04	-104.382	82.6855	-1443.98

0.658333	489.1012	10.46828	-1390.04	-104.346	82.64285	-1444.21
0.666667	489.1008	10.46917	-1390.04	-104.328	82.62372	-1444.35
0.675	489.1008	10.46912	-1390.04	-104.304	82.48636	-1444.5
0.683333	489.1009	10.46905	-1390.04	-104.356	82.39201	-1444.61
0.691667	489.1009	10.46904	-1390.04	-104.354	82.35138	-1444.73
0.7	489.1009	10.46904	-1390.04	-104.278	82.4894	-1445
0.708333	489.0792	10.56664	-1390.03	-104.344	82.43607	-1445
0.716667	489.0764	10.57455	-1390.03	-104.339	82.50093	-1445.1
0.725	489.0954	10.60275	-1389.79	-104.385	82.47939	-1445.18
0.733333	489.0941	10.54343	-1389.79	-104.315	82.58933	-1445.23
0.741667	489.0977	10.53187	-1389.78	-104.311	82.66164	-1445.34
0.75	489.0928	10.66424	-1389.78	-104.286	82.82713	-1445.35
0.758333	489.1011	10.64101	-1389.79	-104.23	83.02261	-1445.38
0.766667	489.1029	10.63499	-1389.79	-104.195	83.2004	-1445.47
0.775	489.0918	10.66862	-1389.85	-104.211	83.3523	-1445.33
0.783333	489.0906	10.67153	-1389.83	-104.253	83.64353	-1445.41
0.791667	489.0909	10.67063	-1389.85	-104.278	83.98883	-1445.36
0.8	489.0934	10.7298	-1389.85	-104.271	84.23922	-1445.26
0.808333	489.0872	10.68147	-1389.85	-104.294	84.58501	-1445.19
0.816667	489.0922	10.66671	-1389.86	-104.207	85.05387	-1445.1
0.825	489.0941	10.72826	-1389.85	-104.203	85.53508	-1444.83
0.833333	489.0872	10.68154	-1389.86	-104.132	86.08598	-1444.61
0.841667	489.0034	10.78483	-1389.87	-104.027	86.70637	-1444.38
0.85	488.9913	10.80909	-1389.85	-103.924	87.33386	-1444.17
0.858333	488.9842	10.86714	-1389.86	-103.889	87.98831	-1443.91
0.866667	489.0019	10.90034	-1389.92	-103.772	88.82645	-1443.7
0.875	488.9852	10.86836	-1389.94	-103.728	89.62357	-1443.42
0.883333	489.0022	10.89759	-1390.06	-103.658	90.44277	-1443.18
0.891667	488.9853	10.86808	-1389.95	-103.037	91.83845	-1443.86
0.9	488.9842	10.86666	-1389.94	-103.095	92.47488	-1443.29
0.908333	488.9868	10.92656	-1390.06	-103.393	92.77564	-1442.52
0.916667	488.9935	10.87398	-1390.07	-102.981	94.13002	-1442.84
0.925	488.9964	10.86507	-1390.06	-102.71	95.37032	-1443.02
0.933333	488.9941	10.80592	-1389.98	-102.605	96.17526	-1442.52
0.941667	489.0001	10.85496	-1390.06	-102.568	96.95815	-1441.98
0.95	488.8936	10.99191	-1390.07	-102.313	98.18444	-1441.69
0.958333	488.8845	11.00623	-1390.09	-102.186	99.25347	-1441.32
0.966667	488.8994	10.93524	-1390.08	-101.899	100.3786	-1441.02
0.975	488.8917	10.99145	-1390.08	-101.723	101.5933	-1440.8
0.983333	488.878	11.03245	-1390.07	-101.451	102.9685	-1440.54
0.991667	488.7974	11.05863	-1390.07	-101.2	104.1771	-1440.35
1	488.7717	11.06642	-1390.05	-101.041	105.2359	-1440.11
1.008333	488.7632	11.04803	-1390.05	-100.952	106.4465	-1439.93
1.016667	488.7641	11.04543	-1390.07	-100.752	107.5973	-1439.8

1.025	488.7462	11.01508	-1390.06	-100.598	108.6384	-1439.65
1.033333	488.7454	11.01436	-1390.04	-100.382	109.6409	-1439.58
1.041667	488.7539	10.89155	-1390.05	-100.187	110.6801	-1439.42
1.05	488.762	10.93464	-1390.06	-99.9901	111.7381	-1439.33
1.058333	488.7384	10.92017	-1390.04	-99.7493	112.7302	-1439.24
1.066667	488.6468	10.97592	-1390.1	-99.5211	113.7267	-1439.15
1.075	488.7422	10.89404	-1390.12	-99.198	114.6388	-1438.98
1.083333	488.7343	10.79821	-1390.06	-98.9641	115.624	-1438.82
1.091667	488.7632	10.80877	-1390.11	-98.7418	116.6657	-1438.71
1.1	488.6743	10.93273	-1390.12	-98.4705	117.6742	-1438.58
1.108333	488.6512	11.01912	-1390.12	-98.1541	118.6101	-1438.47
1.116667	488.6536	11.01669	-1390.12	-97.7791	119.6305	-1438.49
1.125	488.6664	10.94766	-1390.12	-97.4797	120.5909	-1438.45
1.133333	488.6707	11.00136	-1390.11	-97.1219	121.5719	-1438.41
1.141667	488.6376	11.04768	-1390.14	-96.7689	122.6038	-1438.48
1.15	488.6537	11.07974	-1390.13	-96.4661	123.4556	-1438.52
1.158333	488.6667	11.0139	-1390.12	-96.1735	124.2877	-1438.53
1.166667	488.7592	10.94912	-1390.11	-95.8531	125.1037	-1438.54
1.175	488.7483	10.90892	-1390.13	-95.5149	126.0528	-1438.56
1.183333	488.6536	10.97061	-1390.21	-95.218	126.9748	-1438.54
1.191667	488.6453	10.98385	-1390.12	-94.8712	127.8401	-1438.46
1.2	488.6594	10.94634	-1390.11	-94.4975	128.7742	-1438.54
1.208333	488.6503	10.97574	-1390.18	-94.2307	129.6767	-1438.51
1.216667	488.6488	10.97935	-1390.11	-93.8498	130.739	-1438.57
1.225	488.6385	11.04298	-1390.07	-93.5459	131.828	-1438.51
1.233333	488.6547	11.07876	-1390.07	-93.1296	132.9855	-1438.56
1.241667	488.645	11.11153	-1390.08	-92.7484	134.0941	-1438.56
1.25	488.6617	11.14434	-1390.08	-92.4465	135.2518	-1438.57
1.258333	488.6524	11.2079	-1390.06	-92.0424	136.4697	-1438.57
1.266667	488.6466	11.34098	-1390.07	-91.66	137.6301	-1438.51
1.275	488.6532	11.30413	-1390.04	-91.3001	138.8472	-1438.54
1.283333	488.6958	11.32041	-1390.04	-90.953	140.0116	-1438.59
1.291667	488.6765	11.32447	-1390.04	-90.4939	141.2469	-1438.71
1.3	488.663	11.36019	-1390.04	-90.0953	142.6031	-1438.82
1.308333	488.6516	11.42603	-1390.01	-89.5849	143.8362	-1438.87
1.316667	488.6503	11.43014	-1390.05	-89.0881	145.1307	-1438.92
1.325	488.6511	11.42793	-1390.04	-88.5957	146.5163	-1438.99
1.333333	488.5791	11.51635	-1390.03	-88.0691	147.9908	-1439.15
1.341667	488.5541	11.49793	-1390.03	-87.5325	149.5519	-1439.34
1.35	488.5558	11.49295	-1390.03	-86.9028	151.1483	-1439.56
1.358333	488.5464	11.47623	-1390.05	-86.3474	152.7958	-1439.76
1.366667	488.5681	11.37738	-1390.04	-85.7152	154.4035	-1439.96
1.375	488.571	11.37019	-1390.04	-85.0399	156.1615	-1440.21
1.383333	488.5408	11.37583	-1390.04	-84.2815	158.0419	-1440.46

1.391667	488.5497	11.34468	-1390.04	-83.5545	159.8209	-1440.68
1.4	488.5293	11.28285	-1390.04	-82.8352	161.594	-1440.92
1.408333	488.5341	11.24045	-1390.04	-81.9716	163.5603	-1441.21
1.416667	488.5461	11.23905	-1390.04	-81.1221	165.4597	-1441.51
1.425	488.5229	11.24882	-1390.03	-80.3435	167.3851	-1441.71
1.433333	488.5431	11.24496	-1390.03	-79.407	169.2872	-1441.99
1.441667	488.5255	11.19581	-1389.79	-78.4169	171.331	-1442.26
1.45	488.5183	11.0969	-1389.79	-77.511	173.2428	-1442.42
1.458333	488.5193	11.09227	-1389.78	-76.3756	175.2295	-1442.62
1.466667	488.5211	11.15453	-1389.78	-75.2964	177.3252	-1442.99
1.475	488.5363	11.09926	-1389.79	-74.2079	179.4989	-1443.22
1.483333	488.5431	11.10814	-1389.79	-73.1034	181.633	-1443.52
1.491667	488.5427	11.11024	-1389.85	-71.9351	183.8071	-1443.9
1.5	488.5427	11.10992	-1389.83	-70.7752	186.1096	-1444.24
1.508333	488.5427	11.10977	-1389.85	-69.5552	188.2629	-1444.68
1.516667	488.5229	11.03142	-1389.85	-68.3637	190.5062	-1445
1.525	488.6146	10.96611	-1389.85	-67.1198	192.652	-1445.25
1.533333	488.6222	10.95748	-1389.86	-65.8834	194.8011	-1445.5
1.541667	488.619	10.96192	-1389.85	-64.5602	197.0893	-1445.73
1.55	488.6486	10.97792	-1389.86	-63.174	199.2638	-1445.94
1.558333	488.619	10.96501	-1389.87	-61.8115	201.5641	-1446.22
1.566667	488.6179	10.96263	-1389.85	-60.466	203.8513	-1446.43
1.575	488.6184	10.963	-1389.86	-58.9121	206.2726	-1446.62
1.583333	488.6383	11.04182	-1389.92	-57.4507	208.5265	-1446.67
1.591667	488.6372	11.04878	-1389.94	-55.9763	210.9007	-1446.74
1.6	488.6374	11.04624	-1390.06	-54.4045	213.2519	-1446.78
1.608333	488.6032	11.01537	-1389.95	-52.7892	215.7334	-1446.77
1.616667	488.6441	11.10642	-1389.94	-51.1771	218.2265	-1446.73
1.625	488.6444	11.11488	-1390.06	-49.5642	220.7767	-1446.62
1.633333	488.6417	11.05324	-1390.07	-47.8658	223.3348	-1446.61
1.641667	488.6592	11.06706	-1390.06	-46.1309	225.8536	-1446.32
1.65	488.6553	11.07918	-1389.98	-44.4873	228.3774	-1445.98
1.658333	488.6375	11.04737	-1390.06	-42.7612	230.9885	-1445.72
1.666667	488.6373	11.04505	-1390.07	-41.0056	233.6388	-1445.36
1.675	488.5374	11.05135	-1390.09	-39.3037	236.1192	-1445.03
1.683333	488.6294	10.97354	-1390.08	-37.449	238.7159	-1444.66
1.691667	488.646	10.97203	-1390.08	-35.6787	241.2171	-1444.21
1.7	488.6324	11.01005	-1390.07	-33.9	243.7476	-1443.79
1.708333	488.5529	11.09787	-1390.07	-31.8129	246.2845	-1443.23
1.716667	488.5534	11.05238	-1390.05	-30.034	248.9542	-1442.85
1.725	488.5553	11.02491	-1390.05	-27.9522	251.2839	-1442.16
1.733333	488.6471	10.9638	-1390.07	-26.0589	253.9005	-1441.66
1.741667	488.6436	11.01784	-1390.06	-23.9139	256.3754	-1441.05
1.75	488.5521	11.1012	-1390.04	-21.8233	258.8788	-1440.43

1.758333	488.6303	11.03955	-1390.05	-19.7506	261.2058	-1439.81
1.766667	488.6527	11.10215	-1390.06	-17.47	263.6872	-1439.25
1.775	488.6499	11.11009	-1390.04	-15.3542	266.0679	-1438.78
1.783333	488.6322	11.09856	-1390.1	-12.9811	268.4945	-1438.24
1.791667	488.6349	11.09059	-1390.12	-10.8186	270.7738	-1437.8
1.8	488.6563	11.13952	-1390.06	-8.32542	272.9963	-1437.23
1.808333	488.6607	11.14936	-1390.11	-5.95814	275.3113	-1436.91
1.816667	488.6536	11.20426	-1390.12	-3.51552	277.4572	-1436.37
1.825	488.688	11.29044	-1390.12	-1.03607	279.7787	-1436.14
1.833333	488.6752	11.39022	-1390.12	1.450035	281.9998	-1435.81
1.841667	488.694	11.39325	-1390.12	3.994673	283.9808	-1435.35
1.85	488.682	11.36482	-1390.11	6.483597	286.1541	-1435.08
1.858333	488.6921	11.45075	-1390.14	9.339032	288.2582	-1434.72
1.866667	488.6768	11.43394	-1390.13	11.97305	290.4187	-1434.56
1.875	488.6792	11.42434	-1390.12	14.61078	292.5131	-1434.31
1.883333	488.6787	11.42639	-1390.11	17.44573	294.4427	-1434.05
1.891667	488.6697	11.39489	-1390.13	20.13318	296.4858	-1434.06
1.9	488.6786	11.42476	-1390.21	23.02758	298.2798	-1433.71
1.908333	488.6482	11.41448	-1390.12	25.88156	300.3295	-1433.83
1.916667	488.6689	11.39349	-1390.11	28.84932	302.2058	-1433.74
1.925	488.6706	11.39253	-1390.18	31.93007	304.1021	-1433.72
1.933333	488.6807	11.33041	-1390.11	34.7895	305.9518	-1433.8
1.941667	488.6699	11.32885	-1390.07	37.93165	307.7584	-1433.74
1.95	488.7633	11.32574	-1390.07	41.11815	309.5682	-1433.81
1.958333	488.7599	11.26217	-1390.08	44.33236	311.2778	-1433.79
1.966667	488.7776	11.22939	-1390.08	47.58917	313.0472	-1433.86
1.975	488.7787	11.22848	-1390.06	50.92924	314.7541	-1433.96
1.983333	488.7782	11.22957	-1390.07	54.26622	316.4586	-1433.97
1.991667	488.778	11.22979	-1390.04	57.60747	318.1265	-1433.9
2	488.8074	11.2275	-1390.04	60.99573	319.8277	-1434.05
2.008333	488.9	11.16744	-1390.04	64.50821	321.4255	-1434.07
2.016667	488.907	11.15675	-1390.04	68.09281	323.0199	-1434.09
2.025	488.8929	11.19444	-1390.01	71.56088	324.6715	-1434.18
2.033333	488.902	11.16486	-1390.05	75.10798	326.3589	-1434.31
2.041667	488.9013	11.10178	-1390.04	78.73621	327.8326	-1434.25
2.05	488.905	11.09124	-1390.03	82.41012	329.213	-1434.22
2.058333	488.9038	11.09516	-1390.03	86.10896	330.7277	-1434.28
2.066667	488.8994	11.2254	-1390.03	89.74349	332.2393	-1434.42
2.075	489.4068	11.17568	-1390.05	93.42825	333.6114	-1434.41
2.083333	489.4068	11.13534	-1390.04	97.2226	335.0419	-1434.38
2.091667	489.3964	11.16117	-1390.04	100.9239	336.4853	-1434.48
2.1	489.3835	11.252	-1390.04	104.5885	337.8459	-1434.56
2.108333	489.3941	11.345	-1390.04	108.3577	339.0755	-1434.5
2.116667	489.4062	11.42009	-1390.04	112.1634	340.2589	-1434.49

2.125	489.3064	11.40389	-1390.04	115.9753	341.5533	-1434.53
2.133333	489.3031	11.47683	-1390.04	119.7655	342.7133	-1434.58
2.141667	489.2878	11.63112	-1390.03	123.5445	343.7755	-1434.77
2.15	489.2882	11.6158	-1390.03	127.4647	344.865	-1434.89
2.158333	489.2886	11.63838	-1389.79	131.383	345.7031	-1434.89
2.166667	489.2998	11.7007	-1389.79	135.0387	346.4043	-1434.84
2.175	489.2896	11.74177	-1389.78	138.8191	347.2317	-1434.97
2.183333	489.2993	11.86541	-1389.78	142.2801	347.6078	-1434.81
2.191667	489.3112	11.92995	-1389.79	146.0019	348.4169	-1434.94
2.2	489.3022	11.88065	-1389.79	149.0317	348.2993	-1434.27
2.208333	489.2997	11.90206	-1389.85	152.5242	348.7097	-1434.14
2.216667	489.1979	11.91184	-1389.83	156.039	349.2733	-1434.14
2.225	489.2005	11.9774	-1389.85	159.5946	349.8335	-1434.08
2.233333	489.1997	11.97669	-1389.85	162.7792	350.1794	-1433.68
2.241667	489.2132	11.93468	-1389.85	166.1865	350.6398	-1433.6
2.25	489.1704	11.92355	-1389.86	169.3046	351.1069	-1433.4
2.258333	489.2001	11.84188	-1389.85	172.4933	351.5514	-1433.27
2.266667	489.1782	11.99327	-1389.86	175.5571	351.9008	-1432.85
2.275	489.1792	11.95813	-1389.87	178.5023	352.1646	-1432.5
2.283333	489.1702	11.88499	-1389.85	181.4423	352.5252	-1432.23
2.291667	489.1667	11.90796	-1389.86	184.1675	352.8444	-1431.88
2.3	489.1485	12.01187	-1389.92	186.9768	353.2092	-1431.49
2.308333	489.1699	12.05151	-1389.94	189.5486	353.4569	-1431.11
2.316667	489.1741	11.96555	-1390.06	192.2729	353.75	-1430.9
2.325	489.1733	11.94303	-1389.95	194.7517	353.8371	-1430.46
2.333333	489.1512	12.04554	-1389.94	197.3252	354.0095	-1430.07
2.341667	489.1483	12.05492	-1390.06	199.8139	354.2361	-1429.8
2.35	489.1673	12.04784	-1390.07	202.1704	354.3157	-1429.39
2.358333	489.1684	11.98734	-1390.06	204.646	354.5254	-1428.97
2.366667	489.1981	11.91656	-1389.98	207.0114	354.6228	-1428.55
2.375	489.1884	12.03908	-1390.06	209.4663	354.7516	-1428.09
2.383333	489.1561	12.05293	-1390.07	211.8189	354.9371	-1427.59
2.391667	489.1664	12.0498	-1390.09	214.1073	354.9858	-1427.09
2.4	489.1886	11.99003	-1390.08	216.5943	355.1309	-1426.7
2.408333	489.1568	12.01061	-1390.08	218.8338	355.1545	-1426.15
2.416667	489.054	12.10028	-1390.07	221.2887	355.2479	-1425.6
2.425	489.057	12.11993	-1390.07	223.6425	355.1384	-1424.95
2.433333	489.1626	12.1237	-1390.05	225.935	355.1429	-1424.33
2.441667	489.082	12.10526	-1390.05	228.4239	355.3292	-1423.97
2.45	489.0601	12.07653	-1390.07	230.7914	355.3765	-1423.29
2.458333	489.06	12.13116	-1390.06	233.2277	355.3853	-1422.5
2.466667	489.0615	12.17586	-1390.04	235.7186	355.474	-1421.92
2.475	489.0723	12.17218	-1390.05	238.1153	355.5032	-1421.16
2.483333	489.0635	12.14499	-1390.06	240.7826	355.6124	-1420.46

2.491667	489.0909	12.16759	-1390.04	243.4042	355.5227	-1419.58
2.5	489.0808	12.17323	-1390.1	246.0409	355.6171	-1418.78
2.508333	489.0609	12.15249	-1390.12	248.7171	355.6383	-1418.02
2.516667	489.0617	12.13664	-1390.06	251.3392	355.5865	-1417.18
2.525	489.0917	12.20627	-1390.11	254.0641	355.5288	-1416.39
2.533333	489.1017	12.21618	-1390.12	256.8812	355.3998	-1415.54
2.541667	489.0946	12.27396	-1390.12	259.6284	355.3265	-1414.76
2.55	489.1109	12.34905	-1390.12	262.3552	355.272	-1413.92
2.558333	489.1212	12.28462	-1390.12	265.2417	355.0155	-1413.15
2.566667	489.0847	12.37223	-1390.11	268.0025	354.8409	-1412.34
2.575	489.0938	12.32729	-1390.14	270.9247	354.6785	-1411.61
2.583333	489.0942	12.43729	-1390.13	273.8156	354.4899	-1410.8
2.591667	489.1051	12.46953	-1390.12	276.805	354.1383	-1409.95
2.6	489.1062	12.52743	-1390.11	279.7757	353.8284	-1409.19
2.608333	489.0841	12.51047	-1390.13	282.7909	353.4883	-1408.46
2.616667	489.0811	12.56311	-1390.21	285.7182	353.1047	-1407.61
2.625	489.1001	12.63575	-1390.12	288.7051	352.731	-1406.93
2.633333	489.1013	12.70666	-1390.11	291.6787	352.3452	-1406.31
2.641667	489.101	12.63154	-1390.18	294.593	351.818	-1405.5
2.65	489.0904	12.71092	-1390.11	297.5858	351.3932	-1404.93
2.658333	489.0955	12.74848	-1390.07	300.5039	350.9716	-1404.29
2.666667	489.0994	12.80646	-1390.07	303.5746	350.4656	-1403.68
2.675	489.1018	12.7804	-1390.08	306.4527	349.94	-1403.06
2.683333	489.0796	12.81515	-1390.08	309.4608	349.5198	-1402.5
2.691667	489.0763	12.8764	-1390.06	312.3287	348.8599	-1401.93
2.7	489.0773	12.99611	-1390.07	315.2744	348.348	-1401.37
2.708333	489.0994	13.08686	-1390.04	318.2461	347.8456	-1400.86
2.716667	489.1022	13.15004	-1390.04	321.0999	347.1053	-1400.38
2.725	489.1012	13.20638	-1390.04	324.0237	346.5398	-1399.96
2.733333	489.1008	13.38909	-1390.04	326.9337	345.7884	-1399.5
2.741667	489.1008	13.49773	-1390.01	329.7641	345.1824	-1399.07
2.75	489.1009	13.51683	-1390.05	332.4773	344.6205	-1398.56
2.758333	489.1009	13.60663	-1390.04	335.3644	343.8733	-1398.09
2.766667	489.1009	13.65392	-1390.03	338.036	343.1458	-1397.63
2.775	489.0792	13.73072	-1390.03	340.7251	342.528	-1397.25
2.783333	489.0764	13.86318	-1390.03	343.3308	341.7357	-1396.8
2.791667	489.0954	13.80054	-1390.05	345.9522	341.1939	-1396.28
2.8	489.0941	13.80296	-1390.04	348.4005	340.4485	-1395.86
2.808333	489.0977	13.85077	-1390.04	350.7658	339.7692	-1395.36
2.816667	489.0928	13.86509	-1390.04	353.1231	339.148	-1394.93
2.825	489.1011	13.99669	-1390.04	355.3661	338.7012	-1394.49
2.833333	489.1029	14.05367	-1390.04	357.602	338.1585	-1394.13
2.841667	489.0918	13.96281	-1390.04	359.6659	337.4354	-1393.45
2.85	489.0906	14.0426	-1390.04	361.7452	336.8619	-1392.96

2.858333	489.0909	14.12936	-1390.03	363.7002	336.3679	-1392.41
2.866667	489.0934	14.18721	-1390.03	365.7885	335.8044	-1391.81
2.875	489.0872	14.29094	-1389.79	367.5898	335.3619	-1391.33
2.883333	489.0922	14.19795	-1389.79	369.5117	334.7711	-1390.81
2.891667	489.0941	14.25524	-1389.78	371.238	334.2058	-1390.1
2.9	489.0872	14.29673	-1389.78	372.9944	333.7892	-1389.6
2.908333	489.0034	14.31608	-1389.79	374.7596	333.2789	-1388.99
2.916667	488.9913	14.25756	-1389.79	376.306	332.793	-1388.42
2.925	488.9842	14.24073	-1389.85	377.9196	332.3171	-1387.72
2.933333	489.0019	14.20799	-1389.83	379.4989	331.7986	-1387.18
2.941667	488.9852	14.19065	-1389.85	381.1022	331.4723	-1386.62
2.95	489.0022	14.13975	-1389.85	382.5028	330.9451	-1385.87
2.958333	488.9853	14.13431	-1389.85	383.9949	330.3853	-1385.37
2.966667	488.9842	14.11357	-1389.86	385.4908	329.8829	-1384.56
2.975	488.9868	14.0452	-1389.85	386.915	329.5665	-1384.06
2.983333	488.9935	14.13242	-1389.86	388.3985	329.0746	-1383.35
2.991667	488.9964	14.07218	-1389.87	389.6002	328.4939	-1382.78
3	488.9941	14.12084	-1389.85	390.8764	328.0441	-1381.99
3.008333	489.0001	14.13585	-1389.86	392.266	327.7662	-1381.41
3.016667	488.8936	14.1283	-1389.92	393.5415	327.3604	-1380.8
3.025	488.8845	14.16535	-1389.94	394.7372	326.9789	-1380.29
3.033333	488.8994	14.25928	-1390.06	395.9389	326.6352	-1379.57
3.041667	488.8917	14.20622	-1389.95	397.0404	326.183	-1378.84
3.05	488.878	14.22698	-1389.94	398.1335	325.832	-1378.21
3.058333	488.7974	14.34096	-1390.06	399.3755	325.5678	-1377.6
3.066667	488.7717	14.40837	-1390.07	400.468	325.1813	-1377.07
3.075	488.7632	14.40117	-1390.06	401.45	324.79	-1376.24
3.083333	488.7641	14.43453	-1389.98	402.5522	324.4809	-1375.68
3.091667	488.7462	14.34367	-1390.06	403.6375	324.1196	-1375.02
3.1	488.7454	14.44029	-1390.07	404.6519	323.8801	-1374.46
3.108333	488.7539	14.40789	-1390.09	405.6758	323.48	-1373.93
3.116667	488.762	14.41183	-1390.08	406.7779	323.1191	-1373.29
3.125	488.7384	14.38984	-1390.08	407.6901	322.7555	-1372.69
3.133333	488.6468	14.51151	-1390.07	408.6285	322.3406	-1372.05
3.141667	488.7422	14.40251	-1390.07	409.5997	321.9193	-1371.49
3.15	488.7343	14.52174	-1390.05	410.6922	321.6077	-1370.88
3.158333	488.7632	14.47961	-1390.05	411.78	321.3345	-1370.44
3.166667	488.6743	14.44275	-1390.07	412.7031	320.9987	-1369.99
3.175	488.6512	14.56438	-1390.06	413.672	320.4951	-1369.31
3.183333	488.6536	14.55522	-1390.04	414.6423	320.0525	-1368.75
3.191667	488.6664	14.53906	-1390.05	415.6772	319.7043	-1368.41
3.2	488.6707	14.57573	-1390.06	416.6256	319.2223	-1367.94
3.208333	488.6376	14.51896	-1390.04	417.5394	318.9049	-1367.64
3.216667	488.6537	14.60323	-1390.1	418.4711	318.56	-1367.28

3.225	488.6667	14.56379	-1390.12	419.4558	318.1429	-1366.88
3.233333	488.7592	14.53991	-1390.06	420.2832	317.609	-1366.56
3.241667	488.7483	14.52728	-1390.11	421.1244	317.2473	-1366.28
3.25	488.6536	14.56227	-1390.12	421.9203	316.8871	-1365.97
3.258333	488.6453	14.60116	-1390.12	422.8506	316.5845	-1365.74
3.266667	488.6594	14.59725	-1390.12	423.6048	316.2888	-1365.64
3.275	488.6503	14.50462	-1390.12	424.4626	316.0095	-1365.49
3.283333	488.6488	14.43027	-1390.11	425.2172	315.6663	-1365.22
3.291667	488.6385	14.38438	-1390.14	426.0316	315.2758	-1365.03
3.3	488.6547	14.47293	-1390.13	426.6391	314.8638	-1364.86
3.308333	488.645	14.36399	-1390.12	427.2868	314.7224	-1364.95
3.316667	488.6617	14.2685	-1390.11	427.9091	314.38	-1364.88
3.325	488.6524	14.22601	-1390.13	428.5144	314.067	-1364.78
3.333333	488.6466	14.15565	-1390.21	429.1837	313.8538	-1364.78
3.341667	488.6532	14.26598	-1390.12	429.8306	313.512	-1364.78
3.35	488.6958	14.17615	-1390.11	430.4716	313.3137	-1364.79
3.358333	488.6765	14.11417	-1390.18	430.9497	313.0645	-1364.84
3.366667	488.663	14.06683	-1390.11	431.4393	312.6801	-1364.82
3.375	488.6516	14.06049	-1390.07	431.9369	312.3527	-1364.8
3.383333	488.6503	14.07732	-1390.07	432.4138	312.0893	-1364.76
3.391667	488.6511	14.08037	-1390.08	432.9228	311.7368	-1364.77
3.4	488.5791	13.9836	-1390.08	433.4575	311.4016	-1364.81
3.408333	488.5541	13.94379	-1390.06	434.0209	311.12	-1364.84
3.416667	488.5558	13.88675	-1390.07	434.5238	311.1267	-1365.02
3.425	488.5464	13.87712	-1390.04	435.0534	310.6672	-1365
3.433333	488.5681	13.88082	-1390.04	435.4607	310.4087	-1365.12
3.441667	488.571	13.86003	-1390.04	435.9344	310.1096	-1365.23
3.45	488.5408	13.78523	-1390.04	436.4437	309.7716	-1365.33
3.458333	488.5497	13.83989	-1390.01	436.9787	309.5009	-1365.32
3.466667	488.5293	13.84749	-1390.05	437.4191	309.1584	-1365.21
3.475	488.5341	13.87939	-1390.04	437.8404	308.8108	-1365.21
3.483333	488.5461	13.87984	-1390.03	438.3011	308.4625	-1365.17
3.491667	488.5229	13.81831	-1390.03	438.6848	308.1014	-1365.1
3.5	488.5431	13.84928	-1390.03	439.1505	307.8882	-1365.15
3.508333	488.5255	13.84792	-1390.05	439.6568	307.6573	-1365.26
3.516667	488.5183	13.77587	-1390.04	440.0778	307.3623	-1365.31
3.525	488.5193	13.81426	-1390.04	440.4691	307.035	-1365.33
3.533333	488.5211	13.72667	-1390.04	440.9818	306.7479	-1365.42
3.541667	488.5363	13.83701	-1390.04	441.4587	306.4305	-1365.44
3.55	488.5431	13.82172	-1390.04	441.9485	306.1651	-1365.52
3.558333	488.5427	13.72404	-1390.04	442.4051	305.7961	-1365.42
3.566667	488.5427	13.57253	-1390.04	442.8421	305.4419	-1365.49
3.575	488.5427	13.63299	-1390.03	443.1949	305.1564	-1365.6
3.583333	488.5229	13.65345	-1390.03	443.5537	304.8789	-1365.59

3.591667	488.6146	13.63671	-1389.79	443.8866	304.5912	-1365.65
3.6	488.6222	13.57493	-1389.79	444.2181	304.3159	-1365.72
3.608333	488.619	13.56411	-1389.78	444.5917	304.0929	-1365.84
3.616667	488.6486	13.56805	-1389.78	444.9793	303.927	-1365.94
3.625	488.619	13.56967	-1389.79	445.3394	303.7151	-1366.01
3.633333	488.6179	13.58453	-1389.79	445.7262	303.4694	-1365.98
3.641667	488.6184	13.53709	-1389.85	446.1125	303.2365	-1365.99
3.65	488.6383	13.47086	-1389.83	446.5034	303.0738	-1366
3.658333	488.6372	13.55556	-1389.85	446.866	302.8347	-1365.97
3.666667	488.6374	13.554	-1389.85	447.1527	302.7045	-1366
3.675	488.6032	13.49947	-1389.85	447.4595	302.552	-1365.98
3.683333	488.6441	13.45014	-1389.86	447.7828	302.2956	-1365.93
3.691667	488.6444	13.48093	-1389.85	448.1451	302.1928	-1365.92
3.7	488.6417	13.4856	-1389.86	448.3951	302.063	-1365.89
3.708333	488.6592	13.48513	-1389.87	448.7076	301.9271	-1365.82
3.716667	488.6553	13.40585	-1389.85	448.9788	301.8008	-1365.74
3.725	488.6375	13.37966	-1389.86	449.2214	301.6359	-1365.59
3.733333	488.6373	13.39549	-1389.92	449.4739	301.4825	-1365.48
3.741667	488.5374	13.39974	-1389.94	449.7477	301.3598	-1365.29
3.75	488.6294	13.3985	-1390.06	450.0607	301.2498	-1365.1
3.758333	488.646	13.39831	-1389.95	450.2616	301.0634	-1364.94
3.766667	488.6324	13.39904	-1389.94	450.5178	300.9848	-1364.8
3.775	488.5529	13.39893	-1390.06	450.6507	300.8759	-1364.61
3.783333	488.5534	13.43177	-1390.07	450.8848	300.8837	-1364.47
3.791667	488.5553	13.43679	-1390.06	451.0703	300.8368	-1364.33
3.8	488.6471	13.39997	-1389.98	451.1611	300.6664	-1364.04
3.808333	488.6436	13.33677	-1390.06	451.3865	300.5091	-1363.79
3.816667	488.5521	13.39282	-1390.07	451.6232	300.4781	-1363.61
3.825	488.6303	13.44645	-1390.09	451.8477	300.3487	-1363.36
3.833333	488.6527	13.40349	-1390.08	452	300.2531	-1363.15
3.841667	488.6499	13.33816	-1390.08	452.1801	300.0724	-1362.96
3.85	488.6322	13.37292	-1390.07	452.3616	300.0141	-1362.73
3.858333	488.6349	13.4028	-1390.07	452.5096	299.9066	-1362.52
3.866667	488.6563	13.49276	-1390.05	452.6477	299.8637	-1362.44
3.875	488.6607	13.50048	-1390.05	452.7717	299.812	-1362.29
3.883333	488.6536	13.45666	-1390.07	452.9012	299.7675	-1362.16
3.891667	488.688	13.52225	-1390.06	453.0282	299.6877	-1362.05
3.9	488.6752	13.45979	-1390.04	453.1732	299.6693	-1361.99
3.908333	488.694	13.44526	-1390.05	453.2841	299.5442	-1361.84
3.916667	488.682	13.48805	-1390.06	453.4613	299.4846	-1361.74
3.925	488.6921	13.47139	-1390.04	453.5421	299.4189	-1361.61
3.933333	488.6768	13.41814	-1390.1	453.7066	299.6598	-1361.77
3.941667	488.6792	13.50858	-1390.12	453.8195	299.4518	-1361.55
3.95	488.6787	13.48677	-1390.06	453.9145	299.3187	-1361.38

3.958333	488.6697	13.46208	-1390.11	454.036	299.2072	-1361.36
3.966667	488.6786	13.49499	-1390.12	454.1175	299.2365	-1361.34
3.975	488.6482	13.51172	-1390.12	454.2633	299.179	-1361.35
3.983333	488.6689	13.47618	-1390.12	454.3549	299.0634	-1361.21
3.991667	488.6706	13.46532	-1390.12	454.4746	299.0142	-1361.24
4	488.6807	13.50478	-1390.11	454.6093	298.9352	-1361.26
4.008333	488.6699	13.44531	-1390.14	454.6923	298.8373	-1361.25
4.016667	488.7633	13.5002	-1390.13	454.8144	298.7833	-1361.21
4.025	488.7599	13.51613	-1390.12	454.9101	298.7589	-1361.34
4.033333	488.7776	13.48158	-1390.11	455.0159	298.6699	-1361.3
4.041667	488.7787	13.38175	-1390.13	455.1354	298.6205	-1361.32
4.05	488.7782	13.36022	-1390.21	455.2442	298.5757	-1361.4
4.058333	488.778	13.32933	-1390.12	455.3718	298.5705	-1361.4
4.066667	488.8074	13.34412	-1390.11	455.496	298.4863	-1361.5
4.075	488.9	13.24916	-1390.18	455.6084	298.4154	-1361.49
4.083333	488.907	13.18161	-1390.11	455.6741	298.2171	-1361.44
4.091667	488.8929	13.11817	-1390.07	455.7763	298.2488	-1361.53
4.1	488.902	13.11552	-1390.07	455.8849	298.1153	-1361.51
4.108333	488.9013	13.11785	-1390.08	455.9916	298.1035	-1361.58
4.116667	488.905	13.05112	-1390.08	456.1103	298.0543	-1361.59
4.125	488.9038	13.04729	-1390.06	456.1675	297.9407	-1361.61
4.133333	488.8994	13.03604	-1390.07	456.2556	297.8877	-1361.57
4.141667	489.4068	13.04777	-1390.04	456.3107	297.8509	-1361.62
4.15	489.4068	13.03679	-1390.04	456.3678	297.7892	-1361.66
4.158333	489.3964	13.04788	-1390.04	456.4495	297.7174	-1361.71
4.166667	489.3835	12.9876	-1390.04	456.5009	297.6535	-1361.67
4.175	489.3941	13.03128	-1390.01	456.5137	297.5875	-1361.67
4.183333	489.4062	13.05659	-1390.05	456.6238	297.5665	-1361.77
4.191667	489.3064	13.04963	-1390.04	456.6521	297.5242	-1361.79
4.2	489.3031	13.01731	-1390.03	456.6972	297.4417	-1361.83
4.208333	489.2878	13.01577	-1390.03	456.7505	297.4054	-1361.87
4.216667	489.2882	13.11218	-1390.03	456.8105	297.3712	-1361.79
4.225	489.2886	13.1202	-1390.05	456.8581	297.3424	-1361.84
4.233333	489.2998	13.16281	-1390.04	456.9102	297.4058	-1361.9
4.241667	489.2896	13.10653	-1390.04	456.962	297.7023	-1362.2
4.25	489.2993	13.09396	-1390.04	456.9596	297.3471	-1361.94
4.258333	489.3112	13.08582	-1390.04	456.9616	297.3573	-1361.94
4.266667	489.3022	13.11929	-1390.04	456.9691	297.3444	-1361.94
4.275	489.2997	13.10237	-1390.04	456.9849	297.2902	-1361.84
4.283333	489.1979	13.0865	-1390.04	457.03	297.3188	-1361.86
4.291667	489.2005	13.09802	-1390.03	457.0286	297.3076	-1361.85
4.3	489.1997	13.09989	-1390.03	457.0615	297.3214	-1361.78
4.308333	489.2132	13.09959	-1389.79	457.0618	297.3206	-1361.78
4.316667	489.1704	13.05116	-1389.79	457.0551	297.3172	-1361.67

4.325	489.2001	13.01415	-1389.78	457.0322	297.3067	-1361.64
4.333333	489.1782	13.00139	-1389.78	457.0285	297.3454	-1361.53
4.341667	489.1792	13.04583	-1389.79	457.0316	297.3705	-1361.52
4.35	489.1702	12.91224	-1389.79	456.9796	297.405	-1361.46
4.358333	489.1667	12.9278	-1389.85	456.9799	297.382	-1361.39
4.366667	489.1485	12.93415	-1389.83	456.9974	297.3643	-1361.37
4.375	489.1699	12.90196	-1389.85	456.9232	297.3152	-1361.22
4.383333	489.1741	13.02649	-1389.85	456.9362	297.3505	-1361.23
4.391667	489.1733	13.00821	-1389.85	456.9261	297.4404	-1361.21
4.4	489.1512	12.9665	-1389.86	456.9112	297.4243	-1361.2
4.408333	489.1483	12.95198	-1389.85	456.9091	297.4195	-1361.19
4.416667	489.1673	12.95162	-1389.86	456.8815	297.4505	-1361.16
4.425	489.1684	12.98584	-1389.87	456.9033	297.5468	-1361.18
4.433333	489.1981	12.95503	-1389.85	456.9018	297.5359	-1361.17
4.441667	489.1884	12.95139	-1389.86	456.8917	297.4985	-1361.18
4.45	489.1561	12.89052	-1389.92	456.9153	297.8476	-1361.44
4.458333	489.1664	12.85171	-1389.94	456.906	297.5329	-1361.21
4.466667	489.1886	12.91439	-1390.06	456.91	297.8987	-1361.53
4.475	489.1568	12.82509	-1389.95	456.926	297.535	-1361.34
4.483333	489.054	12.75371	-1389.94	456.9166	297.4935	-1361.31
4.491667	489.057	12.81244	-1390.06	456.8857	297.4877	-1361.39
4.5	489.1626	12.8204	-1390.07	456.9392	297.4933	-1361.45
4.508333	489.082	12.8191	-1390.06	456.9861	297.4858	-1361.5
4.516667	489.0601	12.78304	-1389.98	457.0037	297.5112	-1361.6
4.525	489.06	12.72762	-1390.06	457.0508	297.4487	-1361.66
4.533333	489.0615	12.68165	-1390.07	457.0269	297.4149	-1361.64
4.541667	489.0723	12.68172	-1390.09	457.0123	297.4601	-1361.77
4.55	489.0635	12.6843	-1390.08	457.0377	297.3938	-1361.76
4.558333	489.0909	12.62295	-1390.08	456.9913	297.4079	-1361.85
4.566667	489.0808	12.67782	-1390.07	457.0204	297.383	-1361.88
4.575	489.0609	12.69231	-1390.07	456.9996	297.416	-1361.96
4.583333	489.0617	12.71686	-1390.05	457.0006	297.4207	-1361.97
4.591667	489.0917	12.71969	-1390.05	457.0001	297.4187	-1361.96
4.6	489.1017	12.71971	-1390.07	456.9783	297.4526	-1362.04
4.608333	489.0946	12.7071	-1390.06	456.9853	297.4761	-1362.06
4.616667	489.1109	12.7182	-1390.04	456.985	297.5067	-1362.08
4.625	489.1212	12.78194	-1390.05	456.9963	297.4868	-1362.07
4.633333	489.0847	12.7124	-1390.06	457.0005	297.533	-1362.11
4.641667	489.0938	12.70388	-1390.04	456.9682	297.4907	-1362.16
4.65	489.0942	12.58697	-1390.1	456.966	297.487	-1362.16
4.658333	489.1051	12.62396	-1390.12	456.9801	297.5393	-1362.17
4.666667	489.1062	12.75043	-1390.06	456.9397	297.5263	-1362.16
4.675	489.0841	12.66553	-1390.11	456.9044	297.563	-1362.13
4.683333	489.0811	12.66651	-1390.12	456.9045	297.5646	-1362.13

4.691667	489.1001	12.737	-1390.12	456.905	297.5645	-1362.13
4.7	489.1013	12.7421	-1390.12	456.9182	297.5981	-1362.14
4.708333	489.101	12.77321	-1390.12	456.907	297.697	-1362.23
4.716667	489.0904	12.74133	-1390.11	456.8353	297.622	-1362.22
4.725	489.0955	12.61614	-1390.14	456.8456	297.601	-1362.21
4.733333	489.0994	12.60219	-1390.13	456.8312	297.5827	-1362.2
4.741667	489.1018	12.66803	-1390.12	456.8293	297.6411	-1362.22
4.75	489.0796	12.61685	-1390.11	456.8305	297.667	-1362.29
4.758333	489.0763	12.60376	-1390.13	456.8373	297.6889	-1362.31
4.766667	489.0773	12.61923	-1390.21	456.7932	297.6475	-1362.3
4.775	489.0994	12.60949	-1390.12	456.7675	297.6752	-1362.38
4.783333	489.1022	12.68775	-1390.11	456.7701	297.6816	-1362.38
4.791667	489.1012	12.69299	-1390.18	456.7733	297.7257	-1362.41
4.8	489.1008	12.65738	-1390.11	456.7684	297.6828	-1362.52
4.808333	489.1008	12.64155	-1390.07	456.7641	297.6555	-1362.52
4.816667	489.1009	12.67532	-1390.07	456.7819	297.6981	-1362.54
4.825	489.1009	12.69122	-1390.08	456.7939	297.6274	-1362.55
4.833333	489.1009	12.73772	-1390.08	456.7918	297.6218	-1362.55
4.841667	489.0792	12.67924	-1390.06	456.7682	297.5882	-1362.61
4.85	489.0764	12.67211	-1390.07	456.7568	297.6069	-1362.62
4.858333	489.0954	12.70598	-1390.04	456.8211	297.6194	-1362.69
4.866667	489.0941	12.70901	-1390.04	456.8364	297.597	-1362.68
4.875	489.0977	12.67436	-1390.04	456.802	297.5966	-1362.67
4.883333	489.0928	12.57586	-1390.04	456.8141	297.5802	-1362.67
4.891667	489.1011	12.57051	-1390.01	456.8487	297.5305	-1362.73
4.9	489.1029	12.57327	-1390.05	456.858	297.5636	-1362.73
4.908333	489.0918	12.54015	-1390.04	456.866	297.485	-1362.61
4.916667	489.0906	12.46327	-1390.03	456.8992	297.4396	-1362.61
4.925	489.0909	12.51791	-1390.03	456.9012	297.4423	-1362.61
4.933333	489.0934	12.53164	-1390.03	456.9296	297.4134	-1362.64
4.941667	489.0872	12.54276	-1390.05	456.9325	297.4255	-1362.62
4.95	489.0922	12.5966	-1390.04	457.0162	297.4465	-1362.59
4.958333	489.0941	12.53478	-1390.04	456.9837	297.3886	-1362.57
4.966667	489.0872	12.43287	-1390.04	457.0654	297.2846	-1362.49
4.975	489.0034	12.4798	-1390.04	457.0655	297.3098	-1362.51
4.983333	488.9913	12.54312	-1390.04	457.1478	297.3447	-1362.46
4.991667	488.9842	12.54348	-1390.04	457.1772	297.3764	-1362.48
5	489.0019	12.48215	-1390.04	457.1704	297.2281	-1362.35
5.008333	488.9852	12.52924	-1390.03	457.2055	297.2279	-1362.35
5.016667	489.0022	12.48564	-1390.03	457.2966	297.2546	-1362.34
5.025	488.9853	12.59258	-1389.79	457.2932	297.2541	-1362.23
5.033333	488.9842	12.48916	-1389.79	457.3115	297.2587	-1362.21
5.041667	488.9868	12.52899	-1389.78	457.3819	297.5931	-1362.43
5.05	488.9935	12.50972	-1389.78	457.385	297.2127	-1362.1

5.058333	488.9964	12.54093	-1389.79	457.3835	297.5708	-1362.3
5.066667	488.9941	12.60263	-1389.79	457.4248	297.6595	-1362.27
5.075	489.0001	12.54565	-1389.85	457.4823	297.6214	-1362.19
5.083333	488.8936	12.53866	-1389.83	457.4231	297.2766	-1361.88
5.091667	488.8845	12.54001	-1389.85	457.4181	297.2051	-1361.71
5.1	488.8994	12.54061	-1389.85	457.4185	297.2571	-1361.64
5.108333	488.8917	12.54063	-1389.85	457.4794	297.3111	-1361.6
5.116667	488.878	12.54059	-1389.86	457.5416	297.2482	-1361.5
5.125	488.7974	12.50668	-1389.85	457.5146	297.2397	-1361.49
5.133333	488.7717	12.50556	-1389.86	457.4947	297.2426	-1361.36
5.141667	488.7632	12.60153	-1389.87	457.5401	297.2282	-1361.27
5.15	488.7641	12.57428	-1389.85	457.5443	297.2746	-1361.3
5.158333	488.7462	12.49627	-1389.86	457.5902	297.1949	-1361.19
5.166667	488.7454	12.45568	-1389.92	457.576	297.2358	-1361.17
5.175	488.7539	12.48949	-1389.94	457.5852	297.2114	-1361.07
5.183333	488.762	12.50652	-1390.06	457.6009	297.3056	-1361.11
5.191667	488.7384	12.46038	-1389.95	457.6228	297.234	-1361
5.2	488.6468	12.39435	-1389.94	457.59	297.252	-1360.96
5.208333	488.7422	12.39052	-1390.06	457.59	297.255	-1360.96
5.216667	488.7343	12.50078	-1390.07	457.6161	297.2472	-1360.88
5.225	488.7632	12.51045	-1390.06	457.6006	297.3259	-1360.86
5.233333	488.6743	12.50705	-1389.98	457.6019	297.3311	-1360.86
5.241667	488.6512	12.50598	-1390.06	457.6017	297.3298	-1360.86
5.25	488.6536	12.50602	-1390.07	457.6233	297.2961	-1360.78
5.258333	488.6664	12.50611	-1390.09	457.6218	297.2912	-1360.78
5.266667	488.6707	12.50612	-1390.08	457.6082	297.2956	-1360.76
5.275	488.6376	12.50611	-1390.08	457.5971	297.3477	-1360.75
5.283333	488.6537	12.47096	-1390.07	457.568	297.3085	-1360.73
5.291667	488.6667	12.45096	-1390.07	457.5653	297.3538	-1360.74
5.3	488.7592	12.55434	-1390.05	457.5566	297.4147	-1360.71
5.308333	488.7483	12.5202	-1390.05	457.5374	297.4218	-1360.71
5.316667	488.6536	12.5642	-1390.07	457.511	297.4231	-1360.66
5.325	488.6453	12.51569	-1390.06	457.4705	297.429	-1360.64
5.333333	488.6594	12.504	-1390.04	457.4514	297.5099	-1360.75
5.341667	488.6503	12.50463	-1390.05	457.3907	297.5481	-1360.7
5.35	488.6488	12.56633	-1390.06	457.3315	297.4683	-1360.66
5.358333	488.6385	12.51741	-1390.04	457.2811	297.4974	-1360.68
5.366667	488.6547	12.50108	-1390.1	457.2434	297.5335	-1360.71
5.375	488.645	12.57064	-1390.12	457.1679	297.5698	-1360.73
5.383333	488.6617	12.57565	-1390.06	457.1196	297.6644	-1360.8
5.391667	488.6524	12.57285	-1390.11	457.0999	297.7212	-1360.79
5.4	488.6466	12.57218	-1390.12	457.0976	298.1039	-1361.13
5.408333	488.6532	12.57227	-1390.12	457.073	298.1319	-1361.16
5.416667	488.6958	12.57234	-1390.12	457.0278	297.8117	-1360.97

5.425	488.6765	12.57234	-1390.12	456.9233	297.8047	-1360.87
5.433333	488.663	12.51381	-1390.11	456.8934	297.7702	-1360.87
5.441667	488.6516	12.46588	-1390.14	456.8705	297.7499	-1360.93
5.45	488.6503	12.47288	-1390.13	456.8754	297.7787	-1360.94
5.458333	488.6511	12.47371	-1390.12	456.8235	297.7924	-1360.94
5.466667	488.5791	12.43909	-1390.11	456.8167	297.8161	-1361.02
5.475	488.5541	12.43784	-1390.13	456.8137	297.8018	-1361.01
5.483333	488.5558	12.43842	-1390.21	456.7953	297.8668	-1361
5.491667	488.5464	12.43847	-1390.12	456.791	297.852	-1360.99
5.5	488.5681	12.56759	-1390.11	456.7655	297.8858	-1360.98
5.508333	488.571	12.5428	-1390.18	456.7446	297.8947	-1360.99
5.516667	488.5408	12.44286	-1390.11	456.7444	297.8947	-1360.99
5.525	488.5497	12.43468	-1390.07	456.696	297.8015	-1360.94
5.533333	488.5293	12.43764	-1390.07	456.7094	297.861	-1360.96
5.541667	488.5341	12.43857	-1390.08	456.723	297.8999	-1360.93
5.55	488.5461	12.43854	-1390.08	456.7356	297.8356	-1360.88
5.558333	488.5229	12.37669	-1390.06	456.7216	297.8633	-1360.9
5.566667	488.5431	12.46709	-1390.07	456.7479	297.8804	-1360.87
5.575	488.5255	12.47531	-1390.04	456.7475	297.8887	-1360.85
5.583333	488.5183	12.56876	-1390.04	456.7185	297.923	-1360.84
5.591667	488.5193	12.54202	-1390.04	456.7814	297.9061	-1360.78
5.6	488.5211	12.46228	-1390.04	456.7556	297.9053	-1360.72
5.608333	488.5363	12.46881	-1390.01	456.737	297.9134	-1360.72
5.616667	488.5431	12.47279	-1390.05	456.7586	297.88	-1360.65
5.625	488.5427	12.50687	-1390.04	456.7784	297.8929	-1360.64
5.633333	488.5427	12.47556	-1390.03	456.667	297.9265	-1360.68
5.641667	488.5427	12.40034	-1390.03	456.6857	297.8926	-1360.6
5.65	488.5229	12.34144	-1390.03	456.7032	297.8793	-1360.6
5.658333	488.6146	12.39457	-1390.05	456.6754	297.997	-1360.58
5.666667	488.6222	12.56612	-1390.04	456.713	298.0644	-1360.6
5.675	488.619	12.46109	-1390.04	456.5927	298.0478	-1360.52
5.683333	488.6486	12.46284	-1390.04	456.5632	298.0719	-1360.59
5.691667	488.619	12.47431	-1390.04	456.5432	298.1369	-1360.57

D.2 Wiimote

Table D.2: Sample of measuring flexion by Wiimote (raw data)

Rotation around X	Rotation around Y	Rotation around Z
0	0.581792	0.596783
-0.11866	0.249035	0.168663
-0.64501	0.245973	0.168711
-2.09632	0.242533	0.16571
-1.5453	0.239106	0.162694
-0.16613	0.242389	0.159691
0.352535	0.239265	0.156704
1.172141	0.248386	0.159484
1.610928	0.251733	0.159934
0.308393	0.255123	0.159956
1.157223	0.251921	0.160142
-0.47656	0.249617	0.159956
-1.29325	0.23983	0.160142
-1.85492	0.240206	0.156908
-2.93328	0.237155	0.163167
-1.97105	0.233739	0.160617
-1.26152	0.230576	0.160165
0.051547	0.230603	0.160224
0.78739	0.233943	0.160108
2.272658	0.240033	0.160165
3.170995	0.236909	0.160165
3.705806	0.240229	0.163379
2.919899	0.240533	0.163287
2.570624	0.237525	0.16654
2.11028	0.234149	0.167199
1.933954	0.231086	0.170014
2.108906	0.228086	0.174081
1.747443	0.228055	0.180801
2.355158	0.227759	0.186084
4.140151	0.228073	0.186706
5.649931	0.228093	0.187118
9.004246	0.231302	0.187762
12.22951	0.234975	0.184978
15.70815	0.238016	0.184602
20.38293	0.240778	0.183997
22.59479	0.240875	0.183635
25.24649	0.244209	0.180354
29.31678	0.240768	0.17109

31.89456	0.234692	0.164904
36.10111	0.231404	0.162086
41.59027	0.225294	0.159129
50.86913	0.222289	0.158585
66.81563	0.224945	0.164014
77.43985	0.228342	0.171747
84.8832	0.231359	0.185385
92.26791	0.231022	0.211235
96.20399	0.230857	0.240262
97.34162	0.233418	0.257673
97.89623	0.23626	0.279903
99.06964	0.238907	0.295458
102.3491	0.245016	0.310155
105.44	0.251592	0.324571
106.6405	0.26081	0.33577
109.2298	0.26771	0.345275
110.2017	0.283888	0.35755
111.6104	0.287093	0.371494
109.9103	0.294718	0.406483
108.2178	0.302111	0.427753
108.0823	0.309965	0.492635
108.4551	0.321045	0.521174
108.3844	0.329848	0.556514
108.5329	0.330882	0.587556
108.7796	0.335153	0.607728
109.9289	0.336247	0.636467
110.6624	0.336194	0.657711
110.9278	0.33673	0.666039
111.1854	0.337472	0.680436
111.1634	0.33862	0.69247
110.577	0.341358	0.715401
110.6206	0.342301	0.728627
112.3629	0.342307	0.745816
113.8294	0.345618	0.762357
114.6044	0.346588	0.766009
114.9054	0.350615	0.77133
115.2049	0.359293	0.776643
115.1407	0.377651	0.782711
115.0672	0.38422	0.792972
115.3233	0.390507	0.802412
115.9985	0.393298	0.813052
115.8851	0.400762	0.824447
114.8448	0.405403	0.837303
115.2141	0.412484	0.852984

115.914	0.421231	0.871337
115.9137	0.432275	0.890167
115.5161	0.444511	0.903075
114.9818	0.452938	0.911561
115.6154	0.467157	0.919853
116.1243	0.489316	0.928349
116.2643	0.500914	0.935504
116.6574	0.521985	0.941301
116.7298	0.53153	0.941336
116.4147	0.555319	0.940607
116.0627	0.564607	0.939392
116.4377	0.581692	0.94019
116.8454	0.588877	0.942888
117.2523	0.588959	0.95148
117.7687	0.591844	0.956734
117.5228	0.604287	0.96262
117.0865	0.60631	0.961893
117.8541	0.608781	0.95774
117.5946	0.61385	0.95712
116.6267	0.616549	0.947822
116.2953	0.630418	0.945751
116.9976	0.639521	0.942641
116.918	0.667574	0.934776
116.7028	0.684606	0.93508
116.4898	0.692334	0.929161
116.0627	0.701928	0.923209
116.4377	0.709098	0.922373
116.8454	0.715238	0.927231
117.2523	0.723273	0.929156
117.7687	0.732011	0.933157
117.5228	0.736983	0.936619
117.0865	0.740853	0.940642
117.8541	0.741189	0.944511
117.5946	0.736116	0.940683
116.6267	0.730035	0.938176
116.2953	0.72395	0.933581
116.9976	0.718869	0.931057
116.918	0.711702	0.929187
116.7028	0.707459	0.925895
116.4898	0.70637	0.923358

D.3 MotionNode

Table D.3: Sample of measuring flexion by MotionNode (raw data)

Rotation around X	Rotation around Y	Rotation around Z
0.00002	0.000001	0.00013
0.002707	-0.00125	0.00125
0.003498	-0.00254	0.002543
-0.00093	-0.00648	0.006483
0.001613	-0.01663	0.016631
0.003209	-0.01659	0.016591
0.003975	-0.01504	0.015035
0.012215	-0.01926	0.01926
0.01221	-0.01483	0.014831
0.013088	-0.01496	0.014964
0.007516	-0.01251	0.012505
0.021045	-0.01406	0.014064
0.026567	-0.01397	0.013974
0.026215	-0.01844	0.018444
0.024714	-0.01837	0.018374
0.017713	-0.02268	0.022681
0.023732	-0.02918	0.029176
0.022151	-0.02154	0.02154
0.027282	-0.02101	0.021013
0.024779	-0.01394	0.013942
0.017872	-0.00756	0.007557
0.010904	-0.00416	0.004162
0.016781	0.004384	-0.00438
0.015635	0.006937	-0.00694
0.014438	0.011725	-0.01173
0.013384	0.018814	-0.01881
0.019674	0.023141	-0.02314
0.037189	0.015094	-0.01509
0.040816	0.009959	-0.00996
0.058635	0.004048	-0.00405
0.068507	-0.00402	0.004021
0.089797	-0.00722	0.00722
0.100425	0.003381	-0.00338
0.116959	0.006585	-0.00659
0.122174	-0.00171	0.001712
0.140427	-0.01059	0.010589
0.155782	-0.00262	0.002615
0.182804	-0.00543	0.005432

0.194621	0.007675	-0.00767
0.223846	0.013359	-0.01336
0.255489	0.014388	-0.01439
0.285655	0.015744	-0.01574
0.099126	-0.06532	0.065322
0.171336	-0.10094	0.100937
0.243782	-0.08913	0.089125
0.29089	-0.0629	0.062896
0.358863	-0.02769	0.027694
0.441607	-0.00159	0.001586
0.457671	0.030385	-0.03038
0.453324	0.059957	-0.05996
0.499525	0.085055	-0.08506
0.566089	0.082151	-0.08215
0.591183	0.094347	-0.09435
0.643664	0.102121	-0.10212
0.699919	0.122696	-0.1227
0.694549	0.182182	-0.18218
0.719253	0.24094	-0.24094
0.694488	0.266307	-0.26631
0.681139	0.279706	-0.27971
0.645781	0.331601	-0.3316
0.518036	0.381198	-0.3812
0.459497	0.489971	-0.48997
0.391536	0.599539	-0.59954
0.471194	0.773764	-0.77376
0.249558	0.877278	-0.87728
0.166144	0.953802	-0.9538
0.024894	1.029988	-0.00504
-0.08266	1.096246	-0.00537
-0.29726	1.126057	-0.02097
-0.58612	1.196912	-0.03589
-0.83896	1.279474	-0.04416
-1.05026	1.372504	-0.03726
-1.20213	1.436713	-0.02998
-1.25406	1.42816	-0.03479
-1.22344	1.406883	-0.02858
-1.01099	1.370014	-0.02347
-0.70192	1.415922	-0.02684
-0.58231	1.601026	-0.02864
-0.39408	1.974776	-0.03712
-0.40149	2.605316	-0.01878
-0.72292	3.441442	0.012411
-1.04989	4.554413	0.069527

-1.15354	6.005403	0.086515
-1.35925	7.715391	0.064363
-1.78248	9.695577	0.031367
-2.16554	11.45115	-0.02173
-2.5036	13.15426	-0.09215
-2.77703	14.8044	-0.16359
-2.9112	16.21057	-0.22423
-2.89729	17.64422	-0.32647
-2.95278	19.28325	-0.48892
-3.07714	20.75963	-0.77829
-3.16675	21.97977	-1.03851
-3.16762	23.32299	0.000908
-3.17855	25.03939	0.008777
-3.29897	26.94737	0.002415
-3.30675	28.57841	-0.00237
-3.2979	30.08448	-0.00205
-3.31641	31.83528	-0.03162
-3.29987	33.80638	-0.02719
-3.29236	35.78559	-0.08398
-3.35163	37.5139	-0.07358
-3.29255	39.05923	-0.05345
-3.30392	40.57567	-0.03669
-3.35756	42.12499	-0.03216
-3.286	43.88338	-0.06197
-3.30605	45.65183	-0.03915
-3.43267	47.10089	-0.00028
-3.58174	48.42722	-0.02096
-3.07714	49.86906	-0.02544
-3.16675	51.31911	0.007937
-3.16762	53.00883	0.018721
-3.17855	54.58747	0.010665
-3.29897	56.02275	-0.00775
-3.30675	57.34181	0.034922
-3.2979	58.50921	0.035093
-3.31641	59.74112	0.036186
-3.29987	61.11971	0.051615
-3.29236	62.46456	0.000908
-3.35163	63.62222	0.008777
-3.29255	64.73908	0.002415
-3.30392	65.88737	-0.00237
-3.35756	66.98943	-0.00205
-3.286	68.16824	-0.03162
-3.30605	69.48034	-0.02719
-3.43267	70.87062	-0.08398

-3.58174	72.12025	-0.07358
-3.07714	73.23835	-0.05345
-3.16675	74.43913	-0.03669
-3.16762	75.62555	-0.03216
-3.17855	76.72331	-0.06197
-3.29897	77.75125	-0.03915
-3.30675	78.72134	-0.00028
-3.2979	79.82456	-0.02096
-3.31641	81.06358	-0.02544
-3.29987	82.25103	0.007937
-3.29236	83.26953	0.018721
-3.35163	84.28919	0.010665
-3.29255	85.3679	-0.00775
-3.30392	86.50115	0.034922
-3.35756	87.63204	0.035093
-3.286	88.73797	0.036186
-3.30605	90.07497	0.051615
-3.43267	91.53804	-0.27971
-3.58174	92.6524	-0.3316
-3.07714	93.73479	-0.3812
-3.16675	94.92301	-0.48997
-3.16762	96.07607	-0.59954
-3.17855	97.14288	-0.77376
-3.29897	98.10585	-0.87728
-3.30675	98.96322	-0.9538
-3.2979	99.88676	-0.00504
-3.31641	100.7878	-0.00537
-3.29987	101.7144	-0.02097
-3.29236	102.6914	-0.03589
-3.35163	103.5542	-0.04416
-3.29255	104.2581	-0.03726
-3.30392	105.0118	-0.02998
-3.35756	105.7536	-0.03479
-3.286	106.4497	-0.02858
-3.30605	107.0924	-0.02347
-3.43267	107.7616	-0.02684
-3.58174	108.5411	-0.02864
-3.07714	109.3418	-0.03712
-3.16675	110.0317	-0.01878
-3.16762	110.6077	0.012411
-3.17855	111.2635	0.069527
-3.29897	111.9568	0.086515
-3.30675	112.5293	0.064363
-3.2979	112.9997	0.031367

-3.31641	113.4229	-0.02173
-3.29987	113.8438	-0.09215
-3.29236	114.2671	-0.16359
-3.35163	114.6554	-0.22423
-3.29255	115.1325	-0.32647
-3.30392	115.5503	-0.48892
-3.35756	115.9333	-0.77829
-3.286	116.3341	-1.03851
-3.30605	116.7332	0.000908
-3.43267	117.1187	0.008777
-3.58174	117.4887	0.002415
-3.07714	117.8466	-0.00237
-3.16675	118.192	-0.00205
-3.16762	118.4679	-0.03162
-3.17855	118.6949	-0.02719
-3.29897	118.9219	-0.08398
-3.30675	119.139	-0.07358
-3.2979	119.3218	-0.05345
-3.31641	119.5097	-0.03669
-3.29987	119.7254	-0.03216
-3.29236	119.8267	-0.06197
-3.35163	119.9794	-0.03915
-3.29255	120.1866	-0.00028
-3.30392	120.3312	-0.02096
-3.35756	120.4939	-0.02544
-3.286	120.8081	0.007937
-3.30605	121.2321	0.018721
-3.43267	121.6489	0.010665
-3.58174	121.9508	-0.00775
-3.07714	122.1697	0.034922
-3.16675	122.4716	0.035093
-3.16762	122.7548	0.036186
-3.17855	123.0022	0.051615
-3.29897	123.309	0.000908
-3.30675	123.6279	0.008777
-3.2979	123.9641	0.002415
-3.31641	124.4203	-0.00237
-3.29987	124.9143	-0.00205
-3.29236	125.3974	-0.03162
-3.35163	125.8561	-0.02719
-3.29255	126.3279	-0.08398
-3.30392	126.8671	-0.07358
-3.35756	127.3507	-0.05345
-3.286	127.6969	-0.03669

-3.30605	127.9606	-0.03216
-3.43267	128.2007	-0.06197
-3.58174	128.4546	-0.03915
-3.07714	128.8166	-0.00028
-3.16675	129.2442	-0.02096
-3.16762	129.6114	-0.02544
-3.17855	129.8383	0.007937
-3.29897	130.0589	0.018721
-3.30675	130.2428	0.010665
-3.2979	130.4476	-0.00775
-3.31641	130.8125	0.034922
-3.29987	131.148	0.035093
-3.29236	131.4196	0.036186
-3.35163	131.626	0.051615
-3.29255	131.8295	-0.27971
-3.30392	132.0834	-0.3316
-3.35756	132.4121	-0.3812
-3.286	132.7915	-0.48997
-3.30605	133.146	-0.59954
-3.43267	133.4821	-0.77376
-3.58174	133.7498	-0.87728
-3.07714	133.9991	-0.9538
-3.16675	134.2919	-0.00504
-3.16762	134.6113	-0.00537
-3.17855	134.9315	-0.02097
-3.29897	135.2426	-0.03589
-3.30675	135.545	-0.04416
-3.2979	135.7826	-0.03726
-3.31641	136.0221	-0.02998
-3.29987	136.2785	-0.03479
-3.29236	136.5701	-0.02858
-3.35163	136.9062	-0.02347
-3.29255	137.243	-0.02684
-3.30392	137.5416	-0.02864
-3.35756	137.7868	-0.03712
-3.286	138.0352	-0.01878
-3.30605	138.3246	0.012411
-3.43267	138.6424	0.069527
-3.58174	138.9821	0.086515
-3.07714	139.2871	0.064363
-3.16675	139.5473	0.031367
-3.16762	139.8018	-0.02173
-3.17855	140.0915	-0.09215
-3.29897	140.3915	-0.16359

-3.30675	140.6643	-0.22423
-3.2979	140.8649	-0.32647
-3.31641	141.0196	-0.48892
-3.29987	141.1688	-0.77829
-3.29236	141.3534	-1.03851
-3.35163	141.6127	0.000908
-3.29255	141.8778	0.008777
-3.30392	142.0805	0.002415
-3.35756	142.2525	-0.00237
-3.286	142.3969	-0.00205
-3.30605	142.4879	-0.03162
-3.43267	142.5177	-0.02719
-3.58174	142.5259	-0.08398
-3.07714	142.5599	-0.07358
-3.16675	142.5761	-0.05345
-3.16762	142.5906	-0.03669
-3.17855	142.6492	-0.03216
-3.29897	142.7251	-0.06197
-3.30675	142.8299	-0.03915
-3.2979	142.9578	-0.00028
-3.31641	143.1005	-0.02096
-3.29987	143.2011	-0.02544
-3.29236	143.2921	0.007937
-3.35163	143.3814	0.018721
-3.29255	143.4792	0.010665
-3.30392	143.5548	-0.00775
-3.35756	143.6387	0.034922
-3.286	143.7543	0.035093
-3.30605	143.9464	0.036186
-3.43267	144.1953	0.051615
-3.58174	144.4294	0.000908
-3.07714	144.6122	0.008777
-3.16675	144.7977	0.002415
-3.16762	145.0468	-0.00237
-3.17855	145.2892	-0.00205
-3.29897	145.5102	-0.03162
-3.30675	145.7749	-0.02719
-3.2979	146.0701	-0.08398
-3.31641	146.3723	-0.07358
-3.29987	146.6966	-0.05345
-3.29236	147.0173	-0.03669
-3.35163	147.3079	-0.03216
-3.29255	147.5515	-0.06197
-3.30392	147.7222	-0.03915

-3.35756	147.8828	-0.00028
-3.286	148.1229	-0.02096
-3.30605	148.3105	-0.02544
-3.43267	148.4521	0.007937
-3.58174	148.5187	0.018721
-3.07714	148.6205	0.010665
-3.16675	148.7551	-0.00775
-3.16762	148.9653	0.034922
-3.17855	149.177	0.035093
-3.29897	149.3786	0.036186
-3.30675	149.5274	0.051615
-3.2979	149.6261	-0.27971
-3.31641	149.7351	-0.3316
-3.29987	149.8507	-0.3812
-3.29236	149.9862	-0.48997
-3.35163	150.1012	-0.59954
-3.29255	150.2132	-0.77376
-3.30392	150.3008	-0.87728
-3.35756	150.3767	-0.9538
-3.286	150.4813	-0.00504
-3.30605	150.6207	-0.00537
-3.43267	150.7416	-0.02097
-3.58174	150.8136	-0.03589
-3.07714	150.8397	-0.04416
-3.16675	150.8384	-0.03726
-3.16762	150.8491	-0.02998
-3.17855	150.9213	-0.03479
-3.29897	151.0354	-0.02858
-3.30675	151.1351	-0.02347
-3.2979	151.2294	-0.02684
-3.31641	151.333	-0.02864
-3.29987	151.2549	-0.03712
-3.29236	151.3134	-0.01878
-3.35163	151.439	0.012411
-3.29255	151.575	0.069527
-3.30392	151.6766	0.086515
-3.35756	151.7563	0.064363
-3.286	151.821	0.031367
-3.30605	151.9176	-0.02173
-3.43267	151.9632	-0.09215
-3.58174	151.9603	-0.16359
-3.07714	151.9238	-0.22423
-3.16675	151.9305	-0.32647
-3.16762	151.9019	-0.48892

-3.17855	151.8522	-0.77829
-3.29897	151.8579	-1.03851
-3.30675	151.9196	0.000908
-3.2979	151.9601	0.008777
-3.31641	151.9702	0.002415
-3.29987	151.9829	-0.00237
-3.29236	152.0016	-0.00205
-3.35163	152.0085	-0.03162
-3.29255	152.0023	-0.02719
-3.30392	151.9844	-0.08398
-3.35756	151.9913	-0.07358
-3.286	152.0206	-0.05345
-3.30605	152.0587	-0.03669
-3.43267	152.1064	-0.03216
-3.58174	152.1562	-0.06197
-3.07714	152.1976	-0.03915
-3.16675	152.2798	-0.00028
-3.16762	152.5753	-0.02096
-3.17855	152.8948	-0.02544
-3.29897	153.1496	0.007937
-3.30675	153.3181	0.018721
-3.2979	153.4484	0.010665
-3.31641	153.5107	-0.00775
-3.29987	153.5165	0.034922
-3.29236	153.6781	0.035093
-3.35163	153.7959	0.036186
-3.29255	153.9033	0.051615
-3.30392	153.9263	0.000908
-3.35756	153.9654	0.008777
-3.286	154.0256	0.002415
-3.30605	154.0973	-0.00237
-3.43267	154.1593	-0.00205
-3.58174	154.1995	-0.03162
-3.07714	154.2208	-0.02719
-3.16675	154.2215	-0.08398
-3.16762	154.2665	-0.07358
-3.17855	154.3511	-0.05345
-3.29897	154.4346	-0.03669
-3.30675	154.4767	-0.03216
-3.2979	154.5033	-0.06197
-3.31641	154.5293	-0.03915
-3.29987	154.5471	-0.00028
-3.29236	154.5512	-0.02096
-3.35163	154.5468	-0.02544

-3.29255	154.5609	0.007937
-3.30392	154.5664	0.018721
-3.35756	154.5594	0.010665
-3.286	154.5721	-0.00775
-3.30605	154.5946	0.034922
-3.43267	154.5881	0.035093
-3.58174	154.5393	0.036186
-3.07714	154.468	0.051615
-3.16675	154.4112	-0.27971
-3.16762	154.3843	-0.3316
-3.17855	154.3407	-0.3812
-3.29897	154.2747	-0.48997
-3.30675	154.1935	-0.59954
-3.2979	154.1336	-0.77376
-3.31641	154.0745	-0.87728
-3.29987	154.0636	-0.9538
-3.29236	154.0733	-0.00504
-3.35163	154.0633	-0.00537
-3.29255	154.034	-0.02097
-3.30392	154.0065	-0.03589
-3.35756	153.9756	-0.04416
-3.286	153.9312	-0.03726
-3.30605	153.8842	-0.02998
-3.43267	153.8801	-0.03479
-3.58174	153.9064	-0.02858
-3.07714	153.917	-0.02347
-3.16675	153.8956	-0.02684
-3.16762	153.8557	-0.02864
-3.17855	153.8388	-0.03712
-3.29897	153.8546	-0.01878
-3.30675	153.8773	0.012411
-3.2979	153.8947	0.069527
-3.31641	153.8901	0.086515
-3.29987	153.8392	0.064363
-3.29236	153.8105	0.031367
-3.35163	153.7955	-0.02173
-3.29255	153.7659	-0.09215
-3.30392	153.7275	-0.16359
-3.35756	153.6725	-0.22423
-3.286	153.6031	-0.32647
-3.30605	153.5519	-0.48892
-3.43267	153.551	-0.77829
-3.58174	153.5401	-1.03851
-3.07714	153.504	0.000908

-3.16675	153.4551	0.008777
-3.16762	153.4223	0.002415
-3.17855	153.4256	-0.00237
-3.29897	153.4462	-0.00205
-3.30675	153.4485	-0.03162
-3.2979	153.4118	-0.02719
-3.31641	153.347	-0.08398
-3.29987	153.3087	-0.07358
-3.29236	153.313	-0.05345
-3.35163	153.3626	-0.03669
-3.29255	153.3457	-0.03216
-3.30392	153.3148	-0.06197
-3.35756	153.3104	-0.03915
-3.286	153.3194	-0.00028
-3.30605	153.3248	-0.02096
-3.43267	153.3382	-0.02544
-3.58174	153.362	0.007937
-3.07714	153.3608	0.018721
-3.16675	153.3383	0.010665
-3.16762	153.3284	-0.00775
-3.17855	153.3459	0.034922
-3.29897	153.364	0.035093
-3.30675	153.3758	0.036186
-3.2979	153.3584	0.051615
-3.31641	153.3581	0.000908
-3.29987	153.3684	0.008777
-3.29236	153.3794	0.002415
-3.35163	153.4096	-0.00237

Appendix E: Statistical Analysis

E.1 Statistical analysis

SD= standard deviation

LOA (Limit of Agreement) = Mean \pm 1.96 SD/ Square of population size

SEM (Standard Error of Measurement) = SD/ Square of population size

CV (coefficient of Variance) =SD/Mean

E.2 Bland-Altman plot

The Bland–Altman plot is to compare two clinical measurements that each provide some errors in their measure. It can also be used to compare a new measurement technique or method with a gold standard even so the interest of the Bland–Altman plot is contested in this particular case because the error pertains to the sole new measure.

Bland and Altman plots are extensively used to evaluate the agreement among two different instruments or two measurements techniques. Bland and Altman plots allow us to investigate the existence of any systematic difference between the measurements and to identify possible outliers. The mean difference is the estimated bias, and the SD of the differences measures the random fluctuations around this mean. If the mean value of the difference differs significantly from 0 on the basis of a 1-sample t-test, this indicates the presence of fixed bias. If there is a consistent bias, it can be adjusted for by subtracting the mean difference from the new method. It is common to compute 95% limits of agreement for each comparison (average difference \pm 1.96 standard deviation of the difference), which tell us how far apart measurements by 2 methods were more likely to be for most individuals. If the differences within mean \pm 1.96 SD are not clinically important, the two methods may be used interchangeably. Bland and Altman plots were also used to investigate any possible relationship of the discrepancies between the measurements and the true value (i.e., proportional bias). The existence of proportional bias indicates that the methods do not agree equally through the range of measurements (i.e., the limits of agreement will depend on the actual measurement). To evaluate this relationship formally, the difference between the methods should be regressed on the average of the 2 methods. When a relationship between the differences

and the true value was identified (i.e., a significant slope of the regression line), regression-based 95% limits of agreement should be provided.

Consider a set of n samples (for example, objects of unknown volume). Both assays (for example, different methods of volume measurement) are performed on each sample, resulting in $2n$ data points. Each of the n samples is then represented on the graph by assigning the mean of the two measurements as the abscissa (x-axis) value, and the difference between the two values as the ordinate (y-axis) value. Hence, the Cartesian coordinates of a given sample S with values of S_1 and S_2 determined by the two assays is:

$$S(x,y) = \left(\frac{S_1 + S_2}{2}, (S_1 - S_2) \right)$$

E.2 Experiments Data

Table E.1: Validity test of flexion for all of the measurement methods (Motion Capture was used as a reference method)

Goniometer	Wii mote	Motion Capture	MotionNod
140	140.5008	132.9275	133.86
130	138.0679	133.1511	133.3
137	143.2918	132.8541	135.35
135	136.7699	131.8198	137.136
140	133.8953	129.7039	135.62
139	114.6413	131.6951	136.25
145	151.6921	145.528	142.62
155	155.0199	148.474	154.12
158	157.2499	150.3031	154.26
150	156.2926	156.538	155.52
112	106.6237	102.2748	100.55
107	110.8598	104.3836	102.35
112	115.6299	103.992	101.63
145	131.8483	138.992	138.7
140	129.1077	131.0332	131.14
137	132.8548	130.3355	132.35
136	136.3431	125.8687	128.3
135	138.1387	129.6552	128.33
135	137.108	129.1388	139.72
150	145.4368	139.604	142.27
140	144.035	134	130.68

154	145.3578	137.494	148.51
140	146.4845	134.7165	139.41
146	147.1806	140.676	140.4
145	147.4054	142.6484	148.85
150	148.0979	143.825	143.67
137	139.6461	133.9954	134.07
140	141.3	134.254	133.34
147	141.7088	145.2115	147.62
130	116.8222	121.0491	120.54
98	100.8308	88.08991	100.36
110	115.1782	125.0589	127.97
100	94.68567	89.32944	96.65
103	94.85522	89.54404	85.56
95	98.84333	83.99837	82.69
96	109.1131	90.52061	97.29
110	111.6294	101.2909	107.06
115	111.3934	108.3636	108.37
150	148.6331	143.0589	146.87
145	149.0308	141.0491	144.24
140	146.2008	137.4993	132.22
150	168.5333	145.5668	153.34
165	152.5103	159.7061	152.11
165	156.0704	169.7831	162.58

Table E.2: Validity test of adduction for all of the measurement methods (Motion Capture was used as a reference method)

Goniometer	Wiimote	Motion Capture	MotionNod
50	45.7799	48.90188	47.58
50	43.08206	48.75132	51.66
56	51.84256	52.10773	52.6
53	49	51.33925	52.21
50	48	51.33925	51.23
56	50	51.58915	52.39
55	49	52.84832	50.6
50	44.60402	51.58915	47.7
50	46.69507	52.10773	50.67
50	49	46.70091	47.63
53	43.08206	49.67215	46.87
55	44.60402	49.68053	47.158
48	48	52.07519	49.84
48	45.7799	51.20555	48.46
53	50.22355	50.92505	47.44

55	45.2111	50.88197	47.24
60	50	54.3772	50.33
54	51.84256	56.78887	49.6
57	52.88872	54.05108	56.37
65	58.77527	61.70488	65.52
62	54.40108	58.235	60.96
53	49	62.18894	61.01
55	45.03324	50.00978	51.66
57	53.765	51.86038	51.62
55	50.25553	51.07613	51.53
59	56.25	52.86695	51.66
68	57.1232	63.12065	62.14
65	55.42658	58.69696	56.18
67	56.63067	64.3767	66.002
35	33.7221	31.86202	35.41
45	34.59907	38.39372	40.42
40	37.90351	35.32161	41.47
46	37.05524	42.15898	41.5
48	38.94831	44.24734	51.14
47	36.90501	44.07761	51.01
60	59.87722	55.2303	53.15
55	51.74196	51.16938	52.27
55	51.84256	52.18012	51.88
50	43.11554	45.92708	41.42
45	44.09621	43.42763	44.09
45	40.43551	44.03597	40.32
46	39.59128	42.07488	41.68
46	38.15336	42.34808	40.94
45	45.03324	40.50964	41.68

Table E.3: Validity test of internal rotation for all of the measurement methods (Motion Capture was used as a reference method)

Goniometer	Wiimote	Motion Capture	MotionNod
28	32.00315	30.58503	31.51
35	30.00398	34.06127	31.11
35	32.52052	33.92995	31.79
35	33.7221	37.77027	35.37
35	37.05524	37.62371	35.57
40	34.59907	35.59828	37.41
40	43.7799	40.8883	42.05
37	43.08206	40.04757	44.01

43	40.06344	39.7685	41.31
43	32.53352	37.54499	36.19
35	32.52052	36.83755	36.88
35	34.59907	36.32327	36.03
48	42.00315	44.24078	41.94
45	36.06004	41.80177	41.32
43	33.7221	44.93591	40.52
20	18.6795	21.4555	21.21
25	20.96199	25.44847	21.99
28	23.47281	25.87144	20.74
33	30.76637	29.50766	26.28
30	27.05524	25.38793	25.43
30	34.59907	30.57234	28.28
35	37.90351	35.59494	35.95
35	40.05731	38.09192	37.03
35	36.90501	38.07776	36.12
40	36.69865	40.63663	42.59
40	40.43551	41.80177	41.52
45	41.67152	46.09409	41.3
45	46.13176	44.93591	45.91
44	48.07564	48.22424	45.62
45	50.22355	45.21156	46.53
43	45.2111	46.77691	38.71
45	34.99307	40.01939	36.4
42	36.06004	36.81961	36.64
39	46.13176	42.63215	40.16
40	45.7799	43.53014	40.27
40	43.08206	43.89325	36.78
40	40.03324	38.06527	36.25
37	36.06004	34.38506	36.26
40	36.13176	40.17457	46.39
40	37.90351	40.28619	46.38
46	41.84256	44.11557	46.34
43	42.88872	46.46244	46.06
42	46.53796	46.00744	45.97

Table E.4: Reliability test of goniometer for all ROM (flexion, adduction and internal rotation)

Flexion		Adduction		Internal Rotation	
Week1	Week2	Week1	Week2	Week1	Week2
135	130	50	50	30	35
135	135	50	50	35	35
130	135	50	50	35	40
145	145	50	50	40	40
150	150	50	50	40	40
106	107	48	47	35	35
145	140	48	48	45	45
135	130	53	55	25	20
125	132	55	55	25	25
135	135	55	63	30	30
138	140	60	55	30	35
135	140	55	55	35	35
145	145	55	55	40	40
135	135	65	65	45	45
145	125	35	35	45	45
95	120	35	40	45	40
100	103	45	46	40	40
95	93	57	60	40	40
103	105	55	55	40	35
145	145	50	45	40	40
140	150	45	45	45	45
155	165	45	45	45	50
155	155	55	50	50	50

Table E.5: Reliability test of Wiimote for all ROM (flexion, adduction and internal rotation)

Flexion		Adduction		Internal Rotation	
Week1	Week2	Week1	Week2	Week1	Week2
140.5008	138.0679	45.7799	43.08206	32.00315	30.00398
143.2918	136.7699	51.84256	49	32.52052	33.7221
133.8953	124.6413	48	50	37.05524	34.59907
151.6921	155.0199	49	44.60402	45.7799	43.08206
157.2499	156.2926	46.69507	49	40.06344	32.53352
106.6237	110.8598	43.08206	44.60402	32.52052	34.59907
122.6299	131.8483	48	45.7799	32.00315	36.06004
129.1077	132.8548	50.22355	45.2111	33.7221	28.6795
136.3431	138.1387	50	51.84256	20.96199	23.47281
137.108	145.4368	56.88872	58.77527	30.76637	37.05524
144.035	145.3578	52.40108	49	34.59907	37.90351
146.4845	147.1806	55.03324	53.765	40.05731	36.90501
147.4054	148.0979	56.25553	56.25	36.69865	40.43551
139.6461	141.3	57.1232	55.42658	38.67152	36.13176
141.7088	136.8222	46.63067	46.7221	48.07564	50.22355
121.8308	115.1782	34.59907	37.90351	45.2111	44.99307
94.68567	94.85522	37.05524	38.94831	36.06004	36.13176
98.84333	109.1131	39.90501	43.87722	45.7799	43.08206
111.6294	111.3934	51.74196	51.84256	45.03324	46.06004
148.6331	149.0308	43.11554	44.09621	36.13176	37.90351
146.2008	154.5333	40.43551	39.59128	51.84256	52.88872
152.5103	154.0704	48.15336	45.03324	56.53796	53.22355
155.2155	161.2549	44.21549	46.23655	48.07564	45.2111

Table E.6: Reliability test of Motion Capture for all ROM (flexion, adduction and internal rotation)

Flexion		Adduction		Internal Rotation	
Week1	Week2	Week1	Week2	Week1	Week2
132.9275	133.1511	48.90188	48.75132	30.58503	34.06127
132.8541	131.8198	52.10773	51.33925	33.92995	35.77027
129.7039	131.6951	51.33925	51.58915	37.62371	35.59828
145.528	148.474	52.84832	51.58915	40.8883	40.04757
150.3031	156.538	52.10773	46.70091	39.7685	37.54499
102.2748	104.3836	49.67215	49.68053	36.83755	36.32327
133.992	138.992	52.07519	51.20555	44.24078	41.80177
131.0332	130.3355	50.92505	50.88197	44.93591	41.4555
125.8687	129.6552	54.3772	56.78887	25.44847	25.87144
129.1388	139.604	64.05108	61.70488	29.50766	25.38793
134	137.494	58.235	62.18894	30.57234	35.59494
134.7165	140.676	50.00978	51.86038	38.09192	38.07776
142.6484	143.825	51.07613	52.86695	40.63663	41.80177
133.9954	134.254	63.12065	58.69696	46.09409	44.93591
125.2115	121.0491	64.3767	61.86202	48.22424	45.21156
128.0899	125.0589	38.39372	35.32161	46.77691	42.01939
89.32944	89.32944	42.15898	44.24734	46.81961	42.63215
83.99837	90.52061	54.07761	55.2303	43.53014	43.89325
101.2909	108.3636	51.16938	52.18012	38.06527	34.38506
143.0589	141.0491	45.92708	43.42763	40.17457	40.28619
137.4993	145.5668	44.03597	42.07488	44.11557	46.46244
159.7061	169.7831	42.34808	40.50964	46.00744	47.98494
149.3255	147.2515	50.92355	50.47457	49.55962	48.3416

Table E.7: Reliability test of MotionNode for all ROM (flexion, adduction and internal rotation)

Flexion		Adduction		Internal Rotation	
Week1	Week2	Week1	Week2	Week1	Week2
143.86	143.3	57.58	51.66	31.51	31.11
145.35	137.136	52.6	52.21	31.79	35.37
135.62	136.25	51.23	52.39	35.57	37.41
152.62	154.12	46.6	47.7	42.05	44.01
154.26	155.52	46.67	47.63	41.31	36.19
120.55	122.35	46.87	47.158	36.88	36.03
121.63	138.7	46.84	46.46	41.94	41.32
131.14	132.35	47.44	47.24	20.52	21.21
138.3	138.33	49.33	48.6	21.99	20.74
139.72	152.27	68.37	65.52	26.28	25.43
150.68	148.51	66.96	51.01	38.28	35.95
149.41	150.4	51.66	51.62	37.03	36.12
148.85	143.67	61.53	61.66	42.59	41.52
144.07	143.34	32.14	36.18	41.3	45.91
117.62	120.54	36.002	35.41	45.62	46.53
120.36	97.97	40.42	41.47	38.71	36.4
96.65	100.56	51.5	51.14	40.64	40.16
102.69	107.29	51.01	50.15	40.27	36.78
107.06	108.37	42.27	41.88	36.25	36.26
146.87	149.24	41.42	44.09	46.39	46.38
152.22	153.34	40.32	41.68	46.34	46.06
152.11	152.58	50.94	51.68	45.97	43.54
151.91	152.97	50.51	53.84	48.14	45.54

Appendix F: Ethical Approval

F.1 Consent Form

Consent Form

Researchers

Mahhsid Yazdi Far, PhD Student, mahshid.yazdifar@brunel.ac.uk

Prof,Ibrahim Esat, Academic Supervisor, Ibrahim.Esat@brunel.ac.uk

Information for the participants:

Title of the study: Detection of Hip Impingement

This study requires the volunteer participants to take part in the experiments including flex, adduct and internally rotate their hip in Motion Capture lab. Participants hip are flexed, adducted, and rotated to measure the range of motion. Results are collected for the purpose of further analysis. The study will have no harm or risk to the participants. Participants in the study have the right to withdraw from the study at any stage during the research without any penalty. **The collected data from participants will be stored strictly confidentially and participants' identities will be secured. Data with participant's identity will be only accessed by the named researchers for further analysis.** Nameless data will also be analysed by academic supervisor. There will be no other use or access to the participants' data other than this study. **Participants are ensured that their personal information will be destroyed upon the completion of this study.** In the case of publication of the study's results the anonymity of the participants will be preserved. This study has been approved by the School of Engineering & Design Research Ethics Committee.

	Yes	No
I have read the research Participant Information sheet.	<input type="checkbox"/>	<input type="checkbox"/>
I understand the content of the study	<input type="checkbox"/>	<input type="checkbox"/>
I have had the opportunity to ask questions about the study	<input type="checkbox"/>	<input type="checkbox"/>
I understand that I will remain anonymous in any publication of the result	<input type="checkbox"/>	<input type="checkbox"/>
I know that this study will not affect my assessment in the course	<input type="checkbox"/>	<input type="checkbox"/>
I agree willingly to take part in the study.	<input type="checkbox"/>	<input type="checkbox"/>

Signature of the participant

Name

Date:

For researcher's use:

I am satisfied that above person has given informed consent

Witnessed by:

Date:

F.2 Information Sheet

Information Sheet

The aim of the project is to develop and validate the methods that will facilitate patient-specific modelling of hip joint biomechanics. Toward the objective a complete hip model with soft tissues were developed to use in impingement detection of hip.

This study requires the volunteer participants to take part in the experiments including flex, adduct and internally rotate their hip in Motion Capture lab. Participant's hip are flexed, adducted, and rotated to measure the range of motion. Results are collected for the purpose of further analysis.

The experimental takes 5minutes. The participants need to lie down in supine position. The subject volunteers will be asked to bend their knee and bend their leg and bring it as close to their chest as is comfortable for them (fully flexed).

The subject volunteers will be asked to move their leg to the inside toward their opposite leg. The subject was supine in anatomical position.

The subject will be asked to flex the hip 90° and then to rotate their hip out of their body.

The study will have no harm or risk to the participants. Participants in the study have the right to withdraw from the study at any stage during the research without any penalty. **The collected data from participants will be stored strictly confidentially and participants' identities will be secured. Data with participant's identity will be only accessed by the named researchers for further analysis.** Nameless data will also be analysed by academic supervisor. There will be no other use or access to the participants' data other than this study. **Participants are ensured that their personal information will be destroyed upon the completion of this study.** In the case of publication of the study's results the anonymity of the participants will be preserved. This study has been approved by the School of Engineering & Design Research Ethics Committee.

F.3 Ethical Approval

